

Carbon and Platinum Nanostructured Electrodes on Miniaturized Devices for Biomedical Diagnostics

THÈSE N° 6704 (2015)

PRÉSENTÉE LE 11 SEPTEMBRE 2015

À LA FACULTÉ INFORMATIQUE ET COMMUNICATIONS

LABORATOIRE DES SYSTÈMES INTÉGRÉS (IC/STI)

PROGRAMME DOCTORAL EN MICROSYSTÈMES ET MICROÉLECTRONIQUE

ÉCOLE POLYTECHNIQUE FÉDÉRALE DE LAUSANNE

POUR L'OBTENTION DU GRADE DE DOCTEUR ÈS SCIENCES

PAR

Irene TAURINO

acceptée sur proposition du jury:

Prof. J. Brugger, président du jury
Prof. G. De Micheli, Dr S. Carrara, directeurs de thèse
Prof. W. Schuhmann, rapporteur
Prof. V. Van Hoof, rapporteuse
Dr A. Magrez, rapporteur



ÉCOLE POLYTECHNIQUE
FÉDÉRALE DE LAUSANNE

Suisse
2015

L'ultimo passo della ragione è riconoscere
che c'è un'infinità di cose che la sorpassano.
— Blaise Pascal

A mio nonno ...

Acknowledgements

My first big thank goes to Prof. Giovanni De Micheli and to Dr Sandro Carrara for their continuous advices and encouragement throughout the course of my PhD and for the systematic guidance and the great effort they put into training me for doing research.

I wish to express my sincere thanks to the jury members for the evaluation of this research thesis: Prof. Jürgen Brugger, Dr Arnaud Magrez, Prof. Wolfgang Schuhmann and Prof. Viviane Van Hoof. In particular, I want to thank Dr Arnaud Magrez for his support during the collaboration with his laboratory, Prof. Wolfgang Schuhmann for all the suggestions regarding my future career and Prof. Viviane Van Hoof to have inspired part of this research work.

I thank all the CMI people for the help on issues concerning the device microfabrication and Prof. Ali Khademhosseini for giving me the opportunity to work in his laboratory at Harvard University.

A particular acknowledgement to my "LSI mom" Christina Govoni for her kindness and caring and to Rodolphe for helping me in every "laptop-related" problems. Thanks to Sara for the mutual understanding and to be for me the perfect officemate and thanks to Stefano for the confidences and the smiles. Thanks to Cami for her constant availability in every situations during the last five years. Thanks to Michele for the closeness and the useful advices and to Andrea for his enthusiasm and positiveness in doing research. Thanks to Ismael for being an example of fortitude, to Federico for his constant availability and to Francesca for her sensitiveness. Thanks to Fernando, Manuel and Alberto for their useful advices on complex electrochemical subjects.

A very huge thank goes to some people I met during my stay in US: Antonia and her pleasant company and Tugba, one of the best person I have ever met in my life, for making my US experience so amazing.

I would like to express my gratitude to some students I supervised: "la mitica Mitti" and her unique love of life driven by the faith, the sunny and positive Flavia, Gabry for the unique synergy in working together, Francesca and her extreme motivation in learning how to do research and sincere friendship and Mischa for his kindness.

A particular thank to three PhD students of other EPFL laboratories I collaborated with during the last four years: Laurent for his enormous patience and friendliness, Massimo and Federico for their infinite politeness.

I would like to thank current, past and "adopted" members of LSI: Cristina and Matteo, Anna, Jack, Alice, Armando, Julien, Alena, Nima, Shashi, Luca, Giovanni, Somayyeh, Ioulia, Gözen,

Acknowledgements

Wenqi, Hu, Ciprian, Srinu, Jaume and Ludo, Vasilis, Pierre-Emmanuel, Prof. Subhasish Mitra, Prof. Wayne Burlison and Prof. Maciej Ciesielski, Anil and the Nano-Tera staff.

Sincere thanks to some people I met in Lausanne: Ale for supporting me with constant love, Claudia for the everyday friendship, La Vale, Elena, Paoli T. and C., Azzu and Vince, "l'adorabile" Laura, Noelia and finally Iole for the friendship and the "Pizzica" classes we provided.

My deepest gratitude goes to mamma Marcella and papà Fernando for their unconditional love and continuous support and to my sister Marialuisa and her magic power to solve my problems even at distance. Thanks to my grandparents for their sweet love, to my cousins Enrica and Antonio, Giorgio and Elena, to my uncles Salvatore and Giovanni, to my aunts Lella and Antonietta, to Danilo, to Anna and Cate, my two oldest and dearest friends.

Last but not least, a very special thank goes to my grandfather, a true Lover of Life. His smile and his shining eyes are always in my head. This work is dedicated to him.

Lausanne, July 2015

I.T.

Abstract

Nowadays, medical devices face several limitations concerning rapid, reliable and simultaneous quantification of a set of ions and metabolites from a micro-nanoliter volume of undiluted samples. The development of minimally-sized devices is, therefore, of key importance. In such a context, electrochemical sensors are particularly advantageous because of the simple, low cost and reproducible fabrication procedures and the rapid analytical measurements. Moreover, they provide easy possibilities for continuous monitoring. However, sensitive and selective detection of molecules in the physio-pathological concentration range is very challenging when conventional electrochemical devices are employed, especially for long-term use.

Nanostructured electrodes are considered as one of the most promising strategies to overcome issues of sensitivity because of their large surface area and their excellent electrocatalytic properties. They could also address in part the problem of selectivity due to shifts in potential of the measured Faradic currents. In addition, nanomaterials could provide stable and reproducible potential responses when used as solid-contact materials of ion-selective electrodes.

Inappropriate nanointegration methods could decrease the sensor performance so that the development of tailored nanostructuring protocols is extremely important to boost the sensor sensitivity, selectivity and stability over time.

Objective of this thesis was to design and electrochemically characterise novel carbon and metal nanostructures for medical sensors.

First of all, the integration of carbon nanomaterials on specific sensing sites of a microfabricated sensor was considered. Time-consuming, expensive and hardly-reproducible nanostructuring approaches contemplate the co-immobilization of carbon nanomaterials and additives whose presence inevitably masks the nanomaterial promising properties and compromises the time-stability in aqueous environments. The selective CVD growth of carbon nanomaterials was considered as a promising method to enable the coupling nanomaterial-electrode. Deposition parameters were optimised to make the process compatible with CMOS temperatures.

Then, new protocols based on rapid electrodeposition methods were developed to integrate differently shaped and sized Pt and Pt-Au nanostructures on electrochemical platforms. Template-free electrodeposition was selected because of the durably-anchored and the contaminant-free coatings resulting after the process.

Both nanostructuring approaches generated highly-sensitive electrodes to detect human

Acknowledgements

metabolites as compared with the bare counterparts. Unprecedented sensing performance were obtained by both direct and enzyme-mediated detection mechanisms. Selective sensing was achieved thanks to the capability of the proposed nanostructured electrodes to discriminate the detection potentials of biomarkers from those of interfering species. The developed nanostructures were also excellent solid contacts between an electrode and an ion-selective membrane resulting in stable and reliable solid-contact ion-selective electrodes. To prove their stability and reproducibility for long operating lifetimes, these ion-selective electrodes have been successfully used as standard for continuous acute cell death monitoring.

Key words: C and Pt and Au-Pt nanostructured electrodes; CVD growth; electrodeposition; voltammetry; potentiometry; direct metabolite detection; enzyme-mediated metabolite detection; solid-contact ion-selective electrodes; continuous monitoring; diagnostic devices

Résumé

Aujourd'hui, les dispositifs médicaux font face à d'importantes limitations concernant la mesure quantitative rapide, fiable et simultanée d'un ensemble de métabolites à partir d'échantillons non dilués de l'ordre du micro ou nanolitre. La minimisation de la taille des dispositifs acquiert par conséquent une importance grandissante. Dans un tel contexte, le développement de capteurs électrochimiques est particulièrement avantageux, grâce à des procédés de fabrication simples, à bas coût et reproductibles, ainsi qu'à des mesures analytiques rapides. Ces dispositifs permettent la mise en place rapide d'un contrôle continu. Cependant, la détection sensible et sélective de molécules ayant de grandes durées de vie dans la gamme de concentration physio-pathologique est extrêmement difficile lorsque des dispositifs électrochimiques conventionnels sont utilisés.

Les électrodes nanostructurées sont considérées comme une des stratégies les plus prometteuses pour s'affranchir des problèmes de sensibilité, du fait de leurs grandes surfaces et leurs excellentes propriétés électrochimiques. En effet, elles pourraient résoudre en partie les problèmes de sélectivité liés aux décalages de potentiel des courants de Faraday mesurés. En outre, les nanomatériaux pourraient permettre des réponses en potentiel stables et reproductibles lorsqu'ils sont utilisés en tant que matériaux de contact sur des électrodes sensibles aux ions. Cependant, des méthodes de nanointégration inappropriées pourraient conduire à une réduction des performances de ces capteurs. Le développement de protocoles d'intégration adéquats est ainsi d'importance pour augmenter la sensibilité et la stabilité des capteurs dans le temps.

L'objectif de cette thèse est de concevoir et de caractériser électrochimiquement de nouveaux matériaux à base de carbone et de métaux nanostructurés pour application dans les capteurs médicaux.

Premièrement, l'intégration de nanomatériaux en carbone a été considérée. Les approches classiques de nanostructuration telles que la co-immobilisation des nanomatériaux carbonés avec des additifs sont longues, coûteuses et difficilement reproductibles. De plus, la présence d'additifs masque inévitablement les propriétés prometteuses des nanomatériaux et compromet la stabilité en solution aqueuse. Ainsi, une croissance sélective par dépôt chimique en phase vapeur (CVD, de l'anglais chemical vapour deposition) a été considérée pour permettre le couplage nanomatériaux-électrode. Les paramètres de dépôt ont été optimisés pour rendre ce procédé compatible avec les températures de fabrication CMOS. Par la suite, de nouveaux protocoles basés sur des méthodes d'électrodeposition rapide ont été développés

Acknowledgements

pour intégrer des nanostructures de formes et tailles variées en Pt et Pt-Au sur des plateformes électrochimiques. L'électrodeposition sans modèle a été choisie pour permettre des dépôts de couches avec une bonne qualité d'accroche aux substrats et l'absence de contaminations. Les deux approches de nanostructuration ont permis d'obtenir des électrodes fortement sensibles aux métabolites, en comparaison de celles non nanostructurées. Des performances de détection sans précédents ont été atteintes à la fois par détection directe et par détection médiée par les enzymes. Une détection sélective a été obtenue grâce à la capacité des électrodes proposées de distinguer les potentiels de détection des biomarqueurs de ceux des espèces interférentes. Les nanostructures développées ont également constitué d'excellents contacts à l'état solide entre une électrode et une membrane sélective aux ions, ce qui a donné des électrodes sélectives aux ions à l'état solide stable et fiable. Afin de prouver leur stabilité et reproductibilité pour de longs temps d'opération, ces électrodes ont été employées avec succès en tant que standard pour le contrôle continu de mort cellulaire aiguë.

Mots-clé : électrodes nanostructurés en C et Pt et Pt-Au ; électrodeposition ; voltammétrie ; potentiométrie ; détection de métabolites directe ; détection de métabolites par les enzymes ; électrodes à contact solide et sélectives aux ions ; monitoring continu ; dispositifs de diagnostic.

Contents

Acknowledgements	i
Abstract (English and Français)	iii
1 Introduction	3
1.1 Current/future trends in chemical sensors for biomonitoring	4
1.2 Electrochemical sensors	9
1.2.1 Potentiometric sensors	10
1.2.2 Voltammetric sensors	12
1.3 Sensor fabrication techniques	15
1.4 Nanostructured electrodes for enhanced detection performance	16
1.5 Research contributions and outline of the thesis	19
2 Nanostructured electrodes for electrochemical medical sensors	23
2.1 Carbon nanostructured electrodes	24
2.1.1 Electrochemical properties	24
2.1.2 Integration approaches	25
2.1.3 Direct detection	30
2.1.4 Enzyme-mediated detection	30
2.2 Nanoporous Pt electrodes	32
2.2.1 Catalysis	32
2.2.2 Fabrication methods	34
2.2.3 Direct detection	40
2.2.4 Enzyme-mediated detection	44
2.3 Hybrid Pt-based nanostructured electrodes	45
2.4 Potentiometric solid-contact ion-selective electrodes	46
2.5 Summary and contributions	47
3 Direct and selective integration of carbon nanomaterials by a CVD process on a microfabricated Si-based multipanel device	49
3.1 Device microfabrication	50
3.2 Methods	51
3.2.1 Catalyst electrodeposition	51
3.2.2 Synthesis of carbon nanomaterials	52

Contents

3.2.3	Material characterisation	52
3.3	Syntheses at high temperatures from Fe catalyst	53
3.3.1	Selection of the dielectric material and of the deposition time	53
3.3.2	SEM and AFM study	54
3.3.3	Effect of the deposition parameters	59
3.3.4	Micro-Raman spectroscopy	62
3.4	Growths down to CMOS compatible temperatures	64
3.4.1	Catalyst electrodeposition	65
3.4.2	Growths on catalyst nanoparticles	65
3.4.3	Growths on catalyst coatings	66
3.4.4	Implementing two successive growths	68
3.5	Summary and contributions	70
4	Electrochemical characterisation of MWCNTs, nanographite and their hybrids grown by CVD on a Si-based device	71
4.1	Demonstration of the superior performance of MWCNT-based electrodes	72
4.1.1	Direct detection of bilirubin	72
4.1.2	Enzyme-mediated detection of lactate	77
4.2	Detection of molecules by carbon nanomaterials CVD-grown onto microfabricated sensors	80
4.2.1	Methods	81
4.2.2	Nanomaterial activation	82
4.2.3	Direct detection of interferences: the case of uric acid	86
4.2.4	Direct detection of low metabolite concentrations: the case of bilirubin	87
4.2.5	Enzyme-mediated detection of glucose	89
4.2.6	Biofouling evaluation	91
4.3	Comparative study with conventional carbon nanomaterial integration approaches: microspotting and electrodeposition	93
4.4	Summary and contributions	96
5	Direct and selective integration of differently shaped and sized Pt nanostructures by template-free electrodeposition on screen-printed electrodes	97
5.1	Methods	98
5.1.1	Electrodeposition procedures	98
5.1.2	Morphological characterisation	99
5.1.3	Evaluation of electroactive area and roughness factor	99
5.2	Nanostructuring electrodes with nanoPt	100
5.2.1	Synthesis from tetravalent Pt-based solutions	100
5.2.2	Synthesis from divalent Pt-based solutions	105
5.2.3	Double depositions of Pt nanostructures	106
5.3	Coupling Pt and Au nanostructures	107
5.4	Summary and contributions	111

6 Electrochemical characterisation of Pt nanopetals and Pt nanospheres prepared by electrodeposition on screen printed electrodes	113
6.1 Methods	114
6.2 Oxidase-mediated detection of glucose	114
6.3 Direct oxidation of glucose	119
6.4 Measurements with alloy Au-Pt	120
6.5 Summary and contributions	123
7 A biological application of solid-contact potassium-selective electrode based on Pt nanopetals	125
7.1 Methods	127
7.2 Performance evaluation of Pt nanostructures	130
7.3 Characterisation of Pt nanopetal K ⁺ -selective electrodes	133
7.4 Measurements with a fluidic system	133
7.4.1 Fabrication of fluidic system and bioreactor	134
7.4.2 Characterisation in HEPES buffer, DI water and cell media	135
7.5 Acute cell death monitoring	137
7.6 Building an integrated all-solid-state RE	142
7.6.1 Preparation procedures	142
7.6.2 Results	143
7.7 Summary and contributions	144
8 Conclusions and Future Research Directions	147
A Electrochemical sensing parameters	151
A.1 Performance evaluation from voltammetric measurements	151
A.2 Performance evaluation from potentiometric measurements	152
B Taguchi method	155
Bibliography	176
Curriculum Vitae	177

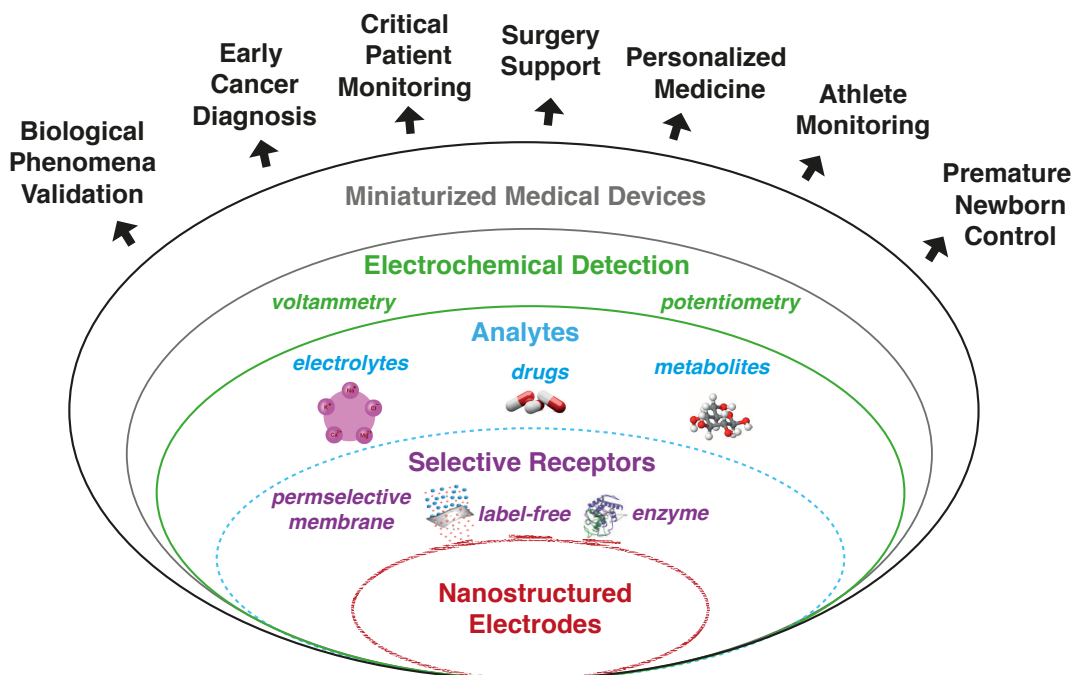
List of Abbreviations

SERS	Surface Enhanced Raman Spectroscopy
SORS	Spatially Off-set Raman Spectroscopy
ECL	Electrogenerated chemiluminescence
MEMS	Micro-Electromechanical Systems
ELISA	Enzyme Linked Immuno Sorbent Assay
GOx	Glucose Oxidase
LOx	Lactate Oxidase
WE	Working Electrode
RE	Reference Electrode
CE	Counter Electrode
ISE	Ion Selective Electrode
PVC	Poly(vinyl Chloride)
CV	Cyclic Voltammetry
CA	Chronoamperometry
DPV	Differential Pulsed Voltammetry
SWV	Square Wave Voltammetry
LSV	Linear Sweep Voltammetry
CMOS	Complementary Metal Oxide Semiconductor
CNT	Carbon Nanotube
MWCNT	Multi-Walled Carbon Nanotube
SWCNT	Single-Walled Carbon Nanotube
NT	Nanotubes
CP	Conducting Polymer
HOPG	Highly Ordered Pyrolytic Graphite
UA	Uric Acid
AA	Ascorbic Acid
LCC	Lyotropic Liquid Crystal
DI	Deionized Water
SS	Solid State

Contents

SEM	Scanning Electron Microscope
EDX	Energy Dispersive X-ray Spectroscopy
AFM	Atomic Force Microscope
RHE	Reversible Hydrogen Electrode
CWE	Coated-Wire Electrode
SC	Solid Contact
ALD	Atomic Layer Deposition
PR	Photoresist
FeNP	Iron Nanoparticle
FeNC	Iron Non-Compact Layer
FeC	Iron Compact Layer
FeCoNP	Iron-Cobalt Nanoparticle
FeCoC	Iron Cobalt Compact Layer
FWHM	Full Weight Half Maximum
BR	Bilirubin
BV	Biliverdin
SPE	Screen Printed Electrode
PBS	Phosphate-Buffered Saline
HEPES	4-(2-Hydroxyethyl)-1-Piperazineethanesulfonic acid) Buffer Solution
DMSO	Dimethyl Sulfoxide
HRP	Horseradish Peroxidase
ABTS	2,2'-Azino-Bis(3-Ethylbenzothiazoline- 6-Sulphonic Acid)
LOD	Limit Of Detection
Rf	Roughness Factor
S/N	Signal to Noise Ratio
QRE	Quasi Reference Electrode
3D	Three-Dimensional
DMEM	Dulbecco's Modified Eagle's Medium
nanoPt	Pt Nanoporous
nanoAu	Au Nanoporous
ISM	Ion Selective Electrode
DOS	Bis(2-Ethylhexyl)sebacate
KTCIB	Potassium Tetrakis(4-Chlorophenyl)borate
THF	Tetrahydrofuran
SSM	Separate Solution Method
RCP	Reversed Chronopotentiometry
C	Capacitance
PDMS	Polydimethylsiloxane
PMMA	Poly(methyl Methacrylate)

1 Introduction



A simultaneous and reliable quantification of ions and metabolites is important in medicine. Nowadays, laboratory tests are mainly performed by big and expensive instrumentation only used by trained staff remote from the patient. Test results are always expected after hours or days.

More often, different diseases and health conditions require continuous biomonitoring for rapid clinical interventions. Therefore, fast laboratory results are highly desirable by employing user-friendly, miniaturised and cheap tools. For instance, reading continuously the concentration

level of different drugs in patients under chemotherapy, would lead to a rational dosage individualisation and fast intervention. Smart portable diagnostic tools are also of crucial importance for early cancer detection and consequent immediate therapy. Patients in intensive care units are typically at high risk of death. Typically the death of these patients is preceded by a Systemic Inflammatory Response Syndrome that can be early diagnosed only by a constant monitoring of some metabolic imbalances. Also premature babies run easily the risk of death if their vital parameters are not regularly checked. Therefore, the development of inline diagnostic tools for accurate and continuous control of some metabolites and electrolytes might significantly reduce mortality of critical patients and newborns. Diabetes is another disease associated with multiple health problems and even death if the level of glucose is not constantly controlled. Detection systems to be partially implanted or partially embedded in external surgical tools would help doctors during a surgery. Sport is another field in which a strategy of multimolecular detection could efficiently reduce risks of injury and/or overtraining while maximising athletic performance.

Among different detection systems, electrochemical sensors are the most powerful because of the high sensitivity and selectivity of the analysis, the opportunities for miniaturisation to afford portable/implantable/wearable devices and the possibility to perform an automated non-stop single- or multi-analyte monitoring. Their combination with nanostructures gives further advantages in terms of sensitivity, specificity and measurement reproducibility.

In this chapter, a first part will be focused on chemical sensors for biosample analysis and on the strengths of using electrochemical sensors for monitoring biomarkers (Section 1.1). Then, an overview of the basic principles of potentiometric and voltammetric devices is given in Section 1.2. Section 1.3 presents the main approaches to fabricate electrochemical sensing platforms for medical use. Finally, a list of advantages concerning the integration of "nano" components onto electrochemical electrodes is provided in Section 1.4. The chapter concludes with an explanation of the thesis objectives and the outline (Section 1.5).

1.1 Current/future trends in chemical sensors for biomonitoring

Nowadays, there is a wide interest in continuous monitoring and controlling the health status of human beings to improve diagnosis and therapy. Most of the clinical analyses are carried out in chemistry laboratories remote from the patient, with expensive instrumentation and time-consuming processes. The analysed human fluids are blood and urine, and common techniques are

- *Chromatography* is a physical method of separation in which the components to be separated are distributed between two phases called stationary and mobile phase (one is static and the other moves in a certain direction). A chromatographic separation requires a sample to be introduced into a flowing stream (mobile phase) that passes through a bed, layer, or column that contains the stationary phase. If the mobile phase

1.1. Current/future trends in chemical sensors for biomonitoring

is a gas, the technique is known as gas chromatography and if it is a liquid, it is called liquid chromatography. Solid/gel or liquid particles compose the secondary phase and the mobile phase carries the sample through the stationary phase. The solutes with less affinity for the stationary phase remain in the mobile phase and travel faster and separate from those that have a high affinity for it. Adsorption, affinity, ion exchange, solubility, and steric exclusion are the main chemical or physical mechanisms for the solute separation. This technique is a valuable clinical laboratory tool to detect and identify certain sugars, amino acids and drugs in body fluids [1].

- *Spectrophotometry* determines mainly the concentration in blood and urine of calcium, magnesium, iron, phosphate, enzymes, albumin, urea, uric acid, glucose, creatinine, cholesterol and bilirubin by the ability of atoms to absorb radiant energy of specific wavelengths [1]. It is based on the adsorption of an opportunely selected electromagnetic radiation in the visible, ultraviolet or infrared range. An opaque block that does not let passing the light is tested and the meter is adjusted to read 0% transmittance. Then, a cuvette containing the blank is inserted and the meter is adjusted to read 100% transmittance. After the calibration, the solution with unknown concentration of the substance is measured and its concentration is determined on the basis of the calibration curve.
- *Immunological methods* are based on a highly specific affinity of an antibody for its antigen¹. The antibodies used for these methods can be (a) monoclonal when produced from a single cell lineage and mostly prepared in laboratory, and (b) polyclonal that are secreted by different B cell lineages and produced by immunisation of animals with antigen. The first ones have excellent specificity but poor ability to precipitate the antigen, the latter possess specificity for complex antigens. Immunological techniques are called **particle-based** when a real antigen-antibody interaction is sensed by agglutination, precipitation, electrophoresis, turbidimetry or nephelometry. In particular, *nephelometry* is a test to measure the concentration of immunoglobulins that are blood proteins helping against the body infections. The test is performed by measuring the scattered light coming from a dilute suspension of reactants. The antibody concentration in solution is kept constant and that of the antigen is variable and proportional to the scatter determined by collecting the light at an angle (usually 30 or 90 degrees) [2]. *Turbidimetry* differs from the previous method only because the adsorbance of the reactants in solution is the measured parameter [3]. Immunological methods are **label-based** when either antigen or antibody is labeled. The antigen-antibody reaction is observed through the label that can be (a) a radio isotope, (b) an enzyme (e.g. ELISA, Enzyme Linked Immuno Sorbent Assay), (c) a fluorescent compound or (d) a chemiluminescent substance. These methods are used for detecting small amounts of biochemical substances (often proteins) [4].
- *In reflectometry* a photodiode senses the intensity of the reflected light from a test strip, which is dependent on the amount of a target (metabolites, ions, proteins) [5].

¹Antibodies are immunoglobins (Y-shaped glycoproteins) containing 4 polypeptides (2 called heavy chains and 2 called light chains). The region of an antigen binding to an antibody is called an epitope. The antigen can be any substance from the environment (e.g., chemicals, bacteria, viruses)

- *Potentiometric ion measurements.* In *indirect* potentiometry the ion is diluted to an activity near to unity and the relative concentration is sensed. *Direct* potentiometry provides the real activity of an ion. The reference methods for measuring some ions as K^+ and Na^+ measure the total concentration of the ions and the indirect potentiometry is used to have a valuable comparative method avoiding confusion.

The previously-described methods possess turn-around-times in clinical laboratories of one/two hours for most common analytes, even when processes are highly automated. More often, the instrumentation is expensive, can analyse only one sample per time and are hardly suitable for miniaturisation. Today, minimally-invasive devices have become extremely interesting to further improve clinical diagnosis. Standard laboratory tests will be replaced by chemical sensors conceived to be worn by or implanted in patients or integrated with tubes/-catheters directly connected with human bodies (e.g., surgery, intensive care medicine). The main objective is to enable the doctor to read continuously patient's vital parameters at any site for fast therapeutic interventions. Beside blood and urine, that are the most well-known human fluids for diagnostic tests, other biosamples (sweat, saliva, interstitial fluids, tears) are starting to be considered as attractive targets for miniaturised medical devices. Detection systems, appropriate for a specific health condition and easy-to-use in different locations (hospital point-of-care settings, by caregivers and/or by patients at home), are becoming an urgent need. However, there is still a lack of technology devoted to a fast and "portable" medical analysis. Such medical sensors should provide highly sensitive and accurate measurements and should sense various molecules in a continuous mode from small volume of undiluted biological fluids.

Sensors are small analytical detectors that record changes of analyte concentration in a sample. Such tools must respond continuously and reversibly without modifying the sample under analysis. Chemical sensors are characterised by a transduction element including or not a biological probe (biosensor). In the presence of the analyte of interest, the traducer produces a signal that is then collected, amplified and displayed by a signal processor (Fig. 1.1). Different types of transducers are available [6].

In **optical** transducers, the measured signal is the light. Many efforts have been done to build wearable optical sensors for continuous healthcare monitoring. For instance, *Surface Enhanced Raman Spectroscopy* (SERS) and *Spatially Off-set Raman Spectroscopy* (SORS) were used to monitor in real-time glucose from interstitial fluids. Raman spectroscopy can detect the vibrational mode of glucose molecules whose signal can be enhanced by using an optical fibre covered with a film of silver nanospheres functionalized with a self-assembled monolayer of decanethiol/6-mercapto-1-hexanol. The sensor, implanted in the abdomen of mice, detected glucose levels between 31 and 79 mg/dl for 17 days [7]. Other authors were able to sense glucose from sweat by employing *Resonance-Enhanced Pulsed Photoacoustic Spectroscopy* with a resonator cell positioned on the skin and characterised by two absorption and resonance cylindrical cavities. The laser beam, irradiating the sample on the far side, induced the photoacoustic effect in the absorption cavity. The acoustic wave was then recorded by an

1.1. Current/future trends in chemical sensors for biomonitors

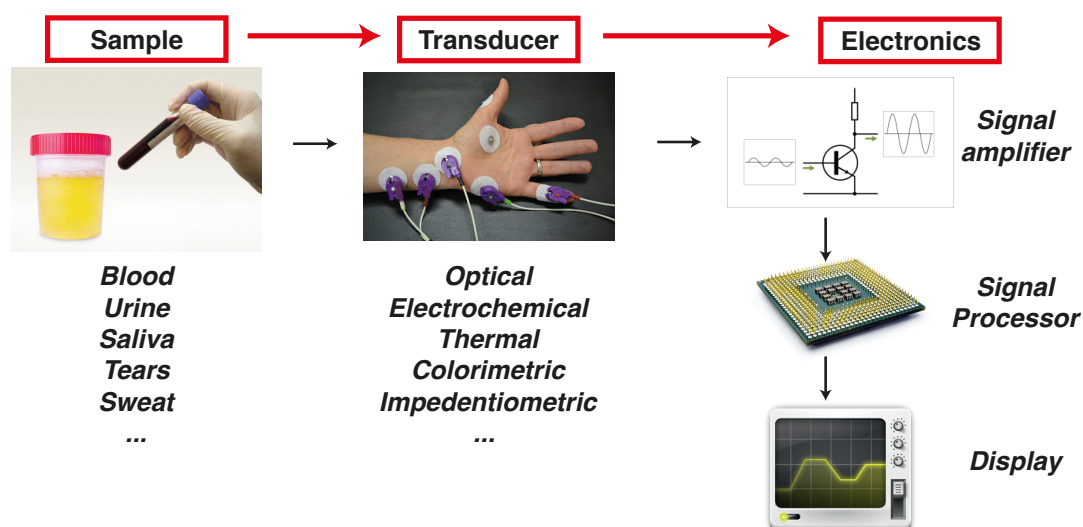


Figure 1.1 – Component of a generic medical sensor.

ultrasound detector positioned at the end of the resonance cavity. Analysis of the principal components of IR spectra showed that glucose was the first principal component [8]. A miniaturisation of the whole system was still necessary. An *electrogenerated chemiluminescence* (ECL) biosensor was realised using a luminol hydrogen peroxide sensitive compound, lactate dehydrogenase and pyruvate oxidase adsorbed onto a carbon nanotube layer to detect lactate from sweat of volunteers. However, in this work, the fabricated device was too big to be worn and the off-line analyses increased the risk of contamination [9]. A system characterised by a light detector, which responded to colorimetric changes of the pH indicator (bromocresol purple, pH sensitive dye), was used to analyse samples directly collected from athletes during training [10]. To make the system really wearable, a further reduction of the dimensions was definitively required. A continuous detection of glucose in tears could revolutionise the life of diabetic people because the constant feedback permits rapid therapeutic interventions and immediate variations of the food intake. Few research groups are investigating systems optically responsive to glucose and sufficiently small to be incorporated on contact lenses [11, 12]. Considering the list of systems before-described, it is clear that the main challenge of optical devices is the possibility to realise compact and versatile instrumentation.

Micro-Electromechanical Systems (MEMSs) are potential technologies to realise implantable devices for metabolic monitoring because of their minimally-invasive sizes leading also to rapid time responses. Xie *et al.* [13] have recently discussed recent developments on mini/micro devices based on **calorimetric** transducers for biochemical/clinical analysis and monitoring. The main drawback of thermal MEMSs include non-specificity and low sensitivity.

A glucose MEMS sensor based on **viscometric** detection was recently developed. Briefly, glucose reversibly forms strong bonds with some moieties of polymer backbones resulting in an increase of the solution viscosity [14]. Huang and co-workers [15] fabricated a MEMS

Chapter 1. Introduction

sensor based on a differential **capacitive** transduction mechanism. The device consisted of two connected microchambers, one containing a glucose-sensitive and the other a glucose-insensitive polymer. A differential measurement of permittivity induced by the glucose binding on the sensing site with respect to a reference (glucose-unresponsive) was correlated to the glucose concentration. In *in vivo* tests of the MEMS sensors were performed by controlling blood glucose concentrations of mice following glucose and insulin administration. Drawbacks of viscometric and capacitive MEMS is the complicated instrumentation.

Among different transduction mechanisms, those based on **electrochemical** events are the most preferred by the industry to build minimally-sized medical sensors. The main reason lies in their unique advantages: miniaturisation with complete system integration retaining excellent detection limits and sensitivities, rapid signal response, low cost, possibility of microfabrication, low power consumption, simple instrumentation and high selectivity [16]. Many medical instruments (laboratory, transportable and portable) based on electrochemical techniques are present in the market for electrolyte and molecular sensing. A list of portable electrochemical analysers is in Table 1.1.

Table 1.1 – Portable electrochemical analysers.

Instrument	Manufacturer	Analyte
Glucomen Day	Menarini Diagnostics, Florence	glucose
Glucometer Elite	Bayer Corporation, Leverkusen	glucose
Advantage Meter	Roche Diagnostics, Basel	glucose
LifeScan OneTouch	Johnson&Johnson, Brunswick, NJ	glucose
Prestige IQ	Home Diagnostics Inc., Fort Lauderdale FL	glucose
Medisensor 2001	MedTest Systems, College Park, MD	glucose, UA
Excel G	Inverness Medical Technology Inc., Inverness	glucose
i-STAT	Abbott, Illinois, IL	Na ⁺ , K ⁺ , Cl ⁻ Ca ⁺ , glucose lactate

On the other hand, few examples of electrochemical sensors for constant health monitoring are commercially available. Among them, the best-known device is the implantable sensor for glucose monitoring (85% of the entire biosensor market in the world) mainly due to the high biomedical significance of the real-time measurement of blood glucose for patients affected by diabetes [17]. Moreover, several small and large companies are currently exploring low-cost technologies to realise non-invasive tools for continuous biochemical sensing with electrochemical transducers. For instance, Google recently announced a novel project to develop a glucose sensor fully integrated into contact lenses (<http://www.gmanetwork.com/news/story/360331/scitech/technology/google-s-smart-contact-lenses-may-arrive-sooner-than-you-think>) that will be inductively powered from the Google Glass platform thanks to the short distance in-

volved. Similarly, Apple will soon announce iWatch (<http://www.idownloadblog.com/2014/06/21/iwatch-blood-glucose-sensors/>), a device designed to be worn on the wrist for electrochemical sensing of glucose.

Medical devices for "non-stop" health monitoring have drew a great interest also in the academic field in recent years. Among a variety of glucose sensors proposed in the last ten years by researchers, one of the most innovative is that proposed by Piechotta [18]. It is based on a polymeric housing, a microperfusion channel and a Pt *working electrode* (WE) modified with *glucose oxidase* (GOx)/agarose/glutaraldehyde covered by silicon pore membrane for antifouling and diffusion control of glucose. The sensor, tested in interstitial fluid, was linear in the range of clinical interest (0.05-20 mM) and stable for one week. In addition to glucose, electrolytes are other important biomarkers to sense. A recent work reports the use of potentiometric fibres modified with carbon nanotubes and partially coated with an ion-selective membrane for pH, K⁺ and NH₄⁺ detection from sweat in the required physio-pathological range. The sensing elements were embedded in cotton yarns making them insensitive to bending or stretching while tested with simulated sweat solutions [19]. Saliva may be another valid source of diagnostic information. To improve wearability of devices, a sensor could be inserted directly in the mouth of a patient. For instance, Wang *et al.* [20] proposed a sensor based on Prussian-Blue and on a polymer layer to entrap an enzyme for sensing lactate over the physiological range (0.1-0.5 mM). However, the system was never tested for in-mouth measurements. As mentioned very briefly before, sensors integrated within a contact lenses may lead to a new real-time monitoring of glucose and of other important biomarkers. The first attempts of electrochemical glucose sensors in tears were too much invasive (thick-film, miniaturised electrodes [21] or needle type [22]). Among different studies, the most recent and promising solution has been proposed by H. Yao *et al.* [23]. Their device was based on three electrodes (reference electrode, activated GOx on WE and de-activated GOx on a control electrode) integrated with an Au antenna and readout/telecommunication circuitry. The differential mode measurement enabled the elimination of interfering species (ascorbic acid, lactate and urea). The signal halved after 4 days from the sensor preparation and a daily replacement was proposed. Similarly, the same mechanism of detection was then proposed for monitoring lactate [24].

1.2 Electrochemical sensors

The present thesis will focus on sensing devices based on two analytical techniques. Potentiometry will be employed for sensing electrolytes (e.g., K⁺) and voltammetric methods for direct (e.g., bilirubin and uric acid) or enzyme-mediated (e.g., glucose and lactate) detection of metabolites (see Fig. 1.2).

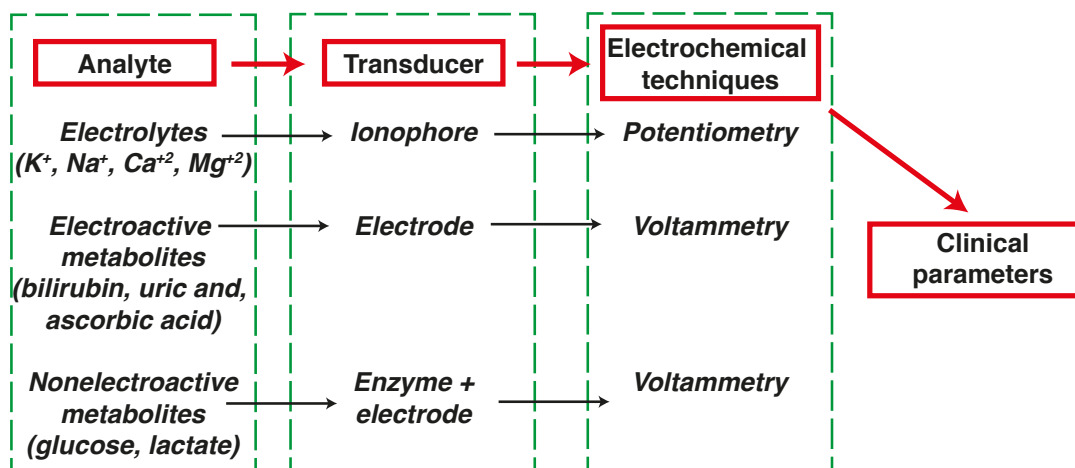


Figure 1.2 – Types of electrochemical sensors for clinical use considered in this research work.

1.2.1 Potentiometric sensors

Ion-selective electrodes (ISEs), that are important sensors for clinical use, are based on potentiometric measurements. K^+ , Na^+ , Ca^{2+} and Mg^{2+} are the most important electrolytes sensed by these classes of electrodes. In many cases, ISEs include a membrane (e.g., glass, inorganic crystal or plasticised polymer).

ISE composition imparts a potential that is associated with the ion of interest *via* a selective binding mechanism. Fig. 1.3 shows an example of potentiometric electrochemical cell including an ISE.

The cell consist of two electrodes: a *working electrode* (WE) that realises the ISE and a *reference electrode* (RE) that must provide a stable potential so that any potential changes in the cell are attributable to the analyte effects on the potential of the WE when zero or negligible current flows between them. Therefore, the cell potential is

$$E_{\text{cell}} = E_{\text{ref}} - E_{\text{ind}} + E_{\text{mem}} + E_j \quad (1.1)$$

Since junction potential (E_j) and the potentials at RE (E_{ref}) and WE (E_{ind}) are constant, any potential variations are due to chemical interactions ion-active sites of the membrane (E_{mem}). Therefore, the potential change is related to the ion activity in a logarithmic manner according to the Nernst equation (25 °C)

$$E_{\text{cell}} = k + (0.05916/z) \log a \quad (1.2)$$

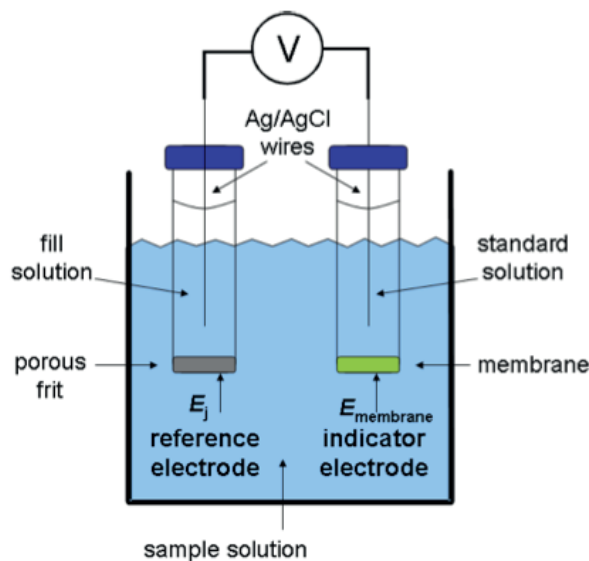


Figure 1.3 – Electrochemical cell for potentiometric measurements with an ISE (indicator electrode). Reprinted from <http://www.asdlib.org/onlineArticles/ecourseware/Welcome.html>.

where k includes all the constant terms in Equation 1.1, z is the charge of the ion of interest and a its activity. The activity (a) of the ion is related to the ion concentration (c) by the following formula $a = cw$ where w is the activity coefficient that can be calculated by the extended Debye-Hückel equation

$$\log w = (-0.51z^2\sqrt{I})/(1 + 3.3d\sqrt{I}) \quad (1.3)$$

where d is the effective diameter of the hydrated ion in nanometers (e.g., 0.3 for K^+), I is the ionic strength of the solution ($I=0.5 \sum_{i=1}^N c_i z_i^2$ where c_i is the concentration of the i ion and z_i is the charge of the i ion) and 0.51 and 3.3 are constants adequate for a water solution at 25 °C. Unfortunately, membranes are not selective towards a single ion and E_{mem} varies as soon as an ion interacts with the active sites of the membrane. Equation (1.1) can be rewritten taking into account the interfering ion (int)

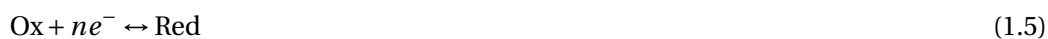
$$E_{cell} = k + (0.05916/z_{ion}) \log(a_{ion} + K_{(ion, int)} z_{ion}/z_{int}) \quad (1.4)$$

where z_{ion} and z_{int} are the charges of the ion of interest and the interfering ion and $K_{(ion, int)}$ is a selectivity coefficient that considers the contribution of the interfering ion to the potential change. More often, microfabricated ISEs use a *poly(vinyl chloride)* (PVC) membrane. The selectivity is given by organic neutral or charged complexing agents (ionophores) that are

included into the PVC membrane.

1.2.2 Voltammetric sensors

Voltammetric techniques have been widely used for quantitative analysis of drugs in biological fluids at concentration below the micromolar range and of metabolites based on enzymatic catalysts (e.g., glucose sensor). The most used configuration for voltammetric measurements is based on three electrodes: a WE, where the electron transfer reaction takes place, a *counter electrode* (CE) that supports the current flow in the cell and a RE, which provides a stable potential with respect to the WE. In response to the potential applied between WE and RE, the current passing the electrolyte from the CE to the WE is measured. It is due to the transfer of electrons during the redox reaction of an electroactive compound at the WE (Fig. 1.4)



where Ox and Red are the oxidised and reduced form of the electroactive compound.

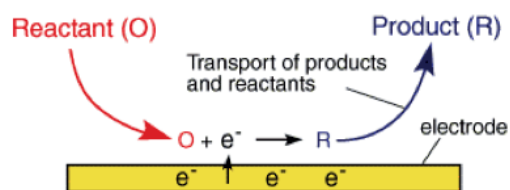


Figure 1.4 – Simple redox reaction at the electrode surface. Reprinted from <http://web.iitd.ac.in/sbasu/ElectrochemistryLectures.pdf>.

The current resulting from the electroreduction or electrooxidation process is called Faradaic current and it is a measure of the rate of the reaction. The rate of the reaction is influenced by two factors: the rate at which electrons pass between the electrode and the reactants and products and the rate at which the reactants and products are transported to and from the electrode (mass transport). There are three modes of mass transport: convection, that relates to the mechanical stirring/flow of the solution, migration, that occurs when charged particles in solution are attracted to or repelled from a charged surface of the electrode, and diffusion when the concentration of the electroactive compound at the electrode surface differs from that in the bulk solution (C_{bulk}). If diffusion is the only significant mode of mass transport, the Faradic current (i) in voltammetric measurements is inversely proportional to the diffusion layer δ (see Fig. 1.5 (a)) that increases with time according to the following equation

$$i = k(C_{\text{bulk}})/\delta \quad (1.6)$$

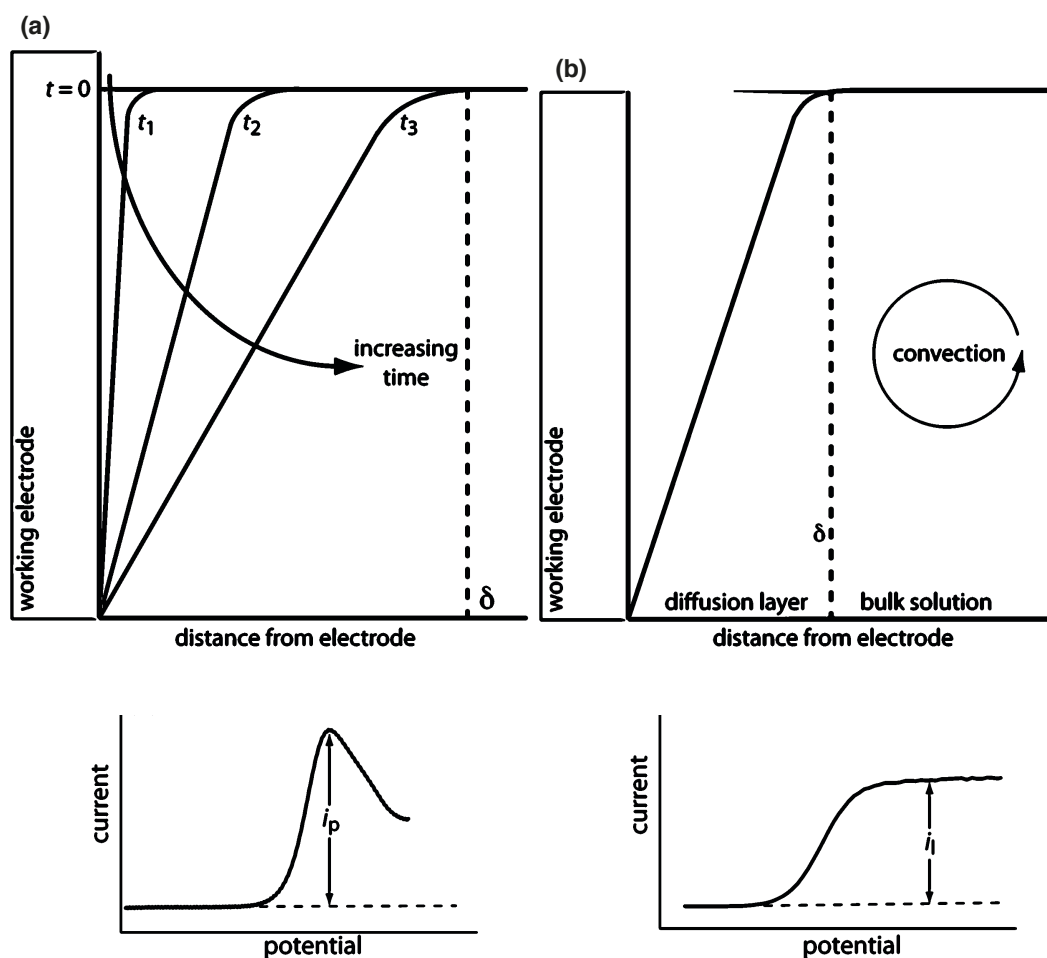


Figure 1.5 – Concentration gradient for a molecule under unstirred (a) and stirred (b) solution and respective voltammogram shapes.

Supporting electrolytes are added to eliminate the migration. If the solution is continuously stirred at the same velocity, δ is constant and a limiting current proportional to the concentration of the compound of interest (see Eq. (1.6)) occurs and the resulting voltammogram shows a limiting current instead of a peak (Fig. 1.5 (b)).

Several potential excitations can be used: *cyclic voltammetry* (CV) (Fig. 1.6), *square wave voltammetry* (SWV) (Fig. 1.7), *differential pulsed voltammetry* (DPV) (Fig. 1.8).

Voltammetry is also particularly attractive to discriminate two or more analytes in the sample (multicomponent analysis - Fig. 1.9).

Chronoamperometry (CA) (Fig. 1.10), is a particular case of voltammetry in which a fixed potential is applied to the WE. Since the potential does not vary, the current-time plot shows a series of steps (steady-state currents) under stirring/flow conditions. The steady-state currents are proportional to the electroactive analyte concentration in the bulk.

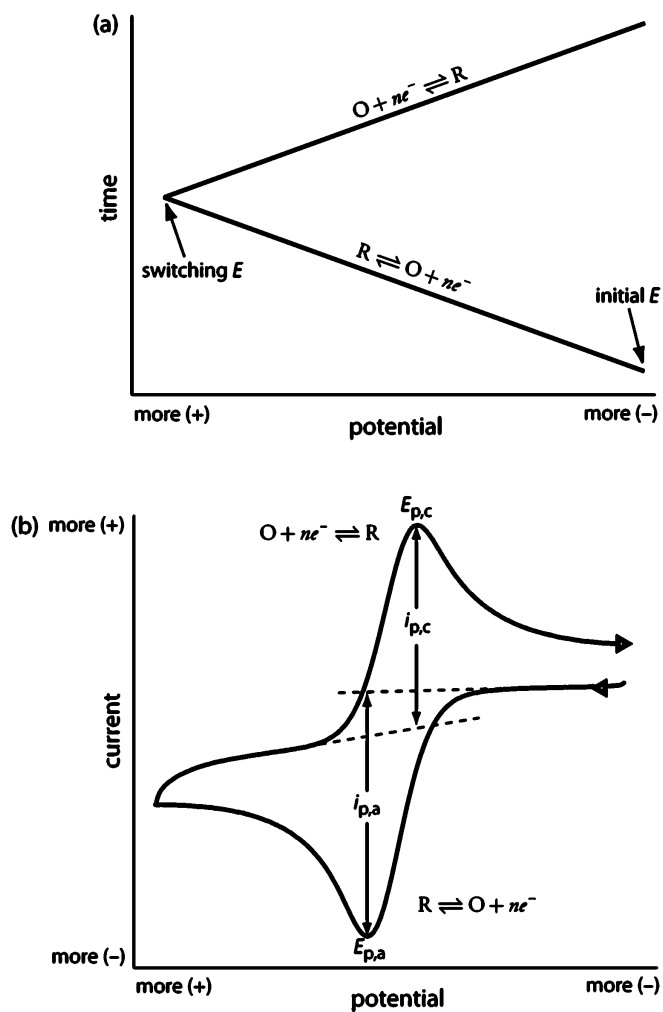


Figure 1.6 – Triangular potential-excitation signal (a) and the resulting cyclic voltammogram showing oxidation and reduction peak currents (b).

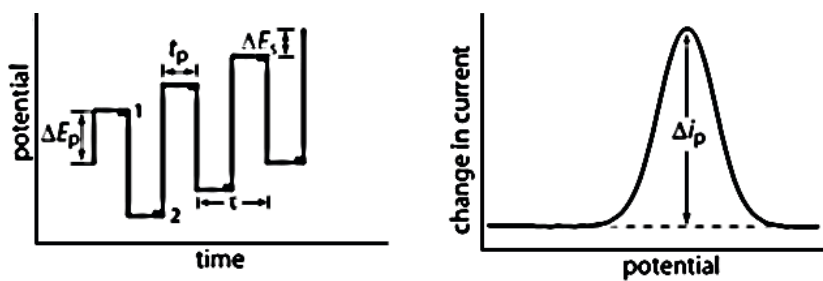


Figure 1.7 – Square wave voltammetry.

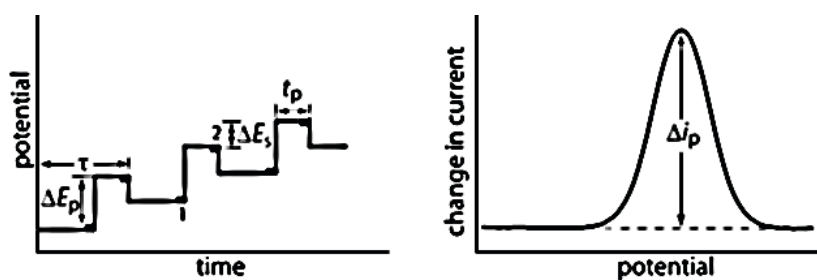


Figure 1.8 – Differential pulsed voltammetry.

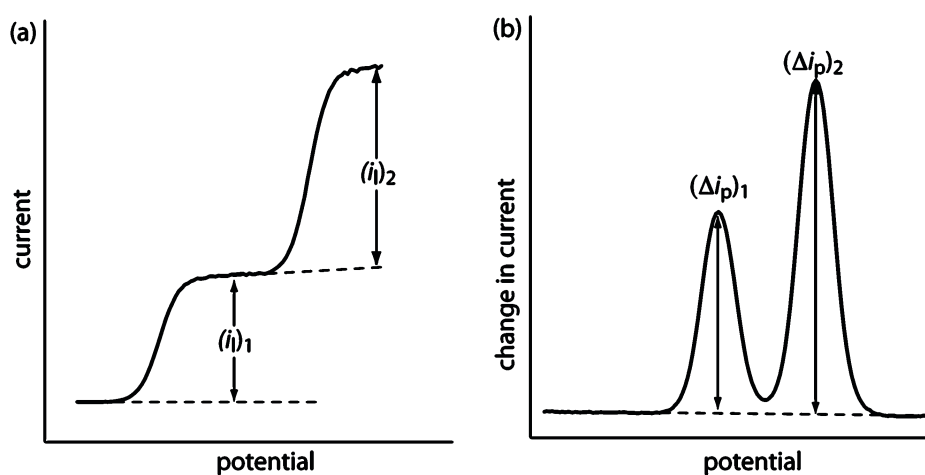


Figure 1.9 – Voltammograms showing two-metabolite detection with limiting currents (a) and peak currents (b).

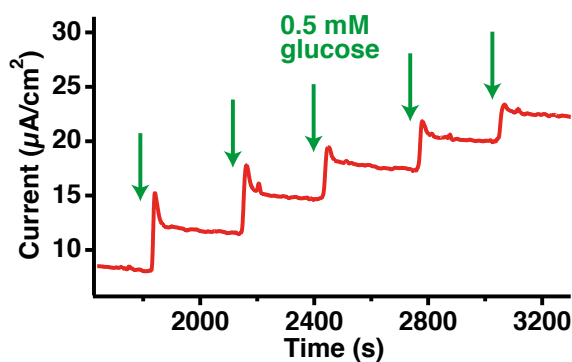


Figure 1.10 – Typical chronoamperometric response of our GOx-carbon nanostructured microfabricated Pt to several injections of glucose.

1.3 Sensor fabrication techniques

An electrochemical medical sensor should be a self-contained integrated system including all the electrodes (one or more than one WE, a RE and a CE) and a potentiostat. In a three-electrode configuration system, the potentiostat is typically an electrical circuit that keeps

constant the voltage between RE and WE while measuring the current passing through the CE and WE. Industrial production of electrochemical platforms can be obtained by both thick- and thin-film technology [25].

Thick-film technology, also called screen printing (Fig. 1.11 (a)), is based on the application of a paste (microparticles of carbon or metal precursors) on a flat surface. The adhesion is assured by a thermal treatment [25]. For instance screen-printed technology has been used to build enzymatic devices for in-mouth analysis [20] as well as "tattoo-electrodes" for monitoring ions and pH [26] and they are commonly used in almost all the glucometers present in the market.

On the other hand, thin-film electrodes (thickness lower than 1 μm) can be obtained by sputtering or evaporation of metals (e.g., Au, Pt) through a mask on a dielectric material such as glass (Fig. 1.11 (b)) and silicon oxide (Fig. 1.11 (c)). By photolithographic and etching processes, integrated electrochemical platforms are structured according to the sensor layout requirements. Minimum structure resolution ranges between 5 and 20 μm [25]. For instance, Liao *et al.* microfabricated a biosensor for glucose detection in tears by a thin-film CMOS (*Complementary Metal-Oxide Semiconductor*) technology which can be easily and conveniently used for large-scale applications.

In this thesis, electrodes prepared by screen printing and by thin-film technologies are employed.

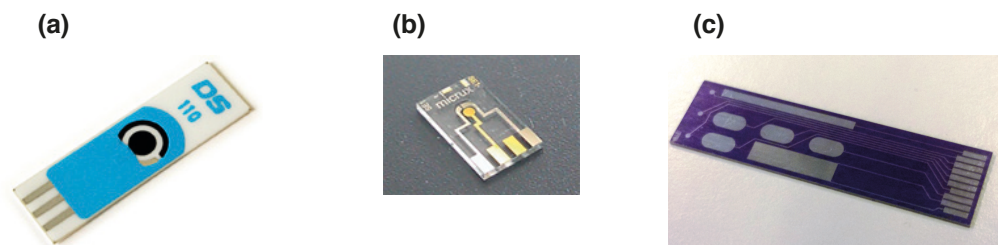


Figure 1.11 – Electrochemical devices prepared by screen printing (a) or by a thin-film technology on glass (b) or on silicon (c).

1.4 Nanostructured electrodes for enhanced detection performance

Section 1.1 explains why electrochemical methods are the most promising technologies for clinical use. However, a continuing challenge in the fabrication of electrochemical devices is still the improvement of the detection performance.

Today, the development of "long-lasting", reliable, ultrahigh-sensitive and selective small medical devices for uninterrupted tracking of vital parameters is helped by the use of nanostructured electrodes. Nanomaterials and nanoporous films have been employed for electro-

1.4. Nanostructured electrodes for enhanced detection performance

chemical sensing and biosensing due to their unique properties such as electrical conductivity, surface-to-volume ratio, structural robustness, catalytic properties, high loading of enzyme if present, excellent stability [27]. A scheme of a variety of nanomaterials employed to improve the electrochemical detection of biomarkers is illustrated in Fig. 1.12.

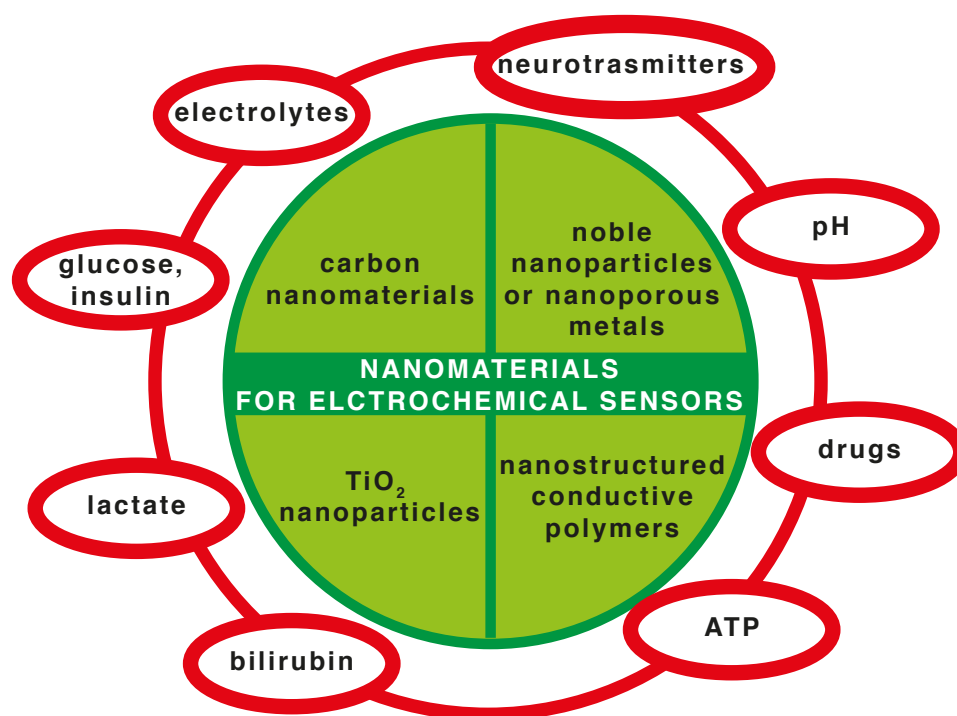


Figure 1.12 – Nanomaterials for voltammetric and potentiometric detection of biomarkers of medical interest.

Carbon nanomaterials moved into the focus of research as interesting materials for the fabrication of electrochemical devices with enhanced sensing parameters. There are different types of carbon nanomaterials (Fig. 1.13 (a) and (b)). *Graphene* [28] is a sheet of sp² planar atoms. Multilayer (2-10) graphene sheets [29] form the so called *graphene platelets*. Thicker multi-layer graphene sheets form *nanographite*. *Single-walled carbon nanotubes* (SWNTs) [30] consist of single graphene sheets that are wrapped into cylindrical tubes with diameters between 0.4 and 2.5 nm. Their high electrical conductivity and small size makes them suitable as individual nanoelectrodes leading to ultrasensitive electrochemical sensors for the detection of biological analytes. *Multi-walled carbon nanotubes* (MWNTs) [31] are rolled cylindrical graphene sheets, having diameters up to 100 nm and lengths ranging from few nanometers to several micrometers. Carbon-nanomaterial modified electrodes have been extensively used as transducers for ion selective sensors based on a PVC-selective membrane, which showed superior performance with respect to sensors having other materials as intermediate layers (e.g., conductive polymers [32]). This class of nanomaterials have also shown the capability to reduce the fouling of enzymes after the protein immobilisation [33] and an improved electron

transfer in electrochemical reactions [34]. Carbon nanomaterials have also exhibited a high response current and a reduced overpotential towards the detection of highly electroactive metabolites as well as a voltammetric discrimination of different electroactive analytes [35].

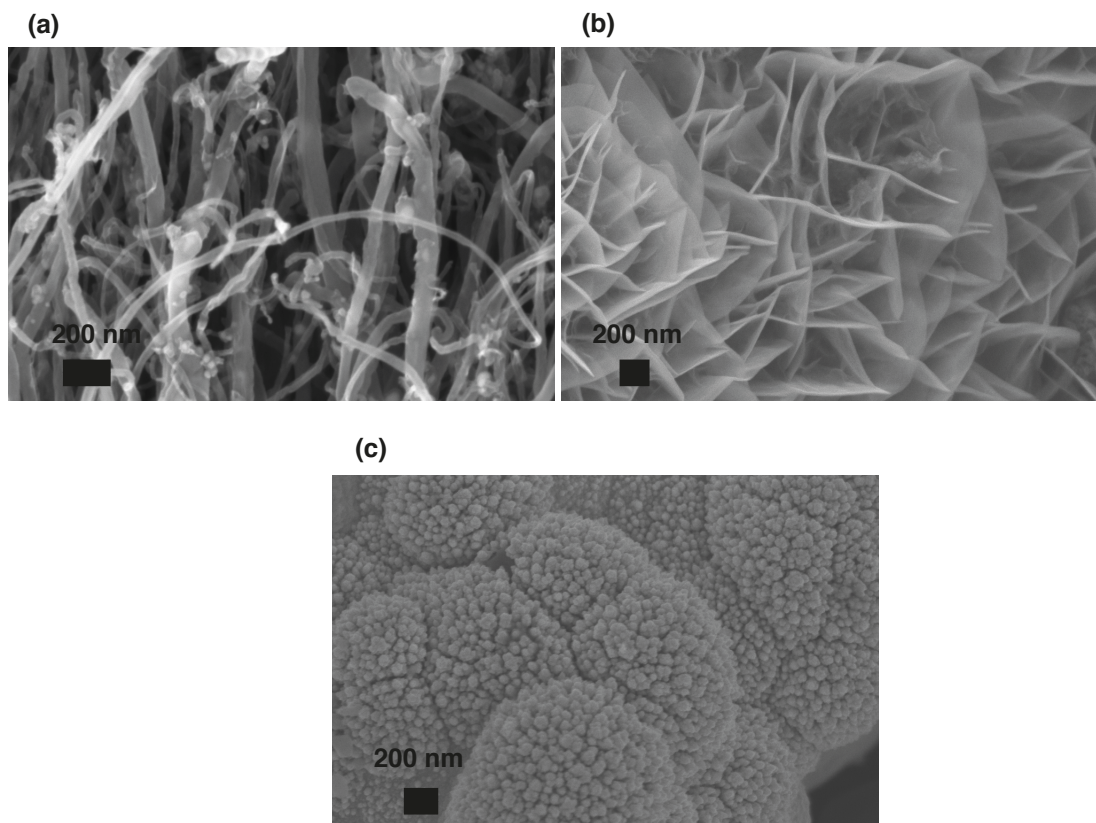


Figure 1.13 – SEM images of MWCNTs (a), graphitic nanopetals (b) and nanoporous Pt (c).

Noble metal nanoparticles (NPs) and *nanoporous films* (Fig. 1.13 (c)) have elicited much interest for important biomedical applications due to their easier production, characterisation and functionalization than carbon nanomaterials. Pt and Au [36] nanostructured electrodes exhibited high catalytic activity especially towards the detection of small molecules (e.g., H_2O_2), a decrease of overvoltage that could be advantageous to solve in such an extent issues related to interferences [37]. The direct electrochemical oxidation of glucose on Pt and Au nanostructured surfaces in a neutral phosphate buffer solution makes these electrodic materials promising substitutes of enzyme-based sensing sites. Nanoporous Pt [38] and Au NPs [39] have been also used to build highly stable potentiometric sensors for detecting pH [38] and ions [39].

Titanium dioxide nanotubes (TiO_2 NTs) have obtained significant research interest due to their ease of preparation by electrochemical anodization of Ti in fluoride-based solutions, high orientation and uniformity, large surface area and good biocompatibility. Therefore, TiO_2 NTs are very promising for the immobilisation of enzyme [40] as well as for other biosensing applications.

1.5. Research contributions and outline of the thesis

Conducting polymer (CP) nanostructures [41] have received an increasing attention as sensing material for ultrasensitive detection because of their chemically tuneable conductivity, high flexibility and easy manipulation. The high surface area favours high enzyme loading so a high sensitive detection. In particular, nanomaterials of polyaniline have a large surface area allowing fast diffusion of gas molecules into the structure. The preparation methods of CP nanofibres follow a chemical route (chemical polymerisation of aniline or polypyrrole nanofibers synthesised in presence of p-hydroxy-azobenzene sulphonic acid). Nanostructured CPs can be prepared by template or non-template methods and seeding approaches. Aluminium oxide or zeolite with channels and polymer porous membranes are used as templates. Electrochemical polymerisation, electrospinning and mechanical stretching are the most commonly used template-free approaches. In recent years, CP nanomaterials-metal NPs hybrids have attracted considerable interest for their high catalytic properties.

It is worth mentioning that the type of nanomaterials or their combination [41] should be selected by looking at the final application from the beginning. Interestingly, nanomaterials confer specificity for sensing a metabolite. Carbon [35, 42] and CP [43] nanomaterials permit to discriminate the voltammetric peak of a molecule of interest from those related to interfering species. Metal NPs or nanoporous films [44] are typically silent towards the detection of highly electroactive interfering species.

Last but not least, the development of tailored integration methods to nanostructure electrodes is quite challenging. Many times nanointegration methods are scarcely reproducible, require long preparation and expensive instrumentation and include the use of binders that can hinder the unique advantages of having "nanocomponents" onto the electrode surfaces. The stability of the nanostructures onto the electrode is another important issue to be considered.

1.5 Research contributions and outline of the thesis

A rapid monitoring of a set of biomarkers in human fluids is of significant importance in medicine. In principle, systems designed for a timely multisensing should be able to do several measurements from a small volume and undiluted sample without losing their performance. To this end, electrochemical devices are particularly advantageous because of the inexpensive and reproducible fabrication procedures, the ease of miniaturisation and the simplicity of the measurements. A continuing challenge in the field of electrochemical medical sensors is the reproducible detection of organic molecules and ions in the physio-pathological concentration range, avoiding problems of interferences. Nanostructured electrodes could be useful tools to solve the mentioned issues.

By keeping this in mind, this research work aims to design novel nanostructured electrodes and to validate their electrochemical performance by sensing electrolytes and metabolites of medical interest. In particular, the main contributions are the following.

- Demonstration of the improved detection of screen-printed sensors based on nanomaterials. MWCNT-screen printed electrodes were employed to detect low concentrations of electroactive compounds with sensing performance enhanced of orders of magnitudes with respect to the bare electrodes. MWCNT-screen printed electrodes were also proved to be a robust platform for the immobilisation of enzymes resulting in catalytic-based biosensors with excellent time-stability, sensitivities and limit of detection.
- Development of a new protocol to integrate a wide range of carbon nanomaterials exclusively onto the WEs of a multisensing device by a direct growth. A Si-based device was microfabricated by employing ordinary thin-film CMOS processes. Selective high yield growths were obtained down to 450 °C, the upper limit temperature for most of the CMOS processes. Thanks to the particular affinity between enzymes and carbon nanomaterials, the nanostructured electrodes were used to build highly sensitive glucose sensors. The capability to detect low concentration of electroactive biomarkers and to discriminate them from interfering biocompounds was also proven by using voltammetric techniques.
- Development of simple and fast template-free electrodeposition methods to produce differently-shaped Pt and Au-Pt nanostructures on electrochemical devices. Devices fabricated by both screen printing and CMOS technology were employed. The nanostructured films were tested for enzymatic detection of glucose at potentials considerable lower than those present in the literature as well as for non-enzymatic glucose sensing.
- While carbon nanomaterials have been extensively used to build highly stable potentiometric ion sensors, in this work, Pt nanostructured films have been successfully applied for the first time as intermediate layers of solid-contact ion-selective electrodes. The sensors were also validated for continuous monitoring of acute cell death by tracking K⁺ levels.

Taking into account this preamble, the thesis is organised in the following way.

Chapter 2 reviews the strategies for nanostructuring electrodes with carbon nanomaterials and nanoporous Pt (nanoPt). The respective catalytic properties towards the detection of ions and metabolites (electroactive and not) are listed.

Chapter 3 describes a new protocol to directly and selectively grow a wide range of carbon nanomaterials (MWCNTs, flower-shaped nanographene, nanographite) onto Pt WEs of a device microfabricated on silicon. Electrodeposition is selected as a very versatile method to efficiently deposit the catalyst onto Pt electrodes in the form of nanoparticles as well as layers with controlled thickness. Then, the integration of carbon nanomaterials onto the electrodes is achieved *via a chemical vapour deposition* (CVD) process. The growth method is optimised to obtain carbon nanomaterials down to 450 °C, the upper limit temperature compatible with the most common CMOS processes, opening the possibility of a direct integration carbon nanostructures/front-end CMOS data acquisition circuit.

1.5. Research contributions and outline of the thesis

Chapter 4 demonstrates the enhanced sensing and biosensing performance of carbon nanostructures used to modify electrodes. Then, this chapter reports the electrochemical measurements of metabolites by using CVD grown carbon nanostructured electrodes. First of all, their excellent sensing performance is proven by detecting low concentration levels of a highly electroactive metabolite independently from interferences. Finally, CVD carbon nanostructured electrodes are proven to be an excellent platform of enzyme immobilisation with excellent biosensing capabilities.

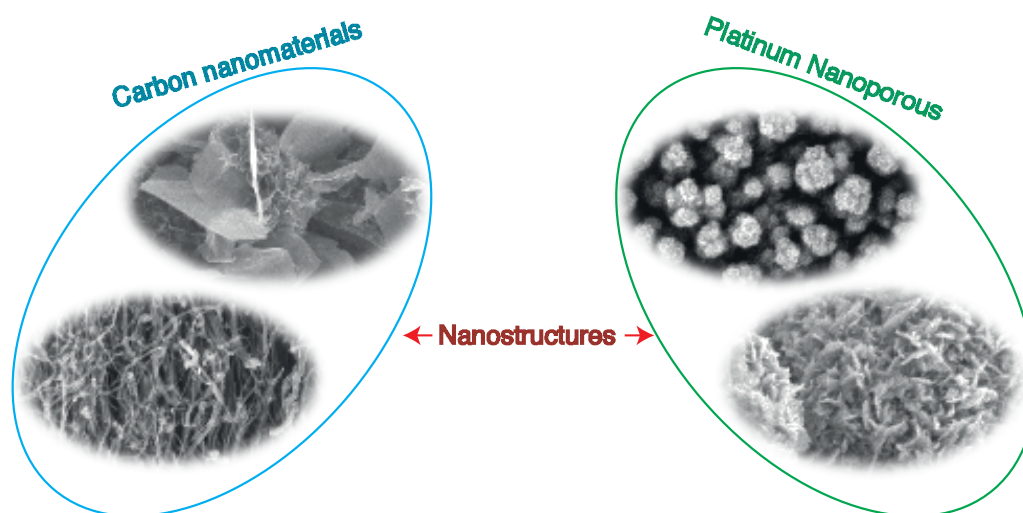
Chapter 5 introduces a novel template-free electrochemical method to produce Pt nanostructured films. By changing the electrodeposition parameters and the type of Pt precursor, differently shaped and sized Pt nanostructures are obtained. Considering the promising catalytic properties of Pt coupled with Au, procedures to obtain bimetallic- and alloy-based nanostructured electrodes are also explained.

In Chapter 6, the electrochemical properties of differently shaped and sized Pt nanostructured films are shown towards the detection of glucose with and without an incorporated enzyme. Then, the catalytic properties of Au-Pt nanostructures are also tested for glucose sensing and biosensing.

In Chapter 7, Pt nanostructured electrodes are used as solid contacts of K^+ selective electrodes. The electrodes are characterised in a buffer solution within the physiological concentration range of K^+ first. Then, the platform containing the ion selective electrode is coupled with a fluidic system and the possibility to use the modified electrode for continuous acute cell death monitoring in incubator is demonstrated. To this aim, the measured K^+ cell efflux is correlated with the cell viability. An efficient procedure to miniaturise the RE is also explored with a view to a fully integrated system for potentiometric measurements.

Finally, Chapter 8 concludes the thesis. A summary of the achievements obtained by exploring the electrochemical properties of the CVD grown carbon nanomaterials and template-free electrodeposited Pt and Au-Pt nanostructures is presented. Considering the accomplished objectives, some perspectives on what should be done in the future are provided.

2 Nanostructured electrodes for electrochemical medical sensors



The unique potentialities of electrochemical nanostructured sensors and biosensors to advantage diagnosis, continuous monitoring of health conditions and treatment of diseases have been listed in Chapter 1.

The aim of the present chapter is to provide an overview of two ways to nanostructure electrochemical sensors.

Section 2.1 is dedicated to carbon nanomaterials. In Subsection 2.1.1 the electrochemical properties of carbon materials and nanomaterials are reviewed. Subsection 2.1.2 describes the principal methods to confine carbon nanostructures onto electrode surfaces. A list of advantages for sensing highly electroactive metabolites is provided in Subsection 2.1.3 and then Subsection 2.1.4 highlights the impact of using carbon nanomaterials for biodetection.

Chapter 2. Nanostructured electrodes for electrochemical medical sensors

The focus of Section 2.2 is on Pt nanoporous. Subsection 2.2.1 explains the catalytic properties of this class of nanostructured electrodes. The state-of-the-art of the Pt nanostructuring protocols is presented in Subsection 2.2.2. Section 2.2 provides some examples of electrochemical sensing and biosensing using Pt nanoporous-coated electrodes (Subsections 2.2.3 and 2.2.4).

Section 2.3 explains the advantages to combine Pt nanostructures with those made of other materials (carbon or other metals).

Finally, the benefits of using either carbon and Pt nanostructures as solid contacts of ion selective electrodes conclude the chapter (Section 2.4).

2.1 Carbon nanostructured electrodes

2.1.1 Electrochemical properties

Carbon-based electrodes exhibit unique electrochemical advantages as the wide potential window, the resistance to surface fouling and the considerable enhancement of the sensing response towards the detection of many analytes (especially highly electroactive biological molecules) with respect to noble metals. It has been established that the origin of the electron transfer for *highly ordered pyrolytic graphite* (HOPG) comes from edge-plane-like sites and defects. Indeed, the basal planes are electrochemically inert. Similar considerations have been extended to carbon nanomaterials (CNTs, graphene nanosheets, nanographite; Fig 2.1). All these materials show an anisotropic electron transfer. Their peripheral ends exhibit an electrochemical behaviour similar to the edge-plane-like sites/defects of HOPG. On the other hand, a slow electron transfer characterises CNT sidewalls, graphene sides, graphite basal planes electrochemically resembling the HOPG basal planes. In our previous work, the sensitivity towards the detection of $[\text{Fe}(\text{CN})_6]^{3+/2+}$ at vertically-aligned MWCNTs, exposing edge-plane-like sites of their tips to the solution, was more than four-fold higher than that at randomly-oriented MWCNTs with exposed sidewalls to the solution [45].

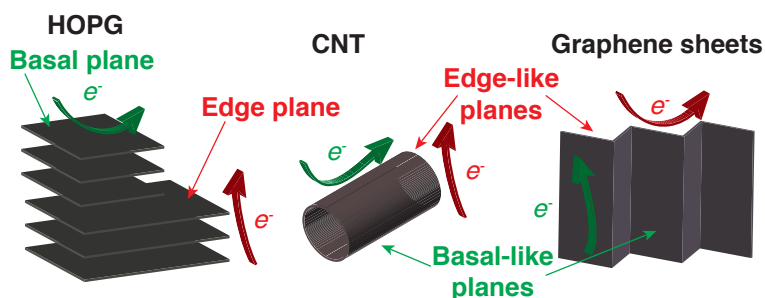


Figure 2.1 – Structure of HOPG, CNT and graphene sheets. The edge-plane-like sites determine the fast electron transfer rate at carbon materials and nanomaterials.

Carbon is prone to react with oxygen and water resulting in a negatively-charged surface that can have possible effects on adsorption of analytes and consequently on their electron

transfer kinetics and electrocatalysis. Therefore, pretreatments of carbon influence the final electrochemical properties towards the detection of a certain analyte. Reactivity differences of carbon surfaces strongly depend on the amount of edge plane-like sites and functional groups and on the redox system involved. Fig. 2.2 shows a classification of redox systems in categories according to their kinetic sensitivity to a particular surface modification of carbon materials and nanomaterials [46].

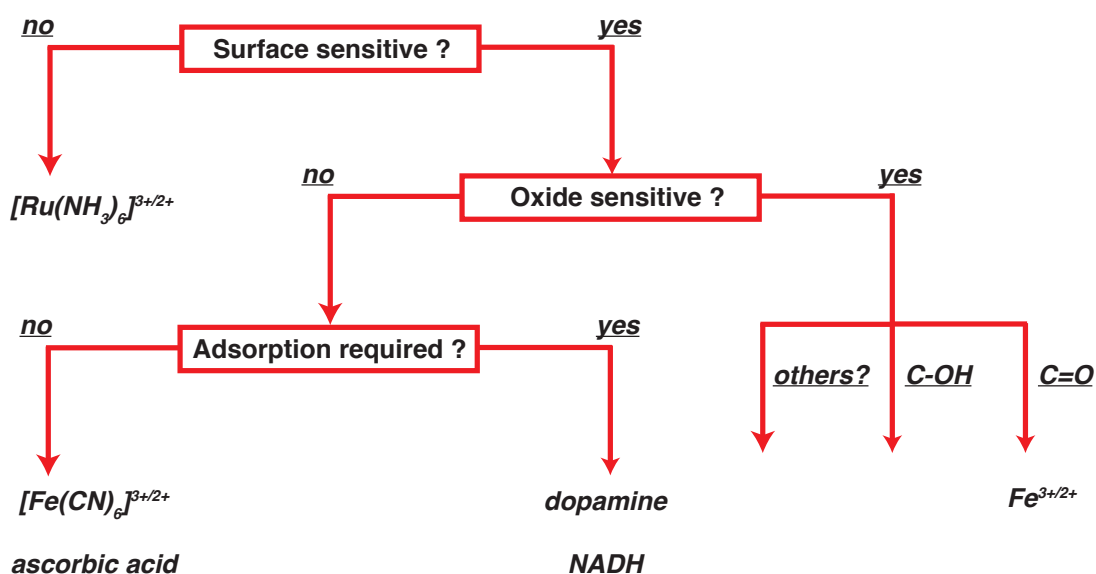


Figure 2.2 – Scheme for determining how carbon surface characteristics influence the electron transfer kinetics of redox systems [46].

2.1.2 Integration approaches

The electrochemical response of electrodes based on carbon nanomaterials strongly depends on the type of material incorporated (pristine or treated, oriented or not, SWCNTs or MWCNTs, multi- or single-layer graphene) and on their incorporation methods.

Carbon nanomaterials are commonly integrated onto electrodes by three methods (Fig. 2.3):

- adsorption onto electrodes with or without a polymer (casting)
- electrochemical methods (electropolymerization of a polymer incorporating CNTs, electrodeposition of graphene, anodic oxidation or cathodic reduction of graphite to obtain graphene flakes)
- direct growth (with or without a transfer) onto the desired electrode surface

The following paragraphs provide an explanation and the state-of-the-art of each electrode nanostructuring approach with carbon nanomaterials.

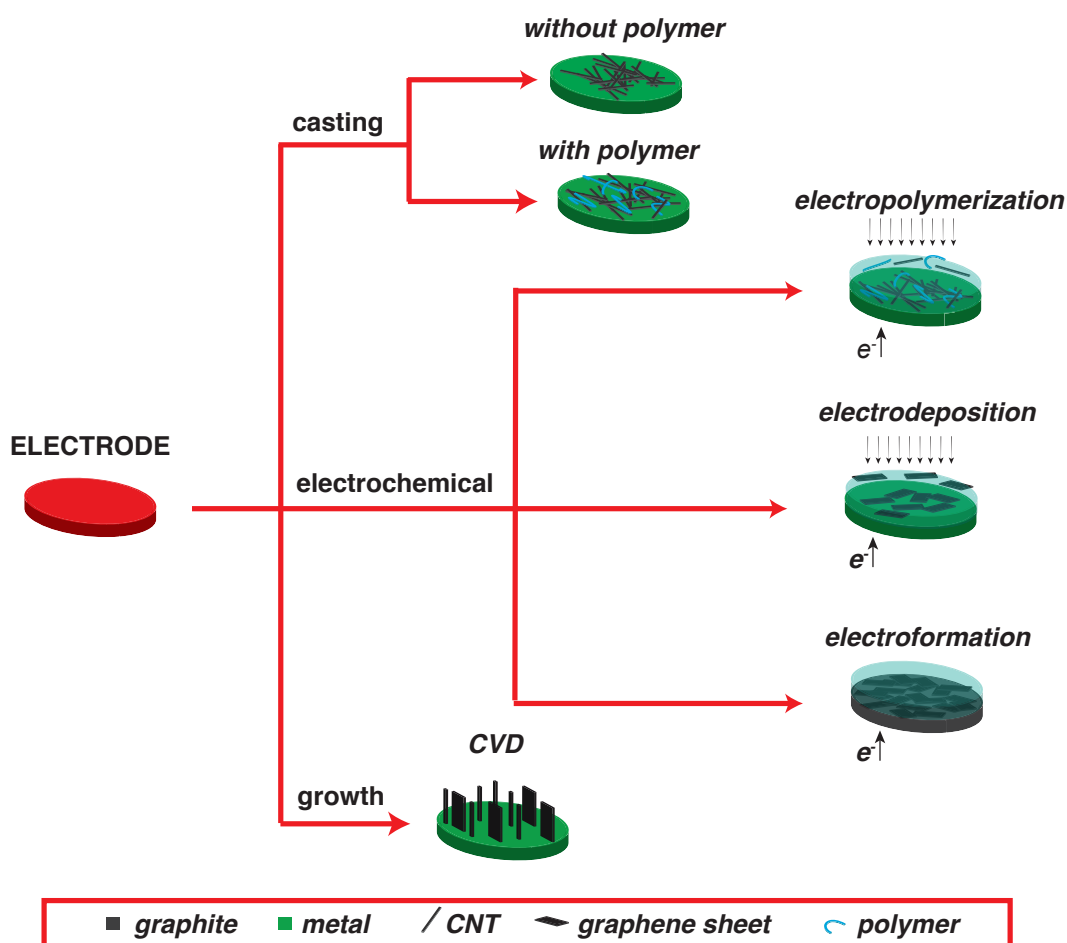


Figure 2.3 – Electrode modification methods with carbon nanomaterials.

Casting One of the major obstacles to apply carbon nanomaterials for electrochemical sensors is the difficulty to handle them. Their characteristic insolubility in almost all the solvents reduces the possibility to form stable and homogeneous films. To overcome this problem, carbon nanomaterials are functionalized with hydrophilic groups first and then dispersed in a solvent with the help of a long-lasting sonication step. Then, a certain amount of the resulted dispersion is cast onto electrodes and is allowed to dry. To this end, many solvents can be used: ethylene glycol [47], ethanol [48], water [49] and N,N-dimethylformamide [30]. Additive-assisted dispersions are also employed to further improve solubility and stability of the nanostructures. For example, Nafion has been extensively used because of its ion exchange, amphiphile structure and biocompatibility properties [50]. The biopolymer Chitosan is also employed because of its excellent film-forming, water permeability, good adhesion and facile surface modification [51]. The employment of surfactants [52], ion liquids [53], and other polymers [43] has been widely reported. The predominance of this nanostructuration method is due to the simplicity despite reproducibility and film stability are very poor.

Electrochemical methods Considering the high demand of miniaturised medical devices, the confining of carbon nanomaterials onto micro-sized electrodes is of urgent importance. Casting approaches are not suitable for a selective nanostructuring because they often result in short-circuits of several electrodes present in the platform. Some authors have already reported the use of the casting technique to nanostructure microelectrodes with a microspotter [54]. However, a precise and automatic positioning of the micro-syringe is challenging and time consuming. A good alternative strategy to prepare nanostructured microelectrodes is the use of electrochemical methods. For CNTs-based sensors, the electrode modification can be easily conducted by an electrochemical polymerisation. Monomers and CNTs are placed in dispersion. By applying a fixed potential, the hydrogen ions located at the electrode interface are reduced to hydrogen and the pH near the electrode surface increases. At high pH monomers (usually Chitosan) become insoluble and polymerise at the electrode entrapping CNTs as dopants [55]. Chen deposited graphene nanosheets through cyclic voltammetric reduction of a graphene oxide colloidal solution and without the use of any binder [56]. Other electrochemical methods used to prepare only nanographene flakes involve the application of cathodic or anodic potentials or currents in aqueous or non-aqueous solutions [57]. However, electroformation is exclusively limited to graphite electrodes.

Direct growth Carbon nanomaterials can be closely coupled with the substrate by directly growing them by *chemical vapour deposition* (CVD) processes. The sensing properties of the as-produced carbon nanomaterials can be tested either directly or after a transfer onto another substrate. Gao [58] prepared aligned MWCNTs on quartz by CVD. Then, a thin gold layer was sputtered onto the tubes followed by a separation of the gold-nanotube electrode from the quartz substrate with an aqueous solution of hydrogen fluoride. The constructed electrode was employed for the indirect detection of glucose. Similarly, Wang and co-workers [59] transferred carbon nanosheets grown on Si to a glassy carbon electrode for sensing *nicotinamide adenine dinucleotide* (NADH). Unfortunately, the transfer of CVD carbon nanomaterials is affected by a loss of nanostructures that reduces the reproducibility of this modification protocol. Moreover, nanomaterials can easily collapse, losing their original orientation.

Avoiding the transfer of CVD grown carbon nanomaterials entails an easy, fast and reproducible integration method. Detection and biodetection properties of CNTs grown onto insulating materials have been extensively studied [60, 61, 62]. Fig. 2.4 shows an example of voltammetric detection of an electroactive drug at MWCNTs grown on Si wafer [61].

More challenging is the CNT synthesis onto metal electrodes. The growth of CNTs on metals requires a pre-deposition of catalyst. The elevated temperatures may activate the diffusion of the catalyst into the substrate inhibiting its activity. To overcome this problem, authors generally utilise thin buffer layers to stop the alloying between the catalyst and the underlayer conductive substrate (e.g., Al [63], silicon oxide [64]). Furthermore, for a selective CNT synthesis onto WEs, also the problem of the spontaneous CNT growth onto insulating materials should be solved. Some authors have reported CNT selective growths onto metal plates with-

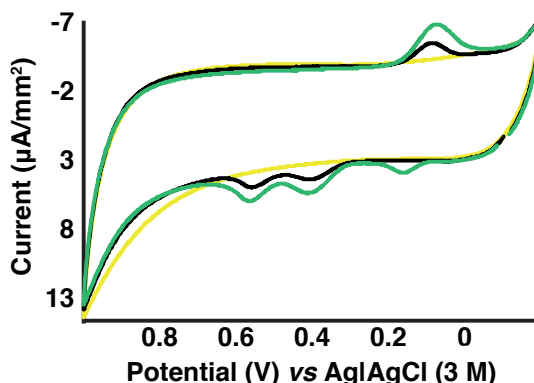


Figure 2.4 – Cyclic voltammograms in solutions containing 0 (yellow), 100 (black) and 200 µM (green) etoposide, an anti-cancer drug, at MWCNTs directly grown on Si wafer.

out the use of buffer layers. Zheng [35] used MWCNTs grown on Ta from a thin Co catalyst film to detect electroactive metabolites. Tominaga [34] successfully synthesised CNTs onto Pt plates by CVD using Fe nanoparticles derived from ferritin molecules. They tested CNTs for an enzymatic determination of D-fructose. Lin [65] firstly reported a growth of aligned CNTs onto chromium-coated silicon substrate. Then, an oxidase was immobilised onto the broken CNT tips to detect glucose.

On the other hand, CVD synthesis of graphene is commonly realised on metals as Ni and Cu. For instance, Brownson [28] studied the electrochemical properties of commercial graphene grown by CVD on Ni towards the detection of various biological analytes.

Commonly used nanostructuring techniques, namely casting and electrochemical methods, suffer from disadvantages as low reproducibility and uncontrollability of the nanomaterial orientation. The preparation of a dispersion, that is very often a mandatory step, makes the before-mentioned approaches time-costly and poorly reproducible. Moreover, these integration methods often employ some binders that inevitably compromise the sensing performance and the stability of the nanostructuring over time. In particular, drop casting approaches are hardly-scalable. A very promising method to nanostructure electrodes is the direct growth. It allows us to obtain uniform film as well as a selective nanostructuring. A CVD synthesis reduces the fabrication steps and benefits from a high reproducibility making it ideal for industrialisation and large-scale production.

Table 2.1 illustrates advantages and disadvantages for each method to integrate carbon nano-materials on electrodes. Note that transfer-free CVD is highlighted as the most promising, although challenging, method to nanostructure electrodes of miniaturised devices.

Table 2.1 – Advantages and disadvantages of different integration methods of carbon nanomaterials onto electrochemical electrodes. Very good choice: (++); Good choice: (+); Not good choice: (-).

CHARACTERISTICS\METHOD	Casting	Electropolymerisation	Electrodeposition	Electroformation	CVD with transfer	Transfer-free CVD
Reproducibility	(-)	(-)	(-)	(++)	(-)	(++)
Large-scale application	(-)	(-)	(-)	(-)	(-)	(++)
Applicability to electrode materials	(++)	(++)	(++)	(-)	(++)	challenging
Binder	(-)	(-)	(++)	(++)	(++)	(++)
Technical effort/costs	(++)	(++)	(++)	(++)	(-)	(-)
Time-consumption	(-)	(-)	(-)	(++)	(+)	(++)
Integration on CMOS devices	(++)	(++)	(++)	(-)	(++)	challenging
Micro-scale applications	(-)	(++)	(++)	(++)	(-)	challenging
Control of orientation	(-)	(-)	(-)	(-)	(+)	(++)
Applicability to all carbon nanomaterials	(++)	(++)	(-)	(-)	(++)	(++)

2.1.3 Direct detection

Carbon nanomaterials provide a very high ratio edge sites/carboxylic groups to basal sites resulting in amplified electrochemical responses towards the oxidation of many electroactive metabolites. Physiological concentrations of biocompounds are often very low (nanomolar range) so the use of carbon nanomaterials favours their direct electrochemical sensing within suitable concentration ranges. Catecholamines, such as dopamine, epinephrine, norepinephrine and serotonin, require an accurate quantitative detection since some mental disorders are due to the change of their concentrations. High electrocatalytic activity of carbon nanomaterials towards catecholamines [43], favoured by adsorption mechanisms [35] (Fig. 2.5), has been widely reported. MWCNTs permit the direct oxidation of insulin, another electroactive metabolite of clinical interest because of its central role in diabetes [66]. Many drugs [67] are also easily electrochemically detectable at carbon nanomaterials. MWCNTs and graphene exhibit good electrocatalytic properties for the oxidation of *uric acid* (UA) and *ascorbic acid* (AA), two electroactive metabolites normally present in biological fluids [53, 35, 28]. The intermolecular CH-O interactions decrease the overvoltages of certain metabolites rather than of others contributing to the discrimination of different voltammetric peaks [42].

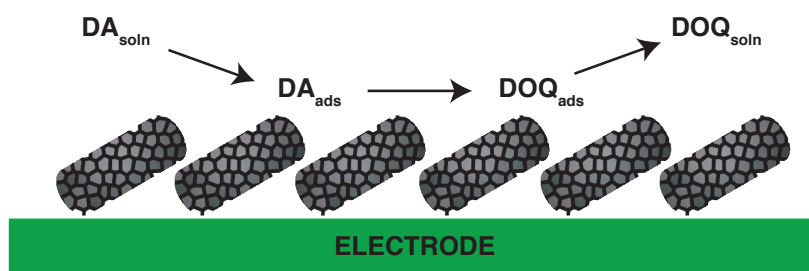


Figure 2.5 – Scheme for the *dopamine* (DA) adsorption-dependent electron transfer at carbon nanostructured electrodes. The mechanism requires an adsorption of DA/electron transfer/desorption of *dopamine-o-quinone* (DOQ).

CNT- [31] and graphene-based [29] sensors are also used for the direct detection of glucose which reaction is very sluggish. However, by using such a kind of nanomaterials, the detection has been performed in alkaline [31] or acid [31] solutions that is not directly applicable for blood and any other human fluids.

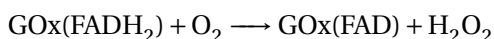
2.1.4 Enzyme-mediated detection

In Subsection 2.1.3, the determination of molecules amenable to a direct electrochemical detection is discussed. Unfortunately, many metabolites are not electroactive at suitable redox voltages. To sense them, specific enzymes are often incorporated into the electrode, thus realising enzymatic biosensors.

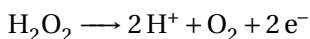
Enzymatic biosensors are divided into three categories:

1. the first generation that is based on the indirect detection of H₂O₂ or O₂, both molecules involved in the enzymatic reactions
2. the second generation that is based on the use of an electron transfer mediator
3. and the third generation that is grounded on the direct electron transfer proteins-electrode substrate.

This thesis will focus only on first generation biosensors *via* H₂O₂ electrooxidation since it occurs at positive potentials and is not subjected to the interference of O₂ reduction. This thesis will study how the presence of nanostructures influences the performance of such biosensors. In the presence of O₂ and of a molecule (e.g., glucose) to detect, the reaction mechanisms of an oxidase (e.g., *glucose oxidase* - GOx) follow the pathways below



Then, H₂O₂ is sensed by applying a suitable potential that oxidises H₂O₂ according to the following reaction



Unfortunately, the electrochemical oxidation of H₂O₂ at carbon electrodes is kinetically slow and the measurements tend to be irreproducible. Moreover, a high overpotential is required to detect H₂O₂ resulting in problems of interferences. Strategies to decrease the overpotential of H₂O₂ oxidation and reduce the irreproducibility include pretreatment protocols [68] or modification of electrode surfaces with redox mediators [69].

Carbon nanomaterials have been largely employed to build more stable and more reproducible first generation biosensors based on oxidases than using other carbon materials. This is due to the fact that they represent a good platform for the immobilisation of proteins and preserve the protein structure and bioactivity. The amount of enzyme that can be effectively immobilised on an electrode strongly depends on the capability of the electrode to "entrap" the protein. All the nanomaterials have the property to stabilise the enzyme better than flat electrodes [70]. In particular, the non-covalent attachment represents the most promising immobilisation technique since it preserves the conformational structure of the enzyme and ensures a high enzymatic loading. This type of immobilisation technique is applicable particularly on carbon nanomaterials thanks to hydrophobic, electrostatic and hydrogen bonding interactions between enzymes and carbon nanostructures [33].

Many research works ascribe the improved electrocatalysis of H_2O_2 at carbon nanostructures also to their intrinsic electrocatalytic activity [71]. In a recent publication, Compton *et al.* demonstrated that the improved oxidation of H_2O_2 reported at MWCNT-based electrodes is mainly due to the iron oxide nanoparticles arising from the CVD synthesis. This phenomenon is not well-understood yet since other studies have shown that the oxidation of H_2O_2 is favoured at carbon nanomaterials showing a large amount of edge-plane-like sites with oxygen functional groups [72]. Fig. 2.6 shows the decrease of the current response when the applied potential diminishes in sensing H_2O_2 at our CVD carbon nanostructured electrodes. This result shows that no decrease of the optimal detection potential arises by the use of carbon nanomaterials for the oxidation of H_2O_2 .

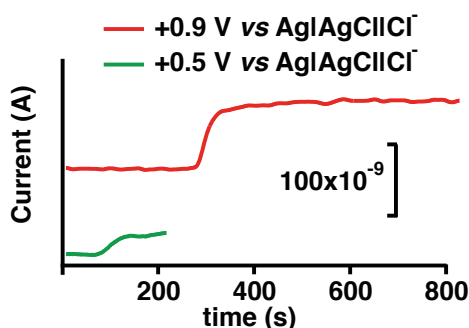


Figure 2.6 – Decrease of the current response in chronoamperometry when the applied potential diminishes from +0.9 V down to +0.5 V in sensing 50 μM H_2O_2 (10 mM *phosphate-buffered saline*-PBS, pH 7.4).

Without doubts, there are nanomaterials that are more suitable for H_2O_2 electrooxidation than carbon nanomaterials. Indeed, it is not by chance that decorating carbon nanostructures with metal nanoparticles (e.g., Au [73], Pt [74, 75, 76]) has been a common practice to increase the performance of first generation biosensors.

2.2 Nanoporous Pt electrodes

2.2.1 Catalysis

The development of electrodes based on Pt nanoporous (nanoPt) has raised large attention due to their high surface area and excellent electrocatalytic activity towards molecules that are generally not sensitive to carbon nanomaterials. The principal reactions promoted at Pt nanopores are the oxidation of hydrogen and small organic compounds (methanol [77, 78], ethanol [79, 80, 81], formic acid [79]) and the reduction of oxygen [82]. The signal amplification at Pt nanoporous films depends on the types of reactions.

Electrooxidations of several interfering electroactive species (AA, UA, drugs) are diffusion-controlled reactions and are particularly enhanced at carbon nanostructured electrodes. In diffusion-controlled reactions and by using metal nanoporous electrodes, the electron transfer is so fast that the reactions occur at the mouths of the pores (red Fig. 2.7 (a) on the right). Therefore, Faradic currents of fast redox reactions are proportional to the electrode area corresponding to the mouths of the pores that is smaller than the geometric area of the electrode (red Fig. 2.7 (a) on the left). On the other hand, highly porous electrodes favours kinetically-controlled sluggish reactions that take place on the entire nanopores (red Fig. 2.7 (b) on the right). In this case, the electrochemical signal is also influenced by the longer residence time of the analytes in the pores that increases the possibilities of collision with the electrode than using flat metal surfaces (red Fig. 2.7 (a) on the left) [83].

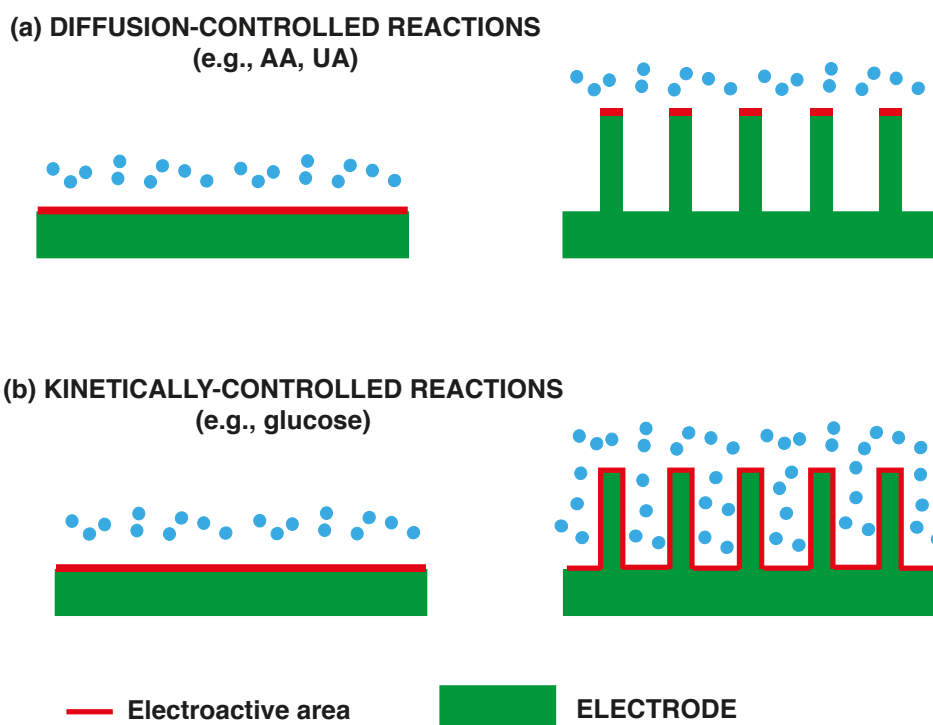


Figure 2.7 – Representation of the effect of Pt nanoporous on electrochemical diffusion-controlled (a) and kinetically-controlled (b) reactions.

It is worth mentioning that if the pore diameter is comparable to or bigger than the thickness of the electric double layer, which increases when the ionic strength in solution decreases [78], the electrochemically active area of the nanoporous electrode may be smaller than the real surface area. Considering the most common electrolyte concentrations, the critical pores are of few nm in diameter.

2.2.2 Fabrication methods

In this subsection, the principal techniques to fabricate nanoPt electrodes are described. These fabrication methods are summarised in Fig. 2.8.

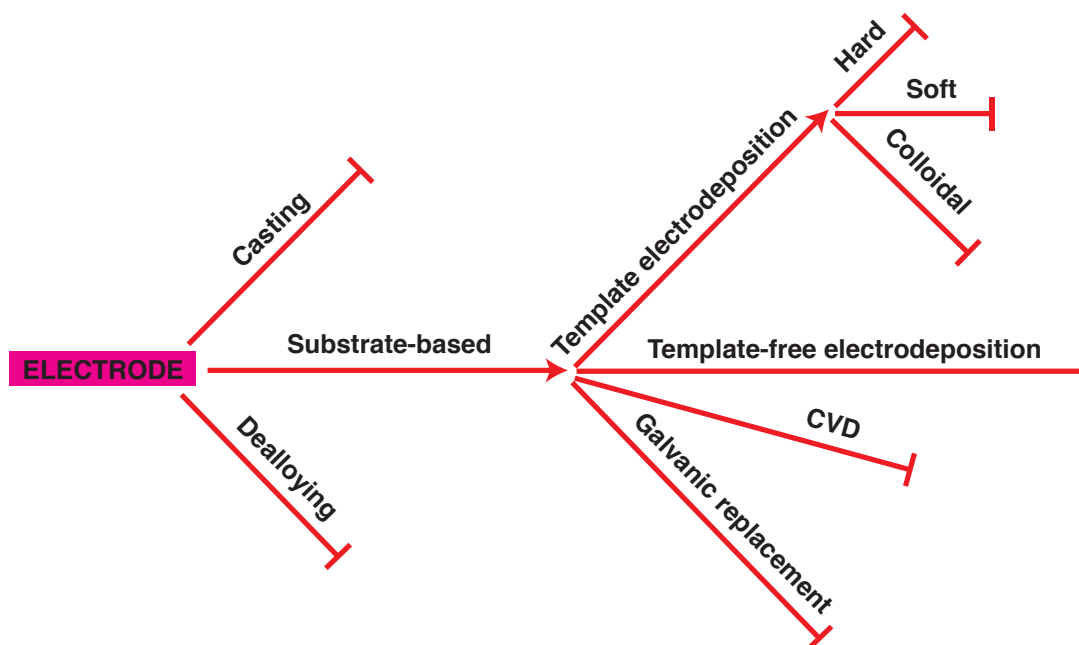


Figure 2.8 – Summary of the principal fabrication approaches of nanoPt electrodes.

Nanoparticle-based Nanoporous electrode from nanoparticles is usually obtained by deposition *via* electro spraying, screen printing, inkjet printing and drop casting usually on a carbon-based electrode. First of all, Pt nanoparticles need to be synthesised from solutions containing a solvent, a platinum salt, a capping agent to avoid particle aggregation and a reducing agent. Then, a dispersion of Pt nanoparticles should be prepared before the deposition onto electrode surfaces. Binders are often used to help the nanointegration step. The presence/absence of a binder [84, 85] as well as a homogeneous nanoparticle dispersion is critical for the final electrocatalytic activity of the electrode. The long preparation and the nanoparticle instability on electrodes have limited the applicability of such methods to fabricate nanoPt electrodes.

Substrate-based The main advantage of substrate-based approaches is the possibility to synthesise nanoPt films directly on electrodes. Commonly-used approaches are: electrodeposition (with or without a template), galvanic replacement and CVD.

Electrodeposition is the most practical and versatile approach to selectively nanostructure conductive substrates. The electrochemical reduction of ligand coordinated Pt complexes is shown in Fig. 2.9. Under an applied voltage the ligand coordinated metal ions move towards the cathode (1). When the ligand coordinated metal ions enter in the diffusion layer, the ligands are aligned to the electric field but the metal ions is still anchored to the ligands (2). Then, the ligand-metal systems move to the double layer where the electric field is so strong to determine the separation of the ligands from the metal ions (3). Finally, the metal is reduced and deposited to the cathode (4). The main advantages of Pt electrodeposition methods for nanostructuring electrodes are the low cost, the high deposition rates, the absence of a post-deposition treatment, the nanofabrication directly on electrodes, the possibility to produce features with different size and shape and to easily form multilayer metal systems and alloys (e.g., Au-Pt) with controlled metal ratio. Moreover, nanostructured films well-anchored on electrodes result from this process with consequent low electrical resistivity. Depositions could be performed by applying voltages or currents using a configuration with two or three electrodes.

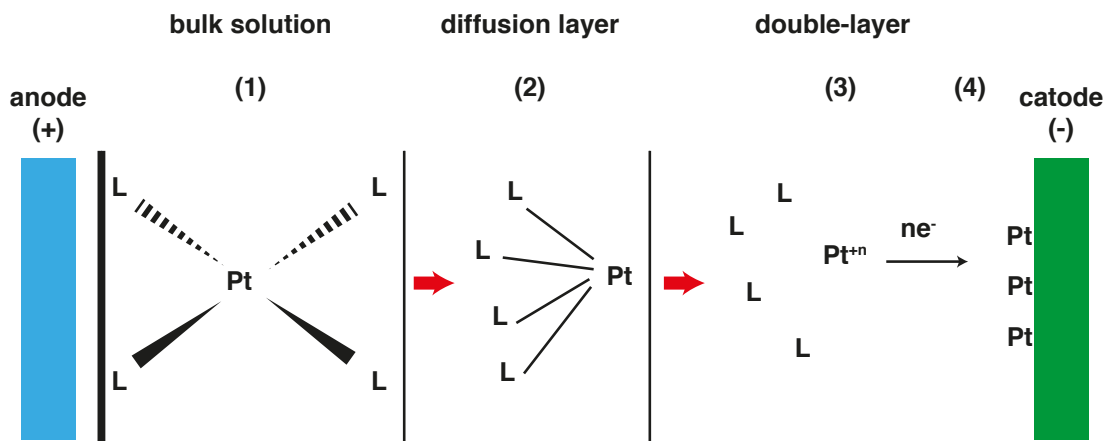


Figure 2.9 – Schematic of electrochemical reduction of a four ligand coordinated Pt complex.

Template electrodeposition requires three steps:

- fabrication of a template (hard, soft or colloidal) with the desired nanoporous structure on the conductive electrode;
- electrochemical filling the pores with a Pt precursor;
- template removal.

The most used **hard** template is the porous anodic aluminium oxide membrane. The vertical structures of these membranes are used to form 1D nanomaterials. If the vertically aligned channels are empty, nanotubes form. When the channels are filled, nanowires result after template removal in acid or basic solutions. Yuan *et al.* [86] fabricated Pt nanotubes through an anodised alumina membrane for glucose sensing. A pretreatment with 3-aminopropyltrimethoxy-silane, that acts as a molecular anchor for the electrodeposited metal nuclei, makes possible the growth along the pore walls. The resulting nanotubules had an outer and inner diameter of (150 ± 10) nm and (70 ± 10) nm, respectively, and thickness of ≈ 40 nm.

Mono- and multilayers (3D and 2D) efficient templates are closely-packed **colloidal** crystals pre-located on electrode surfaces by immersion or evaporation methods. Typically, silica [87] and polymers as polystyrene [88] from nanometer to micrometer sizes are used as template. Also with this approach, the surface modification is extremely important to fill all the voids of the template. Silica spheres are generally removed by etching with hydrofluoric acid [87] and polymeric spheres by using solvents [88]. High temperature processes used for the template removal (calcination, pyrolysis) result in a shrinkage of the pores.

Another method to synthesise nanoPt electrodes is the **soft** templating. A variety of both biological and artificial structures (micelles, reverse micelles in organic solvents, liposomes, vesicles, microemulsions, biomacromolecules and viruses) could be self-assembled onto the electrode surface. After the electrodeposition of Pt, the template removal is obtained by rinsing with water. Examples of soft templates are the *lyotropic liquid crystals* (LLC) formed by C_nEO_m -type surfactant molecules (EO = ethylene oxide) solved in water solutions [38]. The main advantages of the soft templating synthesis is the possibility to change sizes of the pores as well as the coating thickness. The nanopores can have sizes smaller than using hard templates and range from few nanometers to tens of nanometers. However, the application of an electric field during the electrodeposition can cause morphological changes of the surfactants close to the electrode surface making difficult the control of both size and shape. Other disadvantages are the long-lasting procedure and the possibility of an incomplete template removal that causes detachment of the film during an electrochemical measurement. Fig. 2.10 (a) shows the nanoPt synthesised by a soft template electrodeposition on our microfabricated Pt electrodes. The deposition was performed by applying -0.1 V *vs* Ag quasi-reference electrode for hours till a charge of 7 C (electrode diameter of 0.5 mm) was reached. More often, the nanoPt detaches from the electrode surface during Pt activation (Fig. 2.10 (b)) due to the incomplete removal of the template (various immersions of some hours in DI water). The detachment is clearly evident in Fig. 2.10 (c).

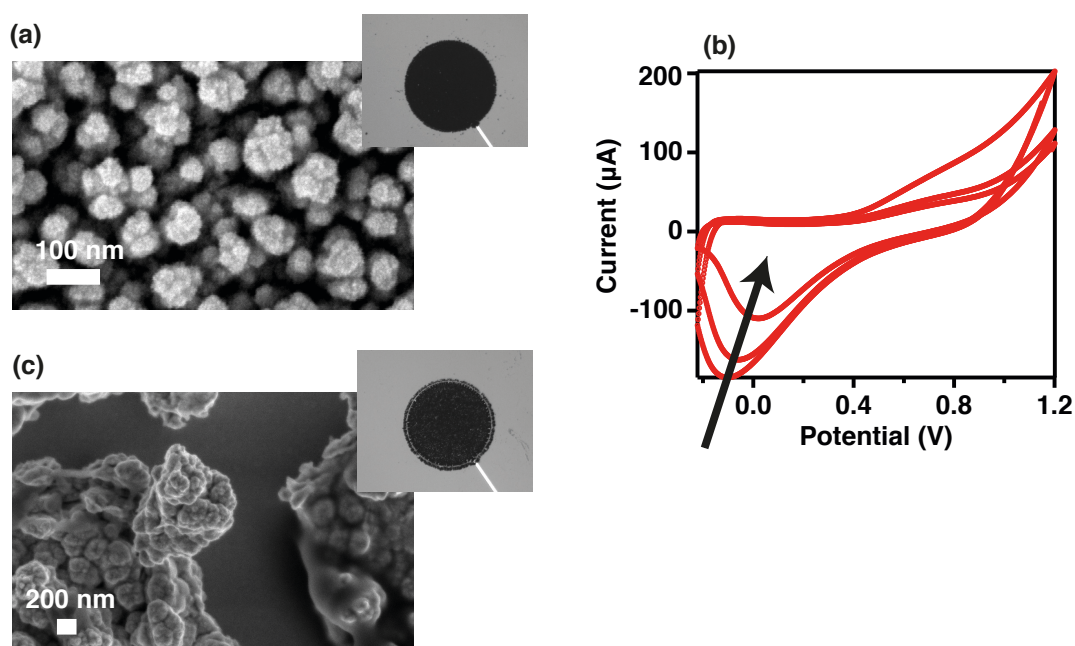


Figure 2.10 – SEM and optical microscope images of nanoPt electrodeposited according to the procedure in [89] on electrodes of our microfabricated platform (see Fig. 1.11 (c)) (a). Material detachment during activation in sulphuric acid (b). SEM and optical microscope images of nanoPt after the detachment (c).

Template-free electrodeposition is the most efficient way to produce nanoPt for the possibility to selectively anchor the coating on electrodes by a one-step room-temperature process in some minutes. As compared with template electrodeposition, it is more challenging to control size and shape of nanostructures. Pulsed electrodeposition is the most used strategy to obtain a narrow distribution of the structure size [77, 90]. High overpotential is applied for a short period of time to create many nucleation sites followed by a low potential to minimise the growth rate and to have a higher control of the growth of Pt nanostructures. Some additives such as ethylen glycol [91] and polyvinylpyrrolidone [92] are commonly used to reduce the size of the surface features of one and three orders of magnitude, respectively.

Only few works concern the control of the shape of electrodeposited nanoPt without template. In general, the addition of additives causes a change of nanoPt shapes. For instance, Pt nanospheres change in clump-like when polyethylene glycol is introduced in solution [90]. Pt nanospheres change in Pt nanoflowers when a lead acetate-containing solution is used [90]. More elaborated post-growth electrochemical treatments could also be adopted to change the shape of Pt from spherical to tetrahedral [79, 80]. The application of square wave potential in the presence of sulphuric and ascorbic acid changes Pt spheres in Pt cubes, tetrahedra, and octahedra that have shown a better catalytic activity for equivalent Pt surface areas towards the detection of small organic molecules [79, 80, 81]. During the treatment, the oxygen atoms adsorb preferentially on the high-index facets and shift the Pt atoms on these facets that

become more pronounced and so highly electroactive.

Template-free electrodepositions in low concentrated sulphuric acid solutions show that the presence of the acid influences the nanoPt shape. During the electrodeposition, the acid anions HSO_4^- and SO_4^{2-} adsorb on specific Pt planes promoting their growth. The growth of the other facets are indeed inhibited. Spherical-like structures result by applying a low voltage for a short period of time. Pt petals are produced by increasing the intensity of the applied voltage or/and by prolonging the growth time [93]. A comparative investigation of the electrocatalytic properties of these as-produced and differently-shaped Pt structures is absent in the literature. No research group has ever studied the influence of sulphuric acid concentration and the type of Pt salt precursor on the resulting nanoPt morphological characteristics.

In **galvanic replacement** reaction, less noble metals or metal oxides, pre-deposited with a particular geometry on electrodes, dissolve in solution and are replaced by a more noble metal that is present in solution. The difference of redox potentials between the two metals is the driving force of this phenomenon. The advantage of this method is that the removal of the template simultaneously occurs with the deposition of the other metal [94]. A variety of nanocrystals could be used as sacrificial templates, resulting in a variety of nanoPt shapes [94, 44].

A **CVD** approach could also be considered for syntheses of nanoPt also on conductive substrates. Lo Nigro fabricated Pt nanocolumns (40-80 nm of diameter and 2 μm of length) on a variety of substrates (conductive and not). Bis-acetylacetonate platinum(II) was used as precursor and the depositions were performed between 220 and 550 $^\circ\text{C}$ for 15-360 min [95]. Besides a high control of both dimensions and shapes of nanoPt produced by CVD, the weak point of this technique compared with substrate-based electrodeposition and galvanic replacement is the required high technical effort.

Alloying-dealloying Other efficient approaches to generate nanoPt-based electrodes are dealloying processes from binary or ternary alloys. An annealing step is required for homogenisation or formation of the alloy. Finally, dealloying is carried out to selectively dissolve the unwanted metal either chemically [96] or electrochemically [97]. After the dealloying, the more noble metal component is left behind with a porous structure. During the electrochemical dealloying two important factors should be considered: concentration limit of the more noble component and critical potential threshold enabling the dissolution of the less noble metal from the alloy. Even though chemical dealloying is much easier to carry out (immersion in an appropriate acid or basic solution), it has many drawbacks because the etching could affect random sites and the process is sometimes too strong to control.

Table 2.2 lists advantages and drawbacks for the described nanoPt incorporation techniques. Template-free electrodeposition (highlighted in the table) emerges as the most favourable nanostructuring approach to implement in terms of time and technical efficiency, reproducibility and film robustness.

Table 2.2 – Advantages and disadvantages of different strategies of nanoPt integration on electrochemical electrodes. Very good choice: (++); Good choice: (+); Not good choice: (-).

CHARACTERISTICS\METHOD	Casting	Template electrodeposition	Template-free electrodeposition	Galvanostatic replacement	CVD	Alloying-dealloying
Reproducibility	(-)	(+)	(++)	(++)	(++)	(+)
Large-scale application	(-)	(-)	(++)	(++)	(++)	(++)
Binder	(-)	(+)	(++)	(++)	(++)	(++)
Technical effort/costs	(++)	(++)	(++)	(++)	(-)	(+)
Time-consuming	(-)	(-)	(++)	(+)	(+)	(-)
Direct integration on CMOS devices	(++)	(++)	(++)	(++)	(++)	(++)
Micro-scale applications	(-)	(+)	(++)	(+)	(++)	(++)
Shape/size control	(++)	(+)	challenging	(-)	(++)	(+)
Film stability	(-)	(-)	(++)	(+)	(+)	(++)

2.2.3 Direct detection

As declared in Subsection 2.2.1, Faradic currents regarding rapid reactions are proportional to the apparent geometric area of the electrode, regardless of its roughness. On the other hand, slow kinetically-controlled electrochemical reactions are sensitive to the real area of the electrode (Fig. 2.7). As a consequence, electrode surfaces enlarged thanks to the use of nanopores boost the electrochemical response of sluggish reactions exclusively. The electrooxidation of the major electroactive interfering species (AA and UA) and of some drugs is diffusion-controlled so their detection at nanoPt-based electrodes is reduced with respect to flat electrodes [98]. A metabolite of extreme importance in medical field and characterised by a sluggish (kinetically-controlled) electrooxidation is the glucose. Pt is the most promising material for the electrochemical oxidation of glucose because the glucose oxidation similarly occurs in solutions with different pH. Cyclic voltammogram of glucose at Pt electrode presents three portions corresponding to three oxidation peaks (Fig. 2.11).

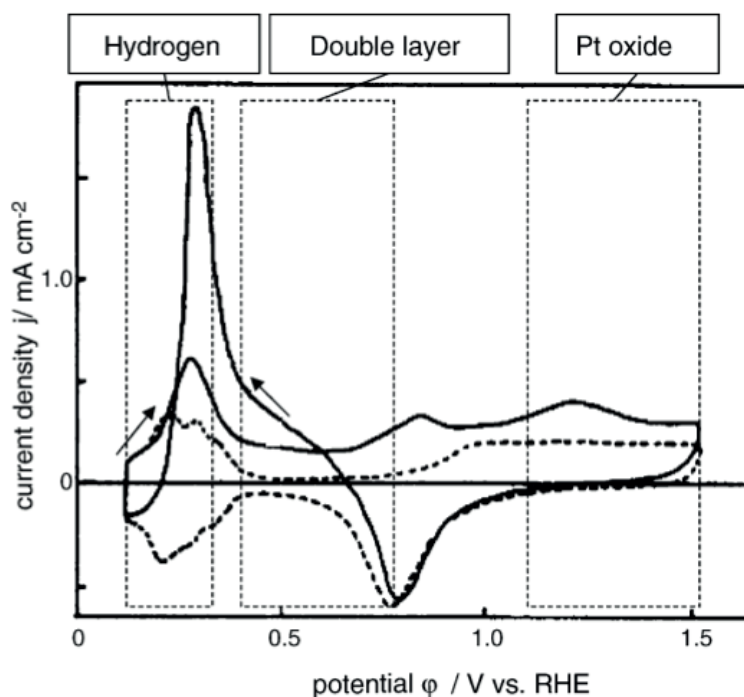


Figure 2.11 – Cyclic voltammogram of glucose oxidation (100 mM) at pH 7, 200 mM phosphate buffer. Reprinted from Fig. 7 in reference [99].

1. The "hydrogen region" between +0.15 and +0.3 V *vs* RHE (*reversible hydrogen electrode*) corresponds to the dehydrogenation of glucose at the hemiacetalic carbon (C₁; see Fig. 2.12 (a)) and the adsorption of the glucose on the Pt surface. This electrochemical oxidation is absent when materials different than Pt are used
2. The "double-layer region" between +0.3 and +0.6 V *vs* RHE. By increasing the potential,

the amount of OH_{ads} increases because of the water dissociation reaction (Fig. 2.12 (b-i)). Then, the OH_{ads} catalyses the oxidation of adsorbed glucose (Fig. 2.12 (b-ii)) in glucono lactone

- The "oxygen region" at a voltage higher than +0.7 V *vs* RHE. By further increasing the potential, the OH_{ads} desorbs and is replaced by O_{ads} that is initially less catalytically active. However, when the Pt surface is completely covered with a monolayer of oxygen species (PtO), the direct oxidation of the bulk glucose occurs (Fig. 2.12 (c))

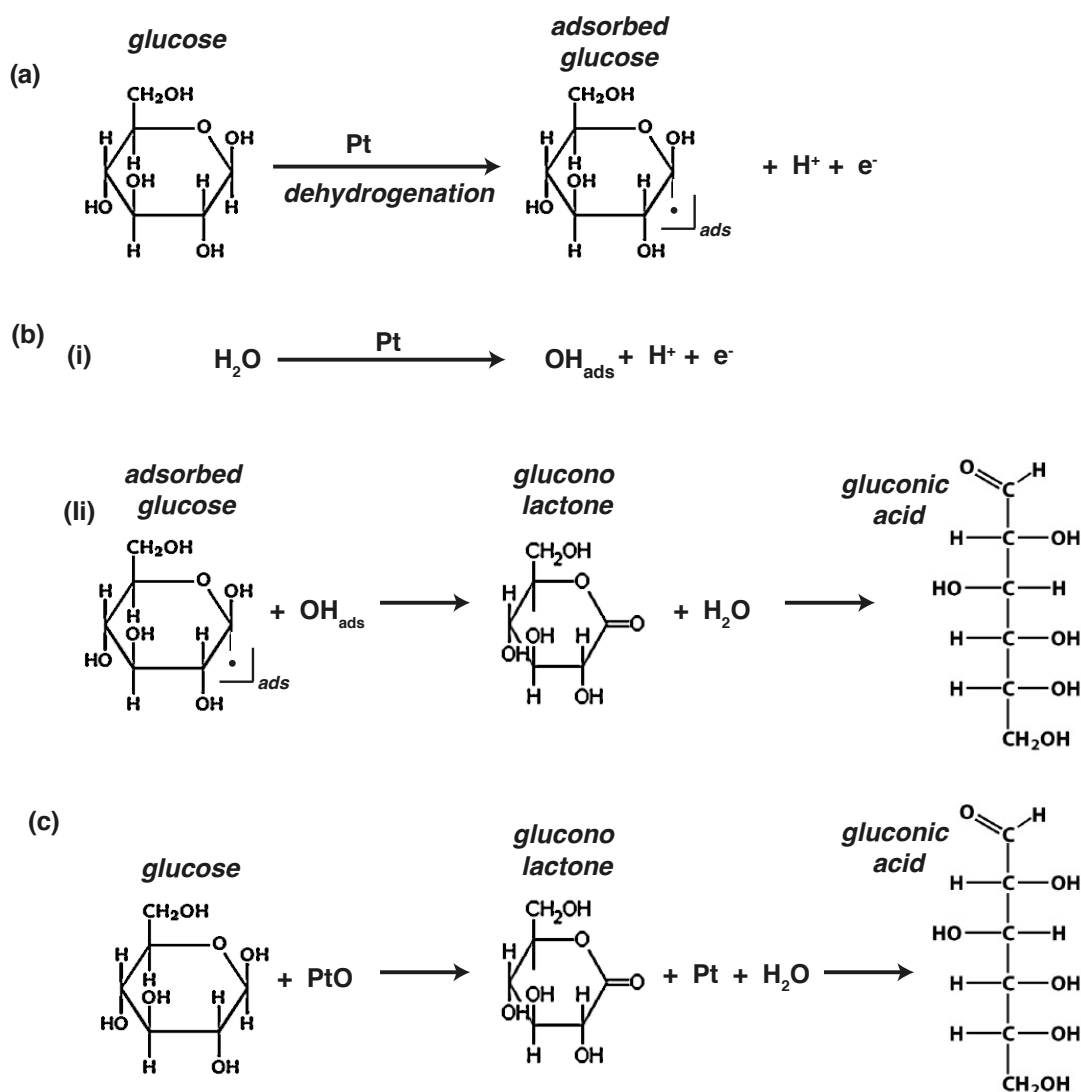


Figure 2.12 – Mechanism of glucose oxidation at Pt electrode.

Note that for all the reactions glucono lactone is an intermediate product and gluconic acid is always the final stable product of reaction (Fig. 2.12 (b-ii) and (c)). Skou *et al.* found that Peak 2 does not alter with the scan rate while Peak 3 was scan rate dependent [100].

Chapter 2. Nanostructured electrodes for electrochemical medical sensors

Concentrations of interfering species such as AA and UA in biosamples are of some hundreds μM . On the other hand, physiological levels of glucose range from 3 to 8 mM. Nevertheless, the Faradic current, originated by interfering species, is much more higher than that related to glucose at bare Pt electrodes. The use of nanoPt with high roughness factor (ratio electroactive-geometric electrode areas; R_f) increases the electrode sensitivity towards the direct glucose sensing [86, 96, 101, 102, 103] and makes the electrode insensitive to interfering species. Park *et al.* [104] demonstrated that the Faradic current for the glucose electrooxidation increases till R_f is equal to 300. This finding implies that, for each sluggish reaction, it is possible to find an optimal thickness of the nanoPt electrode at which the Faradic response is maximum. It has been previously reported that the electrocatalysis of methanol at Pt electrodes depends on the particle size of Pt [105]. This phenomenon could also be valid for the glucose electrooxidation.

Table 2.3 shows all the sensing performance of the most recent non-enzymatic glucose sensors tested at different nanoPt electrodes. Up to now, a full investigation of nanoPt prepared with a template-free electrodeposition towards the direct glucose oxidation is absent in the literature as well as the investigation of different nanoPt shapes towards the direct glucose oxidation.

In addition to the improved sensitivity and selectivity, another advantage linked to the use of nanoPt towards the electrooxidation of glucose is its intrinsic resistance to poisoning by adsorbed intermediates. Even though nanoPt clearly represents a strong alternative to enzyme-based glucose sensors (long stability over time, no oxygen limitation), only one research group used a nanoPt-based sensor to measure glucose in human sample [106].

Table 2.3 – Non-enzymatic glucose sensors based on nanoPt for electrochemical detection. NanoPt type, preparation technique, pH, sensitivity, *detection limit* (LOD), linear range, test with interfering species, R_f , applied voltage and publication year are shown.

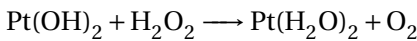
Material	Technique	pH	Sensitivity ($\mu\text{A}/(\text{mM cm}^2)$)	LOD (μM)	Linear Range (mM)	Interf. tested	R_f	Applied Potential	Ref.	Year
porous Pt	filled micropore	neutral	64.1		1-16	yes	-	+ 0.35 V <i>vs</i> SCE	[101]	2011
nanoPt	LC TE	neutral	1.65	97	1-10	-	200.6	+ 0.4 <i>vs</i> Ag AgCl	[107]	2007
mesoPt	LC TE	neutral	9.6	-	0-10	yes	72	+ 0.42 <i>vs</i> Ag Cl	[103]	2003
3D nanoPt	galvanic displ.	neutral	642	-	0.1-1.5	yes	2600	+ 0.4 <i>vs</i> Ag AgCl	[44]	2008
3D nanoPt	sonoelectrochem.	neutral	12.1	1.2	up to 20	yes	-	+ 0.5 <i>vs</i> SCE	[108]	2008
nanoPt	dealloying	neutral	291	-	up to 10	yes	151	+ 0.4 V <i>vs</i> Ag AgCl	[96]	2008
nanoPt	LC TE	neutral	37.5	50	-	yes	375	+ 0.4 V <i>vs</i> Ag AgCl	[102]	2008
Pt nanotubules	PAA TE	neutral	0.1	1	2-14	yes	286	+ 0.4 <i>vs</i> SCE	[86]	2005
3D macroPt	silicon spheres TE	basic	31.3	100	0.001-10	yes	32.5,	+ 0.5 <i>vs</i> SCE	[87]	2005
Pt nanoflowers	sonoelectrochem.	neutral	1.87	48	1-16	yes	1.31	DPV	[109]	2012

2.2.4 Enzyme-mediated detection

As declared in Subsection 2.1.4, hybrid carbon nanomaterials-Pt nanoparticles have shown the highest sensing performance for the indirect quantification of metabolites towards the detection of H_2O_2 , product of oxidase reactions. Indeed, Pt is the most suitable electrocatalytic material for detecting H_2O_2 . However, unlike carbon materials, Pt does not show a stable electrochemical background when used *in vivo*, due to the fast adsorption of biomacromolecules onto its surface and to the easy oxidation (biofouling and fouling). Moreover, to reduce interferences, a permselective membrane (e.g. Nafion) is always required.

In a set of papers, Hall *et al.* [110] have proven that the electrooxidation of H_2O_2 only occurs if a layer of Pt(II) oxide forms on the electrode. This finding explains why the H_2O_2 response is very poor at carbon electrodes. Based on these observations, the H_2O_2 electrooxidation at Pt electrode follows the scheme below.

Firstly, H_2O_2 adsorbs on the oxidised sites of Pt electrodes:



then, since Pt is not stable, the reduced Pt sites are reoxidised and become available to oxidise H_2O_2 again



The lack of available Pt surface sites limits the H_2O_2 electrooxidation resulting in a signal reduction for high concentrations of H_2O_2 so that the oxidation of H_2O_2 at Pt electrodes resembles to a Michaelis-Menten kinetics (Fig. 2.13).

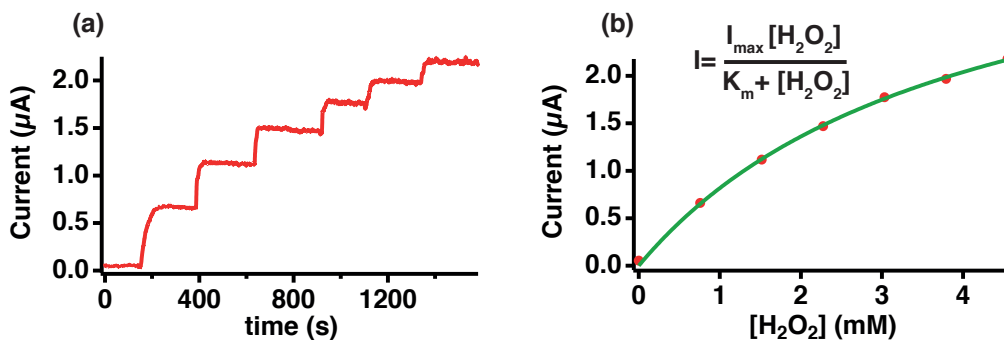


Figure 2.13 – Chronoamperometry at our microfabricated Pt electrode by sensing H_2O_2 (steps: 0.76 mM) (a). The detection mechanism resembles to a typical Michaelis-Menten kinetics (b).

The H_2O_2 electrooxidation at Pt electrodes is under a mixed kinetic and diffusion control. Therefore, for the reasons explained in Subsection 2.2.1, the Faradic currents associated with the slower electrochemical events (kinetically-controlled events of H_2O_2) are sensitive to nanoPt. Up to now, little work has been done on first generation electrochemical biosensors based on H_2O_2 detection using nanoPt. Park [104] investigated the relation between the signal

amplification for an indirect glucose sensing *via* H₂O₂ electrooxidation and the thickness of the nanoporous film. For a R_f lower than 50, the electrochemical response towards the H₂O₂ oxidation increased proportionally to R_f. The oxidative current reached a plateau for R_f higher than 50. By using mesoporous Pt microelectrodes, Evans [37] found not only an enhancement of the catalytic activity but also an excellent reproducibility, precision, and accuracy of measurements over a wider linear range than using flat Pt microelectrodes. In another work, Wang [111] demonstrated that three-dimensionally (3D) ordered freestanding porous Pt nanowires with pores of several nanometers in size are an effective platform to immobilise enzyme. The glucose biosensor performed in a very wide detection range up to 189.5 mM with high sensitivity.

2.3 Hybrid Pt-based nanostructured electrodes

As seen in Section 2.2 nanoPt is the electrode material that has shown superior sensing performance towards the detection of two molecules of clinical interest. The first is the hydrogen peroxide, product of oxidase-based reactions and analyte sensed in the most common first generation biosensors to indirectly quantify an organic molecule (e.g., glucose, lactate) under investigation. The second is the glucose that, with no doubts, is the most relevant metabolite from the medical point of view. NanoPt electrodes electrochemically oxidise glucose without enzyme avoiding problems of enzymatic instability over time.

Even though several fabrication strategies result in nanoPt with many morphologies, continuous efforts are made to obtain nanostructured electrodes with further increased surface-to-volume ratios and with geometries that are not achievable by employing the procedures described in Section 2.2.2. A possible strategy is the combination of Pt nanomaterials with other nanostructures. In particular, it was proven that combining nanostructures of Pt and of other metals further reduces poisoning issues and further favours the detection of small molecules at even lower potential than using monometallic Pt nanomaterials. To sum up, combining nanoPt with other nanostructures provides the following advantages:

1. the possibility to use particular geometries that are impossible to obtain with the deposition techniques previously discussed. Up to now, the most common support materials for Pt nanostructures are CNTs and graphene [74, 75, 76] because of their large accessible surface areas and high electron conductivity. However, the preparation procedures of nanocarbon-based electrodes are either time-consuming (often require the preparation of an homogeneous dispersion) or costly (CVD) and the poisoning of Pt on carbon materials easily occurs.
2. high electrocatalytic performance shown by coupling Pt with other metals towards the detection of some compounds. The improved electrocatalysis of a certain analyte could be due to the higher/lower electronegativity of a second metal than Pt could cause an increase/decrease of the amount of charge being transferred from Pt to the

second metal (electronic effect). Moreover, a larger/smaller lattice constant of the second metal, leads to an increase/decrease of the separation among Pt atoms. The ratio and the surface distribution of Pt and the second metal need to be also considered. A particular arrangement of surface atoms of the two metals suppresses adsorbed poisonous species on surface-active sites of Pt. The shift of the d-band electron density of Pt in the presence of another metal reduces the strength of the molecular adsorption on Pt and, therefore, lower the detection potential. Finally the two metals in the alloys seem to act cooperatively in the electrocatalysis.

Metabolites of medical interest such as H_2O_2 [112] and glucose [113] have been poorly studied with such bimetallic systems. In particular, the improvement of the H_2O_2 electrooxidation is not yet reported.

2.4 Potentiometric solid-contact ion-selective electrodes

Recently, ion selective electrodes have been raised great interest in clinical field to quantify ion concentrations in human fluids. In particular, *solid-contact ion-selective electrodes* (SC-ISEs), that are free from an internal solution, are an interesting option for further improvements due to the possibility of an easy miniaturisation. These advantages are essential for a continuous monitoring of ions from very small biosample volumes.

The initial form of SC-ISEs were the *coated-wire electrodes* (CWEs) in which an ion selective polymeric membrane covered the metal electrode. However, the drift of the electrode potential, due to the high charge-transfer resistance and to the low double-layer capacitance, has limited the use of CWEs for certain medical applications [114].

The use of an intermediate layer that can act as ion-to-electron transducer between the membrane and the electrode could solve the problems of CWEs. Initially, conductive polymers have been used as solid contact. However, these materials suffer from limitations such as the uptake by the membrane and the water uptake due to residues of polymerisation. Sensitivity to light, to redox interfering species, to O_2 , to CO_2 and to pH [114] were other additional drawbacks.

Up to now, nanomaterials are the best candidates as solid contacts because they can satisfy the following requirements

1. reversible transition from ionic to electronic conductivity
2. high electrode capacitance for a long-lasting potential stability
3. high hydrophobicity to eliminate the water layer formation between electrode and membrane and to support the membrane adhesion

Carbon nanostructured electrodes are the most used electrodes to build SC-ISEs [114]. On the

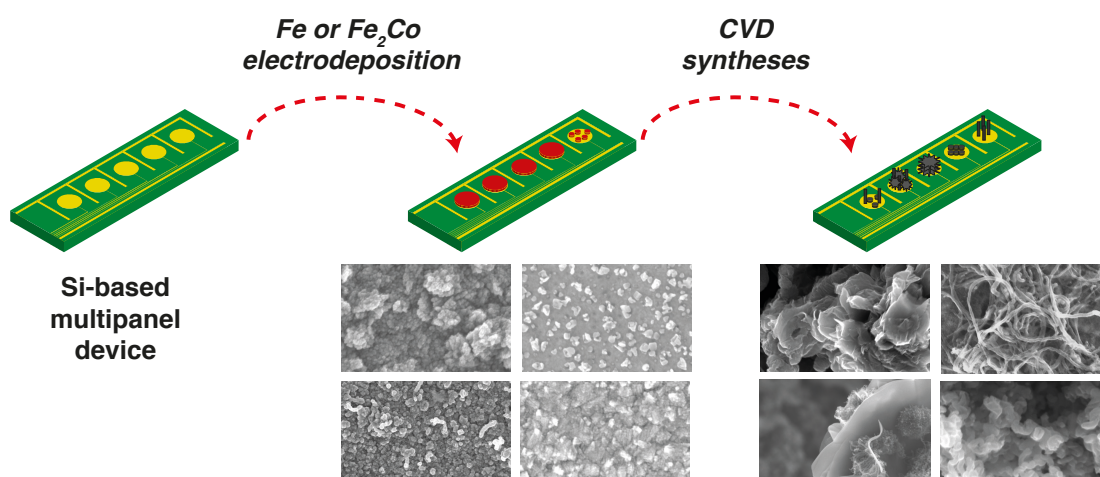
other hand, only one example was found in the literature proposing a SC-ISE fabricated by using nanoPt as intermediate layer [89].

2.5 Summary and contributions

This chapter summarises the most common methods to prepare carbon nanomaterial-based sensors *via* casting, electrochemical methods and direct synthesis and describes the principal strategies to fabricate nanoPt electrodes by casting, electrodeposition with and without a template, galvanostatic replacement, CVD and dealloying. Non-enzymatic fast electrochemical reactions (diffusion-controlled) are particularly favoured by the edge-like planes and defect sites of carbon nanomaterials (e.g., AA, UA and some drugs). For full- or semi-kinetically controlled sluggish reactions nanoPt is preferable (e.g., H₂O₂ and glucose).

The main contribution of the present chapter is the introduction to a critical review of both integration approaches and electrochemistry of carbon nanomaterials and nanoporous Pt for biomedical sensing. For a better understanding of the theoretical background of the present work, some strategies of electrode nanointegration were reproduced on our sensors (screen-printed and microfabricated electrodes) and their robustness was tested (see Fig. 2.10). Some properties of electrodic materials (Fig. 2.13) and of nanomaterials (Fig. 2.4) were verified and some issues clarified (Fig. 2.6). Finally, pro, cons and challenges of different nanostructuring techniques were deduced and then summarised in Table 2.1 and Table 2.2. This study was realised to focus on the development of the most promising and challenging techniques (highlighted in the two tables). The selected nanostructuring methods will be realised on electrodes of screen-printed and thin-film CMOS devices since minimally-sized and, therefore, suitable for continuous biomonitoring. The respective detection capabilities towards biomarkers of clinical interest will be evaluated.

3 Direct and selective integration of carbon nanomaterials by a CVD process on a micro-fabricated Si-based multipanel device



Carbon nanomaterials have been largely employed to enable the detection of molecules relevant for clinical studies. The development of tailored integration methods to nanostructure small electrode surfaces is quite challenging. The most used techniques (casting and electrochemical methods) suffer from scarce reproducibility, long preparation, expensive instrumentation and limitation to some electrodic materials. More often, the presence of binders hinder the nanomaterial properties and make the nanostructuring unstable in aqueous environment. The direct growth of carbon nanomaterials (CNTs, graphene, nanographite) onto electrodes by CVD process would ensure an excellent contact nanostructure-metal that is of crucial importance for high performance characteristics.

Graphene is commonly produced on Ni or Cu. Conversely, growing CNTs on Au or Pt electrodes is difficult because catalytic particles are more active when supported by oxides. When placed on metal surfaces, catalytic particles are often poisoned because of the alloying. Therefore, growths of carbon nanomaterials on only the selected Au or Pt working electrodes of a CMOS multipanel

Chapter 3. Direct and selective integration of carbon nanomaterials by a CVD process on a microfabricated Si-based multipanel device

sensing platform is very challenging. A method to make possible the selective fabrication of CNTs on Au and Pt electrodes is the use of a pre-deposited thin buffer dielectric layer that inevitably reduces the sensor performance by creating a high contact resistance. Moreover, carbon nanomaterials are typically grown at temperatures between 600 and 1200 °C, which are not compatible with direct CMOS integration. A method to obtain various carbon nanomaterials down to 450 °C could open the possibility to a direct integration nanostructures/front-end CMOS data acquisition circuits. To sum up, the three major requirements for an efficient integration of carbon nanomaterials in thin-film electrochemical systems are: (a) selectivity with respect to one working electrode made of Au or Pt of a multisensing platform, (b) contact nanomaterials-electrodes and (c) CMOS compatible synthesis temperatures.

In this chapter, a new protocol to selectively grow carbon nanomaterials by CVD on Pt electrodes of a multipanel Si-based electrochemical platform, microfabricated with thin-film processes, is presented. Section 3.1 describes the process flow for the microfabrication of the device. The procedures for the catalyst deposition, the CVD setup, and the techniques for the nanomaterial characterisation are illustrated in Section 3.2. Section 3.3 focuses on growths at high temperatures (750-600 °C) and on the study of how the deposition variables affect the final characteristics of the nanostructures. Finally, the procedure to synthesise carbon nanomaterials down to 450 °C and, therefore, in a way compatible with CMOS technology, is described in Section 3.4.

3.1 Device microfabrication

The integration of carbon nanomaterials by a direct CVD growth was carried out on the multiple sensing sites (WEs) of a multipanel platform microfabricated on 10 cm Si wafers according to the scheme depicted in Fig. 3.1. Briefly, Si wafers with 500 nm of native SiO₂ were coated with a positive *photoresist* (PR) (Fig. 3.1 (a)). Platinum (200 nm) was deposited by evaporation (Alcatel EVA 600). A buffer layer of Ti (20 nm) was added to improve the adhesion between Pt and SiO₂ (Fig. 3.1 (b) and (c)). After the lift-off, 20 nm of HfO₂ were deposited by *atomic layer deposition* (ALD) (BENEQ TFS200) (Fig. 3.1 (d)). Afterwards, electrodes and contacts were introduced on the dielectric material. HfO₂ was selectively removed by Ion beam etching (Veeco Nexus IBE350) (Fig. 3.1 (e)). Then, a wafer dicing step produced single devices each one with five WEs (diameter of 564 µm). All the WEs share the same CE and RE (Fig. 3.1 (f)). The reason why HfO₂ was selected as passivation layer is explained in detail in Subsection 3.3.1.

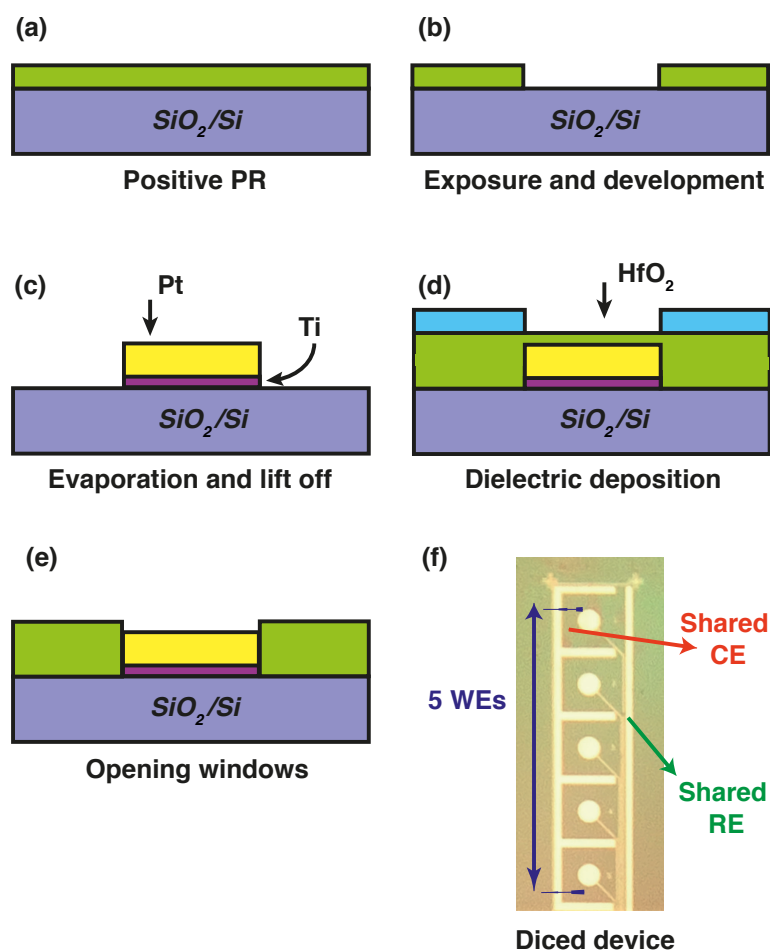


Figure 3.1 – Schematic of the device microfabrication.

3.2 Methods

3.2.1 Catalyst electrodeposition

Cobalt(II) ($\text{CoSO}_4\text{H}_2\text{O}$) and iron(II) ($\text{FeSO}_4\text{H}_2\text{O}$) sulphate heptahydrate were purchased from AppliChem. Depositions of Fe as catalyst were carried out from freshly prepared 0.2 M $\text{FeSO}_4\text{H}_2\text{O}$ solutions while Fe_2Co was deposited on the WEs from mixtures of 0.2 M $\text{FeSO}_4\text{H}_2\text{O}$ and 0.1 or 0.2 M $\text{CoSO}_4\text{H}_2\text{O}$. A buffer solution composed of 0.5 M H_3BO_3 (boric acid, Bio-Chemica, AppliChem) and 0.5 M NaCl (sodium chloride, Sigma) was used. All the solutions were prepared with Milli Q (Millipore) water. All the experiments were performed under aerobic conditions. An Au or Pt circular electrode (diameter = 4 mm), placed in parallel and approximately at 1 cm from the WE, was used as CE to obtain homogeneous depositions. Ag was used as *quasi reference electrode* (QRE). All the experiments were carried out using an Autolab potentiostat under a computerised control.

Fe nanoparticles (FeNPs) were obtained by *linear sweep voltammetry* (LSV) with a potential

Chapter 3. Direct and selective integration of carbon nanomaterials by a CVD process on a microfabricated Si-based multipanel device

window of 0/-1.4 V and a scan rate of 5 mV/s, followed by solution stirring for approximately three minutes (LSV+STIR). Fe non-compact layers (FeNC) resulted from CA at -1.4 V for 15 s followed by solution stirring for approximately three minutes (CA15+STIR). CA at -1.4 V or -1.3 V for 60 s (CA60) was used to produce compact layer of Fe (FeC).

Fe₂Co nanoparticles (FeCoNPs) were deposited by LSV (0/-1.4 V) followed by 5 s of open circuit from 0.2 M of both FeSO₄H₂O and CoSO₄H₂O. Compact Fe₂Co layers (FeCoC) were obtained from solutions containing 0.2 M FeSO₄H₂O and 0.1 M CoSO₄H₂O. Catalyst coatings with different thickness were electrodeposited onto the electrodes by varying the time of deposition (from 2 s to 30 s). Thicknesses were measured with a Dektak XT Profilometer (Bruker). To evaluate the rate of thickness increase with the electrodeposition time, three samples per each deposition time (2, 8, 15 and 30 s) were prepared. For each sample, measurements were taken in triplicate. The thickness showed a linear increase with the electrodeposition time.

3.2.2 Synthesis of carbon nanomaterials

Carbon nanomaterials were grown in a catalytic CVD quartz tube furnace at ambient pressure. Prior to growth, the devices were introduced in the furnace (pre-heated at growth temperature) and kept there for 10 minutes under a H₂ and Ar flow (60 l/h). This resulted in a change of the catalyst morphology. Carbon materials were deposited by Oxidative Dehydrogenation Chemistry [115, 116]; Ar was introduced in the CVD reactor at 45 l/h together with C₂H₂ and CO₂ (with a 1:1 ratio and a flow rate of 0.25 l/h) for 5 minutes. The growth temperature varied between 750°C and 450°C. After the deposition, the chamber was cleaned under Ar flow (60 l/h) for 10 minutes. To sum up, standard growths were obtained with the following parameters (standard parameters): 10 minutes of annealing, 5 minutes of deposition, a C₂H₂ gas flow of 0.25 l/h, a CO₂ gas flow of 0.25 l/h and a growth temperature of 750°C. The system setup is shown in Fig. 3.2.

3.2.3 Material characterisation

The surface morphology and the roughness of the Fe catalyst before and after segregation were examined with a Bruker *Atomic Force Microscope* (AFM). The roughness parameters of the surface were evaluated with a Gwyddion software [117] after plane subtraction and horizontal scar removal. A Zeiss MERLIN *Scanning Electron Microscope* with *Energy Dispersive X-ray Spectroscopy* (SEM/EDX) was used to investigate the morphology of both catalyst and carbon materials and the composition of the catalyst. The covered area of the catalyst NPs and the average CNT diameters were estimated by using the ImageJ software [118]. Raman spectra were acquired using a homemade micro-Raman microscope [119]. The spectra were analysed with a triple grating spectrometer (TriVista 555). The 488 nm laser was focused on a diffraction-limited spot of around 0.65 μm² to reach a power density of 2.2-2.3 mW/μm². The acquisition time varied from 2 to 5 minutes. Particular care was taken to avoid heating of the samples because of the well-known possibility of modifying/damaging the nanomaterials with

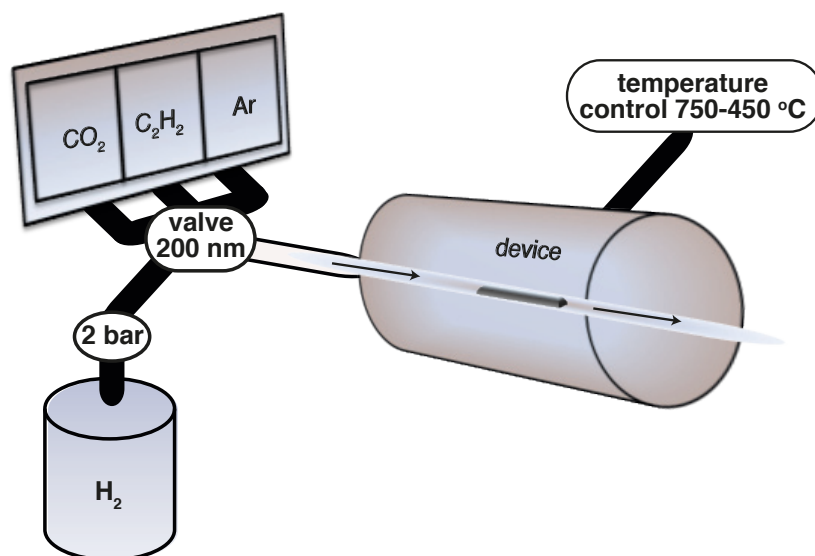


Figure 3.2 – Scheme of the CVD reactor for carbon nanomaterial synthesis.

the laser [120]. The Igor Pro (Wavemetrics, Lake Oswego, OR, USA) software was employed to fit Raman peaks using Lorentzians [121].

3.3 Syntheses at high temperatures from Fe catalyst

The direct synthesis is the principal approach to place carbon nanostructures on an electrode and producing an excellent contact between the nanomaterials and the underlying metal substrate. Unfortunately, this method usually presents several limitations: the tendency of some classes of carbon nanomaterials to grow on dielectric layers complicates their selective positioning on metal surfaces; their growth onto the passivation layer of the device creates short circuits among electrodes of the platform making the detection impossible. The interdiffusion and the alloying between the catalyst and the metal electrode surface prevent the nanocarbon formation at the CVD temperatures [122].

In the following section, a procedure to grow carbon nanomaterials onto Pt electrodes is explained. The influence of both deposition parameters and nature of the catalyst on the characteristics of the obtained carbon nanomaterials is examined.

3.3.1 Selection of the dielectric material and of the deposition time

The adhesion of different passivation layers to the SiO₂ was studied when exposed to the high growth temperature. All the materials deposited by sputtering (V₂O, MgO, SiO₂, TaO₅, TiO₂) have shown poor adhesion to the bottom layer material. On the other hand, both HfO₂ and Al₂O₃ deposited by ALD have shown an excellent adhesion to SiO₂. However, depositions performed for 30 min of carbon flow resulted in spontaneous CNT growths onto these material

Chapter 3. Direct and selective integration of carbon nanomaterials by a CVD process on a microfabricated Si-based multipanel device

substrates (see Fig. 3.3 (a-c)). To avoid not selective CNT growths, the HfO_2 was considered because less CNTs grew on it than on Al_2O_3 and the synthesis time was reduced till no CNTs were seen onto the surface of HfO_2 (Fig. 3.3 (d)).

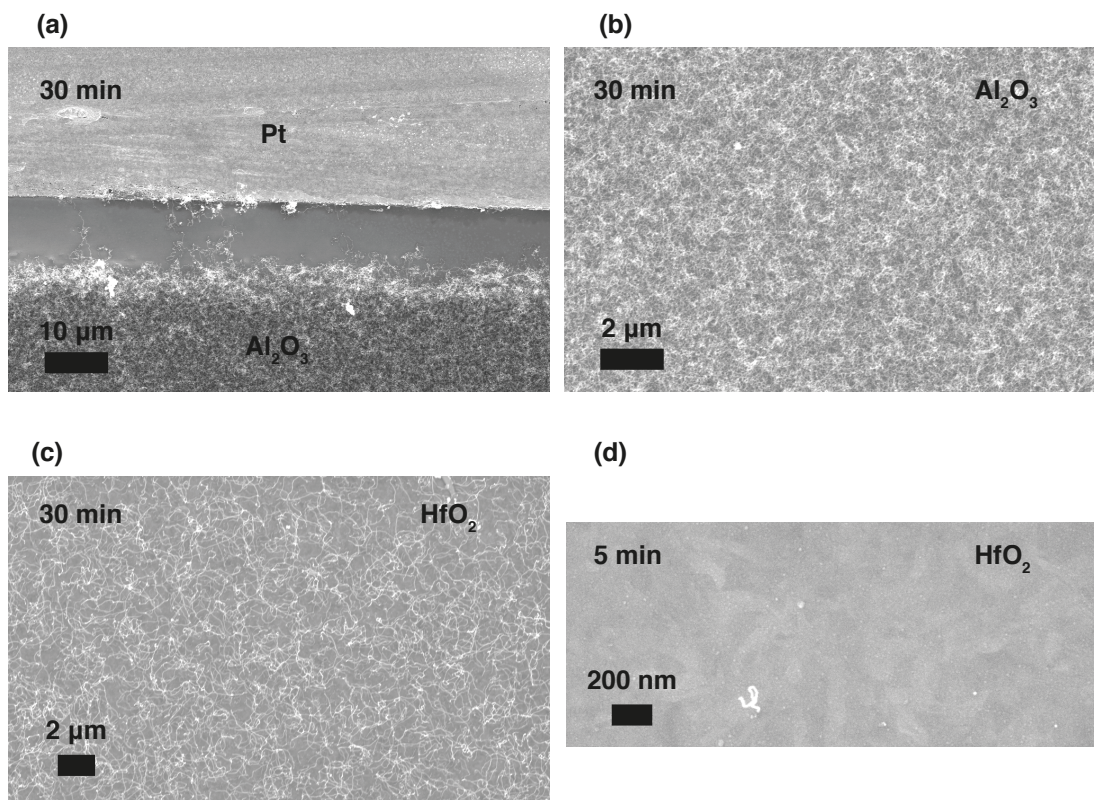


Figure 3.3 – CNT catalyst-free synthesis on ALD Al_2O_3 (a;b) and on HfO_2 (c) after 30 min of carbon flow at 750°C . No CNTs grew on HfO_2 by decreasing the deposition time down to 5 min (d).

3.3.2 SEM and AFM study

Electrodeposition was employed as novel, low-cost, versatile and selective technique, even compatible with the electrochemical platform, to easily obtain different catalyst coatings. Fig. 3.4 (a) and (b) show SEM images of iron nanoparticles (FeNPs) obtained with the LSV+STIR procedure. The covered area is $(27.6 \pm 3.8)\%$ and the perimeter of the particles is (245.7 ± 29.3) nm. The minimum and the maximum near-neighbour distances between nanoparticles were estimated to be (26.6 ± 5.6) nm and (164.8 ± 20.8) nm, respectively. Using the CA15+STIR deposition, platinum electrodes were covered with a non-compact iron layer (FeNC). Arrows in Fig. 3.4 (c) and (d) highlight the presence of cracks on the Fe coating. Conversely, compact iron layers (FeC) do not show any crack and the coating is thicker than FeNC. This is due to the four-fold increase of the electrodeposition time (Fig. 3.4 (e) and (f)).

3.3. Syntheses at high temperatures from Fe catalyst

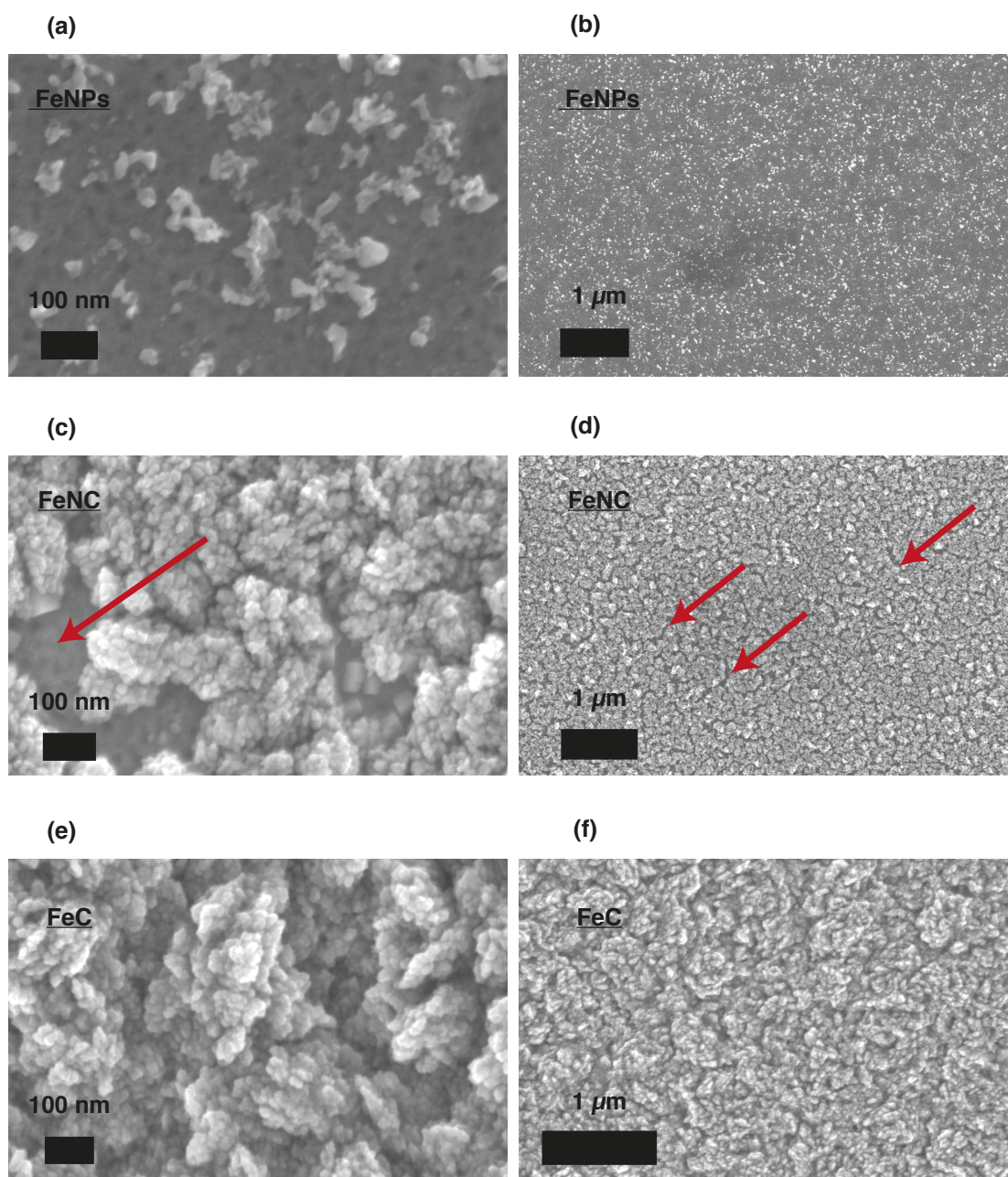


Figure 3.4 – SEM images at high (a;c;e) and low (b;d;f) magnification of iron electrodeposited onto Pt electrodes by using procedure (a-b) LSV+STIR (c-d) CA15+STIR and (e-f) CA60.

Chapter 3. Direct and selective integration of carbon nanomaterials by a CVD process on a microfabricated Si-based multipanel device

Following the iron electrodeposition, coatings were annealed at the growth temperature under an Ar and H₂ flow. Fig. 3.5 (a-c) show SEM images of the different iron layers after 10 minutes of annealing at 750°C.

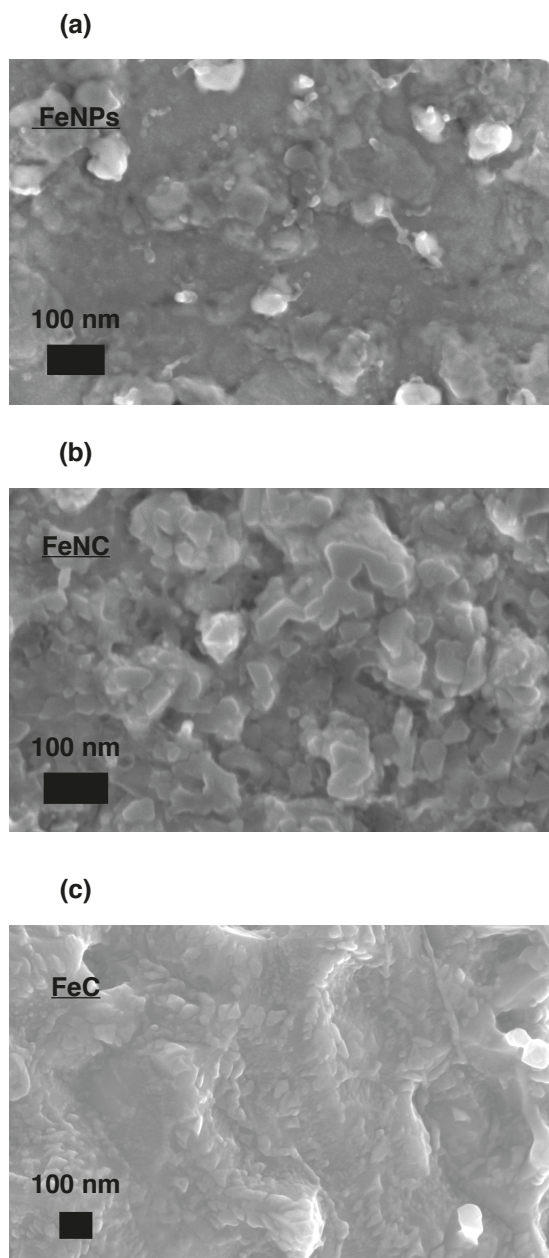


Figure 3.5 – SEM images of iron electrodeposited onto Pt electrodes and obtained with (a) LSV+STIR (b) CA15+STIR and (c) CA60 after 10 minutes of annealing at 750°C.

3.3. Syntheses at high temperatures from Fe catalyst

Roughness, evaluated by AFM (Fig. 3.6), does not differ significantly between FeNPs and FeNC (R_{rms} was 34.8 nm and 29.6 nm for FeNPs, and 22.7 nm and 25.0 nm for FeNC, before and after annealing, respectively). This behaviour is different in the case of FeC for which R_{rms} decreases remarkably after the annealing (from 54.1 nm to 38.6 nm). Particles are still present in FeNPs and FeNC. Undulated surfaces with clear stripes result from FeC.

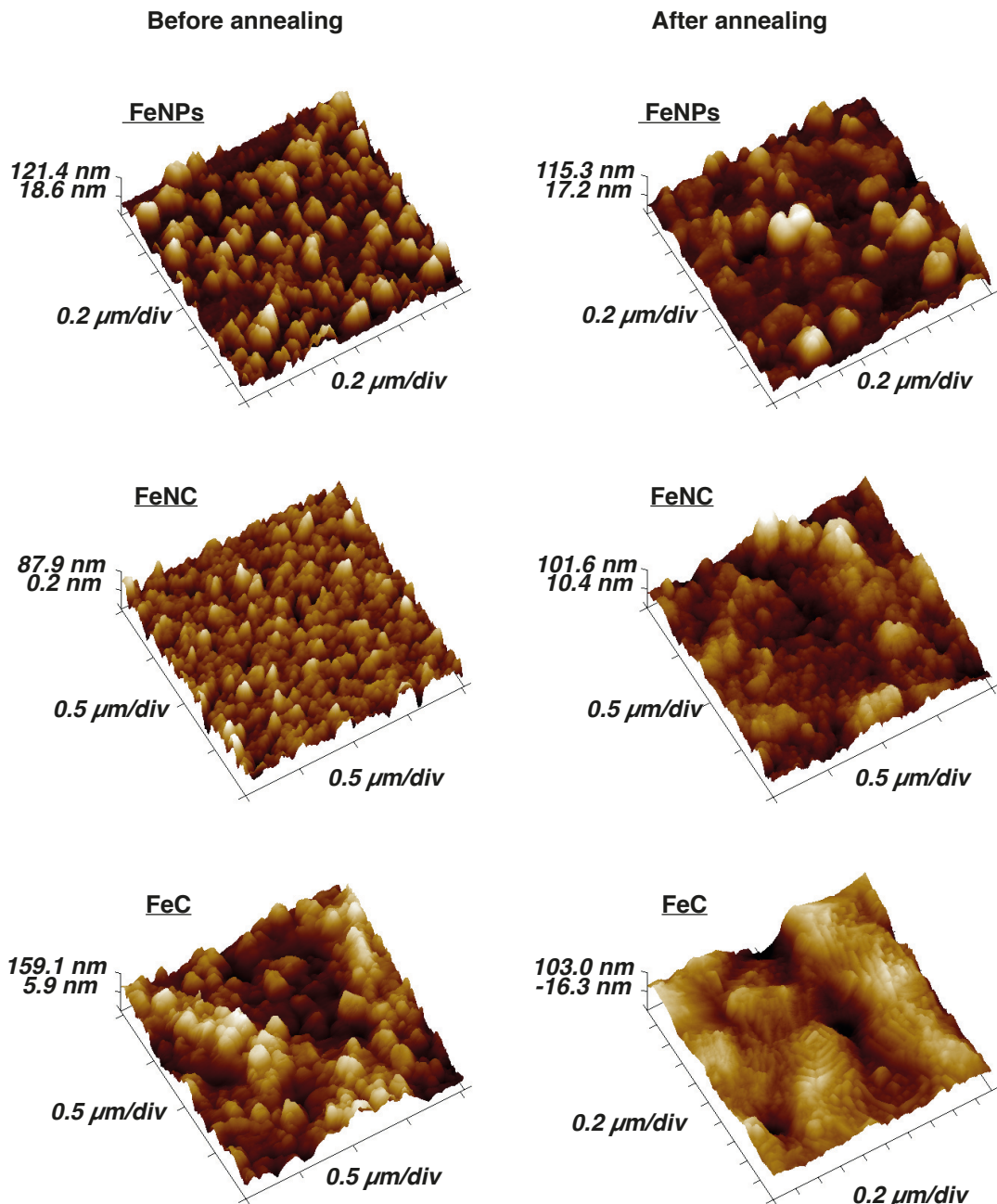


Figure 3.6 – 3D AFM images (Nanoscope Analysis software) before (left) and after (right) 10 minutes of annealing at 750°C (images: 2 μm x 2 μm).

Chapter 3. Direct and selective integration of carbon nanomaterials by a CVD process on a microfabricated Si-based multipanel device

Carbon nanomaterials were imaged by SEM. From FeNPs, sparse rolls of MWCNTs were selectively grown onto the metal electrodes (Fig. 3.7 (a)). Randomly oriented nanotubes resulted from FeNC (Fig. 3.7 (b)). Average diameters of the MWCNTs grown from FeNPs and FeNC were (15.4 ± 4.0) nm and (13.7 ± 3.2) nm, respectively. Fig. 3.7 (c) shows nanographene-shaped flakes resulting from FeC.

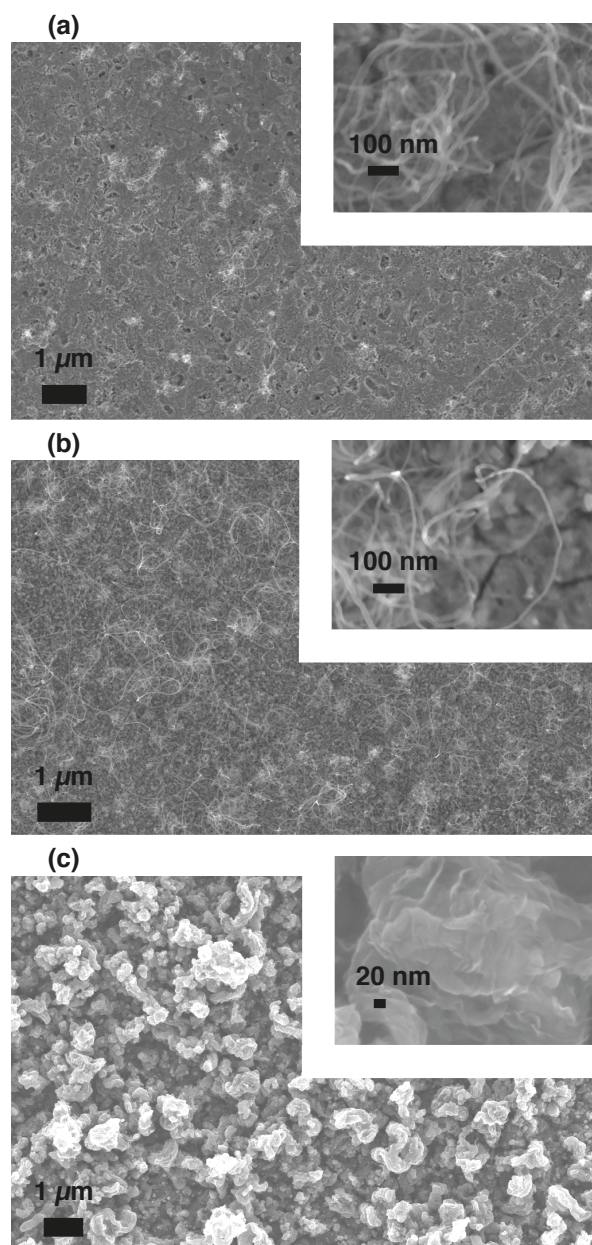


Figure 3.7 – SEM images of MWCNTs (a-b) and nanographene-shaped flakes (c) at low and high magnification (insets) deposited on Pt and obtained from FeNPs (a), FeNC (b) and FeC (c), respectively (annealing time: 10 minutes, carbon growth time: 5 minutes, growth temperature: 750°C).

The selectivity of the present integration approach is clear from SEM image of nanographene-shaped flakes shown in Fig. 3.8.

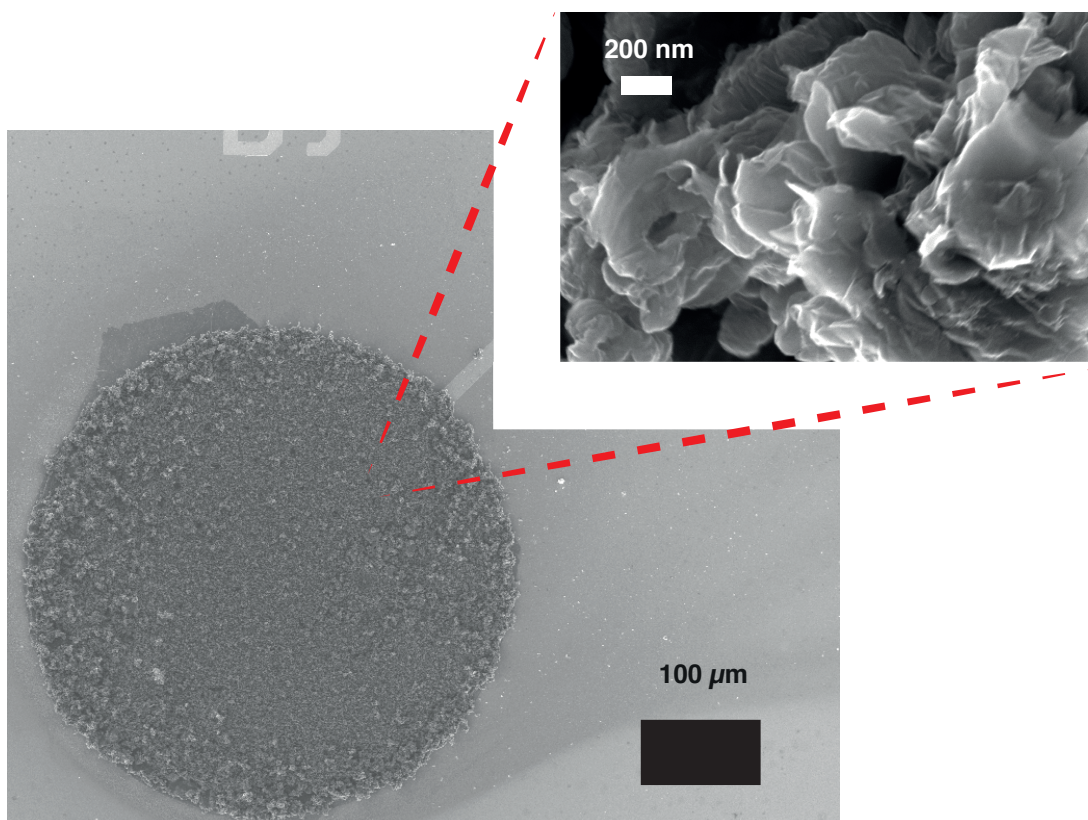


Figure 3.8 – Top view of a nanostructured Pt electrode with nanographene-shaped flakes.

3.3.3 Effect of the deposition parameters

The effect of different deposition variables on the resulting carbon materials was investigated. The same kind of nanographene-shaped flakes was observed when the growth parameters were changed (temperature, flow of the carbon gas, annealing time). An increase in yield resulted from a prolonged carbon growth time and greater catalyst thickness.

Diameter of MWCNTs grown on FeNPs was of (16.9 ± 3.2) nm after 3 minutes of annealing, almost unvaried with respect to that obtained after an annealing of 10 minutes ((15.4 ± 4.0) nm). From FeNC, MWCNT diameter after 3 minutes of annealing was slightly different from that computed by using 10 minutes of annealing ((19.5 ± 5.3) nm and (13.7 ± 3.2) nm, respectively - Fig. 3.9 (a-b)). A shorter annealing time limits the Fe film dewetting, resulting in bigger Fe nanoparticles and, thus, in larger MWCNTs. Indeed, the average diameter of the FeNPs was (14.5 ± 5.3) nm and (16.0 ± 4.7) nm after 10 and 3 minutes of annealing, respectively, while the change of the particle size was more evident from FeNC: (14.2 ± 3.9) nm after 10 minutes and (21.7 ± 8.9) nm after 3 minutes of annealing.

Chapter 3. Direct and selective integration of carbon nanomaterials by a CVD process on a microfabricated Si-based multipanel device

Under the standard growth conditions and by increasing only the carbon flow from 0.25 l/h to 0.5 l/h for both C_2H_2 and CO_2 , the diameter of CNTs unvaried ((11.5 ± 2.1) nm) when grown from FeNPs. Conversely, the doubling of the carbon flow promotes the formation of CNTs with a broader range of diameters (10-70 nm) from FeNC. This is due to the catalytic activation of larger Fe nanoparticles if the furnace is fed with a higher carbon flow, which in turn gives rise to nanotubes with larger diameters (Fig. 3.9 (c)).

The effect of tripling the carbon growth time (from 5 to 15 minutes) was also considered. The average diameter of the tubes grown from FeNPs ((15.8 ± 4.2) nm) unvaried. On the contrary, the diameter of the tubes doubled when obtained from FeNC ((34.9 ± 6.4) nm - Fig. 3.9 (d)). It is reasonable to assume that, in the presence of available catalyst, a prolonged carbon feed results in MWCNTs with more graphitic layers.

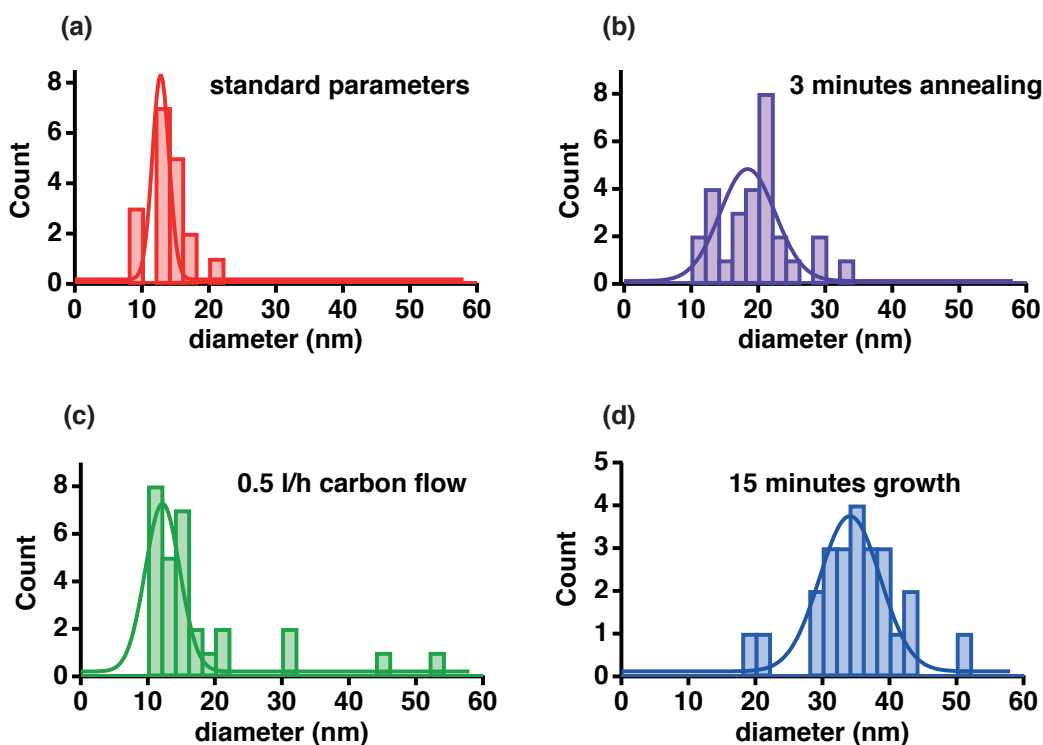


Figure 3.9 – Diameter distribution of MWCNTs produced from FeNC under different growth conditions (first deposition (a), reduced annealing time (b), doubled flow of the carbon precursors (c), tripled carbon growth time (d)).

3.3. Syntheses at high temperatures from Fe catalyst

Then, the influence of the growth temperature on the average MWCNT diameter was evaluated. In general, the MWCNT diameter increased by reducing the growth temperature. The formation of thick and short CNTs was observed at 600°C (Fig. 3.10). When FeNC was used as catalyst, the CNT diameter increased more as the temperature decreased than using FeNPs. Lowering the temperature means that less Fe is catalytically active for CNT nucleation and so the growth kinetics is reduced. This phenomenon results in a decrease of the CNT yield.

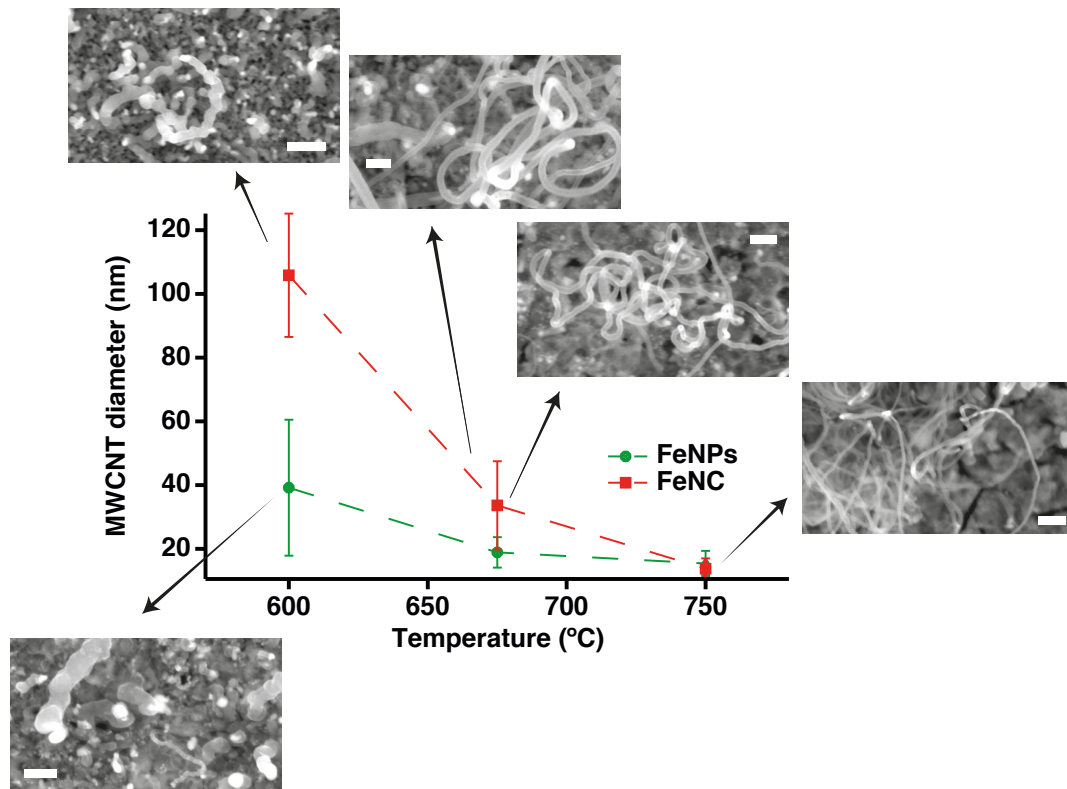


Figure 3.10 – Evolution of the MWCNT diameter with the temperature in case of growths from FeNPs (green line) and from FeNC (red line). SEM images of MWCNTs were selected for each deposition condition (bars: 100 nm).

More in general, it is not possible to exclude the presence of carbon nanofibers together with CNTs in some samples. This is especially true when the catalytically active particles have a big size (e.g., lower synthesis temperature, shorter time interval of annealing).

3.3.4 Micro-Raman spectroscopy

The Raman spectrum of carbon materials consists of three typical bands [123, 124]: D, is the defect- and disorder-induced band ($\approx 1350 \text{ cm}^{-1}$), G that is a measure of the graphitic lattice quality ($\approx 1580 \text{ cm}^{-1}$) and the G' band - overtone of the D peak, $\approx 2710 \text{ cm}^{-1}$ - is also sensitive to the density of defects. The relative integrated peak ratios were considered for the structural evaluation of the materials [123]. For comparison purposes, spectra of amorphous carbon and of graphite were acquired by micro-Raman spectroscopy together with our carbon deposits (Fig. 3.11). The smaller I_d/I_g and *full width at half maximum* (FWHM) and the higher $I_{g'}/I_g$ and $I_{g'}/I_d$ are, the higher is the degree of crystallinity. Indeed, amorphous carbon (red spectrum in Fig. 3.11) shows FWHM of D and G peaks larger than those of other carbon materials (see green spectrum of graphite in Fig. 3.11 for comparison) and the G' peak is completely absent, sign of a disordered material. On the other hand, G' is slightly evident in the spectrum of graphite that shows also a G peak sharper than that of amorphous carbon. The G peak of graphite presents a characteristic shoulder that is due to the structural disorder indicative of sp^2 bonded carbon.

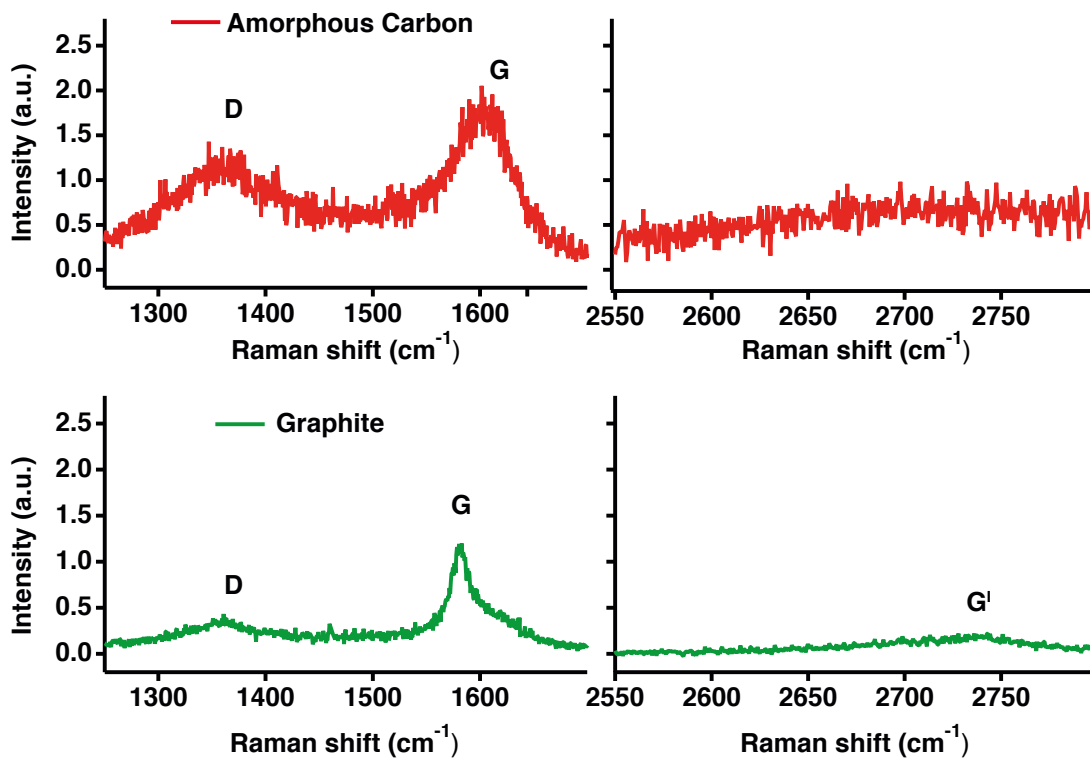


Figure 3.11 – Raman spectra of amorphous carbon (red) and of graphite (green).

The ratio I_d/I_g does not show substantial changes among MWCNTs with diameters in the range 10-20 nm ($I_d/I_g \approx 1$). Conversely, a strong increase of I_d/I_g was observed for wider and shorter tubes (≈ 1.7) grown at 600°C , indicating a less perfect crystalline lattice [121] (see blue and pink spectra in Fig. 3.12). The high defect density of these tubes was also confirmed by the

3.3. Syntheses at high temperatures from Fe catalyst

simultaneous decrease of both $I_{g'}/I_g$ and $I_{g'}/I_d$ ratios [124]. The values of the FWHM of all the three peaks were found to be approximately $20\text{--}30\text{ cm}^{-1}$ higher for CNTs grown at 600°C than for MWCNTs fabricated at higher temperatures, indicating the presence of more disordered and amorphous carbon in the samples prepared at 600°C [125].

Nanographene-shaped flakes showed the lowest value of I_d/I_g (≈ 0.6) and the highest $I_{g'}/I_g$ and $I_{g'}/I_d$ ratios (approximately 3 and 5, respectively) (see violet spectrum in Fig. 3.12). The ratio $I_{g'}/I_g$ resulted to be 9 times higher than that measured from graphite. Also $I_{g'}/I_d$ showed a very high value (13 times higher than graphite).

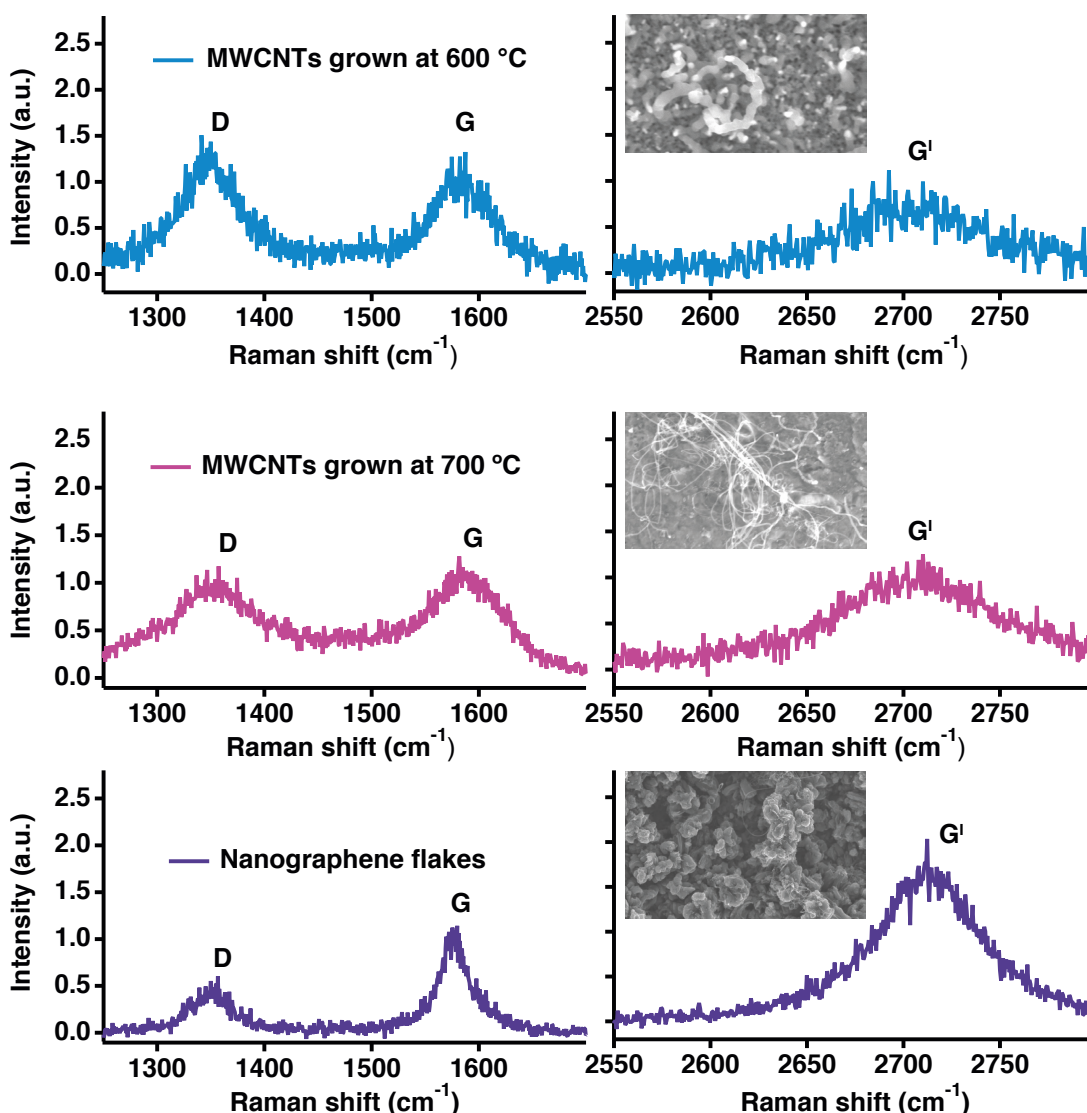


Figure 3.12 – Raman spectra of MWCNTs grown at 600°C (blue) and at 750°C (pink) and of nanographene flakes (violet).

Narrow peaks characterise these carbon nanostructures. FWHM values were about 45 cm^{-1} ,

Chapter 3. Direct and selective integration of carbon nanomaterials by a CVD process on a microfabricated Si-based multipanel device

35 cm^{-1} and 65 cm^{-1} for G, D and G' peaks, respectively. The G band does not present the characteristic shoulder of graphite-based materials. In addition, the position of the G' peak was about 20 cm^{-1} lower than that related to graphite. This peak is also sharper and almost 4 times more intense than the G' peak of graphite. Considering these findings, it is possible to assert that flakes of nanographene were grown from FeC electrodeposited on Pt [126]. Generally Ni and Cu are used as catalysts to grow graphene [127]. Fe layer represents a valuable possibility to produce graphene flakes. In this case, the use of acetylene as the carbon source has been demonstrated to allow a drastic reduction of the growth temperature during the process. This is extremely promising for the direct integration of graphene onto devices with electronic circuits [128]. Up to now, only few studies focus on graphene deposited onto Fe [129] due to the difficulty to control carbon diffusion and precipitation, with consequent formation of mixed phases. Our experimental study reports for the first time the deposition of graphene flakes onto electrodeposited Fe. It is reasonable to assume that a very thin layer of iron remains between the graphene flakes and the Pt. The objective of the present work was to avoid the use of a dielectric underlayer (placed between Pt and iron) for growing carbon nanostructures that would have created a high contact resistance. Certainly, a coupling carbon nanostructures-metal is still present even if a thin layer of iron is interposed between the two materials.

3.4 Growths down to CMOS compatible temperatures

Many efforts have been made so far to integrate carbon nanomaterials onto CMOS-sensors [130, 131, 132] since the compatibility of their fabrication with the low-cost CMOS technology is extremely useful to implement a full parallel process. The most common techniques to integrate carbon nanostructures onto small electrodes are not scalable to the CMOS wafers. The CVD technology is well-known to be easily scalable to wafer size and well-established in the semiconductor industry. However, common CVD systems, as that one described in Section 3.3, usually work at high growth temperatures (>600 °C for CNTs and >1000 °C for graphene) to grow carbon nanomaterials. These temperatures are not compatible with conventional CMOS processes causing irreversible material stresses that inevitably compromise the normal operation of the device with on-board electronic components. To make the whole process compatible with the electronics, the upper limit growth temperature is 450 °C [133]. Recently, many efforts have been made to lower the synthesis temperatures for fabricating graphitic nanomaterials. Nessim *et. al.* have already reported the CNT synthesis on metals at CMOS compatible temperatures by thermal decomposition of the hydrocarbon/hydrogen gas mixture. The nanofabrication consisted of only CNTs and was carried out on Pd and Ta in a non-selective way. Instead, for electrochemical sensing, the need is to grow on specific sites made of Pt or Au of a platform [134]. The present section describes the integration of carbon nanomaterials onto Pt WEs of a microfabricated device by a CVD process down to 450 °C.

3.4.1 Catalyst electrodeposition

In Section 3.3 syntheses and characterisation of carbon nanomaterials from Fe catalyst at temperatures ranging from 600 °C to 750 °C are presented. Below 600 °C, Fe on Pt was proven to be catalytically inactive by using our CVD system. To decrease the synthesis temperature, a previous study was considered in which the maximum yield of MWCNTs was obtained by using Fe/Co alloy as catalyst in a molar ratio 2:1 [115]. The electrodeposition of Fe₂Co was optimised for both catalyst NPs and coatings. Fe₂Co NPs resulted from solutions with equimolar concentrations of the two metals (average molar ratio: 2.15 ± 0.11). On the other hand, Fe₂Co coatings were obtained from sulphate solutions of Fe and Co in a molar ratio 2:1 (average molar ratio from coatings with different thicknesses: 2.12 ± 0.05).

3.4.2 Growths on catalyst nanoparticles

Sparse rolls of MWCNTs with an average diameter of (34.4 ± 19.4) nm were synthesised by using FeCoNPs (Fig. 3.13 (a)). Longer, denser and larger MWCNTs (average diameter: (52.7 ± 22.6) nm) with intercalated nanographite were observed by triplicating the deposition time (from 5 to 15 minutes; Fig. 3.13 (b) and (c)).

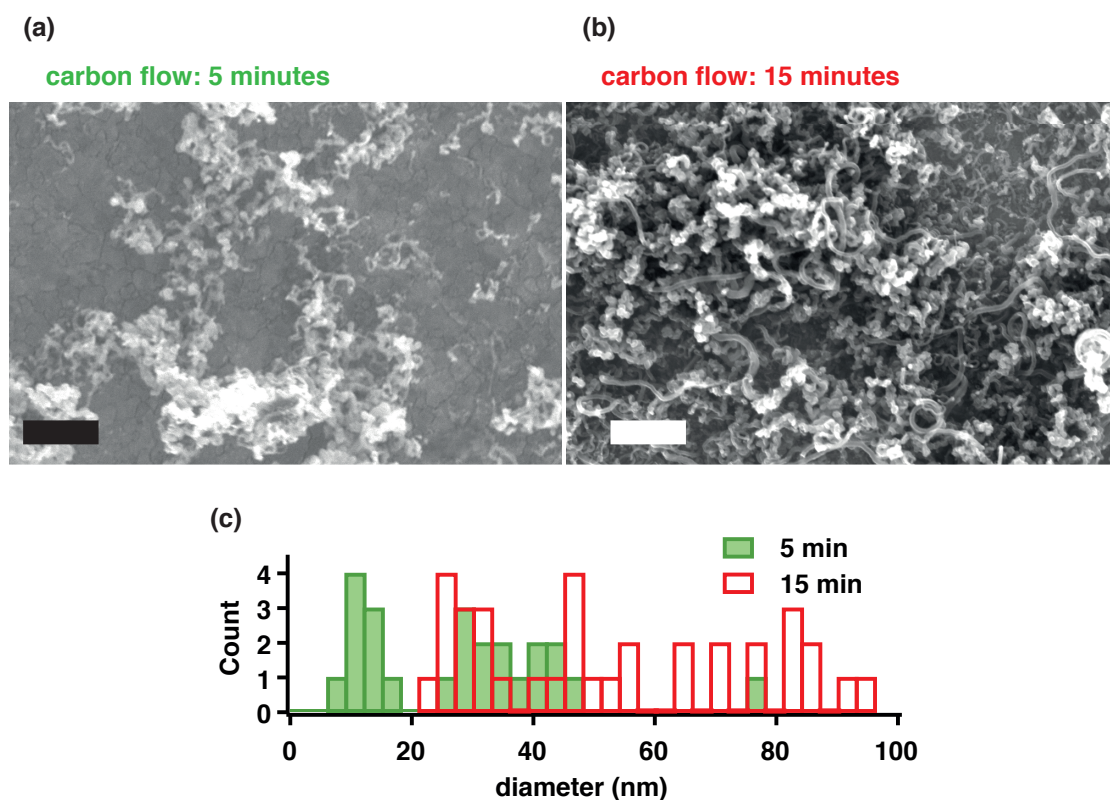


Figure 3.13 – SEM images of carbon nanomaterials fabricated on FeCoNPs at 600 °C under 5 (a) and 15 (b) minutes of carbon flow. Bars: 1 µm. (c) Diameter distribution of MWCNTs produced under two different growth times: 5 (green bars) and 15 (red bars) minutes.

Chapter 3. Direct and selective integration of carbon nanomaterials by a CVD process on a microfabricated Si-based multipanel device

Fig. 3.14 shows that a narrower diameter distribution results by lowering the synthesis temperature. In addition, the average diameter decreases going down with the temperature (from (34.4 ± 19.4) nm at 600 °C to (26.5 ± 6.5) nm at 450 °C). No nanomaterials were grown at temperature lower than 450 °C.

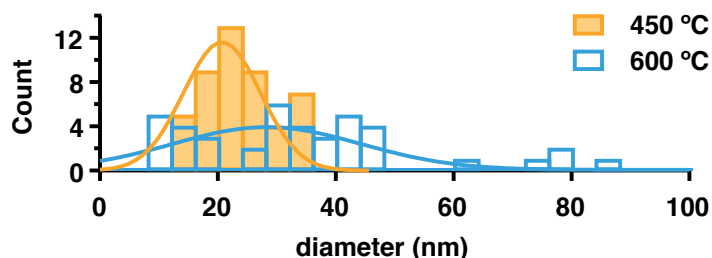


Figure 3.14 – Diameter distribution of MWCNTs grown from FeCoNPs at 600 °C (blue) and at 450 °C (yellow).

3.4.3 Growths on catalyst coatings

Fig. 3.15 (a-c) shows SEM images of carbon growths obtained at 600 °C on FeCoC electrodeposited for different intervals of time. As the Fe₂Co thickness increased, the amount of MWCNTs decreased and nanographite simultaneously started to be produced. The highest carbon yield was obtained from thicker catalyst layers.

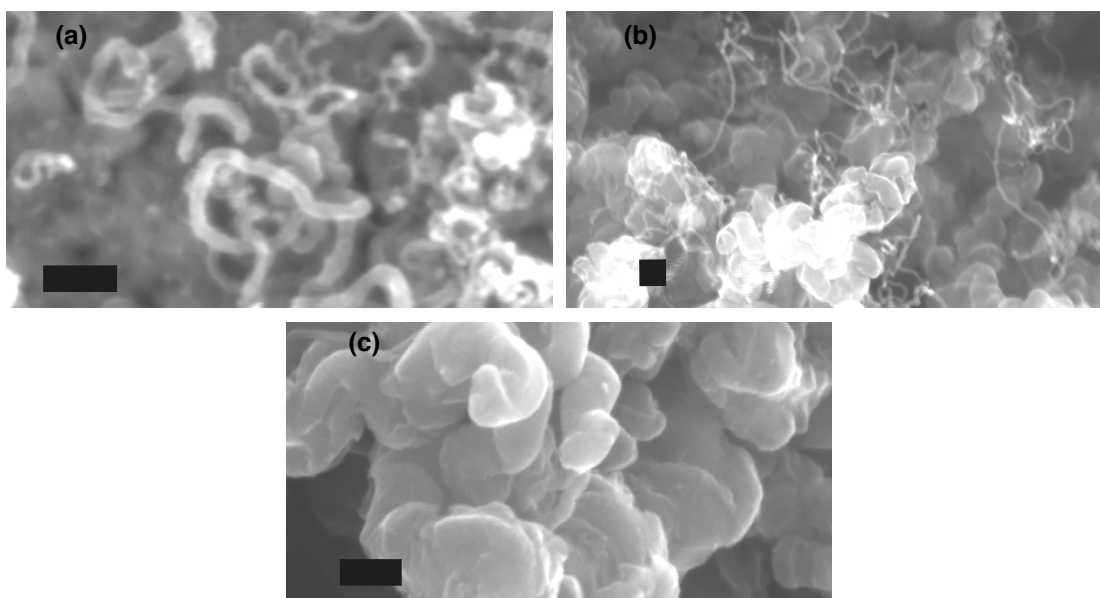


Figure 3.15 – SEM images of MWCNTs (a), hybrid MWCNTs-nanographite (b) and nanographite (c) (bars: 100 nm) obtained on FeCoC deposited at -1.4 V for 4, 15 and 30 s, respectively.

3.4. Growths down to CMOS compatible temperatures

As clearly observable from Fig. 3.16, the MWCNT diameter increased passing from 2 to 4 s of deposited FeCoC. Nanofibers were grown from even thicker catalyst layers (8 s of FeCoC deposition). From 15 s of electrodeposited FeCoC, hybrid nanographite/MWCNTs were produced and the amount of MWCNTs decreased by prolonging the FeCoC deposition time. The MWCNTs diameters decreased once nanographite started to be synthesised.

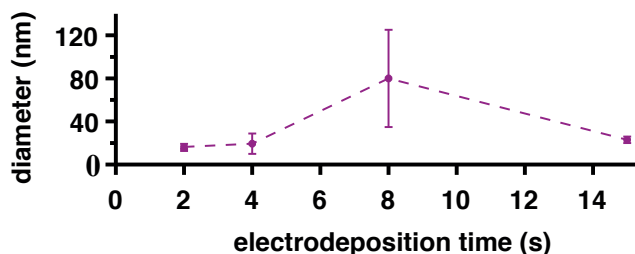


Figure 3.16 – Effect of the Fe₂Co electrodeposition time on the nanotube/nanofiber diameter.

The synthesis of nanographite started from thinner catalyst layers at temperatures lower than 600 °C (Fig. 3.17 (a) and (b)). Also at temperatures lower than 600 °C, once graphite grew, the MWCNT diameter drastically decreased (Fig. 3.18). Very thick catalyst layers were not catalytically active at 450 °C.

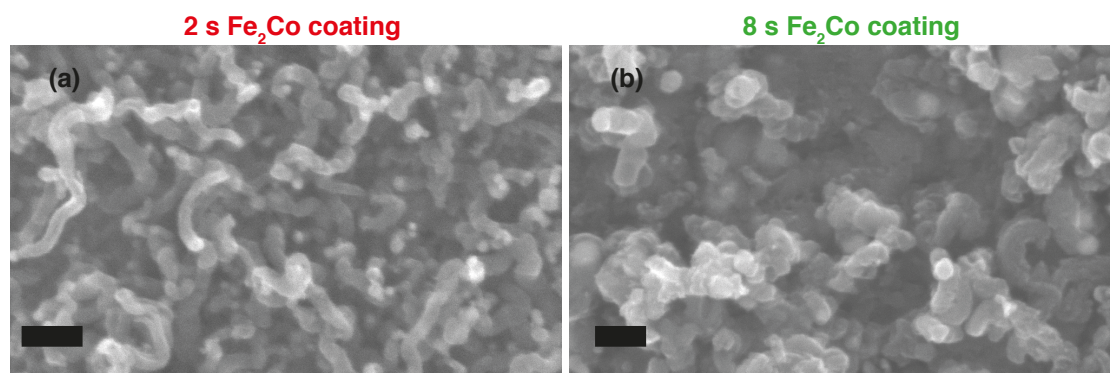


Figure 3.17 – SEM images of nanomaterials produced at 525 °C on 2 s (a) and 8 s (b) of deposited catalyst layers. Bars: 100 nm.

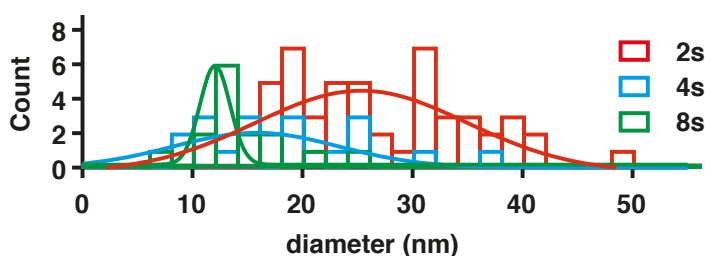


Figure 3.18 – Diameter distribution of MWCNTs grown on FeCoC layers deposited for 2 s (red), 4 s (cyan) and 8 s (green) at 450 °C. The more nanographite is present on the sample, the smaller is the average CNT diameter.

Chapter 3. Direct and selective integration of carbon nanomaterials by a CVD process on a microfabricated Si-based multipanel device

Raman spectra reveal much about the nature of the produced nanomaterials. As expected, the presence of nanographite determined the shift of the G and D bands towards lower values and of G' peak towards higher values, the decrease of the I_d/I_g , $I_{g'}/I_g$, $I_{g'}/I_d$ ratios and sharper G' peaks in accordance with the literature [121]. Peak ratios, peak positions and values of the FWHM are reported in Table 3.1.

Table 3.1 – Values of I_d/I_g , $I_{g'}/I_g$, $I_{g'}/I_d$, D, G and G' positions and FWHM of MWCNTs and MWCNTs/nanographite produced at 525 °C.

	MWCNTs	hybrid MWCNTs+nanographite
I_d/I_g	1.7 ± 0.2	1.5 ± 0.1
$I_{g'}/I_g$	6.8 ± 1.5	1.3 ± 0.2
$I_{g'}/I_d$	4.0 ± 0.9	0.9 ± 0.1
D (cm^{-1})	1352.0 ± 1.3	1349.0 ± 1.4
G (cm^{-1})	1599.7 ± 0.8	1585.9 ± 1.9
G' (cm^{-1})	2678.1 ± 2.4	2698.3 ± 1.0
FWHM(D) (cm^{-1})	109.1 ± 9.7	99.0 ± 3.6
FWHM(G) (cm^{-1})	63.8 ± 4.4	76.2 ± 0.2
FWHM(G') (cm^{-1})	267.1 ± 23.9	116.4 ± 9.3

3.4.4 Implementing two successive growths

In the previous subsections, it was proven the possibility to grow CNTs and nanographite down to 450 °C, the upper limit temperature that makes possible to grow nanomaterials directly onto the front-end of CMOS data acquisition circuits. Generally, only amorphous carbon grows below 600 °C when a CVD system based on thermal decomposition of C_2H_2 is used. Here, the oxidative dehydrogenation reaction of CO_2 and C_2H_2 [115] was proven to improve the activity and the lifetime of the catalyst on metallic surfaces resulting in carbon nanomaterial growths down to 450 °C.

An enhanced electrochemical response and an improved incorporation and stabilisation of biomacromolecules is expected for high yield of nanomaterials due to the increase in the surface area. However, a decrease of carbon yield was observed by lowering the synthesis temperature. To increase the yield of the nanostructures, two successive depositions at 450 °C were implemented.

3.4. Growths down to CMOS compatible temperatures

After the first synthesis, thin layers of Fe_2Co were deposited on the top of nanomaterials grown at the first stage (Fig. 3.19 (a)). Then, a second synthesis was carried out under identical growth conditions. From 2 s of electrodeposited catalyst, more carbon nanomaterials, namely graphitic nanopetals with intercalated MWCNTs (Fig. 3.19 (b)), were obtained. Electrodeposition of Fe_2Co for 4 s results in an increase of only the CNT quantity.

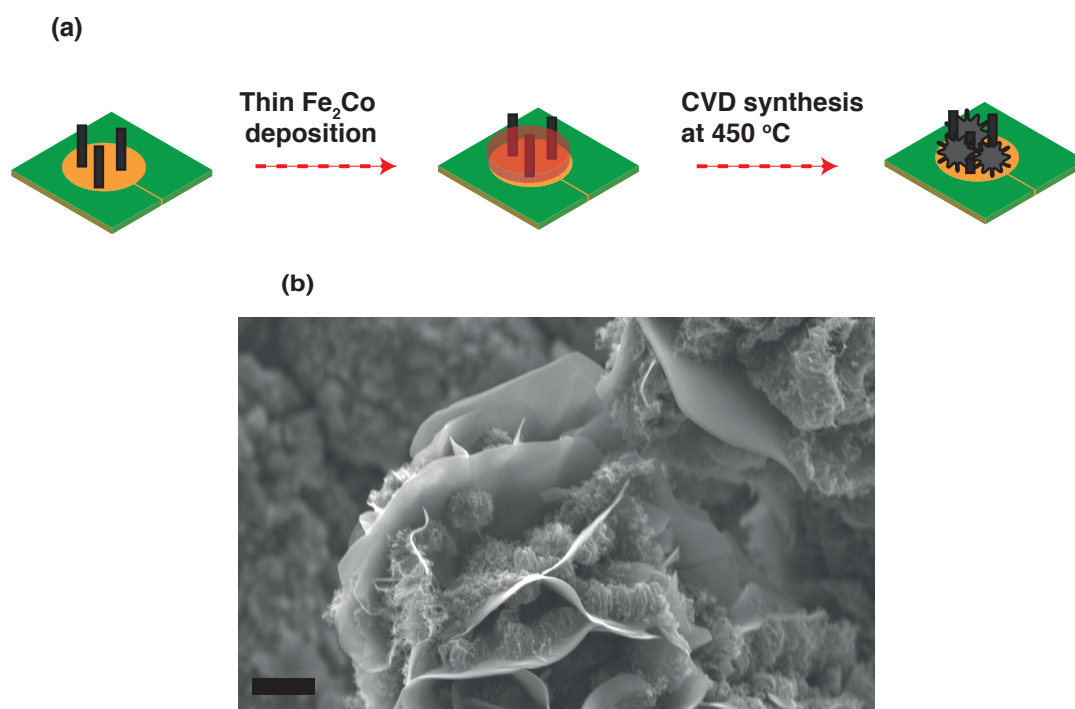


Figure 3.19 – Two-step CVD process (a); graphitic nanopetals and MWCNTs grown onto 2 s of FeCoC electrodeposited onto the overgrown substrate (b).

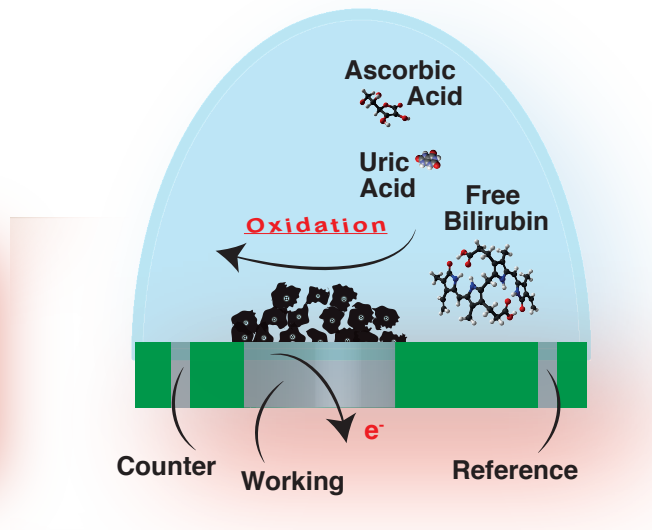
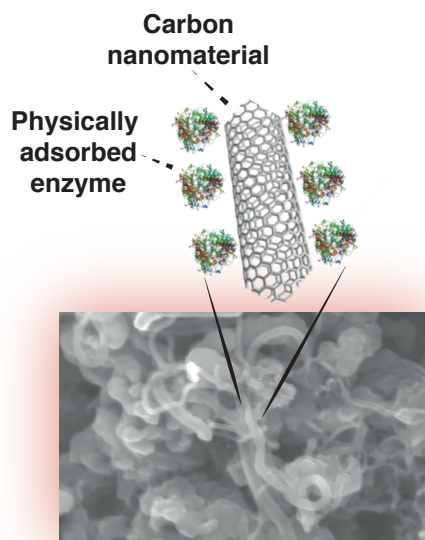
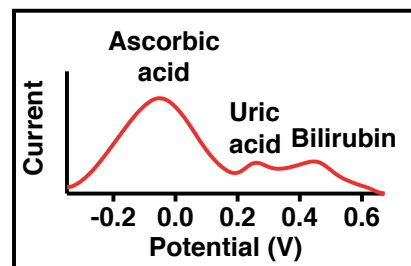
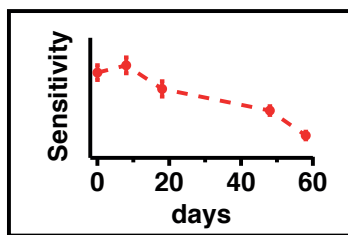
A surface with CNTs not fully covered with FeCoC catalysed the formation of very thin graphitic petals. Other authors have already synthesised graphitic nanopetals by plasma CVD whose growth was catalysed by CNTs [135] and carbon nanofibers [136]. For synthesising MWCNTs, carbon radicals dissolve and precipitate by the metal catalyst forming tubular nanostructures. On the other hand, when MWCNTs remain exposed, carbon radicals insert in the sidewalls and tips of the CNTs (not fully covered by the catalyst layer) forming graphite branches that evolve in graphitic petals.

3.5 Summary and contributions

Conventional methods present in the literature to integrate carbon nanomaterials on miniaturised microfabricated metal electrodes are time-consuming, expensive, hardly-reproducible and often require the incorporation of additives such as polymers that mask the "nano" effects and compromise the lifetime of the device due to the polymer-matrix instability in water-based solutions. This chapter presents a novel protocol to precisely integrate by CVD process a wide variety of carbon nanomaterials on Pt electrode-array of a microfabricated device. An accurate control of the type of material (nanographene flakes, nanographite, MWCNTs), of the MWCNT diameter and of the yield was possible by changing nature and thickness of the catalyst, deposition parameters and growth temperatures. For a successful implementation of this nanostructuring approach the following challenges were overtaken:

- selectivity with respect to one working electrode of the platform (some carbon nanomaterials such as CNTs tend to spontaneously grow on dielectric layers)
- growths on catalyst directly deposited on Pt electrodes avoiding the commonly used thin buffer dielectric layers that could create high contact resistance
- nanodeposits were obtained down to 450°C, the upper limit temperature compatible with CMOS processes, opening the possibility to a direct integration nanostructures/front-end of CMOS data acquisition circuits.

4 Electrochemical characterisation of MWCNTs, nanographite and their hybrids grown by CVD on a Si-based device



Carbon nanostructures have received particular attention in the field of electrochemical sensing for: (a) the determination of electroactive biomarkers at their very low physio-pathological concentration range (nanomolar range); (b) the discrimination of electroactive compounds from

Chapter 4. Electrochemical characterisation of MWCNTs, nanographite and their hybrids grown by CVD on a Si-based device

interfering species normally present in human fluids. By using common electrodes, all the highly electroactive compounds oxidise at almost the same potential resulting in the overlapping of the voltammetric response. (c) enhancing the biodetection performance since carbon nanomaterials can mimic an "enzyme friendly" environment.

The present chapter studies the electrochemical properties of carbon nanostructured electrodes. More in detail, Section 4.1 focuses on enhanced electrochemical behaviour of devices incorporating carbon nanomaterials for sensing electroactive biomarkers (bilirubin) and metabolites thanks to an immobilised oxidase (lactate). Section 4.2 investigates the performance characteristics of CVD carbon nanostructures grown on a microfabricated Si-based sensor. Their sensing capabilities for a direct (uric acid, bilirubin) and enzyme-mediated detection (glucose) are examined. The biofouling resistance of CVD carbon nanomaterials is investigated. A comparative study with the very well-known carbon nanomaterial integration approaches is in Section 4.3. Lastly, the main topics and contributions of the chapter are summarised in Section 4.4.

4.1 Demonstration of the superior performance of MWCNT-based electrodes

In this section, an electrochemical study of bare *screen printed electrodes* (SPEs) coated or not with a film of MWCNTs for detecting bilirubin (BR) is presented first. MWCNTs were considered as a type of carbon nanomaterials. The sensor response was investigated in the physio-pathological concentrations of BR by CV also in the presence of albumin up to its normal level. The concentrations of free BR (not complexed to albumin) were measured in the range typical of newborn jaundice (Subsection 4.1.1). Then, the research objective in Subsection 4.1.2 is to gain fundamental insight into the performance of lactate oxidase (LOx)-MWCNT-based SPEs by evaluating sensing parameters and stability over time. The kinetic behaviour of the enzyme either immobilised on MWCNTs and in solution was studied.

4.1.1 Direct detection of bilirubin

Bilirubin (BR) is a compound of bile produced when the liver breaks down old red blood cells. Two main types of BR are present in human fluids: conjugated and unconjugated BR. Conjugated BR forms a complex with gluconic acid, which renders it water soluble. Unconjugated BR tends to bind to albumin [137]. Therefore, the amount of free unconjugated BR, which is electrochemically detectable, depends on the concentration of albumin and on the intrinsic ability of albumin to bind BR. This binding is very important for the neutralisation of the neurotoxic effect of unconjugated BR. In particular, in neonates, high BR levels in the blood (jaundice) easily occur leading to brain damage and cerebral palsy if untreated. Very often, pathological levels of BR are associated with the accumulation of its oxidised form, a pigment called *biliverdin* (BV) [138]. Therefore, considering the diagnostic significance of BR, the development of an inexpensive device for BR detection is of enormous interest.

4.1. Demonstration of the superior performance of MWCNT-based electrodes

At a first stage, the present subsection aims to proof the superior electrochemical performance of graphite SPEs modified with a film of MWCNTs than bare electrodes to detect physiological concentrations of BR in absence of albumin. The possibility of detecting this molecule with albumin in solution is a problematic aspect that should be considered for developing a BR sensor because of the considerable reduction of the free available electroactive BR from micromolar to nanomolar range caused by the formation of complexes BR-albumin in human blood. By using the modified SPEs, the signal decrease for albumin levels up to its normal concentration is shown. The sensor response for normal albumin level and concentrations of BR corresponding to severe jaundice is studied. It is worth mentioning that the electrochemical detection of BR with MWCNTs has been carried out in previous works but using ferrocene as mediator and only without albumin in solution [139].

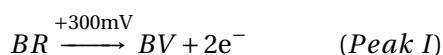
Methods MWCNTs with carboxyl-modification (-COOH groups) were purchased as powder (90% purity) from DropSens. MWCNTs had an average diameter of 10 nm and the length ranged between 1 and 2 μm . A solution of MWCNTs in chloroform was prepared with a concentration of 1 mg/ml. Sonication of the samples was carried out to obtain a homogeneous solution. Stock solutions of BR (Sigma) were prepared in *dimethyl sulfoxide* (DMSO) solvent (10 mM) and then diluted in *phosphate-buffered saline* (PBS; 10 mM pH 7.4) in the presence or absence of fixed bovine albumin concentrations ranging from 0 to 30 mg/ml. PBS and albumin were purchased from Sigma. Since BR is photosensitive, measurements were carried out in a dark room. Electrodes were nanostructured with MWCNT films by casting 30 μl of MWCNT-chloroform solution (six times 5 μl) onto the WE of carbon paste SPEs (model DRP-110) purchased from DropSens. Chloroform was allowed to evaporate from the electrode in between two subsequent deposition steps. The surface area of the WE was equal to 0.1256 cm^2 . The CE was also made of graphite, while the RE was made of Ag. The electrochemistry of BR was investigated by *cyclic voltammetry* (CV) with a Versastat 3 potentiostat (Princeton Applied Technologies). All the experiments were carried out under aerobic conditions at room temperature. For the measurements, the three electrodes were covered with 100 μl of BR-containing solutions. Multiple CVs were acquired using a potential window of -0.4/+0.8 V at a scan rate of 20 mV/s. BR concentrations ranged from 50 to 150 μM (physiologic jaundice) by 25 μM steps or from 200 to 400 μM (severe jaundice) by 50 μM steps. Electrodes with and without a MWCNT layer were tested. Five multiple CVs were applied, alternating them until two subsequent voltammograms overlapped. The adsorption of BR onto a large variety of carbon nanomaterials has been reported [140]. In addition, the well-known adsorption of albumin to the electrodes could also affect the electrochemical measurements [141]. For these two reasons, in between two subsequent measurements a cleaning procedure was performed by applying potential pulses as reported in [142]. Briefly, 3000 fast potential pulses between -0.4 and +0.8 V were repeated 3 times followed by 10 multiple CVs (potential window -0.4/+0.8 V and scan rate 100 mV/s). An oxidation peak currents (Peak II) identified in the V cycle of multiple CVs was used to calculate the sensing parameters. A cubic baseline was subtracted to the voltammogram part (positive scan) between 0 and +0.7 V. The Igor Pro (Wavemetrics, Lake

Chapter 4. Electrochemical characterisation of MWCNTs, nanographite and their hybrids grown by CVD on a Si-based device

Oswego, OR, USA) software was employed to fit the peaks using Gaussians [143] that described their shapes sufficiently well for our aims. The sensitivity and the LOD were calculated as described in Appendix A.

Results Among several possible strategies, the preparation of the BR stock solution using NaOH was deemed unsuitable because of the rapid precipitation [144] and oxidation of BR. Solutions prepared with Tris Buffer (0.05 M, pH 8.0, albumin 30 mg/ml) were excluded since no peak current could be measured with either bare or nanostructured electrodes. DMSO, instead, was proved to be an efficient solvent for BR. Dilutions were prepared in PBS. Solutions were stable for some hours with regard to both oxidation and precipitation of BR just under dark conditions. All the solutions were prepared before the experiments because of the high instability of BR in solutions.

CVs of BR revealed three oxidation processes. The first investigated concentration range (50-150 μM) corresponded to the BR level in the case of physiologic jaundice [145]. The positions of the first two peaks remain almost unvaried in the presence or absence of MWCNTs. The third process occurs only with MWCNT film-based SPEs. All these oxidation processes were found to be irreversible under our experimental conditions, as some authors have already shown [139, 146]. Fig. 4.1 shows the increase of the first (Peak I) and of the second (Peak II) oxidation peak for increasing BR concentration. The lowest electrochemical response was found when bare SPEs (Fig. 4.1 (a)) rather than MWCNT film-cast electrodes were used (Fig. 4.1 (b)). Peak I and II are attributed to the oxidation of BR and of BV, respectively.



This assumption is supported by the disappearance of Peak I when exposing a BR solution to light for a week (Fig. 4.1 (c)). Inset in Fig. 4.1 (c) shows the change in colour from orange to green after this period of light exposure. On the other hand, Peak III is still present under these working conditions and is related to the purpurine oxidation to choletelin



The detection was performed by considering Peak II since its increase exhibited a better linearity. When bare electrodes were used, the sensitivity was one order of magnitude lower than using the modified electrodes (Fig. 4.1 (d)). The intersample reproducibility was studied at MWCNT-SPEs resulting in satisfactory results. Indeed, for 150 μM BR, the average peak potential and the average peak current from four measurements are (471 ± 3) mV and (1.8 ± 0.1) μA , respectively (n=4). The average sensitivity and LOD were (87.6 ± 11.3) $\mu\text{A}/(\text{mM cm}^2)$ and (15.5 ± 1.9) μM , respectively (n=4).

4.1. Demonstration of the superior performance of MWCNT-based electrodes

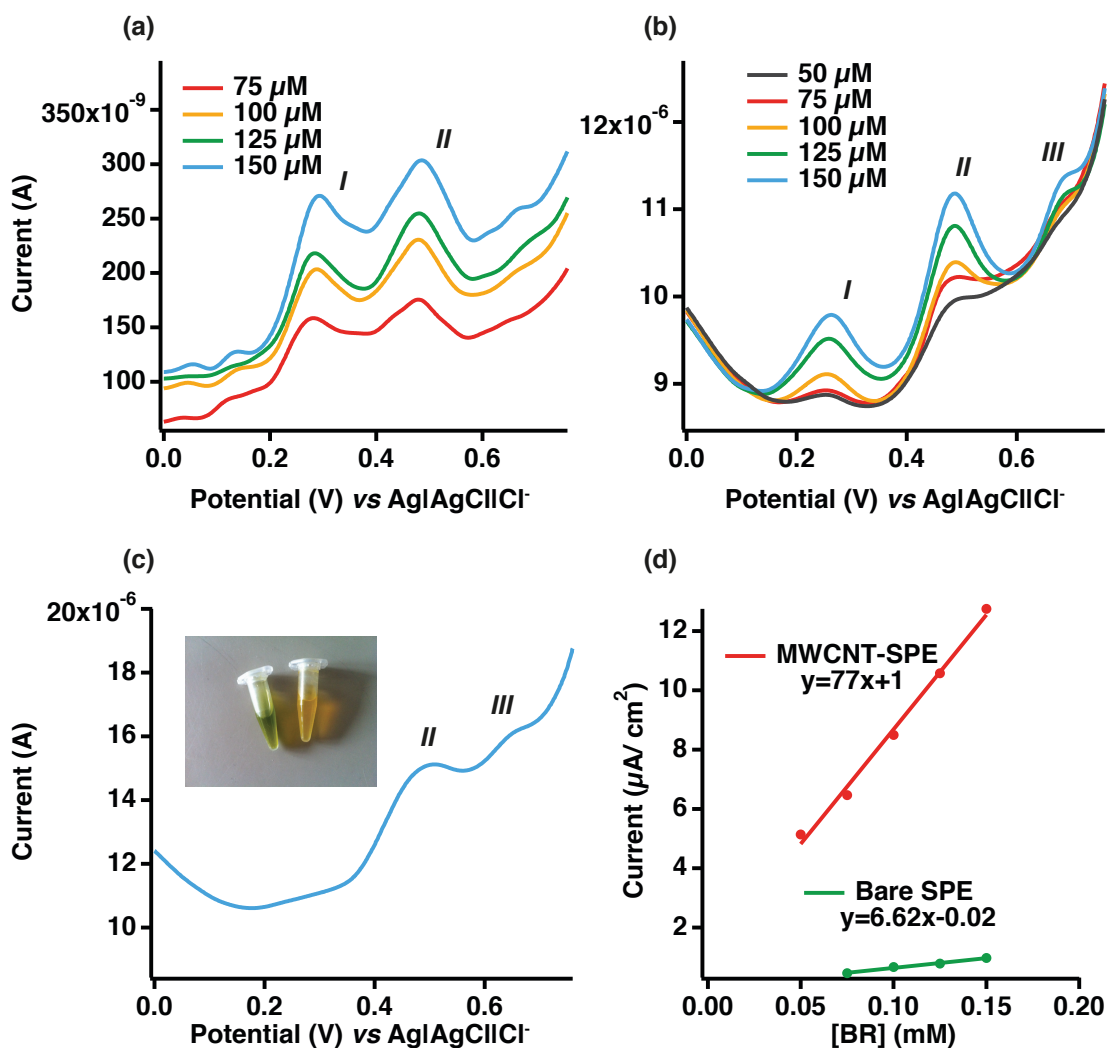
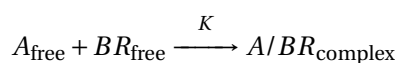


Figure 4.1 – Peaks in CVs at 20 mV/s by changing the BR concentration. Bare (a) and modified (b) SPEs. Disappearance of Peak I after a week of light exposure (BR concentration: 500 μM; scan rate: 20 mV/s) at modified SPEs and change in colour from orange to green of the BR solution due to the BR oxidation in BV (c). Calibration curves at bare and modified SPEs (d).

As mentioned before, unconjugated BR is transported in human plasma bound to a protein carrier, albumin. The association mechanism of BR with albumin can be described by the following equation



Chapter 4. Electrochemical characterisation of MWCNTs, nanographite and their hybrids grown by CVD on a Si-based device

The relation between free albumin, free BR and their complex in terms of concentrations can be expressed by the equilibrium constant [137]

$$K = \frac{[A/BR_{\text{complex}}]}{[A_{\text{free}}][BR_{\text{free}}]} \quad (4.1)$$

Because free BR is present in a small amount relative to the albumin-BR complex, the concentration of the latter is almost equal to that of the unconjugated BR. Therefore, Eq. 4.1 can be written as

$$[BR_{\text{free}}] = \frac{[BR_{\text{unconjugated}}]}{K([A_{\text{free}}] - [BR_{\text{unconjugated}}])} \quad (4.2)$$

The reduction of the peak current as a function of increasing albumin concentrations is shown in Fig. 4.2 (a). The most evident drop in current occurs when passing from 0 mg/ml to 1 mg/ml of albumin concentration. When passing from 1 to 30 mg/ml of albumin in solution, the current decreased only slightly.

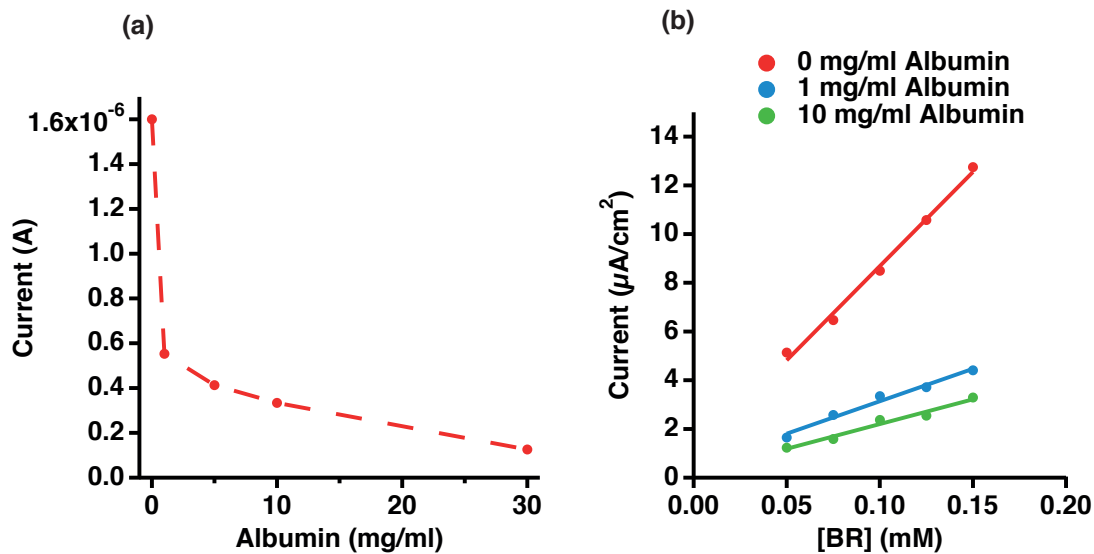


Figure 4.2 – Peak response *vs* albumin concentration (albumin: 0, 1, 5, 10, 30 mg/ml; BR concentration: 150 µM; albumin-BR molar ratios: 0.1, 0.5, 1, 3) (a). Calibration plots for the BR detection in the presence of the following albumin concentrations: 0, 1, 10 mg/ml (b).

Fig. 4.2 (b) shows the decrease of the sensitivity for increased albumin concentrations in solution. With a concentration of albumin equal to 1 mg/ml, the sensitivity decreases almost three fold (26.6 µA/(mM cm²)) with respect to a detection performed in absence of albumin. By

4.1. Demonstration of the superior performance of MWCNT-based electrodes

using 10 mg/ml albumin, the sensing performance further declines (sensitivity: 20.3 $\mu\text{A}/(\text{mM cm}^2)$). The voltammetric response of the MWCNT film-sensor becomes negligible for normal albumin concentration (30 mg/ml). However, the signal is still present even if the molar ratio between BR and albumin is equal to 0.33. Other authors [147] were unable to measure BR for BR/albumin molar ratios below 1.

In very severe jaundice, levels of BR for newborns are greater than 15 mg/dl ($\approx 250 \mu\text{M}$) up to 30 mg/dl ($\approx 500 \mu\text{M}$). The sensitivity was 26.5 $\mu\text{A}/(\text{mM cm}^2)$. The experiments performed in the presence of a normal level of albumin and BR concentrations typical of a severe jaundice, leaves open the possibility to use the proposed sensor to monitor the BR level in babies affected by severe newborn jaundice.

4.1.2 Enzyme-mediated detection of lactate

An important biocompound that needs a reliable monitoring is lactate. The determination of lactate is significant for different aspects of human health [148] (e.g., sepsis, sport). The detection of lactate have been carried out using mainly lactate oxidases immobilised onto the electrodes. In this subsection, the detection mechanism utilised for lactate detection is the same of that described in Subsection 2.1.4 of Chapter 2 regarding the indirect glucose sensing with GOx *via* H_2O_2 electrooxidation. Here, a *lactate oxidase* (LOx) was immobilised on electrode surfaces. To prove the capability of carbon nanomaterials to be an excellent support system for the incorporation of enzymes, a LOx was immobilised on MWCNT-based SPEs. Also in this case, MWCNTs were taken as example of carbon nanomaterials. The protein immobilisation on MWCNTs was accomplished by physical adsorption that is the most promising incorporation strategy to preserve the catalytic activity of the enzyme over time. The final aim of the subsection is to study the reproducibility and the sensing performance after subsequent usages and over time of LOx-MWCNT-SPEs. The kinetic behaviour of the LOx was studied in solutions with increased concentration of lactate while the enzyme was in solution (spectroscopic measurements) or kept dried on MWCNTs (amperometric measurements).

Methods Total protein concentration was determined by UV-Vis absorbance measurements with a Nanodrop ND-1000 spectrophotometer using an extinction coefficient of 51.340 $1/(\text{M cm})$. LOx activity was assayed by quantifying H_2O_2 produced from the coupling reaction with horseradish peroxidase (HRP) (0.05 mg/ml) and 0.5 mM 2,2'-azino-bis(3-ethylbenzothiazoline-6-sulphonic acid) (ABTS). Spectrophotometric LOx activity assays were routinely carried out in a 96-well plate at 35 °C with 40 mM lactate in 0.1 M PBS at pH 7 using a Bio Tek Synergy Mx spectrophotometer and initiated by adding enzyme solution. The assay volume was 200 μl . Oxidation of ABTS was monitored at 420 nm ($\epsilon=36,0001/(\text{M cm})$). The temperature optimum was recorded between 20 °C and 50 °C by following ABTS oxidation in an assay volume of 3 ml using a magnetically stirred, temperature controlled cuvette device. Enzymatic assays were performed in triplicate. One unit was defined as the amount of enzyme that oxidised 1 μM of substrate per minute. In summary, LOx activity was determined with purified enzyme

Chapter 4. Electrochemical characterisation of MWCNTs, nanographite and their hybrids grown by CVD on a Si-based device

by applying a peroxidase-coupled spectrophotometric method, using ABTS and H₂O₂ as substrates at 37 °C in 0.1 M PBS pH 7, which was determined to be optimal.

MWCNT-SPEs were prepared as described in Subsection 4.1.1. The enzyme (26 µg; concentration: 0.4 mg/ml; activity: 9 U/ml) was additionally cast onto the nanostructured WE and kept overnight at 4 °C before the experiments. Each biosensor was washed with distilled water (Eau ultra pure, type Ultra Clear™, BLANCLABO) before the experiments. Control experiments (MWCNT-SPEs and H₂O₂ [149], MWCNT-SPEs and lactate [150], enzyme adsorbed on SPEs and lactate [150]) confirm that lactate electrochemical detection drastically improves by the use of MWCNTs with adsorbed LOx. Lithium l-lactate in form of lyophilised powder (Sigma) was dissolved in distilled water.

The electrochemical response was investigated by *chronoamperometry* (CA) at room temperature under aerobic conditions by applying a fixed potential of +650 mV. A Versastat 3 potentiostat (Princeton Applied Technologies) was used to record the data. Routinely, the electrodes were dipped into a stirred 0.01 M PBS at pH 7.4 with a volume equal to 25 ml. The normal concentration of lactate was varied by steps of 0.2 mM successively adding 10 µl of 0.5 M lactate stock solution in the 25 ml of synthetic buffer. The error related to the final concentration obtained with this type of dilution is negligible. The time-step depended on the current stabilisation. The sensitivity and the LOD were computed according to the procedure described in Appendix A.

Results The sensitivity and the LOD of the lactate sensor (n=4) were among the best reported in the literature (sensitivity= (35.5 ± 3.1) µA/(mM cm²) and LOD= (5.4 ± 2.0) µM)[148]. Subsequent CAs (n=6) did not alter significantly the sensor performance (sensitivity= (31.0 ± 2.5) µA/(mM cm²) and LOD= (18.6 ± 6.9) µM).

The long-term stability of the biosensors is an important measure of its usefulness in a clinical or commercial setting. LOx-MWCNT-SPEs (n=4) showed an unvaried sensitivity ((38.5 ± 3.3) µA/(mM cm²)) one week after the preparation of the modified electrodes. These findings suggest that this biosensor can be applied as a reusable lactate detector within 7 days. Fig. 4.3 shows the sensitivity values computed for four modified electrodes (n=4) within 60 days after their fabrication. It is worth mentioning that the enzyme remains active up to 50 days after the LOx deposition.

4.1. Demonstration of the superior performance of MWCNT-based electrodes

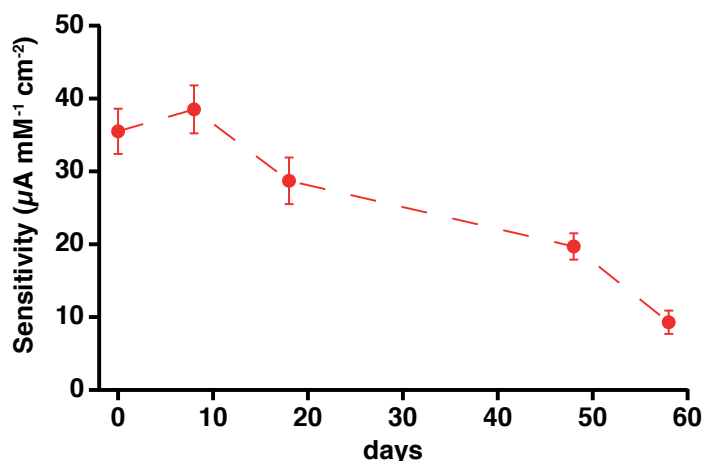


Figure 4.3 – Sensitivity of LOx-MWCNT-SPEs (n=4) computed after 1, 8, 18, 48 and 58 days from the enzyme deposition.

The kinetic behaviour of LOx physically adsorbed onto the MWCNT-based surfaces was evaluated by using electrochemical methods and compared with that of the enzyme in solution (spectrophotometric measurements). Fig. 4.4 (a) shows the CA recorded with a LOx-MWCNT-SPE for successive additions of lactate into a PBS solution. Enzymatic conversion rate of a substrate to a product *vs* the substrate concentration is described by the Michaelis-Menten equation that gives hyperbolic profiles [151]. The equivalent electrochemical equation for the Michaelis-Menten kinetics is

$$I = I_{\max}[S]/(1 + K_m) \quad (4.3)$$

where K_m indicates of the enzyme kinetics on the biosensor surface, I is the steady-state current resulting from the addition of substrate, I_{\max} is the maximum current when the sensor shows saturation by adding analyte to the solution and $[S]$ is the concentration of the substrate. Some enzymes exhibit completely different kinetics [151]. The “stepped” drop in current shown in Fig. 4.4 (a) and starting from ≈ 4 mM of lactate is due to an atypical enzyme kinetics called substrate inhibition [151]. The equivalent electrochemical equation for the substrate inhibition kinetics is

$$I = I_{\max}/(1 + K_m/[S] + [S]/K_i) \quad (4.4)$$

where K_i is the inhibition constant [151]. Interestingly, spectrophotometric studies of the enzyme in solution confirms the substrate inhibition kinetics obtained by electrochemical investigations (Fig. 4.4 (b) and (c)).

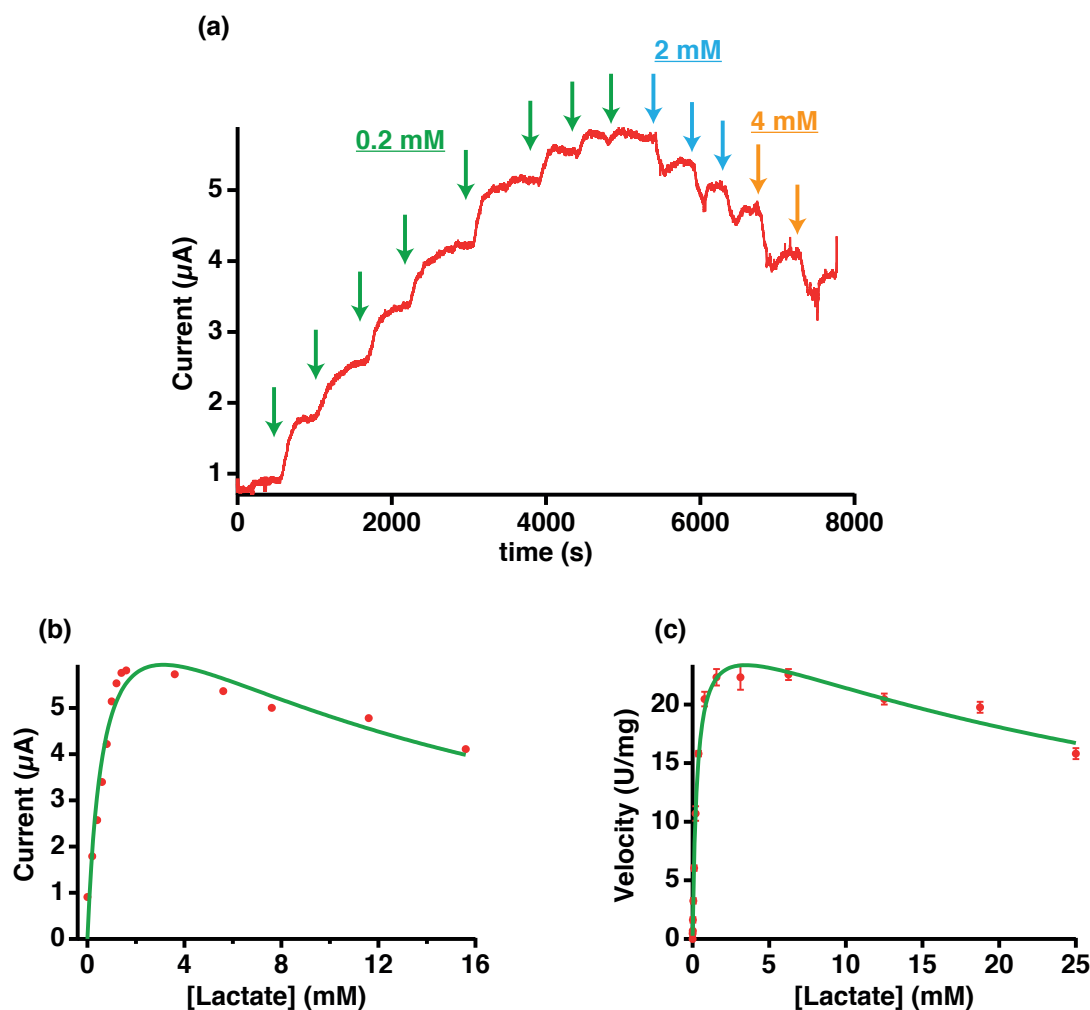


Figure 4.4 – CA acquired with LOx-MWCNT-SPE on successive additions of lactate to a 0.01 M PBS solution pH 7.4 (a). Plot of the observed steady-state current *vs* lactate concentration. The electrochemical equivalent of the substrate inhibition phenomenon (in green) was used for data fitting (b). Kinetic plot obtained with LOx for the lactate oxidation by spectrophotometric measurements (coupled enzymatic assay). The specific activity (U/mg) was plotted *vs* the substrate concentration. The substrate inhibition equation was used for the data fitting (in green). Error bars refer to triplicate determinations (c).

4.2 Detection of molecules by carbon nanomaterials CVD-grown onto microfabricated sensors

In this section, the effectiveness of electrodes nanostructured by CVD-grown MWCNTs, nanographite and their hybrids after a chemical activation is proven by both direct and enzyme-mediated electrochemical detection of medical markers. The suitability of these nanostructures for devices of clinical use is demonstrated. Electrode materials to test hu-

4.2. Detection of molecules by carbon nanomaterials CVD-grown onto microfabricated sensors

man samples should not have a certain tendency to biomolecule adsorption (biofouling). In this section, biofouling of the modified electrodes is also characterised as a function of the exposure time to a real biosample. Finally, two conventional integration methods of carbon nanomaterials are used for a comparative study towards the direct detection of H_2O_2 and the indirect sensing of glucose *via* electrooxidation of H_2O_2 , product of GOx reaction.

4.2.1 Methods

Before the measurements, the nanostructured electrodes were treated in H_2SO_4 (Sigma) solution (6 M) for 5-6 hours [60] to improve the electrochemical properties and to facilitate the enzyme immobilisation by physical adsorption. All the measurements were conducted with Autolab potentiostat controlled by Nova software. The IgorPro software was used for the data analysis. CE and RE of the electrochemical platform, both made of Pt, were used if not declared differently.

UA was purchased from Sigma. A H_3BO_3 buffer solution (0.02 M; pH 9.0 at 25 °C) was employed to prepare 3.57 mM UA stock solution. It was freshly prepared before each measurement. All the dilutions were carried out in PBS (10 mM, pH 7.4) solution. AA (Sigma) was dissolved in distilled water obtained with Eau ultra pure, type Ultra Clear™ (BLANCLABO). Measurements of UA were carried out by *differential pulse voltammetry* (DPV) at 10 mV/s in 0.01 M PBS (pH 7.4) between -0.1 and +0.45 V at bare electrode and between -0.2 and +0.35 V at nanostructured electrodes.

BR (Sigma) was dissolved in DMSO solvent (10 mM). Dilutions were prepared in PBS (0.01 M, pH 7.4, Sigma) containing bovine albumin (30 mg/ml, Sigma) or in human serum (VWR). Measurements were carried out in a dark room. CVs and *square wave voltammetries* (SWVs) were acquired at scan rates of 10 mV/s and 15 mV/s, respectively, for concentrations of BR ranging from 100 to 500 μM by steps of 100 μM . The sensitivity and the LOD were calculated as described in Appendix A. Peak positions and peak heights were computed by curve fitting with Gaussians. A cubic baseline was subtracted before each fitting.

Electrodes were modified with GOx from Roche by physical adsorption (drop casting). A solution of the enzyme was freshly prepared (concentration: 15 mg/ml) and 1 μl was cast onto the electrodes and kept overnight at 4 °C in a dry condition. The concentration of D-glucose (Sigma) was increased by steps of 100 μM up to 500 μM and of 250 μM up to 4.5 mM (applied potential: +650 mV). Enzyme-electrodes were stored at 4 °C under dry conditions. Electrodeposition of GOx-Chitosan on CVD carbon nanomaterials was carried out by applying a fixed potential of +1.5 V *vs* Ag QRE from a GOx-polymer dispersion (GOx: 55 mg/ml; Chitosan 0.7%w/v in a water solution, pH 5) [55]. Cross-linking of GOx with glutaraldehyde was achieved by casting 1 μl of GOx solution (25 mg/ml, Roche in 2.5% glutaraldehyde) onto nanostructured electrodes. The solution of glucose was prepared at least the day before the measurements to allow the glucose mutarotation [152] and stored in the fridge at 4 °C. To study the electrode fouling in biosample, a Dulbecco's Modified Eagle Medium (Gibco, Life

Chapter 4. Electrochemical characterisation of MWCNTs, nanographite and their hybrids grown by CVD on a Si-based device

Technologies) containing phenol red was employed. CAs of glucose were performed in PBS (10 mM, pH 7.4, Sigma) at +650 mV.

4.2.2 Nanomaterial activation

Before studying the electrochemistry of the nanostructured Pt electrodes, the CVD-grown nanomaterials were activated. Treatments of pristine carbon nanostructures are necessary for three main reasons.

- Elimination of amorphous carbon that may negatively affect the electrochemical responses [153]
- Improvement of the electrochemical properties by creating edge-like-plane sites [45, 61]
- Decrease of hydrophobicity of the as-grown carbon nanomaterials because of the introduction of functional groups facilitating their functionalization with bioprobes [60, 61, 62].

Chemical, electrochemical and thermal treatments or combination of them are mainly used. Chemical modifications imply the use of strong acid or basic solutions more or less diluted, alone or mixed, at different temperatures [60, 61, 62]. This treatment produces edge-like-plane sites and functional groups, eliminating also impurities like amorphous carbon. Annealing procedures at moderate temperatures (400-500 °C) remove functional groups and purify graphitic nanomaterials from amorphous carbon [154]. Electrochemical treatment at a constant or variable potential can be also applied at carbon nanostructured electrodes immersed in an appropriate solution and resulting in the production of functional groups mainly on CNTs caps and graphene edges. This method was proven to be useful for the immobilization of enzymes in a covalent way [65]. Thermal annealing and electrochemical treatment of carbon materials are both very used procedures. However, these methods compromise the mechanical stability of the nanomaterials on the electrodes. In addition, electrochemical procedures are not suitable for our carbon materials because they produce functional groups and defects onto the graphene sheet edges and CNT caps [65]. Our carbon nanomaterials (nanoflakes, MWCNTs) are randomly oriented with respect to the Pt surface and extensively expose their walls. Therefore, a chemical activation was chosen. Carbon nanomaterials were pretreated in a sulphuric acid solution [60, 61, 62] and the activation time was optimised to avoid material detachment from the surface (6 hours). In our previous work, this treatment was proven to improve the electrochemical performance of CVD grown MWCNTs randomly oriented with respect to a Si substrate and to considerably decrease their hydrophobicity [45, 61, 62].

To prove the efficacy of this activation protocol, CVs in solution of ferricyanide, a very well-know defect-sensitive electroactive compound, were carried out before and after the acid activation. Since an increase in the number of defects is expected after the activation, treated nanostructures should lead to better electron transfer in electrochemistry.

4.2. Detection of molecules by carbon nanomaterials CVD-grown onto microfabricated sensors

Fig. 4.5 shows the faster heterogeneous electron transfer of carbon nanomaterials after the activation, more pronounced when electrodes nanostructured with high yield nanomaterials were used (Fig. 4.5 (b)). The peak-to-peak separation (ΔE_p) was 122 mV before and 103 mV after the acid treatment for low yield nanostructures (Fig. 4.5 (a)). It showed a more marked reduction at high yield nanostructured electrodes (260 mV before and 88 mV after the acid treatment; Fig. 4.5 (b)).

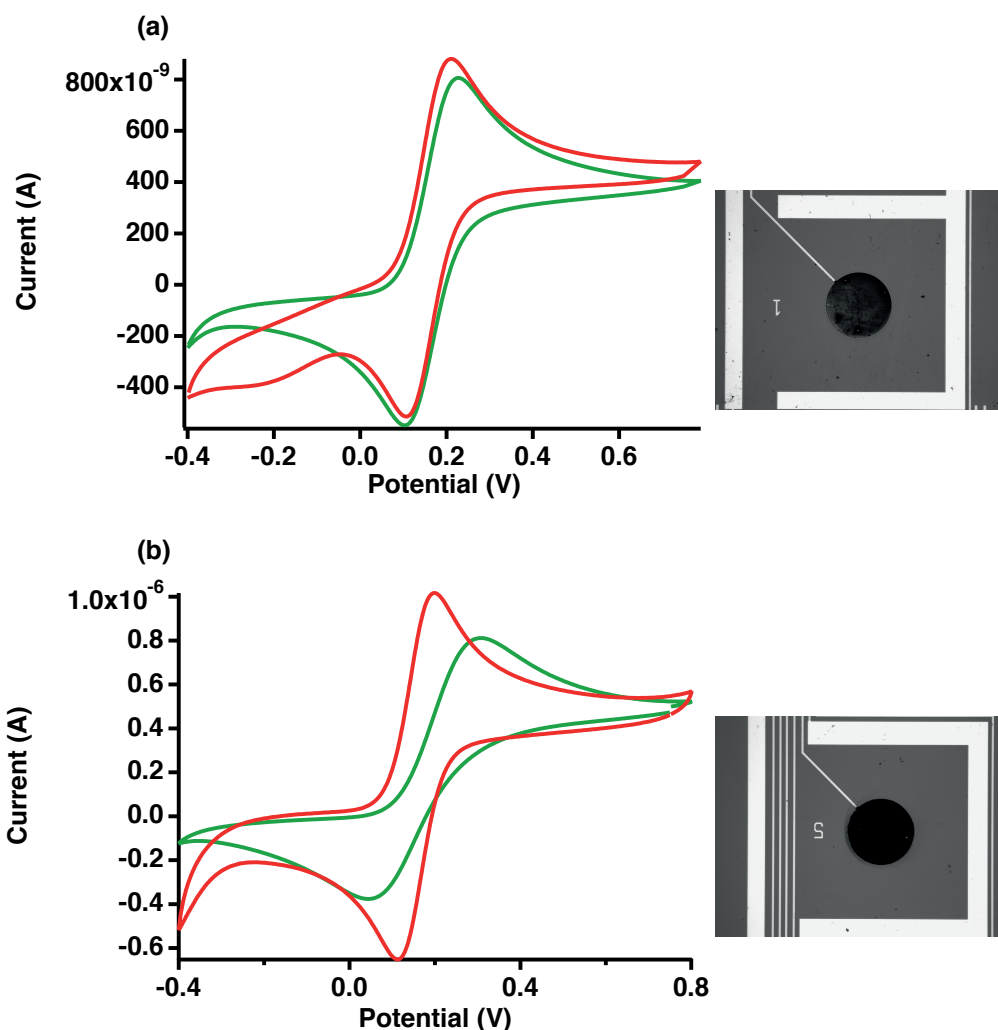


Figure 4.5 – CVs (V cycle) of nanostructured electrodes with hybrid MWCNTs/nanographite grown at 525 °C from 2 s of electrodeposited catalyst in 2.5 mM $K_3[Fe(CN)_6]$ /PBS (10 mM; pH 7.4) solution (a) and with hybrid MWCNTs/nanographite grown at 525°C from 8 s of electrodeposited catalyst in 2.5 mM $K_3[Fe(CN)_6]$ /PBS (10 mM; pH 7.4) solution (b). The green and red lines refer to CVs before and after the chemical activation in 6 M sulphuric acid, respectively. Potential window: -0.4/+0.8 V. Scan rate: 0.05 V/s. The effect of the treatment is evident from the increase of the peak current and the decrease of the peak-to-peak separation, both more pronounced for high yield nanostructured electrodes. Optical microscope images on the right.

Chapter 4. Electrochemical characterisation of MWCNTs, nanographite and their hybrids grown by CVD on a Si-based device

Both peak currents increased especially when high yield treated carbon nanostructures were employed (reduction peak current I_{pc} increased of $\approx 10\%$ and $\approx 30\%$ at low and high yield nanostructured electrodes, respectively).

Also an increase of the capacitive current, more evident when the electrode is covered with a largest amount of nanomaterials, demonstrates the efficiency of this treatment in forming defects and functional groups. Values of total capacitance for low and high yield carbon nanomaterials synthesised from Fe and Fe_2Co catalyst are also shown in Fig. 4.6 and Fig. 4.7, respectively. This activation step is very important also because it increases the number of sites enabling an efficient immobilisation of proteins.

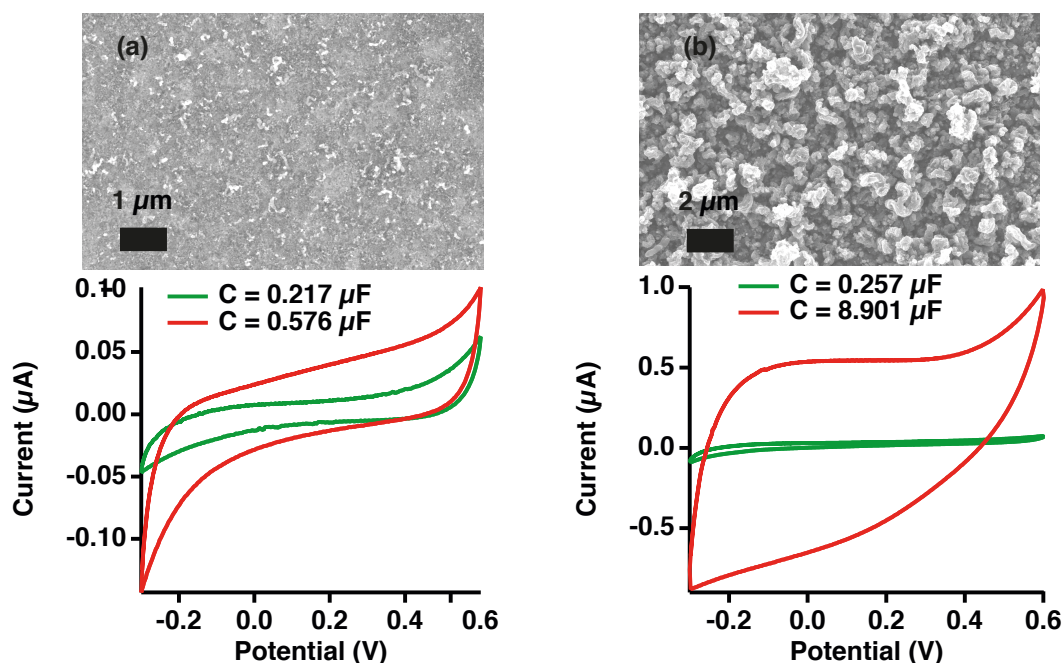


Figure 4.6 – CVs (V cycle) of electrodes nanostructured with MWCNTs (a), and with hybrid MWCNTs/nanographene (b) grown at 600 °C from Fe catalyst. Scan rate: 0.1 V/s. The green and red lines refer to CVs before and after the chemical activation in 6 M sulphuric acid, respectively. Solution: 10 mM PBS; pH 7.4. Potential window: -0.3/+0.6 V. The effect of the treatment is evident from the increase of the background current, more pronounced for high yield nanostructured electrodes. SEM images of the nanostructures are on the top of each subfigure.

4.2. Detection of molecules by carbon nanomaterials CVD-grown onto microfabricated sensors

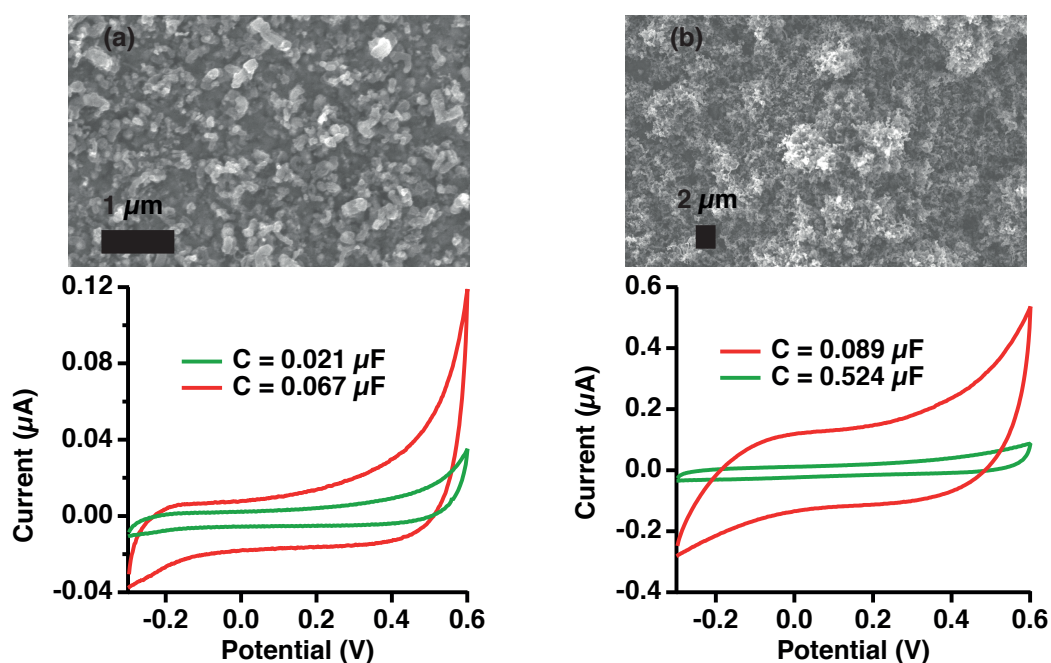


Figure 4.7 – CVs (V cycle) of electrodes nanostructured with hybrid MWCNTs/nanographite synthesised at 525 °C from 8 s of electrodeposited Fe₂Co (a) and grown at 600 °C from 15 s of electrodeposited Fe₂Co (b). Scan rate: 0.1 V/s. The green and red lines refer to CVs before and after the chemical activation in 6 M sulphuric acid, respectively. Solution: 10 mM PBS; pH 7.4. Potential window: -0.3/+0.6 V. The effect of the treatment is evident from the increase of the background current, more pronounced for high yield nanostructured electrodes. SEM images of the nanostructures are on the top of each subfigure.

To further confirm the efficacy of the activation, Raman spectra were taken before and after the treatment. The increase in the peak intensity in the frequency region beyond 2900 cm⁻¹ is indicative of the O-H stretching of acid-produced carboxylic groups. Table 4.1 (a) shows the increase of the ratios between the peaks related to the introduction of defects after the activation (G + D peak at 3000 cm⁻¹ and 2D2 peak at 3200 cm⁻¹) and the G peak.

Table 4.1 – Increase of $I_{(g+d)}/I_g$ and I_{2d2}/I_g ratios after the carbon activation.

	Before activation	After activation
$I_{(g+d)}/I_g$	0.42 ± 0.01	1.52 ± 0.62
I_{2d2}/I_g	0.213 ± 0.003	1.23 ± 0.54

4.2.3 Direct detection of interferences: the case of uric acid

To investigate the electrochemical behaviour of nanostructured electrodes for a direct detection of biomarkers, *uric acid* (UA) was considered as example of electroactive metabolite of significant importance in medical sensing. Fig. 4.8 (a) shows the improvement of the sensing parameters with the yield of the deposited carbon nanomaterials (sensitivity changes of two orders of magnitude and LOD of one order of magnitude).

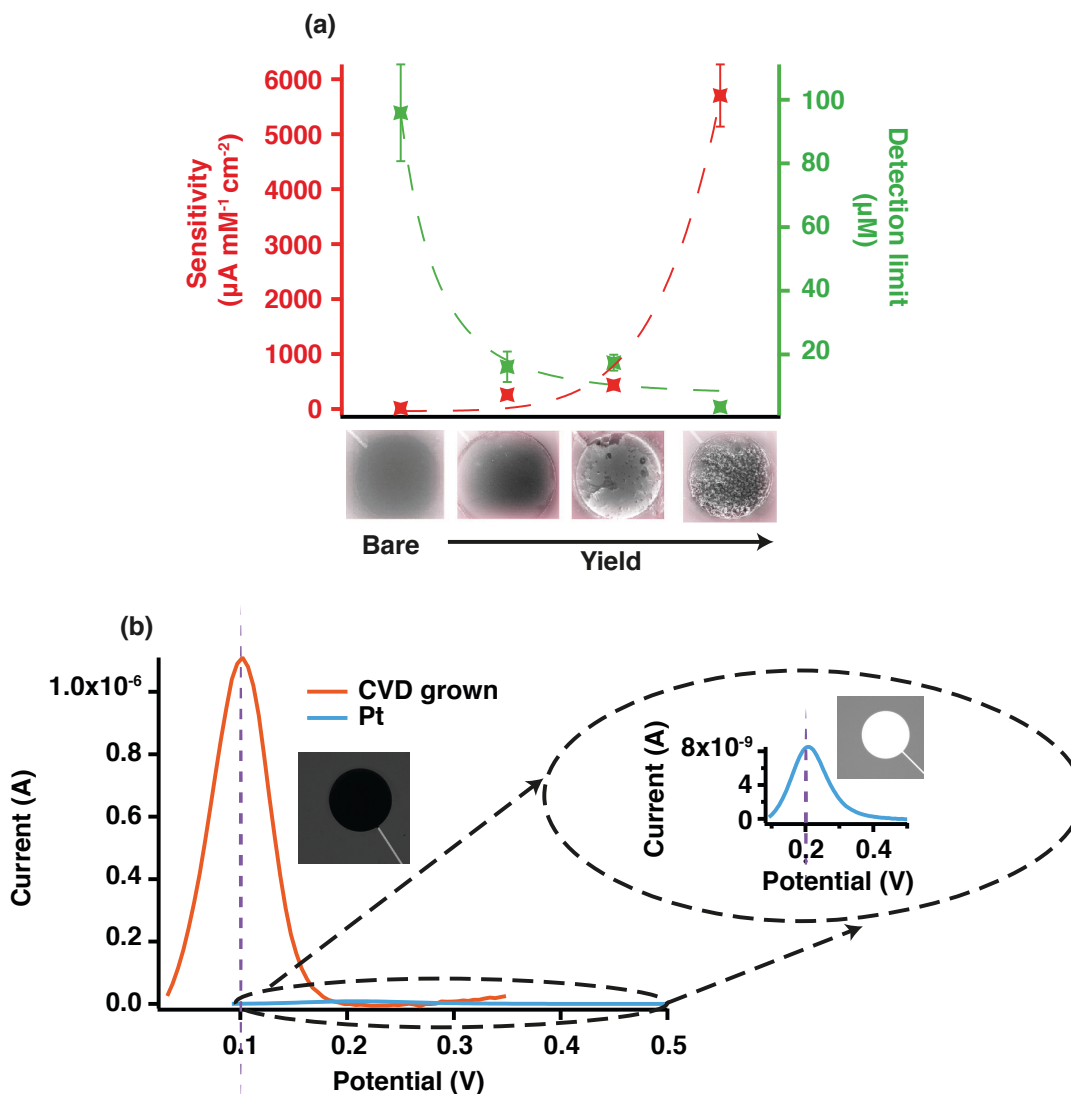


Figure 4.8 – Sensitivities and LOD by detecting UA at bare electrode, at electrodes with MWCNTs and with MWCNTs-nanographite grown at 525 °C and at 600 °C. Error bars refer to standard deviation of triplicate intrasample measurements (a). Difference of peak positions and heights by DPV at bare and nanostructured electrode (b).

4.2. Detection of molecules by carbon nanomaterials CVD-grown onto microfabricated sensors

Hybrid nanomaterials grown at 600 °C with the highest yield and consequently the largest surface area have shown the best sensing properties. Electrodes based on carbon nanomaterials attract UA thanks to weak interactions (e. g. hydrophobic, hydrogen bondings). The oxidative peak shifts towards less positive values which entails less required energy for the oxidation to occur at carbon nanostructured electrodes (from $\approx +200$ mV to $\approx +100$ mV; Fig. 4.8 (b)).

4.2.4 Direct detection of low metabolite concentrations: the case of bilirubin

Subsection 4.1.1 of the present chapter demonstrates the possibility to detect BR in the presence of normal levels of albumin for BR concentrations typical of severe jaundice with MWCNT-SPEs. The electrochemical determination of BR is challenging because the most part of BR is attached to albumin so the free BR concentration is very low (some hundreds of nanomolars). Moreover, other electroactive metabolites as UA and AA are normally present in human serum. By using common electrodes, BR and interfering species oxidise at almost the same potential resulting in overlapping of the voltammetric response. In this subsection, a Pt electrode nanostructured with CVD grown nanographite and having a geometric area 50-fold lower than that one of the SPEs is used as WE. The sensor capability to discriminate the oxidation peaks of BR, UA and AA is proven and studies regarding the BR peak identification in human serum are shown.

Fig. 4.9 shows a CV of nanographite modified electrode in solution containing 600 μM BR and a normal concentration of albumin (30 mg/ml). The three peaks fitted with Gaussian curves and related to the oxidation of BR (I) and of the BR products (II and III) are evident.

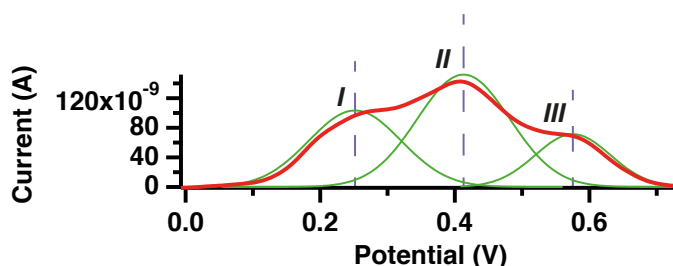


Figure 4.9 – Background subtracted voltammogram portion comprising the three oxidation peaks of BR at the nanostructured electrode (BR: 600 μM ; albumin: 30 mg/ml). Peak I: BR oxidation to BV. Peak II: BV oxidation to purpurine. Peak III: purpurine oxidation to choletelin.

SWV was then employed as a more sensitive analytical technique to detect concentrations of free BR in the respective physio–pathological range than CV. Fig. 4.10 (a) depicts the current peaks of the sensor measured for an increased BR concentration. The sensing parameters were evaluated by looking at the increase of Peak II as in Subsection 4.1.1 and from a linear regression of the plot peak currents *vs* concentrations of BR (Fig. 4.10 (b)). The sensitivity and the LOD were 154 $\mu\text{A}/(\text{mM cm}^2)$ and 56 μM , respectively.

Chapter 4. Electrochemical characterisation of MWCNTs, nanographite and their hybrids grown by CVD on a Si-based device

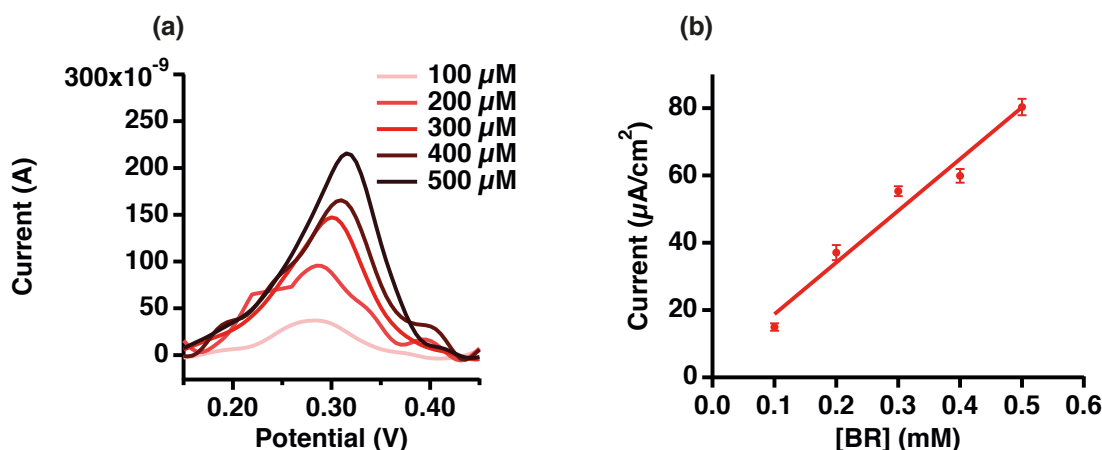


Figure 4.10 – SWVs in PBS solutions containing 100, 200, 300, 400 and 500 μM BR and a normal level of albumin (a). Calibration curve (b).

UA and AA are interfering species that oxidise at the same potential of BR by using common electrodes. The use of carbon nanomaterials has been already proven to be a powerful tool for the discrimination of the oxidation peaks of different metabolites in voltammetry [35, 42]. Therefore, the detection of BR in the presence of both AA and UA even in solutions with physiological levels of albumin (30 mg/ml) was examined. Fig. 4.11 shows the discrimination of the three metabolites by SWV.

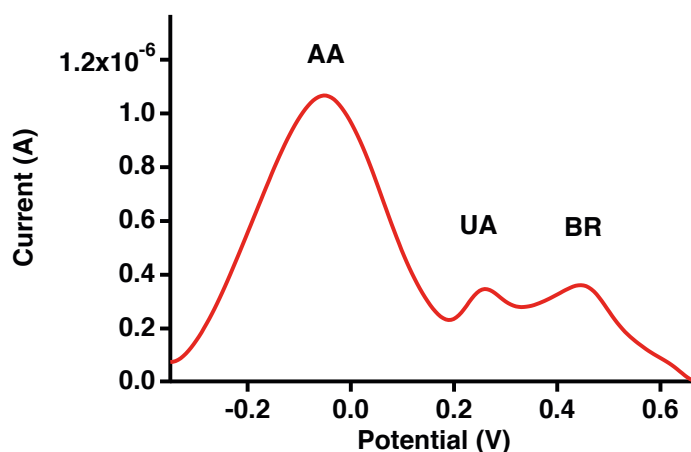


Figure 4.11 – Electrochemical oxidation of AA (200 μM), UA (100 μM) and BR (400 μM) by SWV in PBS solution containing 30 mg/ml albumin.

Sensing parameters did not vary even in the presence of the two interfering species (sensitivity: 151 $\mu\text{A}/(\text{mM cm}^2)$; LOD: 56 μM). Experiments were also carried out in serum containing 500 μM BR. The height of Peak II decreased of five-fold with respect to that obtained by using a synthetic buffer (Fig. 4.12 (a) and (b)).

4.2. Detection of molecules by carbon nanomaterials CVD-grown onto microfabricated sensors

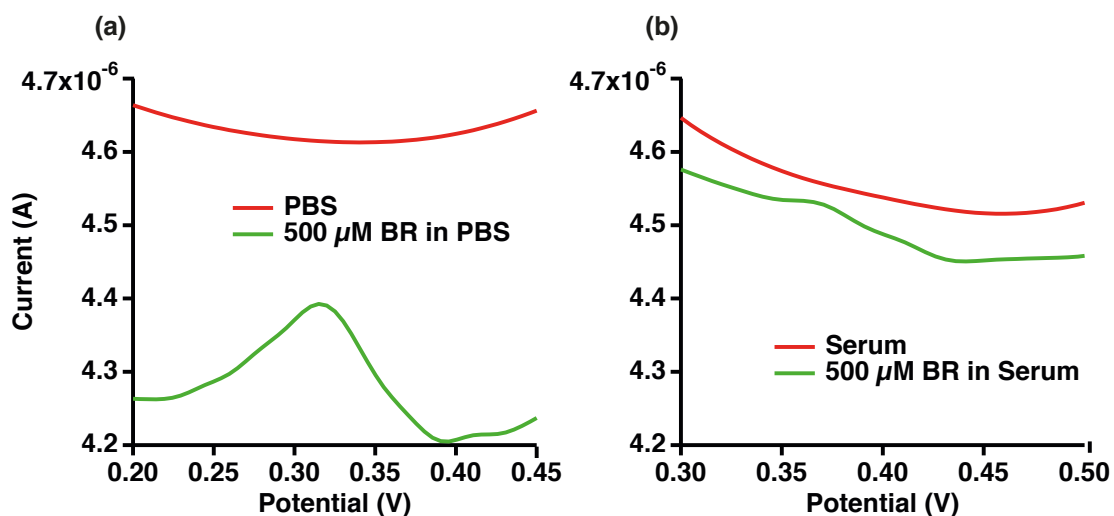


Figure 4.12 – Peak II in PBS solution containing albumin (red line) and in PBS solution containing albumin and 500 μM BR (green line) (a). Peak II in serum (red line) and in serum containing 500 μM BR (green line) (b).

4.2.5 Enzyme-mediated detection of glucose

As in the case of electroactive biocompounds, the enzyme-mediated detection of glucose was proven to be dependent on the amount of material grown onto the electrode. Fig. 4.13 shows an increased current response for high yield nanostructured electrodes. In particular, the highest response resulted by using most packed nanographite produced at 600 $^{\circ}\text{C}$. The value of sensitivity was higher than those found with other nanostructuring approaches [155].

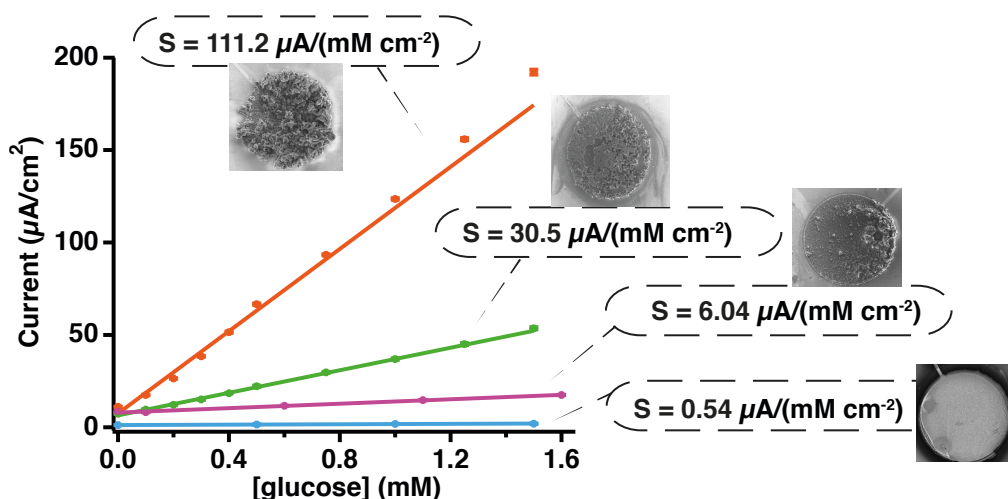


Figure 4.13 – Calibration curves for glucose detection of GOx-based electrodes modified with an increased amount of CVD grown carbon nanomaterials, respective SEM images and sensitivities (S).

Chapter 4. Electrochemical characterisation of MWCNTs, nanographite and their hybrids grown by CVD on a Si-based device

The large surface area of the high yield carbon nanomaterial-based electrodes favours the adsorption of a huge amount of GOx thus improving the sensitivity of the enzyme-based sensors. Fig. 4.14 shows SEM images taken before (a) and after (b) the GOx adsorption on carbon nanomaterials. In Fig. 4.14 (b) it is clearly evident that the enzyme glues the nanomaterials. The diameter of MWCNTs increases from (22.6 ± 2.7) nm to (34.3 ± 17.1) nm (see red arrows in Fig. 4.13 (a) and (b)). This finding confirms previous computations [156] proving that each MWCNT and nanographite fragment is surrounded by a single enzyme layer.

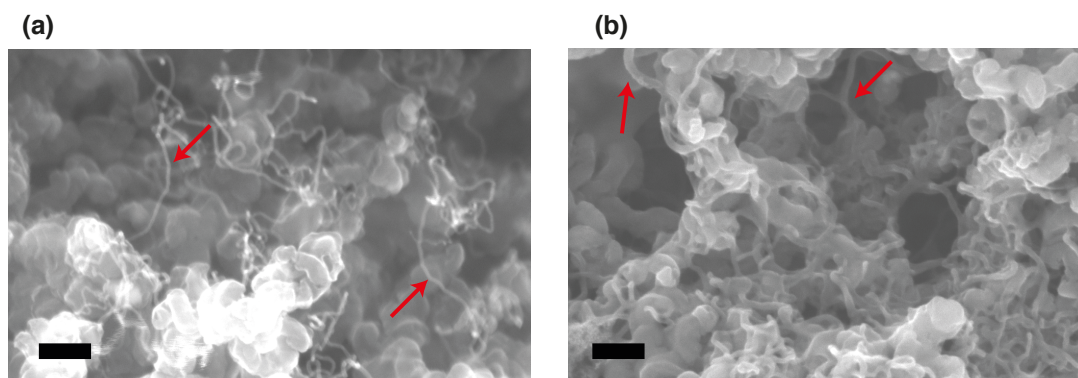


Figure 4.14 – SEM images of hybrid MWCNT-nanographite before (a) and after (b) the GOx immobilisation. Bars: 200 nm

The enzyme adsorbed on the as-grown carbon nanostructures had a life-time of one day. To improve the enzyme stability over time two alternative immobilisation strategies were tested.

- GOx electrodeposition in a Chitosan matrix.
- Cross-linking with glutaraldehyde.

The morphological change of the nanostructures after the incorporation of the enzyme is clear in Fig. 4.15. By keeping constant the yield of carbon nanostructures, the presence of Chitosan and glutaraldehyde onto the electrode surface did not compromise the biosensor sensitivity. However, the polymers decrease the linear range towards glucose detection (Fig. 4.16 (a)). The more the yield is, the more the linear range is reduced (Fig. 4.16 (b)). The biosensors fabricated by electrodeposition of the enzyme were excluded from the life-time investigation since deposition was not selective enough to assure the reliability of the data (Fig. 4.15 (c) red arrows). The sensor with cross-linked GOx and maximum yield was linear up to 1 mM (Fig. 4.16 (a)). Glutaraldehyde prolonged the time-stability of the enzyme. The sensitivity decreased of about 35% three days after the enzyme incorporation. Five days after the biosensor preparation, the enzyme lost its activity towards the glucose detection.

4.2. Detection of molecules by carbon nanomaterials CVD-grown onto microfabricated sensors

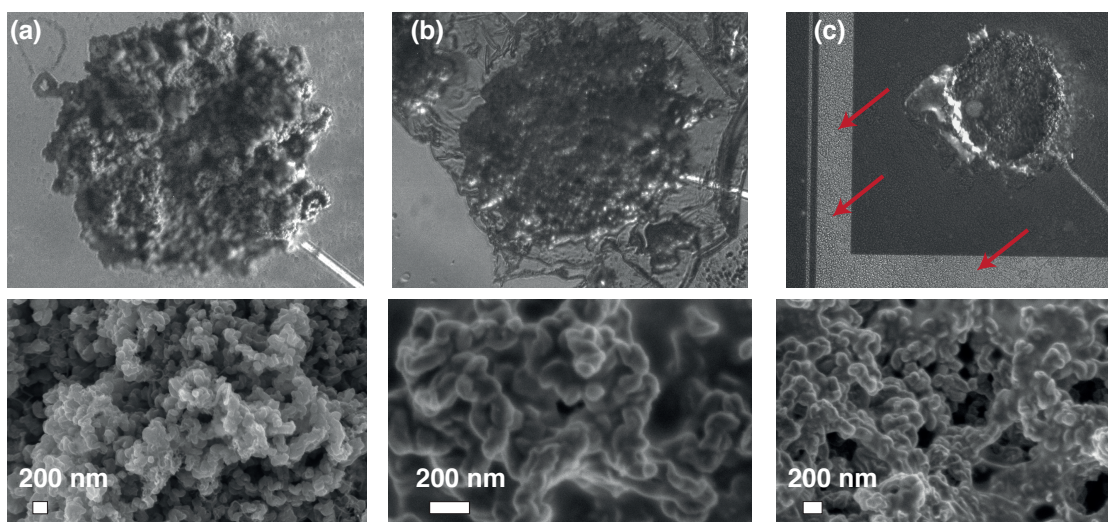


Figure 4.15 – Optical microscope and SEM images of CVD carbon nanomaterials before (a) and after the immobilisation of GOx by cross-linking with glutaraldehyde (b) and by electrodeposition in Chitosan (c).

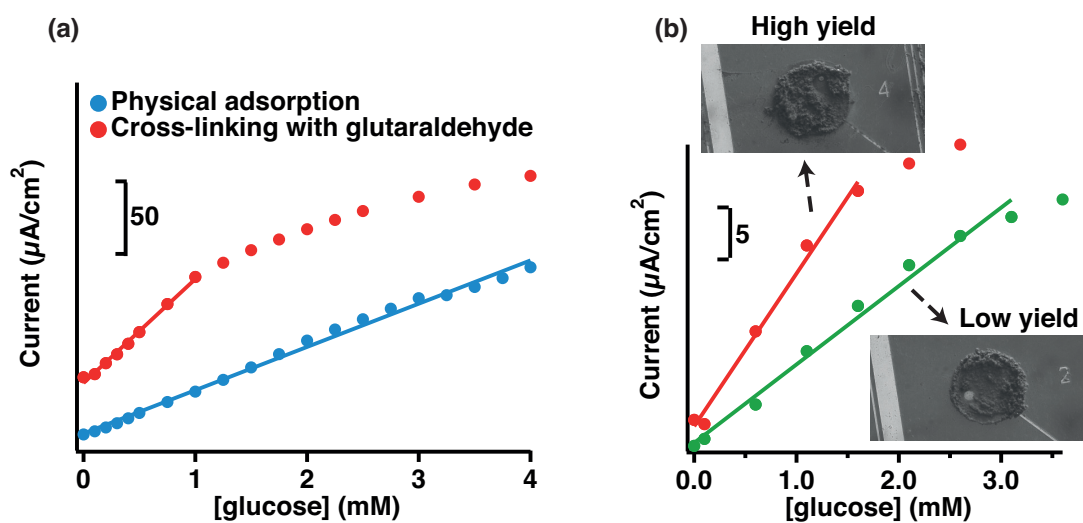


Figure 4.16 – Decrease of the linear range when a polymer is utilised for incorporating GOx onto the electrode (a). This reduction is more evident when high yield nanostructured electrodes are used (b).

4.2.6 Biofouling evaluation

It is well-known that electrode fouling in real biosample is an issue for reproducible and accurate measurements. Taken this into account, the biofouling of low (Fig. 4.17 (a)) and high (Fig. 4.17

Chapter 4. Electrochemical characterisation of MWCNTs, nanographite and their hybrids grown by CVD on a Si-based device

(b) yield nanostructured electrodes was investigated according to the approach in [157]. Initially multiple CVs in solutions containing 2.5 mM $K_3[Fe(CN)_6]$ /PBS (10 mM, pH 7.4) were acquired. The nanostructured Pt electrodes were then inserted for 10 minutes in a cell culture medium containing a wide range of biocompounds. An attenuation of the electroanalytical response was expected because of possible adsorption of biomolecules either on the polar sp^2 carbon created after the treatment and by hydrophobic interactions. The electrodes were then removed from the biosample, reinserted in the initial solution containing $K_3[Fe(CN)_6]$ and multiple CVs were recorded again. The increase of the peak-to-peak separation ranged between 29 mV and 164 mV (Fig. 4.17 (c)) and the reduction of the peak currents ranged between 16% and 26% (Fig. 4.17 (d)). The highest fouling characterised the electrodes with low yield of carbon nanomaterials exposing Pt (Fig. 4.17 (a)). Then, the procedure was repeated by keeping the electrodes in the cell medium for extra 45 and 60 minutes and both peak heights and potential positions unchanged for samples fully covered with nanomaterials (high yield).

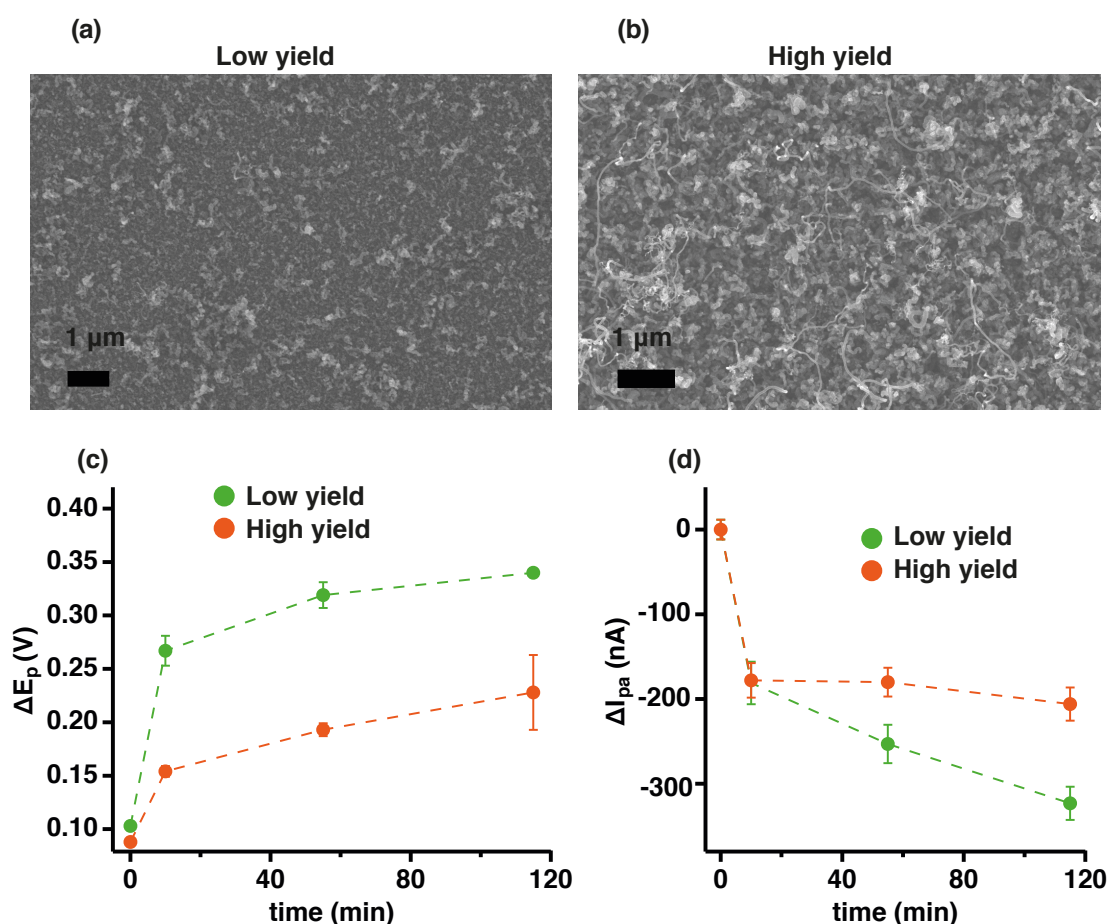


Figure 4.17 – SEM image of low yield (a) and high yield (b) nanostructured electrodes employed for biofouling studies. Peak-to-peak separation ΔE_p (c) and anodic peak current I_{pa} reduction (d) at low yield and high yield nanostructured electrodes in 2.5 mM $K_3[Fe(CN)_6]$ /PBS (10 mM, pH 7.4) before and after exposure to cell media (0, 10, 55 and 115 min). Error bars refer to standard deviation of triplicate measurements.

4.3. Comparative study with conventional carbon nanomaterial integration approaches: microspotting and electrodeposition

4.3 Comparative study with conventional carbon nanomaterial integration approaches: microspotting and electrodeposition

The final performance of the sensor is strongly affected by the kind of interaction nanostructures - electrode surfaces. Therefore, the nanostructuring procedure plays inevitably a crucial role. The aim of this section is to gain a particular insight into the influence of the incorporation method of carbon nanomaterials on sensing parameters. Microfabricated Pt electrodes of a sensor were modified with carbon nanomaterials by a direct CVD growth as described in Chapter 3 (Fig. 4.18 (a)), with MWCNTs by an embedment into Chitosan *via* electrodeposition (Fig. 4.18 (b)) and with MWCNTs by microspotting from a Nafion-based dispersion (Fig. 4.18 (c)). MWCNTs were taken as example of carbon nanomaterials to incorporate onto Pt electrodes. First, carbon nanostructured electrodes were used for the direct sensing of H_2O_2 , a small molecule product of oxidase-based reactions. Then, GOx-based biosensors were fabricated and sensing of glucose, indirectly sensed *via* H_2O_2 electrooxidation, was evaluated.

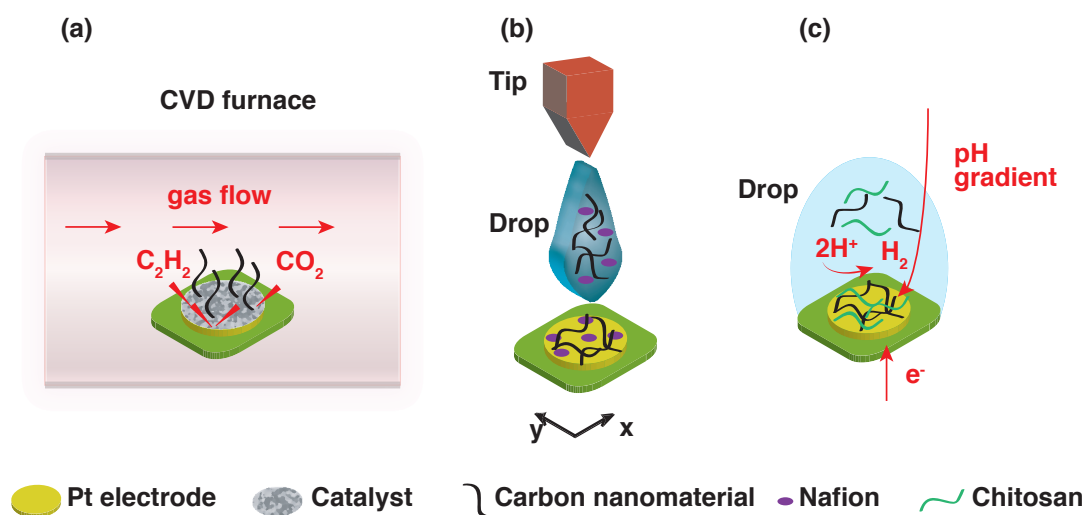


Figure 4.18 – Direct growth of carbon nanomaterials according to the procedure described in Chapter 3 (a). Microspotting of MWCNTs from a Nafion-based dispersion.(b). Electrodeposition of MWCNTs-Chitosan composite (c).

The employed carbon nanostructuring methods are described below.

- Carbon nanomaterials were grown on Pt microelectrodes by using Fe or Fe_2Co as catalysts, pre-electrodeposited onto the electrodes (nanoparticles or layers of various thicknesses) from sulphate-based solutions (see Chapter 3). Synthesis was carried out in a catalytic CVD quartz tube furnace at ambient pressure by introducing C_2H_2 and CO_2 both with a flow ratio of 0.25 l/h for 5 minutes after 10 minutes of catalyst annealing at 600 °C. The grown carbon nanomaterials were activated in 6 M H_2SO_4 for 6 hours (Fig. 4.18 (a)).
- Electrodes with incorporated MWCNTs and Nafion were obtained by casting tens of

Chapter 4. Electrochemical characterisation of MWCNTs, nanographite and their hybrids grown by CVD on a Si-based device

nanoliters of MWCNTs-Nafion dispersion (distilled water 50 v/v% and ethanol 50 v/v%, with 0.5 wt% of Nafion, MWCNTs: 1 mg/ml). A microspotting system was used to assemble MWCNTs onto small Pt electrodes. A CNT-Nafion dispersion was transferred to the probe tip by a micropump. After an accurate positioning of the probe by using a computer-controllable micromanipulator, drops were deposited onto the desired location. Nafion was preferred to chloroform since the latter is too volatile for the manipulation of small volumes (400 pl). A commercially available non-contact spotter was used to deposit multiple layers of MWCNT-Nafion. Solvents were allowed to dry in between two subsequent deposition steps (Fig. 4.18 (b)).

- Electrodeposition of Chitosan and MWCNTs on Pt WEs was carried out by applying a fixed potential of +1.5 V *vs* Ag QRE from a MWCNTs-Chitosan dispersion (MWCNTs: 4-8 mg/ml, Chitosan: 0.7%w/v in a water solution, pH 5) [55]. In this case, when +1.5 V *vs* Ag QRE is applied, the hydrogen ions are reduced to hydrogen at the electrode interface and the pH near the electrode surface increases. At higher pH, Chitosan becomes insoluble and deposits onto Pt entrapping CNTs (Fig. 4.18 (c)).

Fig. 4.19 shows the optical microscope and SEM images at two different magnification of the three modified Pt electrodes. It is evident the presence of the polymer that glues MWCNTs in Fig. 4.19 (b) and (c).

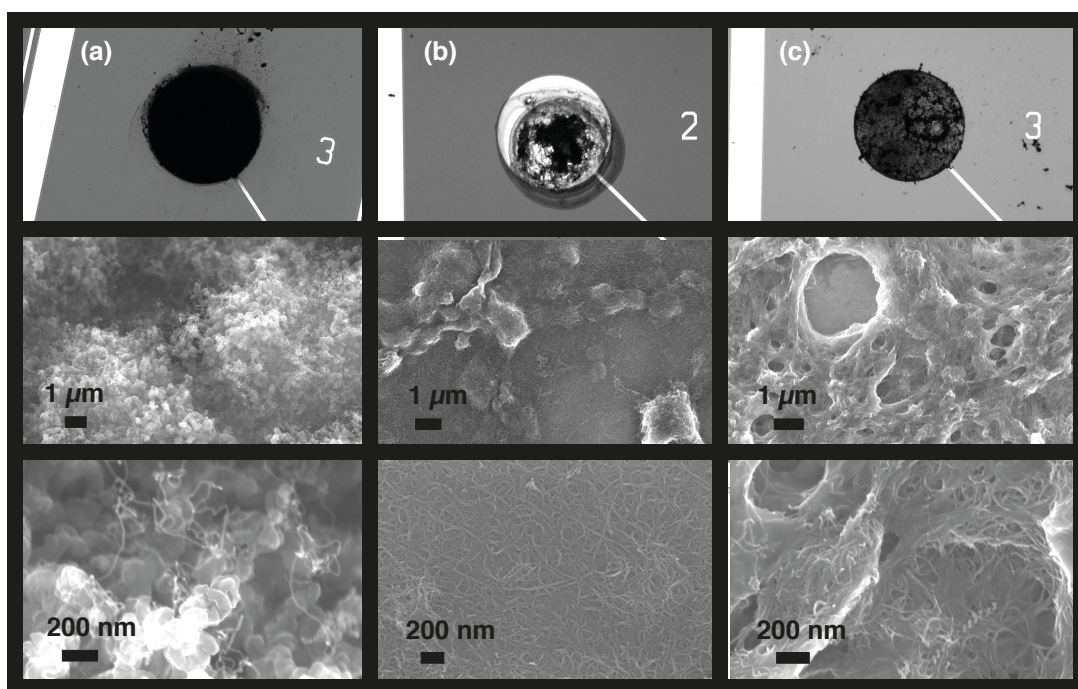


Figure 4.19 – Optical microscope and SEM images at low and high magnification of hybrid MWCNTs-nanographite synthesised by CVD (a), MWCNTs spotted from a Nafion-based dispersion (b), MWCNTs electrodeposited in a Chitosan matrix (c).

4.3. Comparative study with conventional carbon nanomaterial integration approaches: microspotting and electrodeposition

To address the detection performance of the three types of nanostructuring approaches, the electrocatalytic oxidation of the H_2O_2 was studied in CA. Fig. 4.20 (a) shows the sensitivity values towards H_2O_2 at Pt modified with spotted Nafion-MWCNTs, with electrodeposited Chitosan-MWCNTs at high (HY) and low (LY) density and with directly grown carbon nanomaterials at high (HY) and low (LY) density. Detection parameters at spotted CNTs in Nafion worsened largely (about one order of magnitude). These results indicate the Nafion creates an insulating layer on Pt. The presence of MWCNTs does not compensate the negative effect of the cast polymer. To understand the influence of Nafion, CVs were acquired by using bare and Nafion-CNTs based electrodes. Fig. 4.20 shows a typical CV obtained at bare (in green) and at spotted Nafion-MWCNT-based (in red) electrodes. The reduction of the peak currents at spotted Nafion-MWCNTs is due to the presence of the polymer that masks the catalytic properties of the electrode.

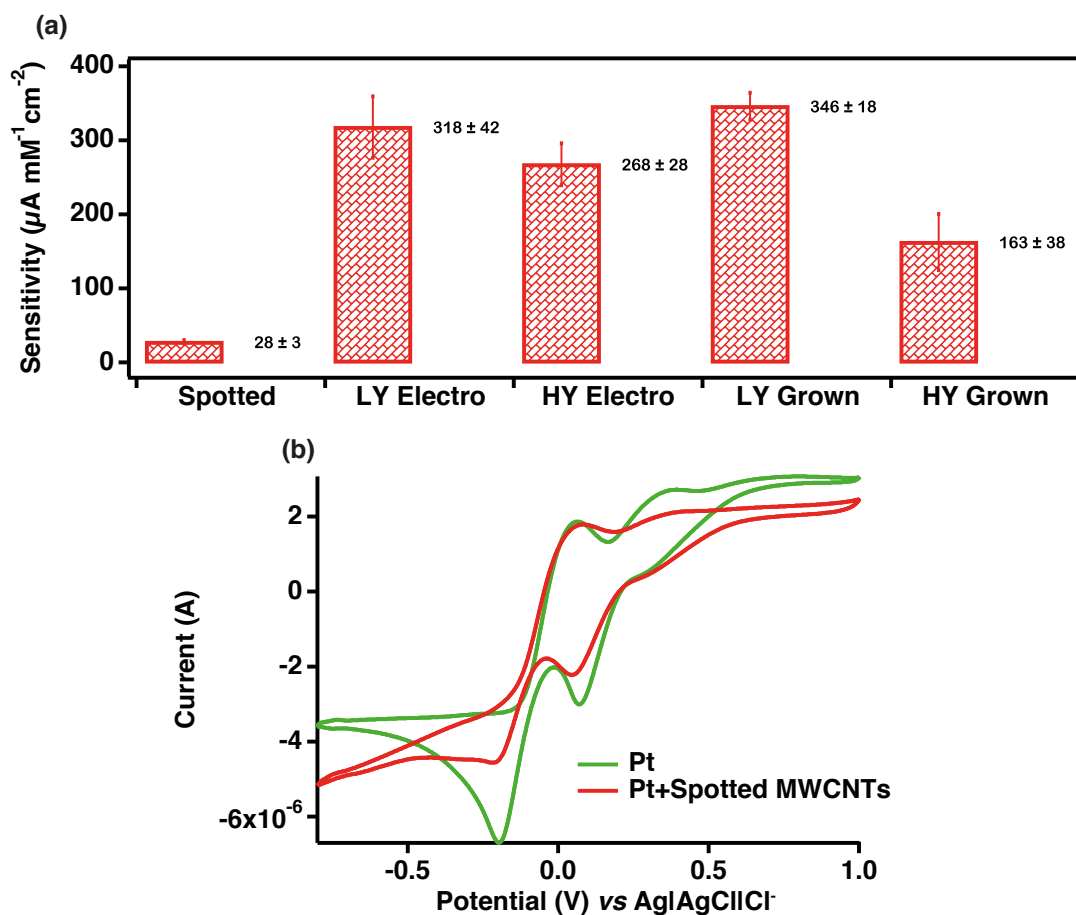


Figure 4.20 – Sensitivities of carbon nanomaterials differently integrated onto microfabricated Pt electrodes towards H_2O_2 detection (100-500 μM). Error bars refer to the standard error of three intrasample measurements. Applied potential +0.5 V vs Ag|AgCl|Cl⁻ (a). CVs in 5 mM H_2O_2 (PBS 10 mM, pH 7.4) at Pt bare (green) and Pt nanostructured with Nafion-MWCNTs (red) (b).

Chapter 4. Electrochemical characterisation of MWCNTs, nanographite and their hybrids grown by CVD on a Si-based device

Based on previous results, spotted Nafion-MWCNTs were excluded from the following comparative study. To evaluate the performance of the modified electrodes for enzyme-mediated biosensors, the electrodes were modified with the highest amount of nanomaterials by CVD and electrodeposition in Chitosan. The yield of nanomaterials was optimised to prevent the detachment from the electrode surface when in use. Then, a GOx was immobilised by adsorption. The signal response obtained with the two types of nanostructuration was similar meaning that both the modified electrodes offer a large available surface area for the incorporation of an enzyme. However, nanostructuring with CVD grown nanomaterials was more controllable than using electrodeposition of Chitosan and MWCNTs. The preparation of a new dispersion MWCNT-Chitosan required each time an optimisation of the electrodeposition time to maximise the yield of MWCNTs deposited on Pt electrodes.

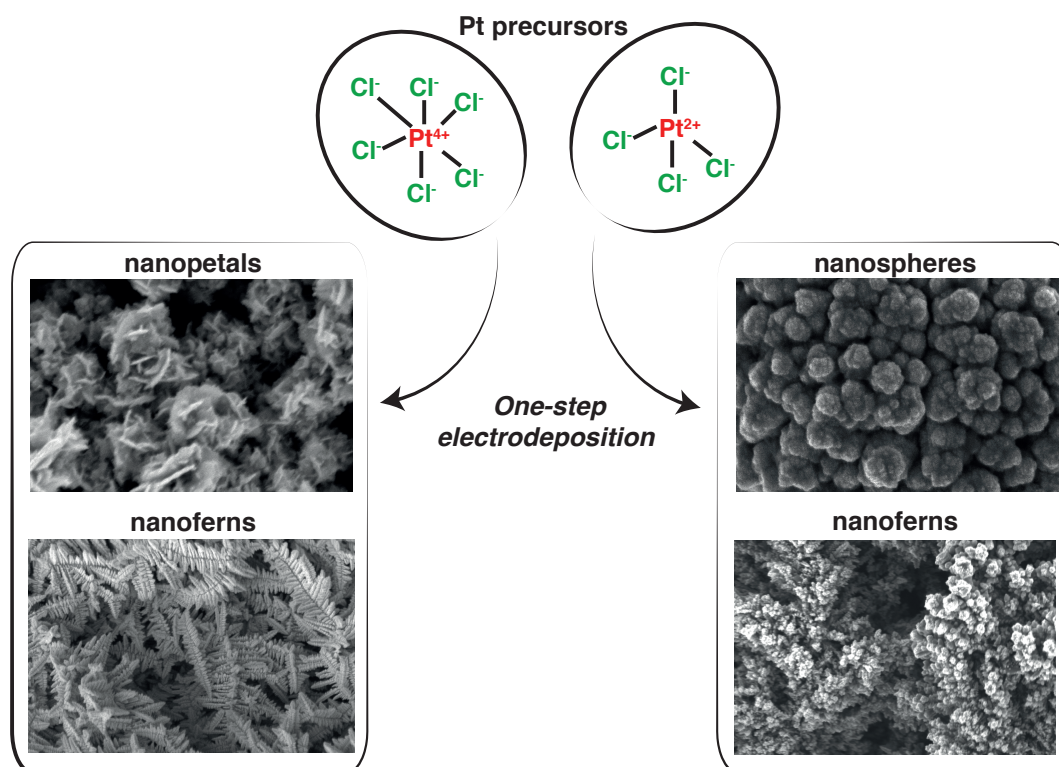
4.4 Summary and contributions

A fast monitoring of a set of metabolites in human fluids is of significant importance in medicine and their detection in the relative physio-pathological concentration range is extremely challenging. To solve this issue, two strategies are currently employed. The miniaturisation of electrodes increases the mass transport rates, reduces the ohmic drop and significantly enhances the S/N ratio. The use of carbon nanomaterials offers unique advantages related to their excellent electrocatalytic activity and to the easy enzyme immobilisation by physical adsorption as demonstrated in Section 4.1.

Binder-assisted nanostructurations are notoriously hardly reproducible, unstable in water environments and not compatible with the low-cost CMOS technology. The selective CVD growth of carbon nanomaterials is one of the most promising methods to modify electrodes without employing other materials (e.g., polymers) enabling a close coupling nanomaterials-electrode surfaces in a full parallel process. Novelties of this chapter are described below.

- Microfabricated and miniaturised Pt electrodes modified with CVD grown carbon nanomaterials enabled the detection of biomarkers within low concentration ranges corresponding to the respective physio-pathological levels.
- Despite the voltammetric discrimination of the oxidation peaks related to different electroactive molecules is a well-known property of carbon nanomaterials, CVD grown carbon nanomaterials enabled the sensing of an electroactive biomarker (free bilirubin) at very low concentrations regardless the presence of interfering species (uric and ascorbic acid) showing unaffected sensing parameters.
- Both direct and enzyme-mediated sensing exhibited competitive sensitivities taking advantage by the use of a more robust, more reproducible and simpler nanostructuration than conventional approaches.

5 Direct and selective integration of differently shaped and sized Pt nanostructures by template-free electrodeposition on screen-printed electrodes



In the past decades, nanoporous metals have received particular attention because they offer larger surface area and higher electrical conductivity than the equivalent bare electrodes. The electrocatalytic properties depend on the pore structure (dimensions and shapes).

Pt-based nanostructured electrodes have shown unique electrochemical properties. Surface composition, morphology and contaminations of Pt nanostructures have an enormous influence on

Chapter 5. Direct and selective integration of differently shaped and sized Pt nanostructures by template-free electrodeposition on screen-printed electrodes

the final electrocatalytic performance. Therefore, an ideal fabrication method of nanostructured Pt coatings should be not only fast and low cost but also controllable, reproducible and free of surface impurities.

In the literature, different techniques have been reported so far to obtain nanoporous Pt. All these methods either include the use of additional materials as templates or are time-costly (e.g., dealloying) and technically difficult to implement (e.g., CVD). Therefore, a simple and contaminant-free approach to synthesise Pt nanostructured layers is highly desirable. Free-template electrodeposition is the simplest, the fastest and the cheapest method to confine nanostructured films onto electrodes. However, it was argued that the resulting shape and size of the nanostructures of the produced film are difficult to control with this approach. In addition, a comparative study of nanostructures obtained from divalent and tetravalent Pt salt precursors is absent. The influence on shape and size of sulphuric acid concentration, of applied potential and of deposition time has never been studied.

In Section 5.2 of the present chapter, a new method to prepare differently-shaped Pt nanostructured coatings on a platinum substrate by a one-step template-free electrodeposition is reported. Four- and two-valent chloride-complexes hexachloroplatinate (Subsection 5.2.1) and tetrachloroplatinate (Subsection 5.2.2) are used as Pt precursors. The change in size and shape of the nanostructures is proven to be dependent on the deposition parameters. To further improve the electrochemical properties of electrodes, depositions of Pt nanostructures on already Pt nanostructured electrodes is performed (Subsection 5.2.3).

The integration of nanostructures of Pt with those of Au was proven to further improve the catalytic activity and resistance to poisoning. In Section 5.3, two protocols to fabricate hybrid Au-Pt nanostructured films are described: a two-step approach consisting in pores made of Au nanocorals covered with Pt nanostructures and a one-step electrodeposition of Au-Pt nanostructured alloys with three-dimensional pores. The fabrication of the pores is achieved by a potentiostatic deposition using hydrogen bubbles as dynamic templates.

5.1 Methods

5.1.1 Electrodeposition procedures

Pt nanostructured electrodes were prepared using an Autolab potentiostat under a computerised control (Metrohm, Switzerland) from solutions containing H₂SO₄ (95-98%, Sigma) and tetravalent and divalent Pt salts, H₂PtCl₆ (Aldrich) or K₂PtCl₄ (FisherSci), respectively. Depositions were carried out by applying -0.2 V or -1 V at room temperature under stirring. A carbon electrode was used as counter electrode and placed in parallel to the *working electrode* (WE). Ag electrode was used as *quasi reference electrode* (QRE). Nanostructured films have been deposited on Pt *screen printed electrodes* (SPEs) (Metrohm; 12.56 mm²). All the bare electrodes were cleaned before the nanostructuring step by applying +2 V for 60-120 s. After the deposition process, a material activation was carried out consisting in acquiring

multiple CVs between -0.2 V and +1.5 V at 100 mV/s in 0.1 M H₂SO₄ till the overlapping of two subsequent voltammograms [38]. Then, the cleaning procedure was repeated. Depositions of macroporous gold on the gold WE of SPEs (DropSens, 12.56 mm²) was carried out according to a previously reported protocol [158]. Gold (III) chloride hydrate (10 mM HAuCl₄, Sigma) and ammonium chloride (2.5 M NH₄Cl, BioChemica) were utilised to realise pores of Au nanocorals by applying -3 V for 120 s. The codeposition of Au-Pt alloy was obtained by applying -2 V from two solutions containing 4.4 mM HAuCl₄, 2.2 M NH₄Cl, 5.5 mM H₂SO₄ and 2.8 mM K₂PtCl₄ or 4.3 mM HAuCl₄, 2.2 M NH₄Cl, 6.8 mM H₂SO₄ and 3.4 mM H₂PtCl₆.

5.1.2 Morphological characterisation

The morphology of the obtained nanostructures were investigated with a Zeiss Merlin high resolution *Scanning Electron Microscope* (SEM) and with a Bruker *Atomic Force Microscope* (AFM). Nanopetal dimensions and nanosphere diameters were computed from SEM images with the ImageJ software [118] and from AFM images with the Nanoscope Analysis software.

5.1.3 Evaluation of electroactive area and roughness factor

The integral of the Pt oxide reduction peak in CV (see Fig. 5.1), acquired in 0.1 M H₂SO₄ (Autolab, Metrohm, Switzerland), was computed using the IgorPro software (Wavemetrics, Lake Oswego, OR, USA) after subtraction of the electrochemical double layer current [159]. The related charge value (Q) was evaluated by dividing the integral (A V) by the scan rate (V/s).

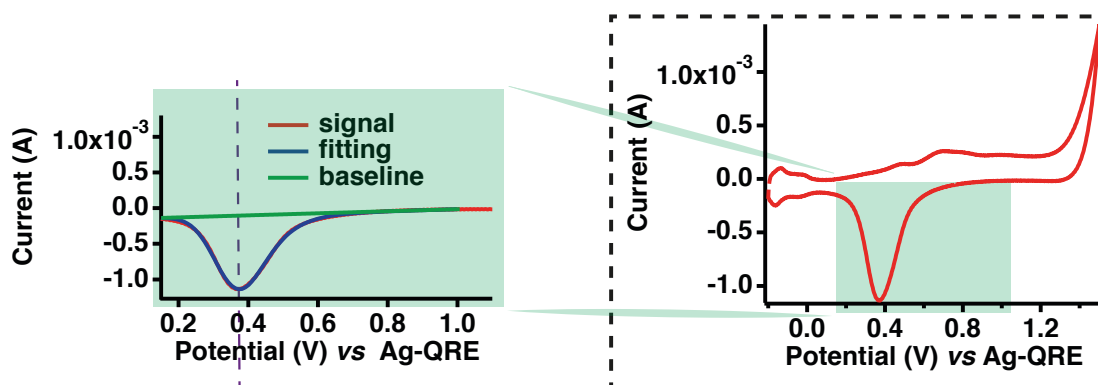


Figure 5.1 – Zoom of the Pt oxide reduction peak in CV whose integral has been taken after baseline subtraction.

The value of electroactive area was calculated as $Q (\mu\text{C})/420 \mu\text{C}/\text{cm}^2$ where $420 \mu\text{C}/\text{cm}^2$ is related to the theoretical estimation for an atomically 1 cm^2 smooth Pt electrode [159]. The roughness factor R_f was estimated by dividing the electroactive area by the geometric area of the electrode (0.1256 cm^2).

5.2 Nanostructuring electrodes with nanoPt

5.2.1 Synthesis from tetravalent Pt-based solutions

Fig. 5.2 shows a SEM image of high density Pt nanopetals produced by applying -1 V for 90 s from a solution containing 25 mM H_2PtCl_6 and 50 mM H_2SO_4 . The nanopetal average size was (68 ± 20) nm. Pt flower-like nanostructures were similar to those obtained by a chemical reduction with NaBH_4 [160]. However, our nanostructures adhere strongly to the electrode and were advantageously grown by a one-step deposition process directly and selectively onto the electrode surfaces.

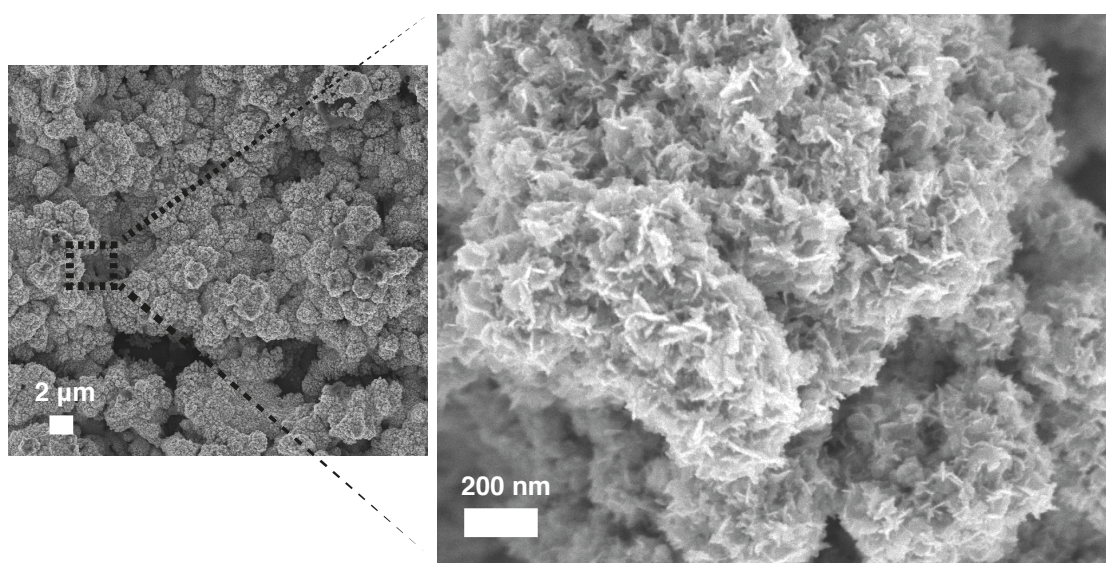


Figure 5.2 – SEM image of Pt nanopetals at low (left side) and high (right side) magnification (-1 V; 90 s; 25 mM H_2PtCl_6 and 50 mM H_2SO_4).

To study the influence of the deposition parameters on the formation of nanopetals, an experimental design, namely the Taguchi method, was used (see Appendix B). Three experimental parameters with two levels of variation each were considered leading to four experiments of a L4 Taguchi matrix [161]. Taguchi technique allows us to design and perform only a limited number of experiments and to identify the principal factors influencing the results of the process [161]. More details on this experimental design approach are described in Appendix B. The three deposition parameters were: applied potential (-1 V and -0.2 V), concentrations of H_2PtCl_6 and H_2SO_4 (respectively 3 mM and 500 mM and 25 mM and 50 mM) and electrodeposition time (90 s and 200 s).

Table 5.1 shows the parameters per each experiment reporting also the respective R_f , density and dimension of petals. SEM images in Fig. 5.3 show the morphology of the modified electrodes.

5.2. Nanostructuring electrodes with nanoPt

Table 5.1 – Taguchi experimental L4 array showing deposition conditions (applied potential, composition of solution, electrodeposition time) and respective outputs (R_f , percentage density and dimension of nanopetals).

Experiment	I	II	III	IV
Potential (V)	-1	-1	-0.2	-0.2
Solution composition	3 mM H_2PtCl_6 + 500 mM H_2SO_4	25 mM H_2PtCl_6 + 50 mM H_2SO_4	3 mM H_2PtCl_6 + 500 mM H_2SO_4	25 mM H_2PtCl_6 + 50 mM H_2SO_4
Time (s)	90	200	200	90
R_f	26.5 ± 0.1	201.8 ± 0.7	23.9 ± 0.1	62.7 ± 0.6
Coverage area (%)	1	100	0	50
Petal dimension (nm)	102 ± 37	65 ± 16	0	142 ± 40

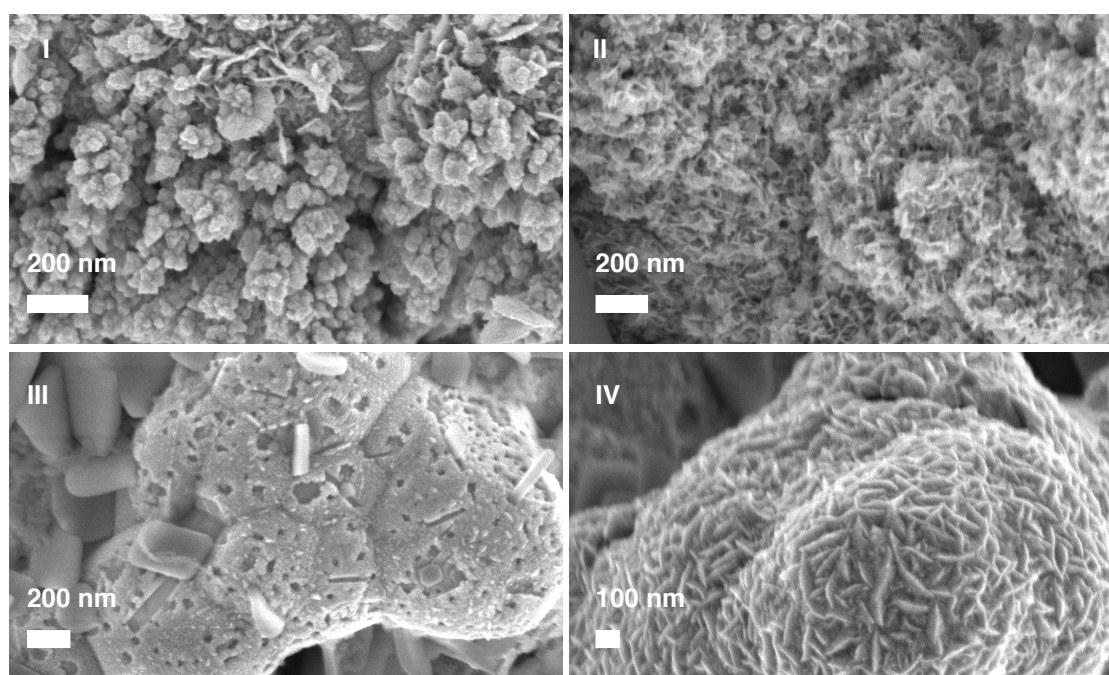


Figure 5.3 – Morphology of electrodeposited nanoPt coatings after experiment I, II, III, IV.

From experiment I, Pt with a very low density of petals was obtained. On the other hand, an electrode fully covered with Pt nanopetals with the smallest dimensions (65 ± 16) nm was observed after experiment II was carried out. Electrode modified according to parameters in experiment III does not show any nanostructure. Electrodes half-covered with big nanopetals

Chapter 5. Direct and selective integration of differently shaped and sized Pt nanostructures by template-free electrodeposition on screen-printed electrodes

((142 ± 37) nm) were obtained from experiment IV. Such electrodes showed a R_f one order of magnitude lower than the electrode full of nanopetals with the smallest size (≈ 63 and ≈ 202 , respectively). These findings confirm the fundamental role of both the petal density and size for a significant increase of the electrode R_f .

To maximise density of nanostructures and R_f and to minimise petal dimension, the *signal-to-noise ratio* (S/N) was computed. For minimising a deposit characteristic (in our case petal dimension), the *smaller-is-better* S/N ratio is used and calculated according to the following Equation 5.1

$$S/N_i = -10 \log \frac{1}{N_i} \sum_{u=1}^{N_i} y_u^2 \quad (5.1)$$

To maximise deposit characteristics (in our case coverage area of nanostructures and R_f), *larger-is-better* S/N ratio is used and calculated according to the following Equation 5.2

$$S/N_i = -10 \log \frac{1}{N_i} \sum_{u=1}^{N_i} \frac{1}{y_u^2} \quad (5.2)$$

where:

- N_i is the number of variations of each parameter (applied potential, solution composition and time) under investigation and
- y_u is the u^{th} value of the deposit characteristic (R_f , coverage area of nanostructures and petal dimension) reported in Table 5.1

Fig. 5.4 shows the influence of all the synthesis parameters on the deposit characteristics. The major factor influencing both density of petals and R_f is the concentration of sulphuric acid and Pt salt in solution. Zhang *et al.* have already observed the importance of the H_2SO_4 to synthesise Pt nanopetals [93]. The acid anions selectively adsorb on specific Pt surface planes favouring their growth and resulting in an anisotropic material. Interestingly, our study demonstrates that the ratio $\text{H}_2\text{PtCl}_6/\text{H}_2\text{SO}_4$ plays a determinant role on the Pt nanopetal growth. The higher the ratio is, the more likely the nanosynthesis occurs (Fig. 5.4 (a) and (b)). Depositions from a solution with the highest ratio $\text{H}_2\text{PtCl}_6/\text{H}_2\text{SO}_4$ produce a film covered with Pt nanopetals having the highest R_f (Fig. 5.4 (a) and (b) - Experiment II and IV in Table 5.1 and Fig. 5.3). The applied potential seems to play the most important role in influencing the petal size (Fig. 5.4 (c)). It is well-known that, depletion zones form around Pt particles at high overvoltages, so the distance between secondary nuclei increases resulting in the growth

of ramified structures [162]. The higher the absolute value of the potential is, the smaller is the nanopetal dimension (Fig. 5.4 (c) - Experiment I and II in Table 5.1 and Fig. 5.3).

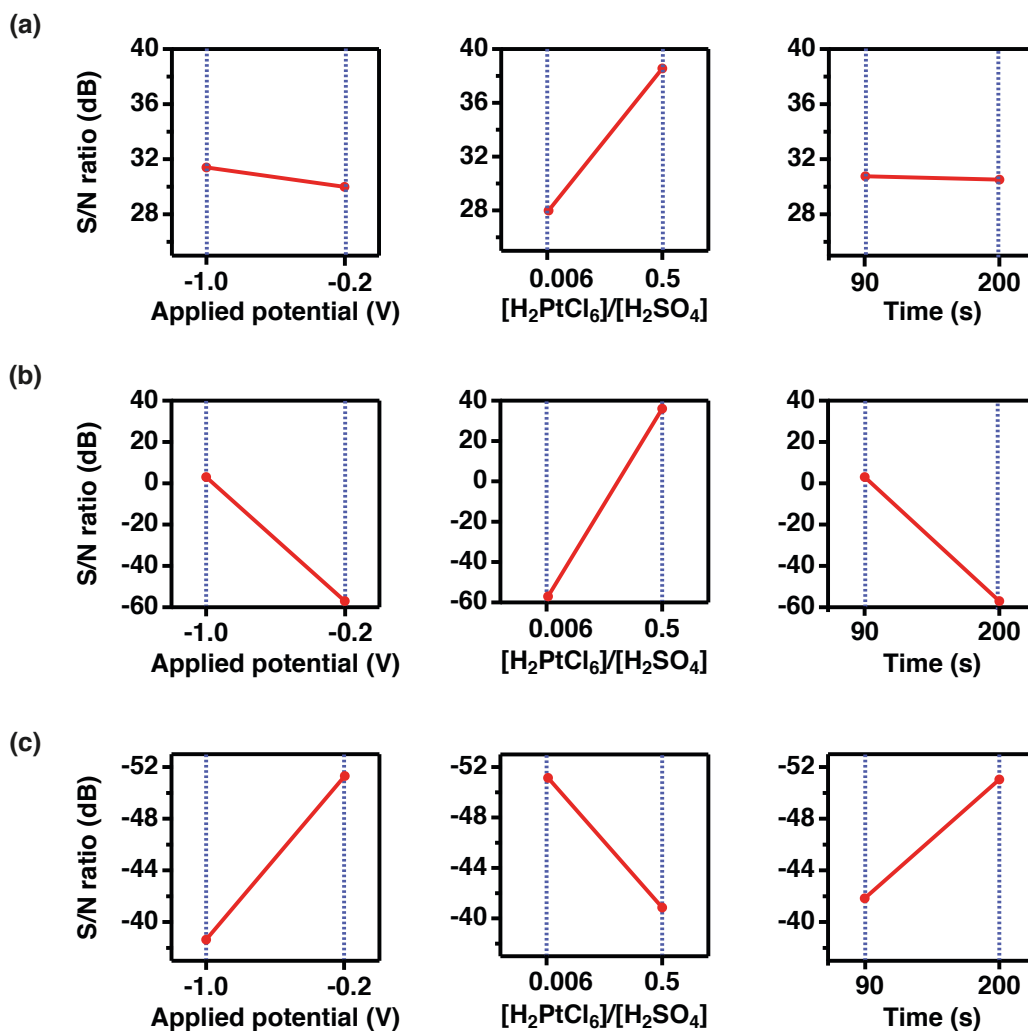


Figure 5.4 – Response graphs of S/N ratio (see Appendix B) for *larger-is-better* analysis of R_f (a) and of nanopetal coverage area (b). Response graph of S/N ratio for *smaller-is-better* analysis of nanopetal dimension (c).

The effect of the electrodeposition time on the electroformation of Pt nanopetals was also investigated. A set of syntheses was carried out at -1 V from a solution containing 25 mM H_2PtCl_6 and 50 mM H_2SO_4 which resulted in the highest density of nanostructures with the smallest size. It is clearly evident from Fig. 5.5 that spherical structures were obtained after 30 s of electrodeposition. High density sharp-cornered nanostructures start to appear after 60 s of applied voltage [93] corresponding to a R_f halfway between that one related to electrodeposited Pt for 15 s and the R_f of an electrode fully-covered with Pt nanopetals. From the graph R_f vs deposition time (Fig. 5.5) a sigmoidal trend was obtained.

Chapter 5. Direct and selective integration of differently shaped and sized Pt nanostructures by template-free electrodeposition on screen-printed electrodes

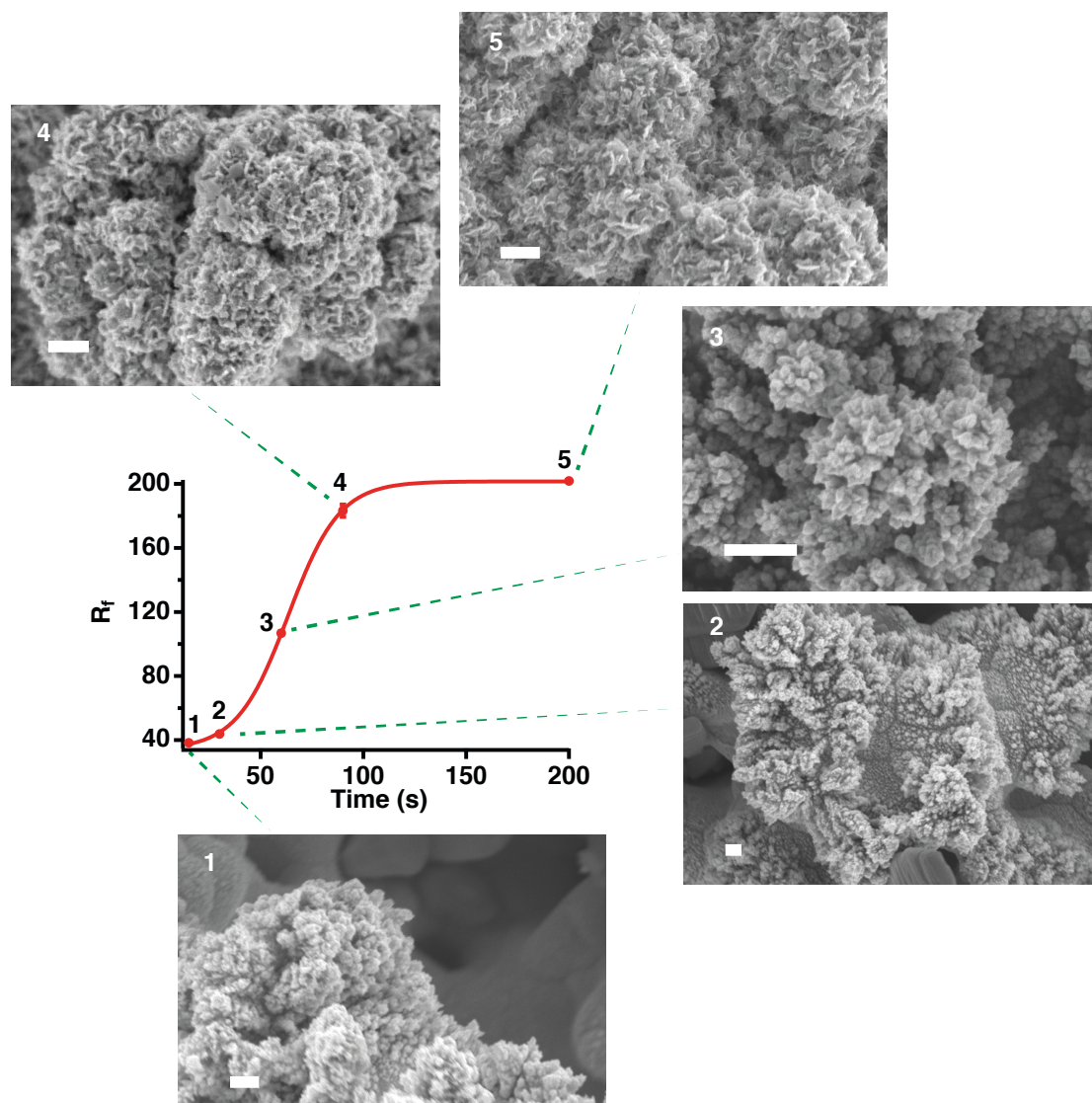


Figure 5.5 – Evolution of the R_f with the deposition time (potential: -1 V; solution: 25 mM H_2PtCl_6 and 50 mM H_2SO_4). SEM images of Pt coatings obtained at different deposition times (bars: 200 nm).

Interestingly, the R_f was 85 % of the maximum value by using the electrode almost totally covered with nanopetals and obtained by applying -1 V for 90 s. The maximum value of R_f is obtained after (167.5 ± 2.5) s of electrodeposition corresponding to the time at which nanopetals covers all the electrode surface. This value has been extrapolated from a sigmoidal fitting.

5.2.2 Synthesis from divalent Pt-based solutions

The effect of applied potential and deposition time on the formation of nanostructured Pt layers was investigated by using a solution containing 25 mM K_2PtCl_4 and 50 mM H_2SO_4 . The morphology of the obtained deposits are shown in Fig. 5.6 (a-d).

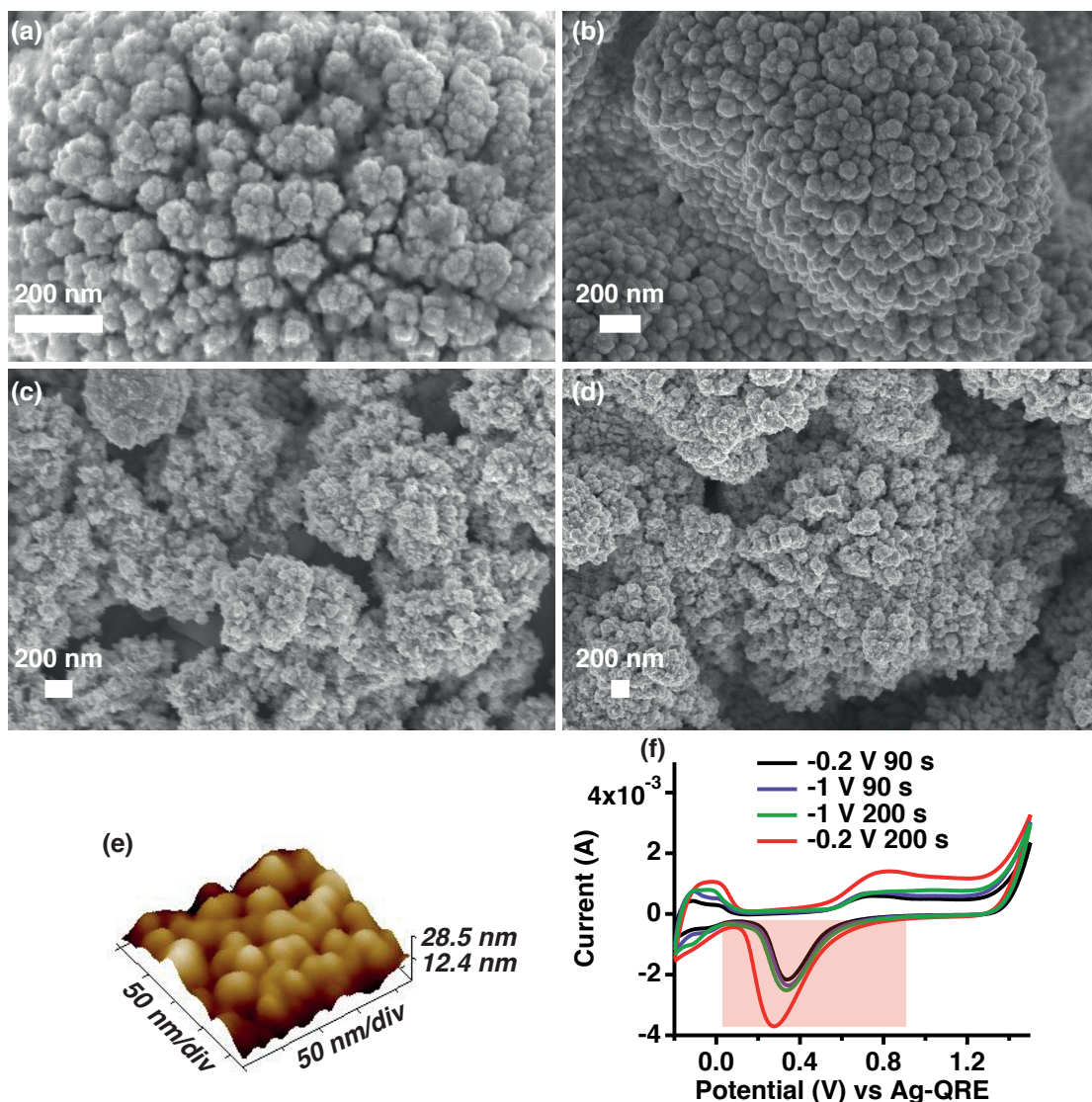


Figure 5.6 – SEM images of Pt electrodeposited by applying -0.2 V for 90 s (a) and 200 s (b) and -1V for 90 s (c) and 200 s (d) from solutions containing 25 mM K_2PtCl_4 and 50 mM H_2SO_4 . AFM 3D image of Pt nanospheres deposited by applying -0.2 V for 200 s from divalent Pt-based solutions (e). CVs acquired with the modified electrodes in 100 mM H_2SO_4 at 100 mV/s (f).

Regular nanospheres with the lowest diameter were obtained by applying the lowest voltage (-0.2 V) for the maximum time (200 s). The average diameter of the structures evaluated from SEM images was (52 ± 18) nm. A similar value was obtained from AFM images ((51 ± 16) nm - Fig. 5.6 (e)). Interestingly, these structures (Fig. 5.6 (b)) have shown the highest R_f with

Chapter 5. Direct and selective integration of differently shaped and sized Pt nanostructures by template-free electrodeposition on screen-printed electrodes

respect to the other three fabrications (Fig. 5.6 (a; c; d)) obtained from K_2PtCl_4 -based solutions. This finding is evident from Fig. 5.6 (f) illustrating the CVs of the four differently modified electrodes in which the largest Pt-oxide reduction peak (highlighted in red) characterises the deposit with the smallest feature size (Fig. 5.6 (b)). The value of R_f of Pt nanostructures in Fig. 5.6 (b) (198.0 ± 3.7) was similar to the best value obtained with petal-like nanostructures. This result confirms the importance of both size and amount of nanostructures for a high value of R_f .

It was observed that the increase of K_2PtCl_4 concentration in solution led to bigger nanospheres (Fig. 5.7) due to the availability of more Pt ions for reduction [163].

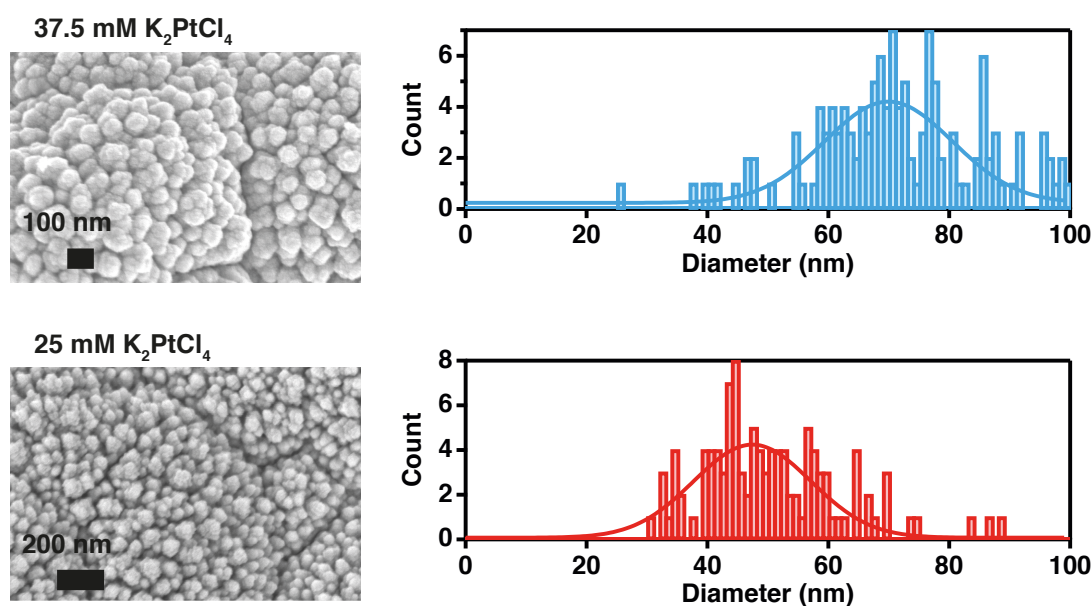


Figure 5.7 – SEM images of Pt nanospheres deposited from solutions containing two different concentrations of K_2PtCl_4 and respective histograms of the nanosphere diameters.

By increasing the deposition potential up to -2 V, nanopetals were grown even from K_2PtCl_4 -based solutions. The anions present in the electrodeposition solution inhibit the reduction to Pt of divalent Pt more than tetravalent Pt. Indeed, divalent Pt requires the availability of several adjacent sites because of the planar geometry, while tetravalent Pt is not inhibited to the same extent because of its 3D geometry and the requirement of only one site available [164]. Therefore, tetravalent Pt deposits easier than divalent Pt. This phenomenon explains why, by using H_2PtCl_6 -based solutions, Pt nanopetals form at a potential lower than using solutions containing K_2PtCl_4 with equal concentrations.

5.2.3 Double depositions of Pt nanostructures

For an extra increase of R_f of the electrodes, two successive depositions were carried out. After the deposition of nanospheres (-0.2 V, 200 s, 25 mM K_2PtCl_4 + 50 mM H_2SO_4), Pt nanopetals

were synthesised onto the overgrown electrode (-1 V, 90 s, 25 mM H_2PtCl_6 + 50 mM H_2SO_4). Pt nanopetals grown on nanospheres are shown in Fig. 5.8. The presence of both the nanomaterials is clearly evident. The double-coated electrode has shown a R_f higher (224.6 ± 2.9) than the highest value of R_f obtained with one-step depositions of both nanospheres and nanopetals.

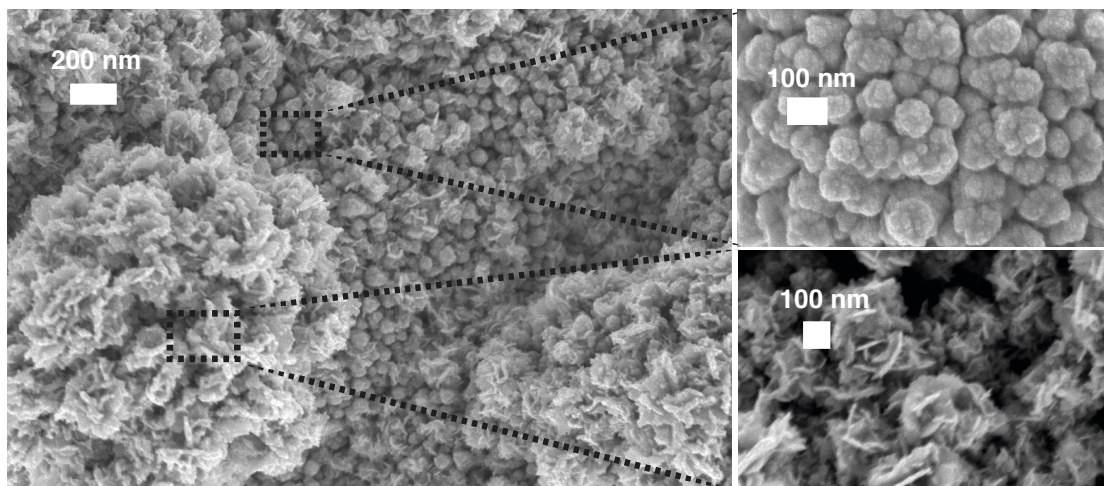


Figure 5.8 – SEM image of Pt nanopetals (on the right; -1 V for 90 s from tetravalent Pt-based solution) electrodeposited on Pt nanospheres (on the left; -0.2 V for 200 s from divalent Pt-based solution).

5.3 Coupling Pt and Au nanostructures

As discussed in Subsection 2.2.2 of Chapter 2 the main advantages related to the combination of Pt nanostructures with those of another material are two: integration on electrodes of Pt nanostructures with geometries that are impossible to obtain with the conventional nanoPt fabrication strategies and improved electrocatalytic properties. In particular, when other metal nanostructures are combined with those of Pt a further reduction of overpotential for sensing molecules and a decrease of the Pt poisoning under highly oxidising conditions could be achieved.

Cobalt, iron, nickel, chromium added to Pt are prone to dissolution so the combination of a noble metal (Pd, Au) with Pt is more promising. In particular, Au seems to be very attractive because it is inert and it shows high catalytic activity at nanoscale (nanoAu) [36]. The combination of nanoPt with nanoAu results in a material with different properties than nanoPt. The presence of Au in Pt increases the lattice distance of Pt. Due to the higher electronegativity of Au than Pt charges are transferred from Pt to Au resulting in an increase of the d-orbital vacancy in Pt.

Chapter 5. Direct and selective integration of differently shaped and sized Pt nanostructures by template-free electrodeposition on screen-printed electrodes

Hydrogen bubble dynamic templates have been recently explored because of the fast formation of 3D macroporous metal films and because the solid template to remove is absent [158] (Fig. 5.9). Chen [158] developed a protocol to produce Au macropores characterised by nanocoral-like structures by hydrogen bubble template electrodeposition. NH_4^+ was added in solution as a source of hydrogen.

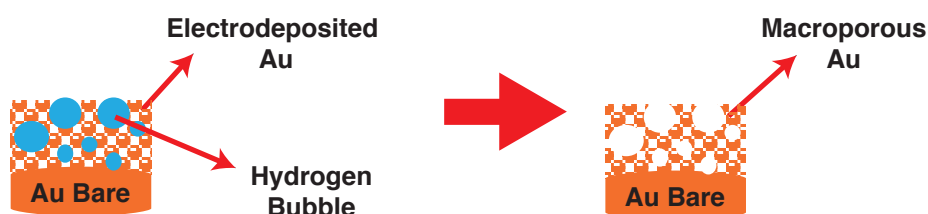


Figure 5.9 – Schematic of the hydrogen bubble dynamic template electrodeposition of Au.

Unfortunately such a protocol was not applicable for the synthesis of nanostructured 3D pores made of only Pt because of the precipitation of both H_2PtCl_6 and K_2PtCl_4 in the presence of 2.5 M NH_4^+ . On the other hand, to obtain 3D Au-Pt macropores by employing this technique, two procedures were devised.

Two-step procedure First of all, 3D macropores of Au nanocorals (Fig. 5.10 (a)) were deposited onto a Au bare electrode according to the procedure (see Fig. 5.9) previously described by Chen and coworkers [158]. This geometry was then exploited by decorating the borders of the pores with both Pt nanopetals (Fig. 5.10 (b)) and Pt nanospheres (Fig. 5.10 (c)). Fig. 5.10 shows the borders of Au macropores free from Pt nanostructures (a) and coated with Pt nanopetals (b) and with Pt nanospheres (c). Pt nanostructures have been effectively loaded on macropores of nanoAu. These findings demonstrate that our Pt nanointegration method is highly versatile allowing us to nanostructure a wide range of electrodes with different geometries from flat surfaces to macropores of nanostructured surfaces.

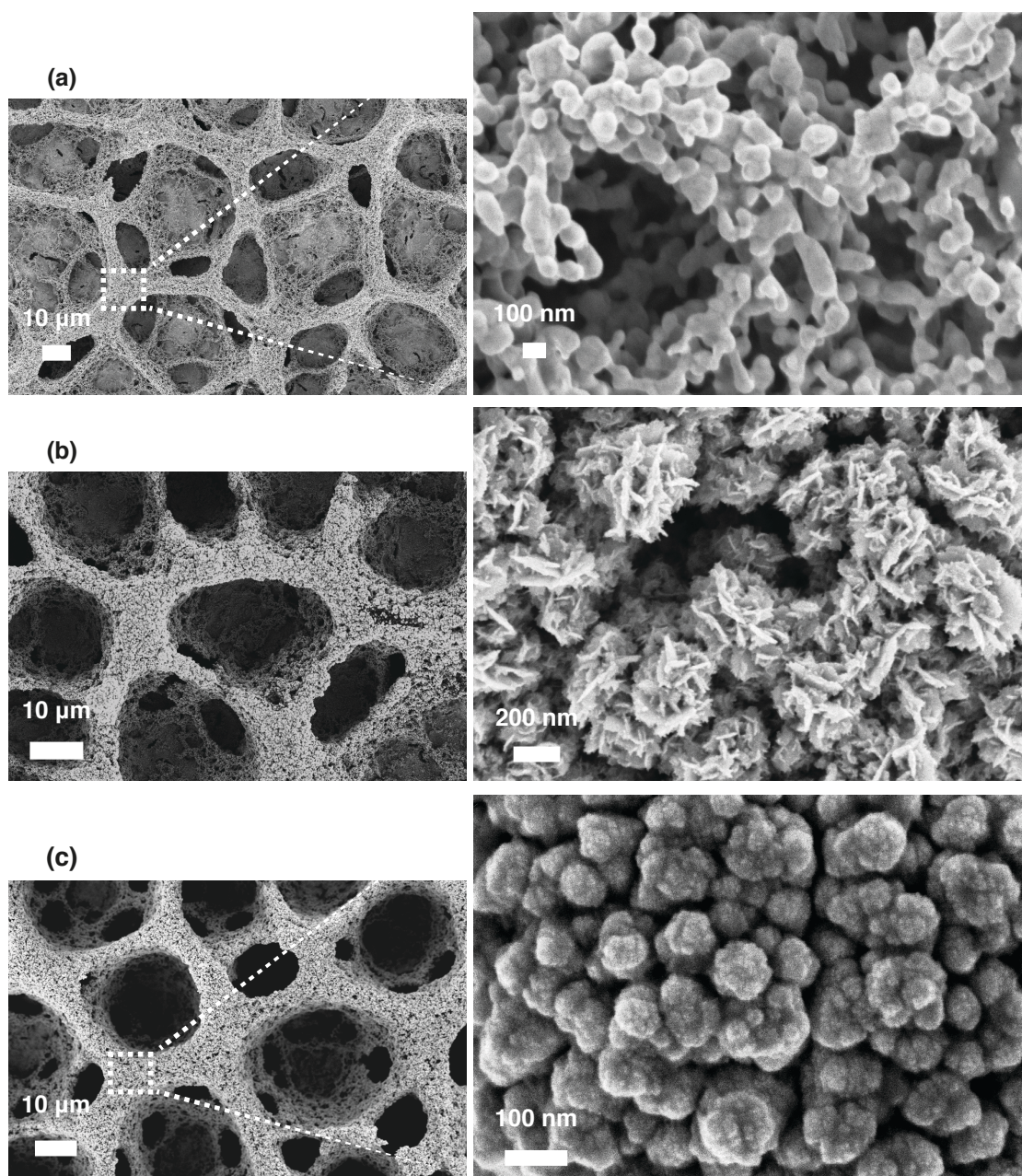


Figure 5.10 – SEM images of nanocoral-like Au macropores (a), Au macropores decorated with Pt nanopetals (-1 V for 90 s from tetravalent Pt-based solution) (b) and with Pt nanospheres (-0.2 V for 200 s from divalent Pt-based solution) (c).

One-step procedure Among various methods, the one-step template-free electrodeposition is the most powerful and simplest approach. For this reason, a one-step simultaneous electrodeposition of Au-Pt nanostructures was carried out *via* hydrogen bubble dynamic template working with very low concentration of Pt (see Section 5.1) to avoid precipitation phenomena. Fig. 5.11 depicts the 3D structures of Au-Pt. Both H_2PtCl_6 and K_2PtCl_4 were used. Well-defined

Chapter 5. Direct and selective integration of differently shaped and sized Pt nanostructures by template-free electrodeposition on screen-printed electrodes

pores composed of nanoferns were obtained from K_2PtCl_4 -based solutions. Bigger nanoferns were deposited from H_2PtCl_6 than using K_2PtCl_4 (Fig. 5.11).

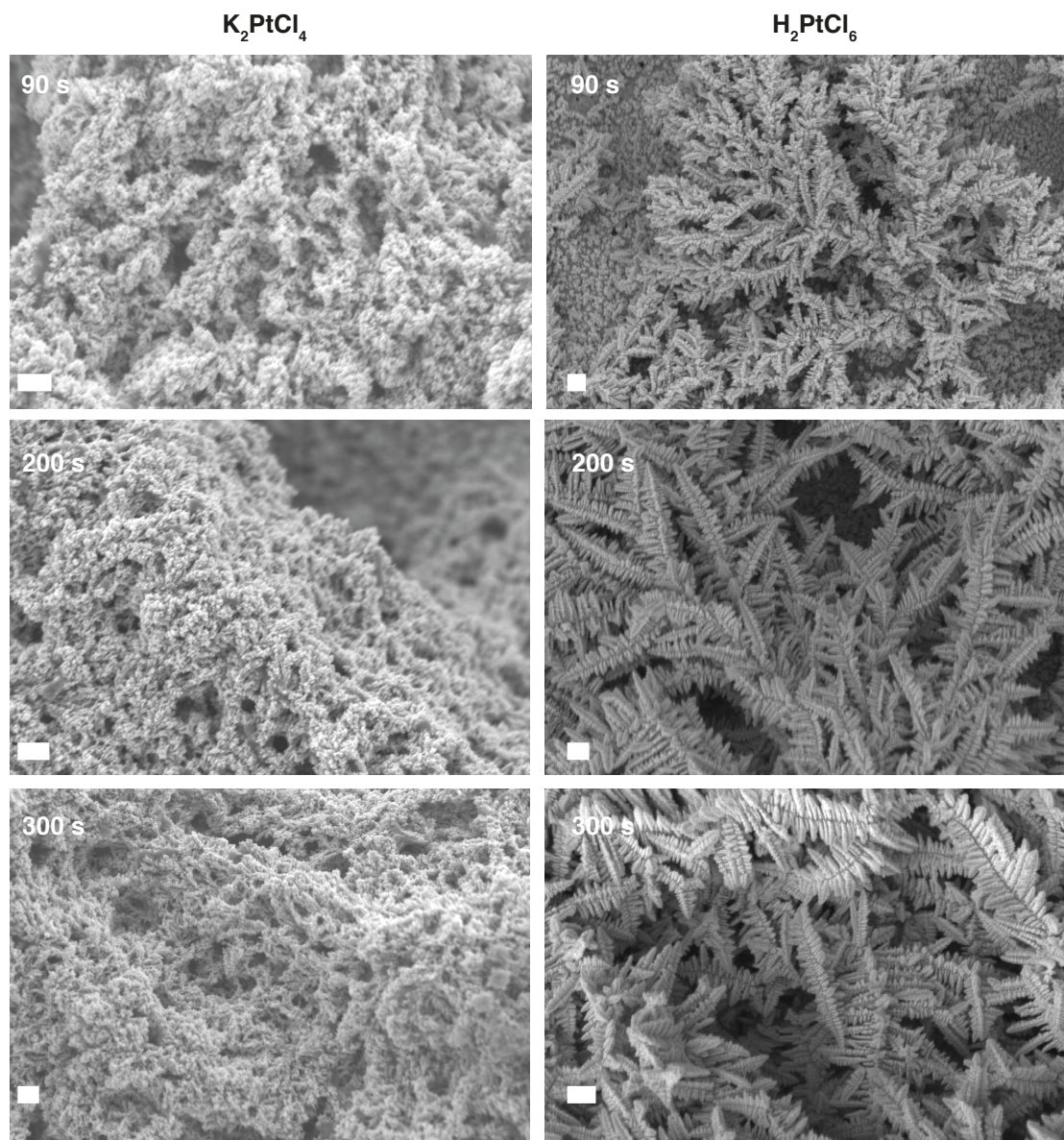


Figure 5.11 – SEM images of Au-Pt nanostructured alloys produced from divalent and tetravalent Pt-based solutions at different deposition times (bars: 200 nm).

From solutions based on H_2PtCl_6 , the prolongation of the deposition time increased the nanofern size and the pores became more evident (Fig. 5.12). From EDX analysis the average Pt content was about 35% and 25% of the total alloy when K_2PtCl_4 - and H_2PtCl_6 -based solutions were used, respectively. It does not correspond to the ratio Au-Pt in solution because the electrodeposition of Au occurs at a potential lower than Pt [112].

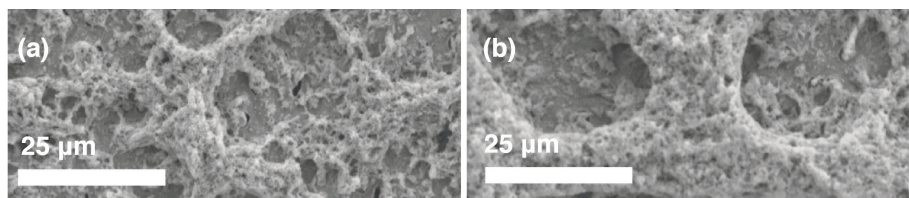


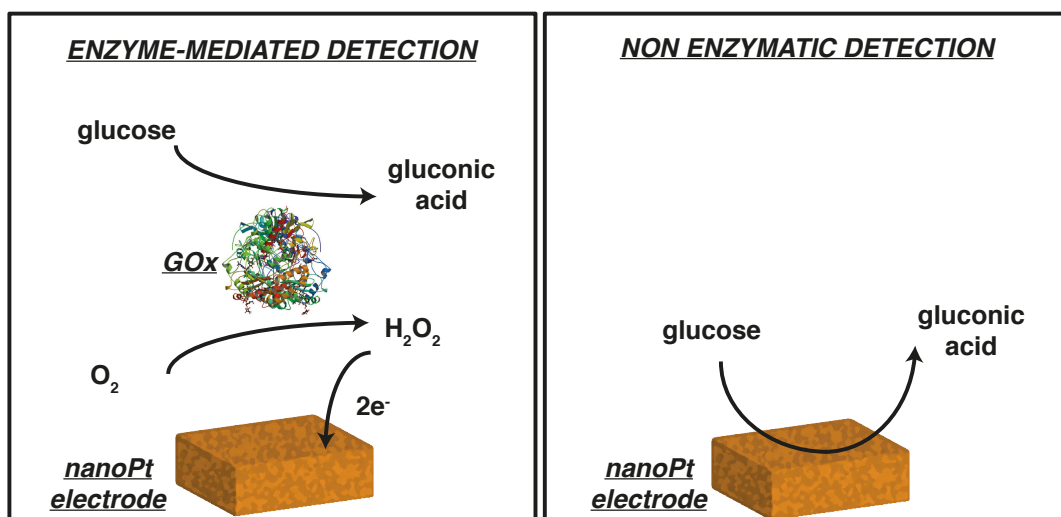
Figure 5.12 – SEM images of Au-Pt pores synthesised from H_2PtCl_6 -based solutions by applying -2 V for 90 s (a) and 300 s (b)

5.4 Summary and contributions

This chapter focused on the following topics and contributions

- For the first time the role of type of Pt salt precursor (four- and two-valent chloride-complexes) and of Pt salt/sulphuric acid ratio was investigated in nanostructuring electrodes by fast one-step template-free electrodeposition. By optimising deposition conditions, nanostructures with two defined shapes (spheres and petals) were obtained although a control of the shape is notoriously difficult by template-free electrodeposition methods. Interestingly, some parameters affecting the nanostructure size were also identified. Another definitely novel electrode modification was also invented, characterised by a monometallic nanocomposite Pt-Pt including nanopetals and nanospheres.
- Considering the convenient and very recently discovered catalytic potentialities of Au-Pt systems, two novel types of nanostructurations were invented: the first consists of Au macropores made of nanocoral-like structures decorated with Pt nanospheres or Pt nanopetals, the second includes nanoferns of Au-Pt with different sizes obtained by one-step process. Hydrogen bubbles were used as dynamic templates.

6 Electrochemical characterisation of Pt nanopetals and Pt nanospheres prepared by electrodeposition on screen printed electrodes



Recently, Pt nanostructured electrodes have been utilised to build electrochemical sensors because of the high surface area and the high electrocatalytic efficiency. Their nanoscale size has been largely proved to enhance the electrochemical sensing of kinetically-controlled electrochemical events that characterise: (a) some metabolites of medical interest such as glucose and (b) important molecules as hydrogen peroxide. Oxidases produce hydrogen peroxide as side reaction product that is sensed for indirectly measuring biocompounds metabolised by oxidases.

In the present chapter, measurements with Pt nanostructures, electrochemically synthesised on Pt bare electrodes according to the procedures described in Chapter 5, are shown for both enzymatic and non-enzymatic sensing of glucose. The latter detection is of increasing industrial interest considering the absence of an enzyme that limits the device costs and time stability. Section 6.2 describes the performance of the modified electrodes towards the enzymatic detec-

Chapter 6. Electrochemical characterisation of Pt nanopetals and Pt nanospheres prepared by electrodeposition on screen printed electrodes

tion of glucose with respect to bare Pt electrodes. The potential corresponding to the highest electrochemical response is identified at the modified electrode. Then, the influence of electroactive interferences is shown at the optimum detection potential. Similarly, in Section 6.3, the capability of these electrodes to voltammetrically detect glucose without enzyme is investigated. The evaluation of the resistance to the biofouling of the nanoPt electrodes is shown by using both the mechanisms for detecting glucose. Finally, Section 6.4 focuses on studies concerning both enzyme-mediated and direct detection of glucose at Au-Pt nanostructured electrodes.

6.1 Methods

An Autolab potentiostat (NOVA software) with a three-electrode configuration was utilised to perform electrochemical measurements. *Chronoamperometries* (CAs) of glucose were carried out at a fixed potential vs Ag|AgCl|Cl⁻ in *phosphate buffered saline* (PBS) solution (Sigma, 10 mM, pH 7.4) or cell media (Dulbecco's Modified Eagle's Medium - DMEM, D5030, Sigma) under stirring and aerobic condition by consecutively adding H₂O₂ (Reactolab SA, Switzerland) or glucose (Sigma). *Glucose oxidase* (GOx), purchased from Roche, was immobilised by cross-linking with glutaraldehyde (glutaraldehyde solution, Grade II, 25 % from Sigma). A drop of 10 µl of solution containing GOx (15 mg/ml in PBS; glutaraldehyde 2.5 %) was cast onto the electrodes and kept dried at 4 °C before the use. Calibrations were carried out with the IgorPro software (Wavemetrics, Lake Oswego, OR, USA). To study the direct glucose oxidation voltammetries were acquired in a 10 mM PBS solution (Sigma, pH 7.4) or cell media (DMEM, D5030, Sigma). *Cyclic Voltammetries* (CVs) were acquired at 20 mV/s while *Square Wave Voltammetries* (SWVs) at 15 mV/s (potential window: -0.6 V/+0.8 V). The sensitivity and the LOD were calculated as described in Appendix A.

6.2 Oxidase-mediated detection of glucose

CA was employed to determine the electrochemical response of electrodes towards the indirect detection of glucose *via* H₂O₂ electrooxidation (applied potential +700 mV). GOx was immobilised by cross-linking onto the electrodes and the current arising from the electrooxidation of a product of enzymatic reaction (H₂O₂) was then monitored as an indirect measurement of glucose. It was found that all the nanostructured electrodes exhibited a higher electrochemical response towards the indirect glucose detection than bare electrodes. The sensitivity of Pt nanopetals and Pt nanospheres was three-fold higher than that related to bare electrodes (Fig. 6.1). A further improvement of 25% was recorded by using the hybrid electrode Pt nanopetals on Pt nanospheres (Fig. 6.1). These findings indicate that the nanoporosity of the modified electrodes offer a larger area for the enzyme incorporation and favours the H₂O₂ electrooxidation, in part kinetically-controlled, resulting in an electrochemical signal for sensing glucose higher than that of unmodified electrodes [104].

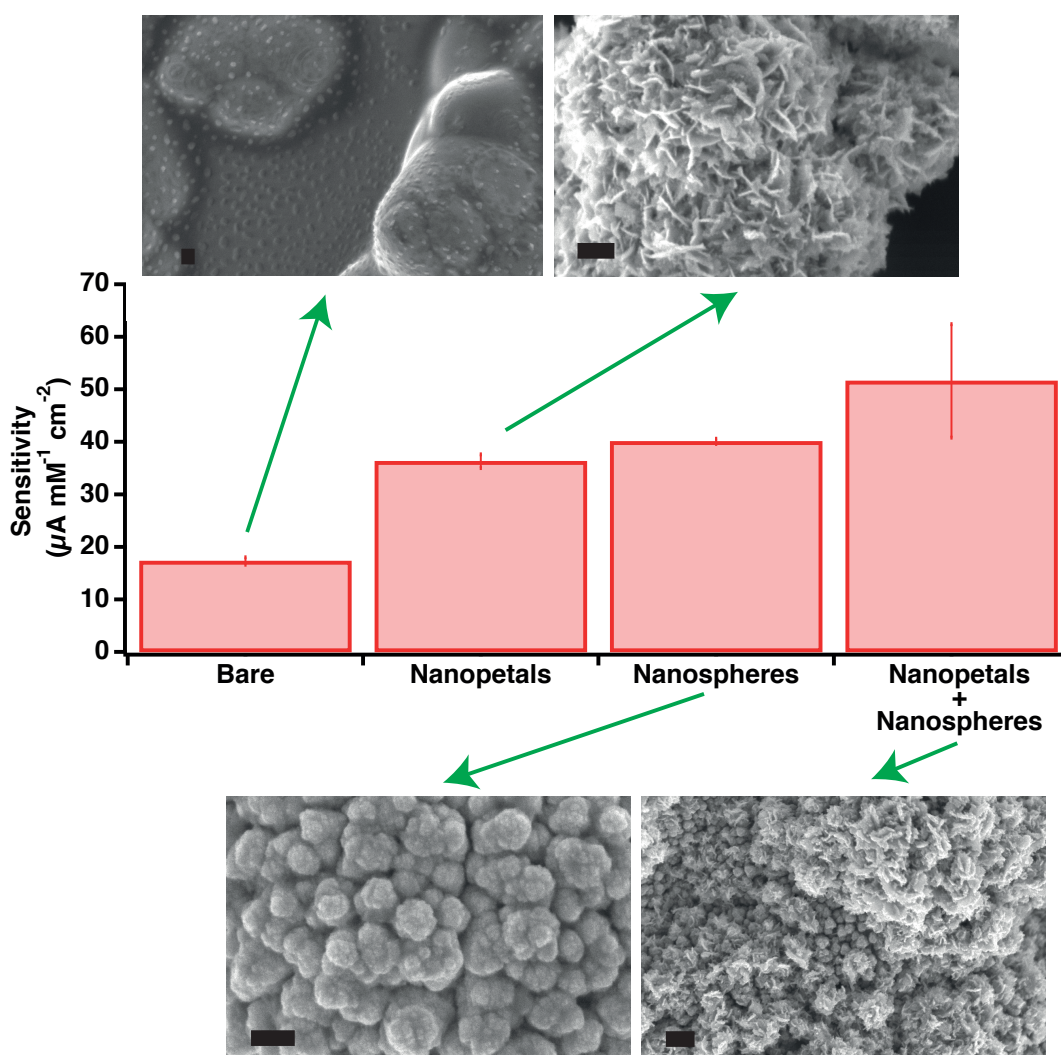


Figure 6.1 – Sensitivities towards glucose at bare Pt electrodes, Pt nanospheres (-0.2 V; 200 s, divalent Pt-based solution), Pt nanopetals (-1 V; 200 s, tetravalent Pt-based solution) and Pt nanopetals (-1 V; 90 s, tetravalent Pt-based solution) grown on Pt nanospheres (-0.2 V; 200 s, divalent Pt-based solution) with an immobilised GOx. Error bars refer to the standard error of three intersample measurements. Glucose concentration: from 100 to 500 μM , 100 μM each step. Bars: 100 nm.

The nanostructured electrode based on Pt nanopetals and Pt nanospheres is the first example reported so far presenting hybrid monometallic nanostructured electrode having also the advantage of being fabricated by two simple electrodeposition steps. As shown in Fig. 6.1, this electrode exhibited the highest sensitivity at an applied potential of +700 mV. In general metal nanomaterials have exhibited an efficient catalytic activity towards the electrooxidation of H_2O_2 at low potentials [165]. The investigation of the electrode response at different applied potentials towards the detection of a fixed concentration of H_2O_2 (20 μM) was performed at bare and monometallic hybrid electrodes.

Chapter 6. Electrochemical characterisation of Pt nanopetals and Pt nanospheres prepared by electrodeposition on screen printed electrodes

As shown in Fig. 6.2 the amperometric response of both bare and nanoPt hybrid electrodes increased by reducing the potential below +700 mV. The maximum value of current signal was obtained at +450 mV for bare electrodes and at +300 mV for the hybrid electrodes. The signal reduces by a further lowering of the applied potential. It is worth to note that the maximum signal at bare electrodes was more than two-fold lower than that found at the hybrid nanoPt electrode at their optimal applied voltage. Therefore, the hybrid nanostructuring increases the current response lowering, at the same time, the optimal detection potential.

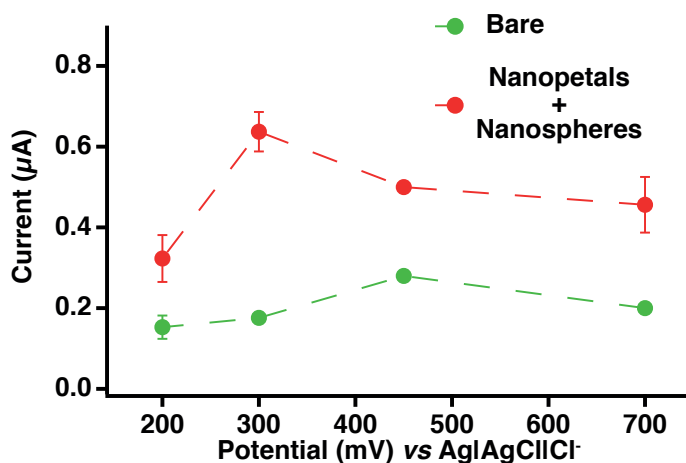


Figure 6.2 – Current response *vs* applied potential at bare (green) and at hybrid nanoPt (red) electrodes towards the detection of 20 µM H₂O₂ (PBS 0.01 M, pH 7.4). Error bars refer to the standard error of three intersample measurements.

Then, GOx was cross-linked onto the hybrid nanoPt electrode and glucose was chronoamperometrically sensed at +300 mV. The linear response was up to 4 mM (1 mM at bare Pt) with a sensitivity of $(28.8 \pm 2.1) \mu\text{A}/(\text{mM cm}^2)$ and a LOD of $(6.6 \pm 1.5) \mu\text{M}$ ($n=3$). Our biosensor has shown good to excellent sensing parameters with respect to those based on nanoPt and on Pt nanoparticles present in the literature (Table 6.1), paving the way for its use at a considerable low potential with advantages in circuit design.

The decrease of the detection potential is particularly useful due to the reduction of interferences from electroactive biomolecules such as AA. Glucose concentrations relevant for many clinical applications range between 0 and 20 mM. Therefore, our sensor, showing a linearity up to 4 mM, can be used for analysis of five-fold diluted human samples. Consequently, also the concentration of the interfering species are proportionally diluted (e.g., AA $\approx 20 \mu\text{M}$). Fig. 6.3 shows the amperometric response of the hybrid nanoPt electrode by adding 20 µM AA in a stirred buffer solution at the applied potential of +300 mV. The introduction of AA in solution shows a very slight increase of the current signal demonstrating a good reliability of the sensor in rejecting interfering species as AA.

6.2. Oxidase-mediated detection of glucose

Table 6.1 – Sensing performance of different glucose biosensors characterised by GOx immobilised on Pt nanoparticles (NPs) or Pt nanostructured layers (nanoPt).

Biosensor	Applied potential (V)	Linear range (mM)	Sensitivity ($\mu\text{A}/(\text{mM cm}^2)$)	LOD (μM)	Ref
GC/ BNNTs/ PANI/PtNPs	+ 0.55 <i>vs</i> SCE	0.01-5.5	19.02	0.18	[166]
PtNPs/ MWCNTs	+ 0.60 <i>vs</i> Ag AgCl	0.001-23	58.9	1	[75]
GOx/GC PMPD-GOx/ Pt μ Ps/	+0.60 <i>vs</i> SCE	0.002-12	-	-	[84]
nanoPANI/ GOx/nanoAu/ nanoPt/	+0.60 <i>vs</i> SCE	0.5-16.5	-	-	[167]
CNT/gold Nafion/Chit/ GOxPtNCs/Pt	+0.60 <i>vs</i> Ag AgCl	0.001-8	35.92	0.5	[85]
PtNanowires/ GOx	+ 0.55 <i>vs</i> Ag AgCl	0.0045-89.5	8.74	4.5	[111]
PtNanopetals/ PtNanospheres/ GOx	+0.30 <i>vs</i> Ag AgCl Cl⁻	0.02-4	28.8 \pm 2.1	6.6 \pm 1.5	This work

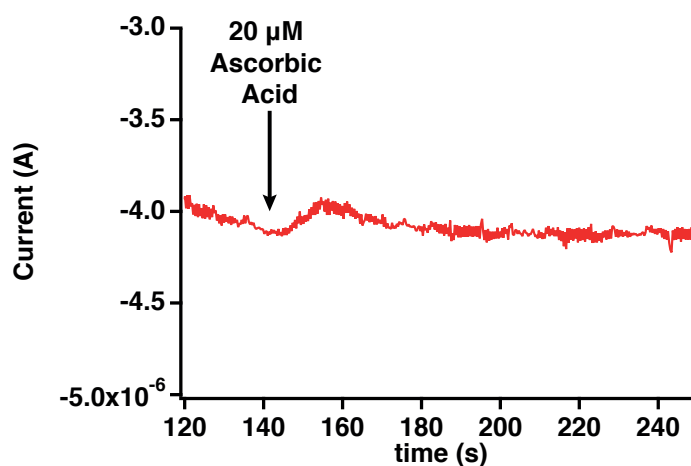


Figure 6.3 – Effect of the addition of 20 μM AA in solution on the current response of hybrid nanoPt electrode (+300 mV *vs* Ag|AgCl|Cl⁻; PBS 0.01 M, pH 7.4).

Chapter 6. Electrochemical characterisation of Pt nanopetals and Pt nanospheres prepared by electrodeposition on screen printed electrodes

Poisoning is a phenomenon of physical and chemical change of the electrode surface due to the presence of certain substances in solution which reduce the electrocatalytic properties of the electrode. The poisoning of Pt electrodes when used in a direct contact with real sample has limited their use for continuous metabolite monitoring [168]. The electrooxidation of H_2O_2 (used here to indirectly measure any metabolite by a proper oxidase) resulted in a two-fold sensitivity decrease of the hybrid nanoPt electrode when cell media was used rather than a synthetic buffer solution (Fig. 6.4 (a)). The presence of big biomacromolecules mask the catalytic activity of the Pt nanostructures. These findings were also confirmed by measuring glucose with the GOx-hybrid nanoPt sensor. The sensitivity was almost two-fold lower and the LOD two-fold higher than that obtained by using synthetic buffer solutions (Fig. 6.4 (b)). The current response of the biosensor was linear up to 1 mM in the media (Fig. 6.4 (b)).

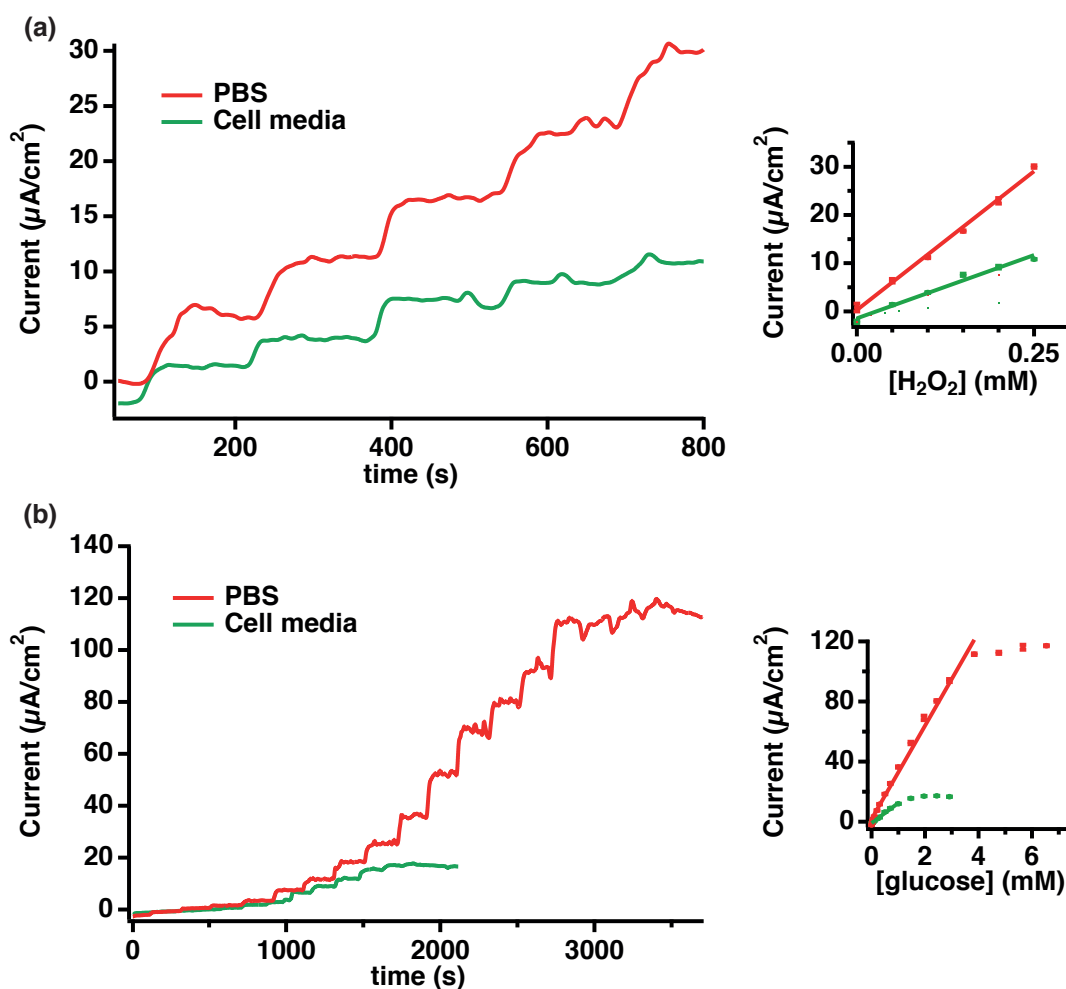


Figure 6.4 – CVs and calibration curves at hybrid nanoPt electrode and at GOx-hybrid nanoPt electrode towards H_2O_2 (a) and glucose (b) detection, respectively. Measurements in PBS (10 mM; pH 7.4; red) and in cell media (green).

6.3 Direct oxidation of glucose

Lots of studies on glucose detection are based on GOx immobilised on electrode surfaces, in which H_2O_2 is produced from the catalytic oxidation of glucose in the presence of oxygen, and then electrochemically oxidised (or reduced). The principal problem of enzymatic sensors is the lack of enzymatic stability over time. Moreover, the enzyme is easily affected by pH, temperature, other chemicals and humidity [169] and its incorporation increases the cost of the final device. To overcome these issues, researchers have focused their attention on a direct bioprobe-free detection of glucose.

Therefore, the capability of our Pt nanostructured electrodes to detect glucose without an immobilised enzyme was also investigated. Pt usually suffers from problems of poisoning by adsorbed species that reduce the Pt catalytically active sites for detecting glucose. Fig. 6.5 shows CVs acquired in the presence of physiological concentration of chloride ions and phosphate anions both well-know inhibitors of the glucose adsorption onto the Pt surface and therefore of its oxidation [169]. The glucose oxidation peaks, clearly evident in Fig. 6.5 for the two nanostructured electrodes, demonstrate the capability of the modified electrodes to retain a high sensitivity towards the direct detection of glucose. Three oxidation peaks for the direct glucose electrooxidation were found at Pt nanopetals and Pt nanospheres similarly to those reported in the literature [169].

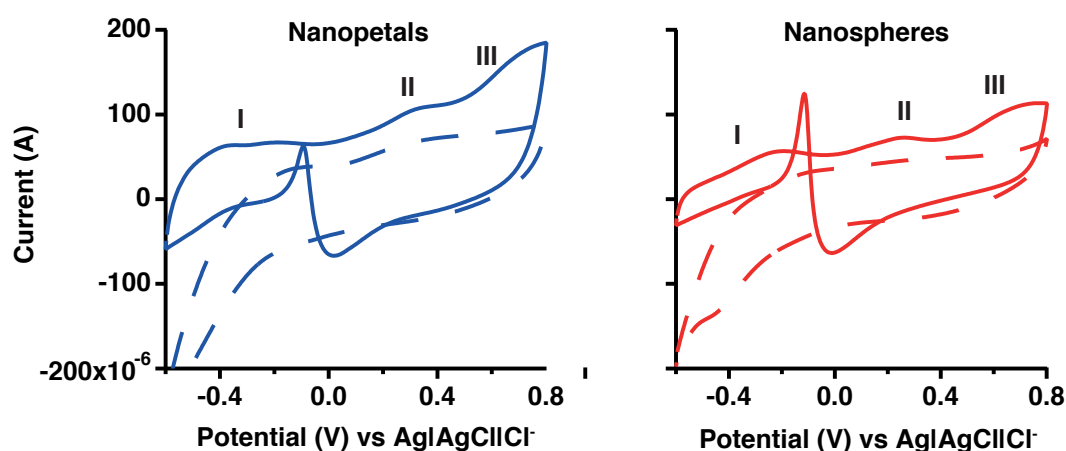


Figure 6.5 – CVs in PBS (dotted line) and in 20 mM glucose/PBS at electrodes nanostructured with Pt nanopetals (left side in blue; -1 V; 200 s, tetravalent Pt-based solution) and with Pt nanospheres (right side in red; -0.2 V; 200 s, divalent Pt-based solution). Scan rate: 20 mV/s. PBS solution: 10 mM, pH 7.4.

Pt nanospheres were used to verify the enzymeless detection of glucose directly in cell media. Peak current II, commonly used to detect glucose at Pt electrodes (Table 2.3 in Chapter 2), showed a three-fold reduction by measuring glucose in the media due to poisoning effects. However, in spite of the strong oxidising conditions, an increase of the peak current has been acquired for increasing glucose concentration within the physio-pathological range (Fig. 6.6). The sensitivity value was $(2.9 \pm 0.1) \mu A / (mM \text{ cm}^2)$, even higher than those obtained by other

Chapter 6. Electrochemical characterisation of Pt nanopetals and Pt nanospheres prepared by electrodeposition on screen printed electrodes

authors in synthetic buffer solutions (see Table 2.3 in Chapter 2). So far there are no other examples of direct glucose detection in undiluted cell media in the literature.

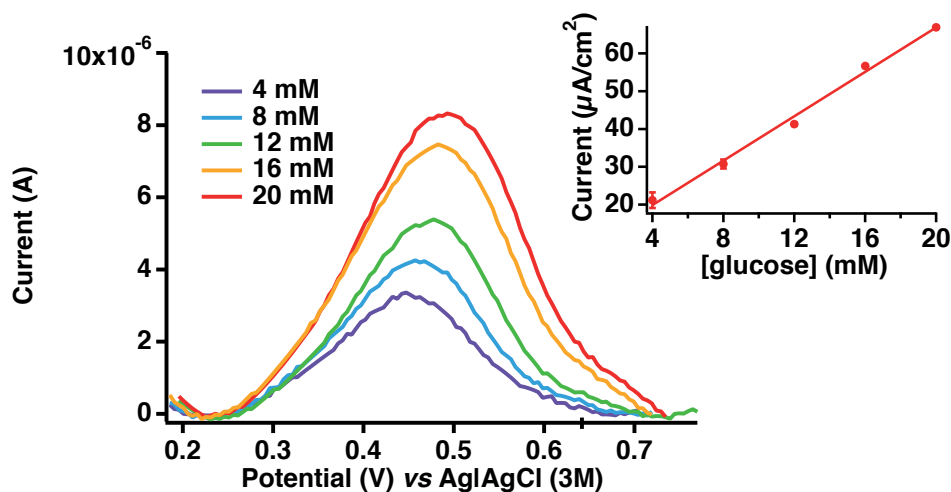


Figure 6.6 – SWVs at 15 mV/s in cell media containing glucose concentrations equal to 4, 8, 12, 16, 20 mM and respective calibration curve (estimation of standard deviation from duplicate measurements).

6.4 Measurements with alloy Au-Pt

As seen in previous sections, the principal drawback associated with the use of nanoPt, even in a smaller extent with respect to bare Pt, is the poisoning when used in a direct contact with real samples due to the adsorption of molecules onto its surface. In Section 5.3 of Chapter 5 new protocols to build bimetallic nanostructures Au-Pt by a one- and a two-step electrodeposition processes are described. The combination of Pt with another metal potentially reduces the oxidation potential to detect hydrogen peroxide, enhancing at the same time the signal stability and intensity of the glucose oxidation. The reduction of the detection voltage and of the poisoning at bimetallic systems has been previously reported by detecting a variety of compounds [112, 113, 170].

Studies were carried out with Au-Pt nanoferns produced by a one-step electrodeposition at -2 V for 300 s from solutions containing H₂PtCl₆ or K₂PtCl₄ (description of the one-step deposition procedure in Section 5.3 of Chapter 5). These nanostructured electrodes were selected because they showed the highest peak related to an electrochemically deposited oxygen monolayer (≈ 0.4 V Fig. 6.7 in violet) and the highest peaks of the hydrogen monolayer adsorption and desorption (below 0 V Fig. 6.7 in yellow). The integration of the before-mentioned peaks is used to compute the electroactive area of Au and Pt [36].

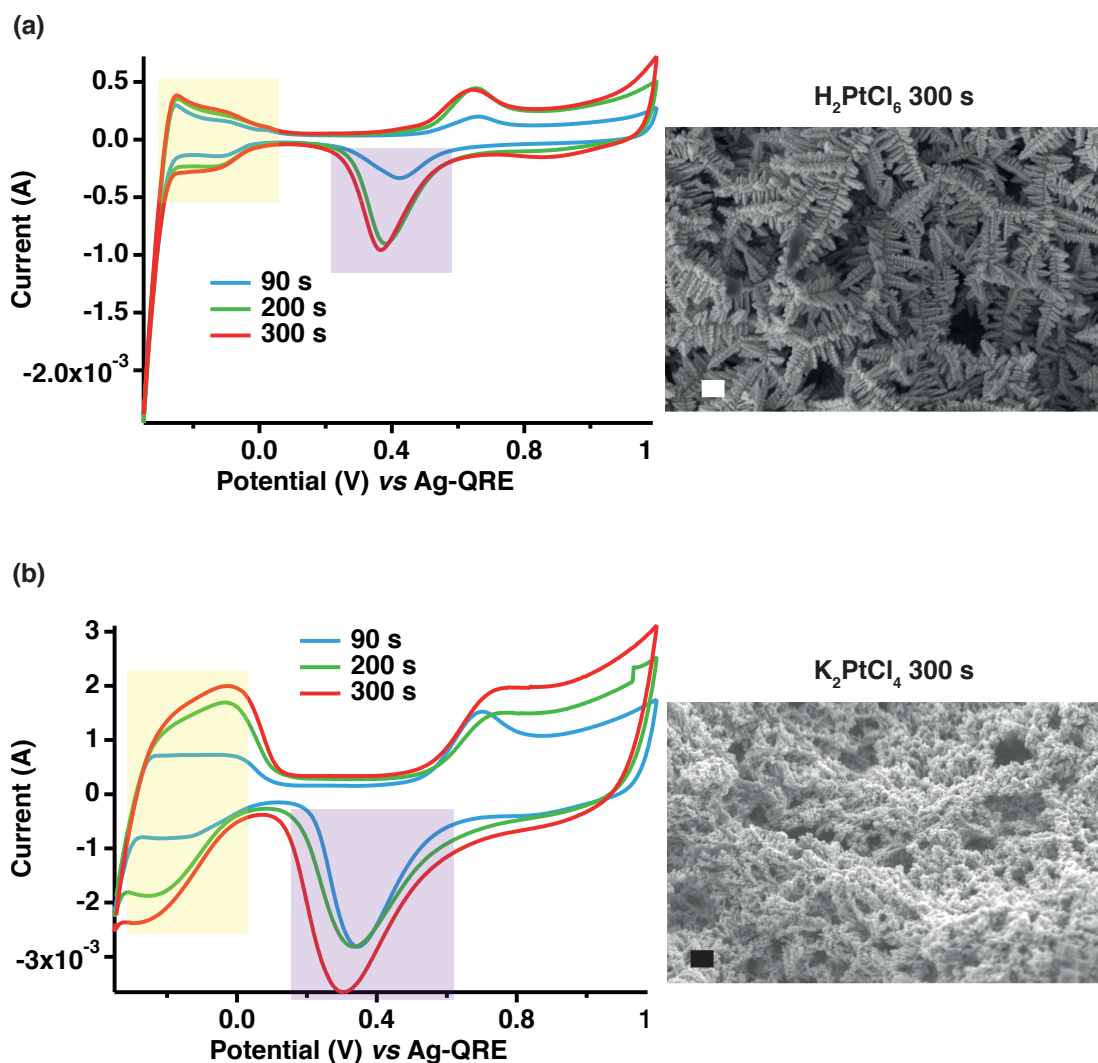


Figure 6.7 – CVs at 100 mV/s in 0.1 M H_2SO_4 at Au-Pt nanostructured alloys produced from tetravalent (a) and divalent (b) Pt-based solutions at different deposition times (applied potential: -2V).

Interestingly, the electrooxidation of hydrogen peroxide was experimentally observed at an optimal potential lower than +300 mV (value found with the hybrid monometallic Pt-Pt nanostructures). As shown in Fig. 6.8, the current response at the Au-Pt electrodes prepared with the two Pt salts increased passing from +700 mV to +200 mV as applied potential then a drop of the current was observed. It is interesting that the absolute value of the current is higher when electrodes modified with Au-Pt nanoferns are smaller in size and that the optimal potential acquired with Au-Pt nanomodified electrodes was lower than that acquired with Pt-Pt hybrid nanostructures. The increase of electrochemical signal passing from higher to lower potentials characterised Au-Pt and hybrid Pt-Pt nanostructures only. On the other hand,

Chapter 6. Electrochemical characterisation of Pt nanopetals and Pt nanospheres prepared by electrodeposition on screen printed electrodes

nanocoral-like structures of Au showed a similar response passing from +700 mV to +450 mV of applied potential and then a signal drop was recorded (Fig. 6.8). Au bare showed the lowest signal response and a signal drop by decreasing the applied potential from +700 mV.

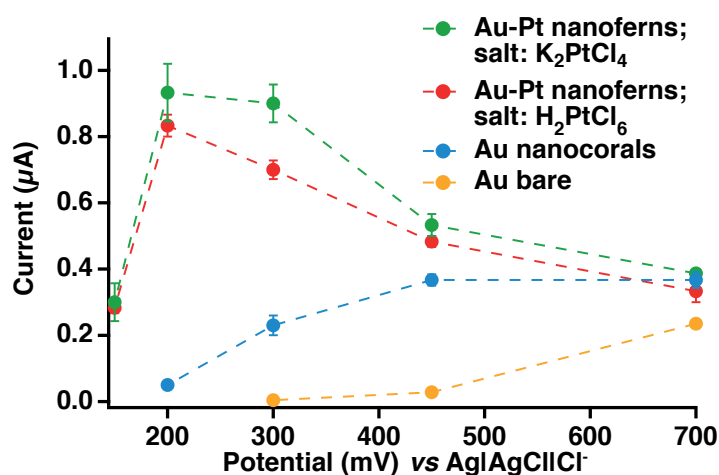


Figure 6.8 – Effect of the applied potential on the response of Au-Pt nanostructures (deposition time: 300 s; applied voltage: -2 V) grown from solutions containing H₂PtCl₆ (red) and K₂PtCl₄ (green). Effect of the applied potential on the response of Au nanocoral-like (cyan) and of Au bare electrodes (yellow). Error bars refer to the standard error of three intersample measurements.

Fig. 6.9 shows CVs acquired with Au-Pt nanostructures deposited for 300 s at -2 V in PBS without and in the presence of glucose (10 and 20 mM). Au-Pt nanostructures produced from H₂PtCl₆-based solutions (Fig. 6.9 (a)) show a peak related to the oxidation of glucose at \approx +215 mV while those obtained from K₂PtCl₄ solutions (Fig. 6.9 (b)) show a peak at \approx +550 mV. Similar potentials for glucose detection are present in the literature [171, 172]. The difference in shape and size of the Au-Pt nanoferns explains the change of potential for detecting glucose. Both the alloyed nanostructured electrodes show the appearance of only one peak in the presence of glucose in solution. CVs have a shape closer to those obtained at nanoAu electrode than to those obtained at nanoPt that are characterised by three peaks. This is probably due to the Au concentration higher than Pt in the alloy. Note the decrease of the reduction peaks caused by the adsorption and electrooxidation of glucose on the electrode surface, which reduce the formation of the oxides during the forward scan [173].

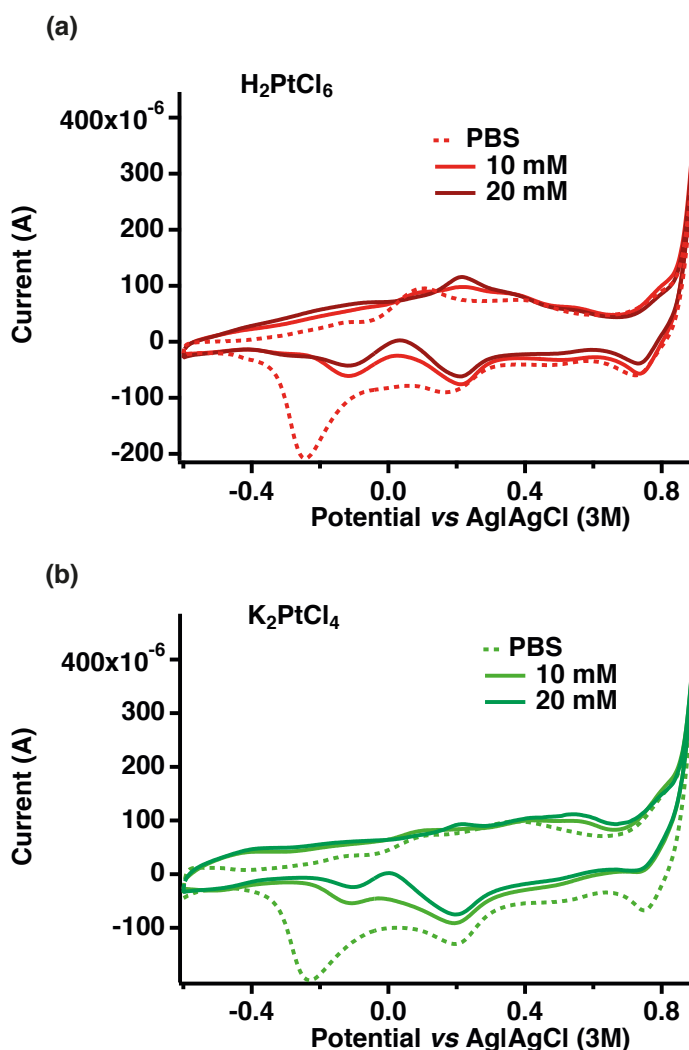


Figure 6.9 – CVs at 20 mV/s without and in the presence of glucose (10 and 20 mM) at Au-Pt nanostructured electrodes (deposition time: 300 s; applied voltage: -2 V) from solutions containing tetravalent (a) and divalent (b) Pt salts.

6.5 Summary and contributions

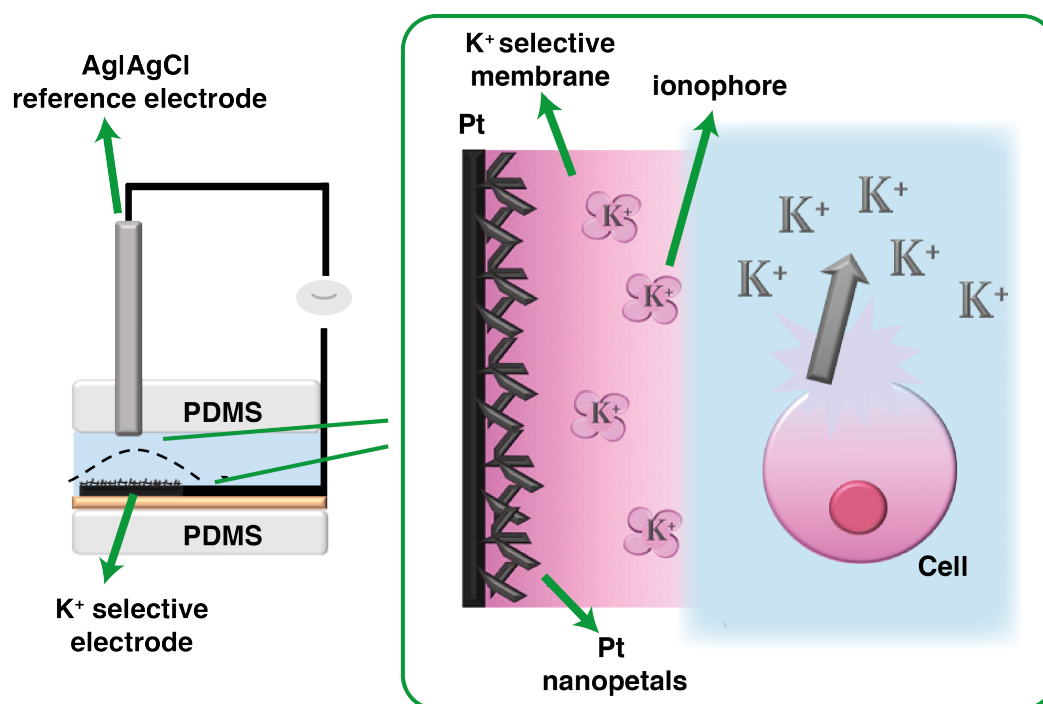
Without doubt, glucose is one of the most relevant molecule in medicine [106]. In this chapter, the superior properties of template-free electrodeposited Pt nanostructures in sensing glucose is proven as compared with bare Pt electrodes. Two ways to detect glucose with Pt nanostructured electrodes have been explored: (a) by using GOx immobilised on nanostructures thanks to the quantification of H_2O_2 , generated by the enzymatic reaction and (b) by direct enzymeless electrochemical oxidation [106].

Chapter 6. Electrochemical characterisation of Pt nanopetals and Pt nanospheres prepared by electrodeposition on screen printed electrodes

Achievements and contributions presented in this chapter are listed below.

- The principal novelty is the reduction of the H_2O_2 electrooxidation potential (≈ 150 mV) and the simultaneous increase of signal current at hybrid monometallic Pt-Pt nanostructured electrodes as compared with bare Pt electrodes. Sensing parameters related to glucose detection with an immobilised oxidase were among the best ones found in the literature having as additional advantage a considerably low working potential.
- Both potential reduction and signal increase are more pronounced when Au-Pt bimetallic nanostructured films are used rather than Pt-Pt hybrid nanostructures. The obtained findings demonstrate for the first time that the combination Au-Pt plays an important role for further enhancing the H_2O_2 electrooxidation.
- Another strength of the chapter is the demonstration of enzymeless glucose detection at Pt nanostructures in a real biosample. Sensing glucose in real samples is notoriously challenging because the adsorption on Pt of species from such a complex environment reduces the Pt catalytically active sites. Interestingly, the evaluated sensing parameters were similar to those found in the literature when synthetic buffers were employed.

7 A biological application of solid-contact potassium-selective electrode based on Pt nanopetals



Potassium is the predominant intracellular ion [174]. In homeostasis cells keep a high internal K⁺ concentration of 150 mM while in extracellular medium K⁺ level remains at 4 mM. The ionic balance is controlled by Na⁺/K⁺ ATPase that introduces K⁺ into cells while removing Na⁺ [175]. The disruption of the pump Na⁺/K⁺ and consequently of the membrane generates K⁺ effluxes that can be used to diagnose cellular dysfunctions and eventually to predict cell death [176].

A number of sensing approaches for detecting K⁺ have been already published including radiometry [177], flame photometry, specific electrode photometry and atomic absorption photometry

Chapter 7. A biological application of solid-contact potassium-selective electrode based on Pt nanopetals

[178], optical fluorescence (OPTICA, Roche Diagnostics) and patch clamp [179]. However, all of these techniques suffer from some limitations such as the off-line detection with repetitive sampling and problems of selectivity. Potentiometric devices are the most promising tools for continuous sensing of ions in concentration ranges of interest. They could also selectively detect an ion with respect to interfering ions always present in biosamples. Potentiometry is based on acquisition of a potential difference between a reference (RE) and a working electrode (WE), the latter covered with a membrane selective to the ion of interest. The main challenges of this method is to provide a stable potential over time and to miniaturise the sensing site. Solid-contact ion-selective electrodes (SC ISEs) are recently employed to obtain small sensing sites with satisfactory potential stability and measurement reproducibility. Self-assembled monolayer of a lipophilic redox-active molecule on gold electrode was proven to enable excellent ion-to-electron exchange properties [180]. However, the redox capacitance of the monolayer is very low. To overcome this problem, conducting polymers were initially utilised as intermediate layers because of their high redox capacitance [181]. Their high sensitivity to light and the high probability of water-layer formation have oriented researchers to use nanostructured materials as solid-contact ion-to-electron transducers. Nanostructures provide both high redox capacitance, essential requirement to obtain the potential stability, and high hydrophobicity to eliminate the unwanted water layer between metal electrode and selective membrane [39, 182]. The use of carbon [182] and gold nanomaterials [39] has been widely explored. However, the employed nanofabrication procedures were time consuming [39] or limited to a specific electrode material [182]. Few recent studies suggest that nanoPt could be successfully used in potentiometry and not only in voltammetry. Chung et al. [89] demonstrated the possibility to build miniaturised pH and REs combining nanoPt with polyelectrolyte junction. NanoPt has been not used yet as solid contact of potentiometric sensors for electrolytes of clinical interest (e.g., K^+ , Na^+ , Ca^{2+}). Furthermore, the use of a one-step template-free electrodeposited nanoPt as solid-contact of ISE and fabricated on a multisensing microfabricated platform has never been explored till now.

In the present chapter, a K^+ selective electrode based on nanoPt is proposed for the first time. Pt nanostructured layers are produced by a simple and fast one-step template-free electrodeposition on a microfabricated Pt electrode of a multipanel Si-based sensor. The potential stability over time is examined (Section 7.2). The main performance characteristics (sensitivity, LOD and selectivity) are studied in HEPES (4-(2-hydroxyethyl)-1-piperazineethanesulfonic acid) buffer solutions (Section 7.3). Then, the sensor is inserted in a polydimethylsiloxane (PDMS) fluidic system and used to monitor K^+ released by cells if exposed to DI water. The effect of a drug treatment on cells is studied by measuring K^+ effluxes produced by necro-apoptotic mechanisms (Section 7.4). Furthermore, the developed nanoPt- K^+ selective electrode (K^+ SE) is employed to continuously monitor in incubator K^+ released by cells in a bioreactor. The bioreactor consists of a chamber distinct from the main chamber of the sensor enabling the sensor to read K^+ effluxes at a distance (Section 7.5). Considering the demand of sensors with a stable on-board RE, the chapter concludes with the description of a protocol to build a miniaturised reliable RE integrated into the platform (Section 7.6).

7.1 Methods

Nanostructured Pt electrodes were synthesised using an Autolab potentiostat under a computerised control (Metrohm, Switzerland) from solutions containing 25 mM H_2SO_4 (95-98 %, Sigma) and 50 mM Pt salts. H_2PtCl_6 (Aldrich; applied potential: -1 V) or K_2PtCl_4 (FisherSci; applied potential: -0.2 V) were employed to synthesise Pt nanopetals and Pt nanospheres, respectively, as described in Chapter 5. Depositions were carried out for 200 s at room temperature under stirring. NanoPt was deposited on the Pt electrode (geometric area = 7.14 mm^2) highlighted in Fig. 7.1 where the main dimensions of the microfabricated platform are reported. After the deposition, a cleaning was carried out as described in Section 5.1 of Chapter 5. *Scanning electron microscope* (SEM) images of the nanostructures were acquired with a Zeiss Merlin high resolution SEM (5 kV).

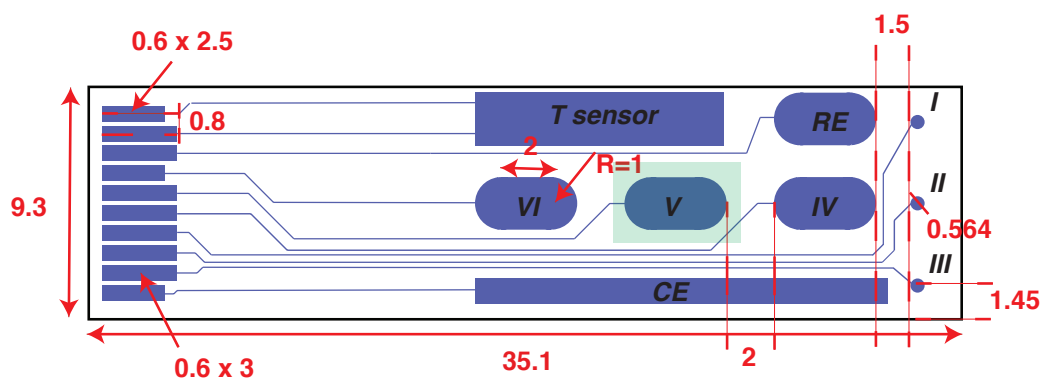


Figure 7.1 – Top view of the microfabricated electrochemical multisensing platform. The size of device and electrodes and respective distances (in mm) are reported. Highlighted with a green box, the electrode used for potentiometric K^+ detection.

K^+ *ion-selective membrane* (ISM) was obtained by dissolving 33.5% poly(vinyl chloride) high molecular weight (PVC, Fluka), 65% bis(2-ethylhexyl)sebacate (DOS, Fluka), 0.5% potassium tetrakis(4-chlorophenyl)borate (KTClB, Fluka) and 2% potassium ionophore I (Fluka) in 1 ml tetrahydrofuran (THF, Fluka) per each 100 mg of mixture. Bare and nanostructured electrodes were coated with 8 μl of K^+ ISM and used as working electrodes. The membrane was kept dried for 24 h and then conditioned in 10 mM KCl (Sigma) for at least 12 h before starting the experiments. An appropriate conditioning of the membrane is important because, after the membrane preparation, K^+ ions are not present inside the membrane. In the conditioning solution, the membrane gets slowly filled with K^+ . This step is very important because big K^+ concentration differences across membranes cause movement of K^+ in or out from the membrane, which leads to potential instability. A conditioning solution of 10 mM KCl was chosen since this concentration was close to the physio-pathological concentration level of K^+ in human fluids. SEM images of the membrane were acquired with a Zeiss Ultra55 high resolution SEM (15 kV). The ImageJ software [118] was used to evaluate the thickness of the

Chapter 7. A biological application of solid-contact potassium-selective electrode based on Pt nanopetals

membrane.

Fig. 7.2 shows a picture of the Si-based device (a) and the lateral view of the membrane (b). The average thickness of the membrane was of $(11.7 \pm 2.3) \mu\text{m}$.

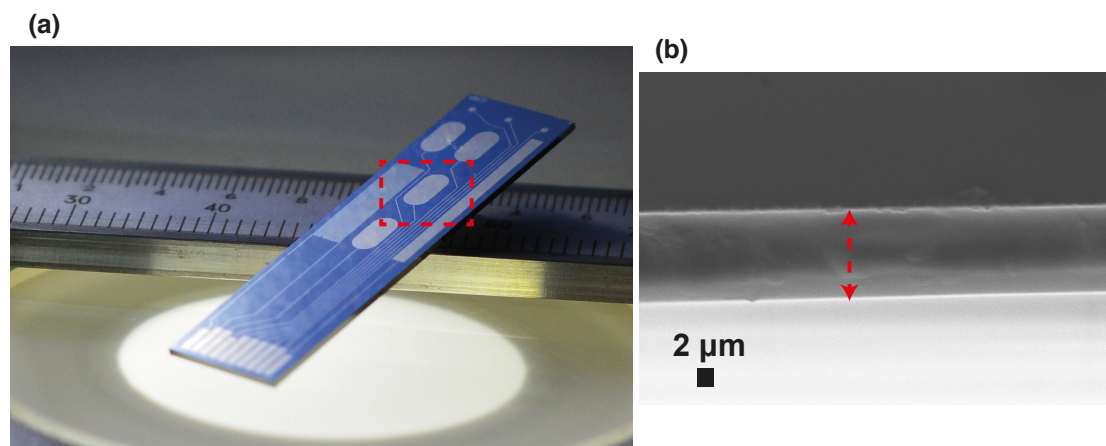


Figure 7.2 – Picture of the microfabricated device (highlighted the electrode used for building a nanostructured K^+ selective electrode) (a). SEM image of the K^+ ISM (lateral view). The double arrow covers the whole thickness of the membrane (b).

The potentiometric measurements were carried out in a beaker under stirred solution by using a double-junction RE (Metrohm, Switzerland, $\text{Ag}|\text{AgCl}$, 3 M KCl). The sensitivity was computed from the slope of the linear curve as shown in Fig. 7.3. The *detection limit* (LOD) was evaluated as the K^+ activity corresponding to the intersection (see Fig. 7.3) of the curve fitting the data points in the linear range and the average potential corresponding to K^+ activities at which the electrode is insensitive [183]. Further details on sensitivity and LOD evaluation procedures are in Appendix A.

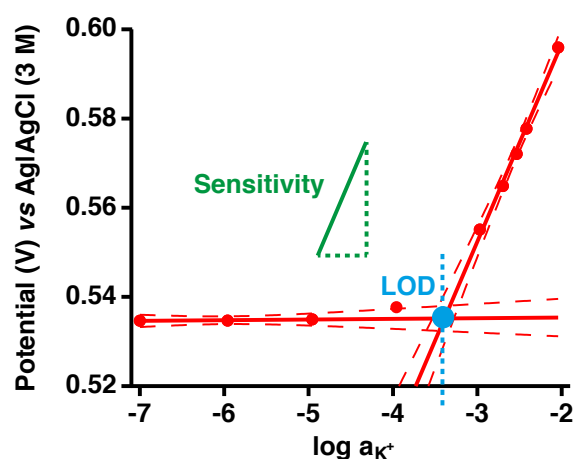


Figure 7.3 – Calibration plot of the solid-contact K^+ -selective electrode based on Pt nanopetals (stirring: 110 rpm).

The analytical performance of K⁺ selective electrodes were studied within a concentration range between 10⁻⁷ M and 10⁻² M KCl. The activity coefficients were computed using the Debye-Hückel equation [184]. The inter- and intra-sample reproducibility was evaluated by using a solution stirred at 80 rpm. Then, the solution was stirred from 80 rpm to 170 rpm and the effect of the stirring on sensitivity and LOD was evaluated. The *separate solution method* (SSM) was used to calculate the selectivity coefficients [183]. Briefly, the zero-current potential of the cell was measured in three separate solutions, the first containing K⁺ (0.1 M) and the second containing Na⁺ (0.1 M) and the third containing Ca²⁺ (0.1 M). The selectivity coefficient ($K_{(\text{ion}, \text{int})}$) was calculated from the equation below [183]

$$\log K_{(\text{ion}, \text{int})} = ((E_{\text{int}} - E_{\text{ion}})z_{\text{ion}} / (0.059 \text{ V})) + (1 - z_{\text{ion}} / z_{\text{int}}) \log a_{\text{ion}} \quad (7.1)$$

where z_{ion} and z_{int} are the charges of K⁺ and of the interfering ion (Na⁺ or Ca²⁺) and a_{ion} and a_{int} are the activities of K⁺ and of the interfering ion (Na⁺ or Ca²⁺), respectively. E_{ion} and E_{int} were the measured potentials in solutions containing only K⁺ and only Na⁺ or Ca²⁺, respectively. The selectivity coefficient is a number that provides a measure of how well the membrane can discriminate the ion of interest against interfering ions. If an electrode has equivalent responses to K⁺ and Na⁺, $K_{(\text{K}^+, \text{Na}^+)}$ is 1. The smaller $K_{(\text{ion}, \text{int})}$ is, the less the interfering ion is affecting our measurements. For instance, a $K_{(\text{K}^+, \text{Na}^+)}$ of 0.1 means that the electrode is 10 times more responsive to K⁺ over Na⁺.

Measurements in a fluidic system and with cell media were performed using a 600E Potentiostat (CH instrument, Inc.) and Ag|AgCl RE with porous Teflon Tip (1 M, CH instrument, Inc.). Cell media was prepared with DMEM 1X medium (Gibco, Life Technologies), 10% fetal bovine serum (Gibco, Life Technologies) and 1% penicillin-streptomycin (Life Technologies). Calibrations in DI water were carried out by using concentrations of K⁺ equal to 0.05, 0.1, 0.5, 1, 5, 10 mM. Calibrations in cell media were carried out for concentrations of K⁺ ranging between 6 and 16 mM by steps of 2 mM.

HepG2/C3A cell line (ATCC) was cultured at 37 °C with 5% CO₂ in T-175 cell culture flasks. Cell media was used in culture and replaced every 48 hours. Inocula begun at 2x10⁶ single cells. Cells were harvested at an 80% confluency. Cells were counted with a hemocytometer before static and dynamic experiments.

Viability images were obtained using a Zeiss Axio Observer D1 Fluorescence Microscope (Carl Zeiss, Germany). LIVE/DEAD® Viability/Cytotoxicity Kit (Life Technologies) was used to assess cell viability under DI water exposure and acetaminophen treatment. The ImageJ software [118] was used for cell quantification and analysis.

Single cells were seeded at 1x10⁶ and cells in spheroids at 10-20x10⁶ (1-2x1000 cells/spheroid) in 96 well plates and kept at 37 °C with 5% CO₂. After 24 hours, two plates, one containing

Chapter 7. A biological application of solid-contact potassium-selective electrode based on Pt nanopetals

single cells and the other spheroids, were exposed to DI water for 1, 5, 15 and 30 minutes. The third plat containing single cells underwent a treatment with 5, 25 and 50 mM acetaminophen for 36 hours. Then, DI water and media were collected and K^+ was measured for each condition with our K^+ selective electrode. Live and dead assays were immediately carried out after each of the before-described experimental condition.

7.2 Performance evaluation of Pt nanostructures

Potentiometric water-layer test is a common procedure to detect the formation of an aqueous layer between the selective membrane and the electrode surface after ISE exposure to the solution. Such water layer causes disadvantages as: (a) high sensitivity to osmolality changes inside the sample, (b) slow stabilisation time following ionic changes in solution, (3) drifts when interfering ions are introduced in (positive drift) or removed from (negative drift) the sample. Briefly, water layer tests were carried out by recording changes of the zero-current potential *vs* time when K^+ was substituted by Na^+ and vice versa. When a K^+ selective membrane is exposed to a solution of Na^+ , ion-exchange processes at the interface membrane-solution cause changes in ion composition of the membrane and of the aqueous layer when present (top part of Fig. 7.4). Considering the small volume of the aqueous layer, even little ionic fluxes determine big concentration variations. These variation are the source of a signal drift that is positive passing from K^+ - to Na^+ -containing solutions and negative when the change is in the opposite direction (bottom part of Fig. 7.4). A schematic illustration of the fluxes and of the potential drifts in the presence of a water layer is in Fig. 7.4.

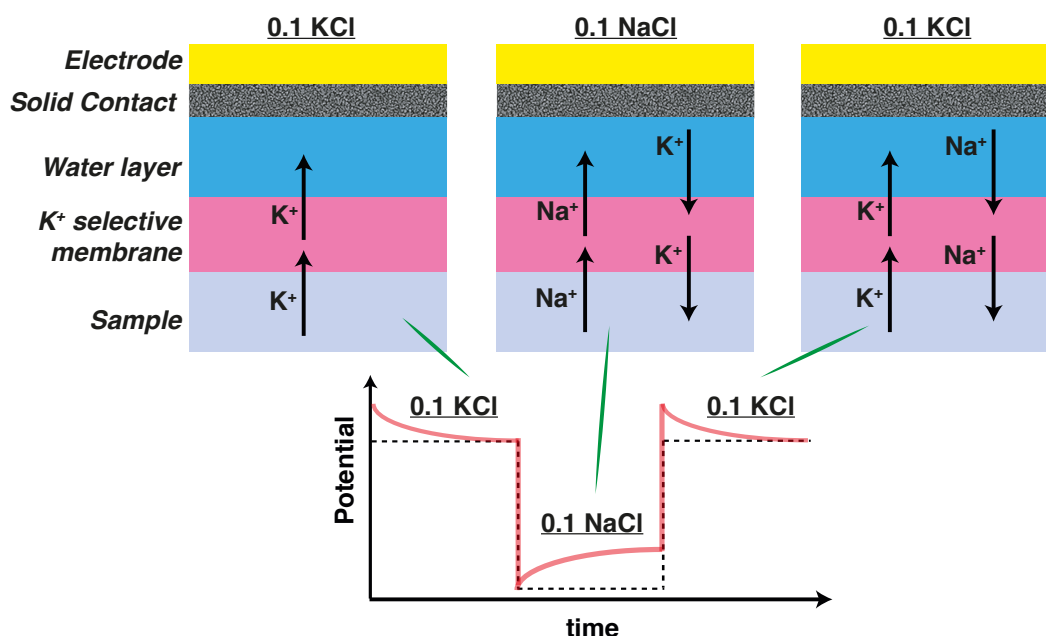


Figure 7.4 – K^+ and Na^+ fluxes and potential transients (solid line) after the formation of a water layer between solid contact and K^+ membrane. Dotted line: absence of a water layer.

7.2. Performance evaluation of Pt nanostructures

A PVC K^+ ISM was cast on bare electrodes and on electrodes modified with Pt nanopetals and Pt nanospheres. Measurements were carried out in sequence by using the following solutions: 0.1 M KCl, 0.1 M NaCl and 0.01 M KCl. Inset in Fig. 7.5 shows the potentiometric response of bare and of the two nanostructured electrodes in 0.1 M KCl, in 0.1 M NaCl and again in 0.1 M KCl. Only by employing ISEs without nanostructures, a positive and a negative drift was found passing from KCl- to NaCl-containing solutions and then from NaCl- to KCl-containing solutions. The directions of the two drifts indicate the formation of a water layer when the membrane is cast on bare electrodes. On the other hand, no drift characterised our nanostructured electrodes meaning the absence of a water layer between membrane and our solid contacts.

Besides evaluating the potential drift during the equilibration processes, the mid-term potential stability of three sensors in a constant environment (0.1 M KCl) was also evaluated. As clearly evident in Fig. 7.5, electrodes based on nanostructures exhibited a better stability over time (Pt nanopetals: $(32 \pm 2) \mu\text{V/h}$; Pt nanospheres: $(98.8 \pm 3) \mu\text{V/h}$ than Pt bare ($(7.698 \pm 0.005) \text{ mV/h}$) and similar to the better results reported in the literature [32, 185, 186, 187]. The lack of adhesion between the two sides of the membrane in absence on nanostructures is the cause of such high drifts.

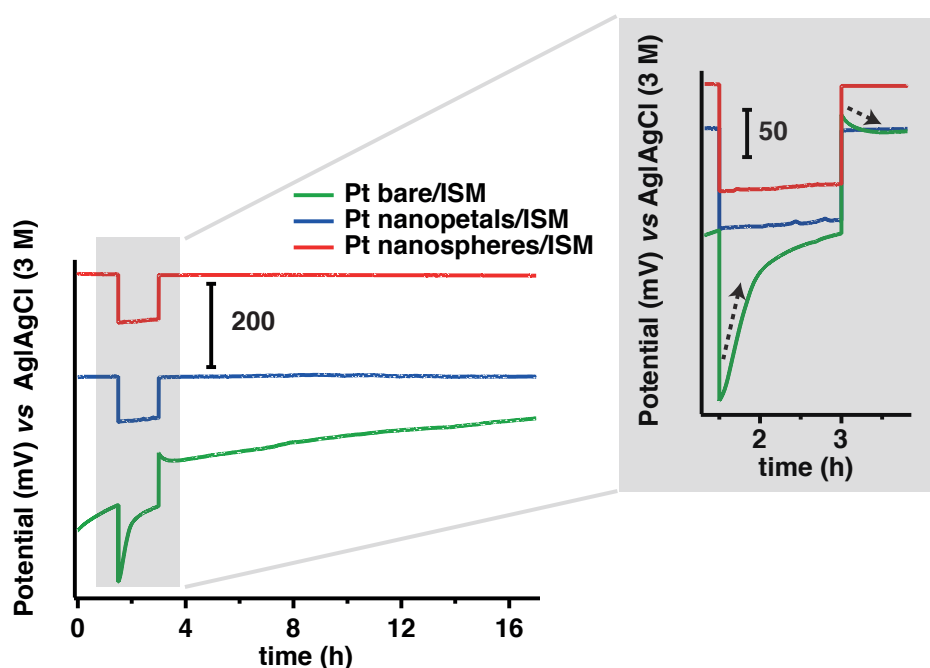


Figure 7.5 – Water-layer test for Pt- K^+ SE (green line), Pt nanospheres- K^+ SE (red line; -0.2 V for 200 s from divalent Pt-based solution) and Pt nanopetals- K^+ SE (blue line; -1 V; 200 s, tetravalent Pt-based solution). Inset highlights positive and negative drifts upon changing the solution from 0.1 M KCl to 0.1 M NaCl and vice versa indicating a water layer formation only between bare Pt and K^+ ISM.

Chapter 7. A biological application of solid-contact potassium-selective electrode based on Pt nanopetals

The potential stability of a SC ISE can be also determined in chronopotentiometry avoiding long-term stability experiments as suggested by Bobacka [188]. Polarisation of ISEs with current of some nA causes a potential jump (E) followed by a slow drift ($\Delta E/\Delta t$). The chronoamperometric technique proposed by Bobacka [188] and called *reversed chronopotentiometry* (RCP) was employed to evaluate potential stability and electric capacitance of our electrodes. Currents of ± 1 nA and ± 5 nA were applied for 60 s at each working electrode (Fig. 7.6 to see). From the potential jump (E), the total resistance of the electrode (R) was estimated according to the Ohm's law ($R=E/I$). The total resistance of the electrodes decreased of one order of magnitude in the presence of nanostructures as solid contacts passing from ≈ 3 M Ω to ≈ 0.3 M Ω . The potential drift was computed from the slope of the plot E vs t ($\Delta E/\Delta t$) and the capacitance (C) of the solid contacts was computed according to the equation $\Delta E/\Delta t = I/C$ where I is the applied current. Table 7.1 shows potential drifts and capacitances related to bare electrode and to electrodes where Pt nanopetals and Pt nanospheres were used as solid contacts. All the measurements reported in the next sections refer to Pt nanopetals- K^+ SEs.

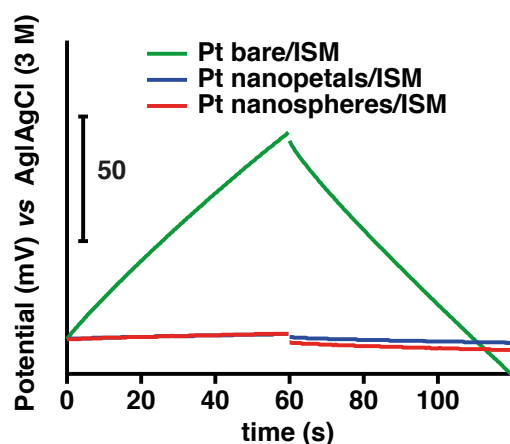


Figure 7.6 – RCP for Pt- K^+ SE (green line), Pt nanospheres- K^+ SE (red line) and Pt nanopetals- K^+ SE (blue line). The applied current was +5 nA for 60 s and -5 nA for 60 s in 0.1 mM KCl.

Table 7.1 – Potential drifts ($\Delta E/\Delta t$) and capacitances (C) of bare electrode and of electrodes nanostructured with Pt nanopetals and Pt nanospheres.

	Applied Current (nA)	$\Delta E/\Delta t$ ($\mu V/s$)	C (μF)
Pt bare	± 1	297.2 ± 11.2	3.4 ± 0.1
	± 5	1441.3 ± 106.6	3.5 ± 0.3
Pt nanopetals	± 1	6.7 ± 1.8	155.1 ± 42.5
	± 5	33.0 ± 1.9	151.6 ± 8.9
Pt nanospheres	± 1	7.9 ± 0.9	127.8 ± 14.8
	± 5	42.2 ± 6.8	120.2 ± 19.3

7.3 Characterisation of Pt nanopetal K⁺-selective electrodes

The sensitivity and the LOD values were estimated by measuring the open circuit potential and varying K⁺ concentration from 10⁻⁷ to 10⁻² M in a stirred solution. The average sensitivity of four sensors tested under the same condition (stirring: 80 rpm) was (31 ± 6) mV/dec and the average LOD was (-3.21 ± 0.07). The same sensor three-fold tested showed an average sensitivity of (30 ± 5) mV/dec and the average LOD was (-3.18 ± 0.03), values similar to those obtained from inter-sample measurements.

The selectivity coefficient, also called selectivity ratio, indicates the preference of an electrode for the ion of interest (our case K⁺) over the interfering ions. The selectivity coefficients calculated by SSM (stirring: 100 rpm) were: $\log K_{(K^+, Na^+)} = (-2.9 \pm 0.3)$ and $\log K_{(K^+, Ca^{2+})} = (-4.4 \pm 0.5)$ (n=3).

The sensing performance improved by increasing the stirring rate. The Nernstian slope was obtained by stirring the solution at 100 rpm. Above 140 rpm of stirred solution, the linear range increased from 1-10 mM to 0.1-10 mM and the average LOD decreased down to -4.6. By increasing the stirring velocity from 80 to 170 rpm, the response time reduces from some minutes to seconds. The concentration of K⁺ at the interface between membrane and solution must be kept as constant as possible to minimise the concentration gradients across the membrane during sample changes. Indeed, K⁺ concentration gradients at the interface membrane-sample cause a worsening of the sensing performance. Therefore, any measure to make ion fluxes more efficient (e.g., stirring, rotating electrode potentiometry) is helpful [189].

7.4 Measurements with a fluidic system

Monitoring in a continuous manner the status of cultured cells was conceived as the step preceding *in vivo* tests of sensors designed for healthcare analysis. In the past decade, the combination of sensing technology and cell-based microfluidic systems has increased the capabilities of *in vitro* studies [190], especially for non-stop monitoring of cellular events [191]. Small novel sensors coupled with a fluidic system could evaluate cellular functions and monitor cell behaviour by detecting a wide set of targets, ranging from ions to macromolecules. In this section, *solid contact K⁺ selective electrodes* (SC K⁺ SEs) based on nanopetal-like structures were coupled with a PDMS fluidic system and used to detect K⁺ released by cells. The effect of DI water on HepG2/C3A cells was evaluated by measuring the K⁺ effluxes due to osmotic shock in real time. The cells were also exposed to an acetaminophen treatment and the K⁺ effluxes produced by necro-apoptotic mechanisms were measured with the electrode. The novel electrode worked at 37 °C in a sterile environment (incubator) with an externally-located bioreactor enabling for the first time measurements of K⁺ effluxes from cells at a distance.

Chapter 7. A biological application of solid-contact potassium-selective electrode based on Pt nanopetals

7.4.1 Fabrication of fluidic system and bioreactor

Fig. 7.7 shows top (a) and lateral view (b) of the fluidic system hosting the sensor and the external RE and a picture of the bioreactor (c).

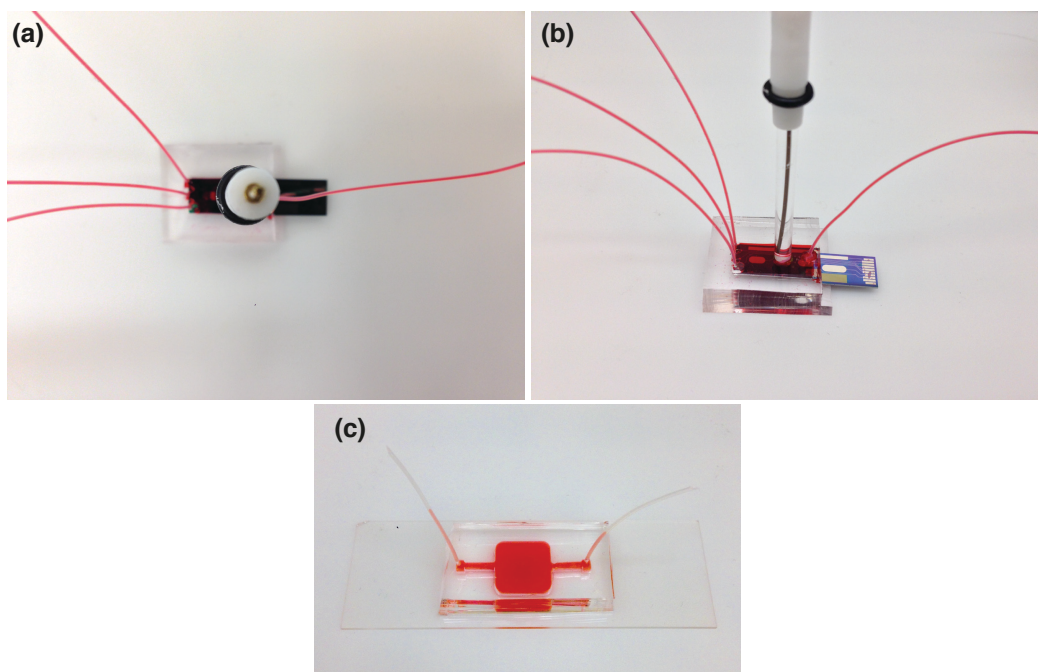


Figure 7.7 – Top (a) and lateral view (b) of the device assembled with the RE and the fluidic system. Picture of the bioreactor (c).

The fluidic chamber of the microfabricated sensor containing the SC K^+ SE was cut by using PDMS casting methods. Briefly, two *poly(methyl methacrylate)* (PMMA) molds of appropriate size and geometry designed by using the CorelDRAW®X5 Software (Corel Corporation) were prepared with a laser cutter first (Fig. 7.8 (a-1)) and stuck to Petri dishes (Fig. 7.8 (a-2)). A mixture of PDMS and curing agent (Sylgard 184, Dow Corning) was prepared in a ratio 10:1 and degassed under vacuum for 30 minutes. Then, 4 mg and 18 mg of the mixture were cast onto the Petri dishes containing the molds to build the bottom and the top layer of the fluidic system, respectively (Fig. 7.8 (a-3)). After a curing at 80 °C for 60 min, the PDMS layers were peeled off their molds (Fig. 7.8 (a-4)) and cut with a rectangular shape (Fig. 7.8 (a-5)). The chamber included one inlet, three outlets and a hole to host an external RE (Fig. 7.8 (a-6)). The bottom part of the fluidic chamber of the device was aligned with the sensor before being bonded with the upper part (Fig. 7.8 (b)). The bonding was realised by oxygen plasma treatment.

The bioreactor consisted of a glass layer permanently plasma bonded to a PDMS chamber (Sylgard 184, Dow Corning). The PDMS chamber and channels were cast around laser cut PMMA molds designed as previously described. After the integration of inlet and outlet 30AWG tubing (Cole Palmer) the bioreactor was perfused with a 50 $\mu\text{g}/\text{ml}$ Type I Collagen Solution

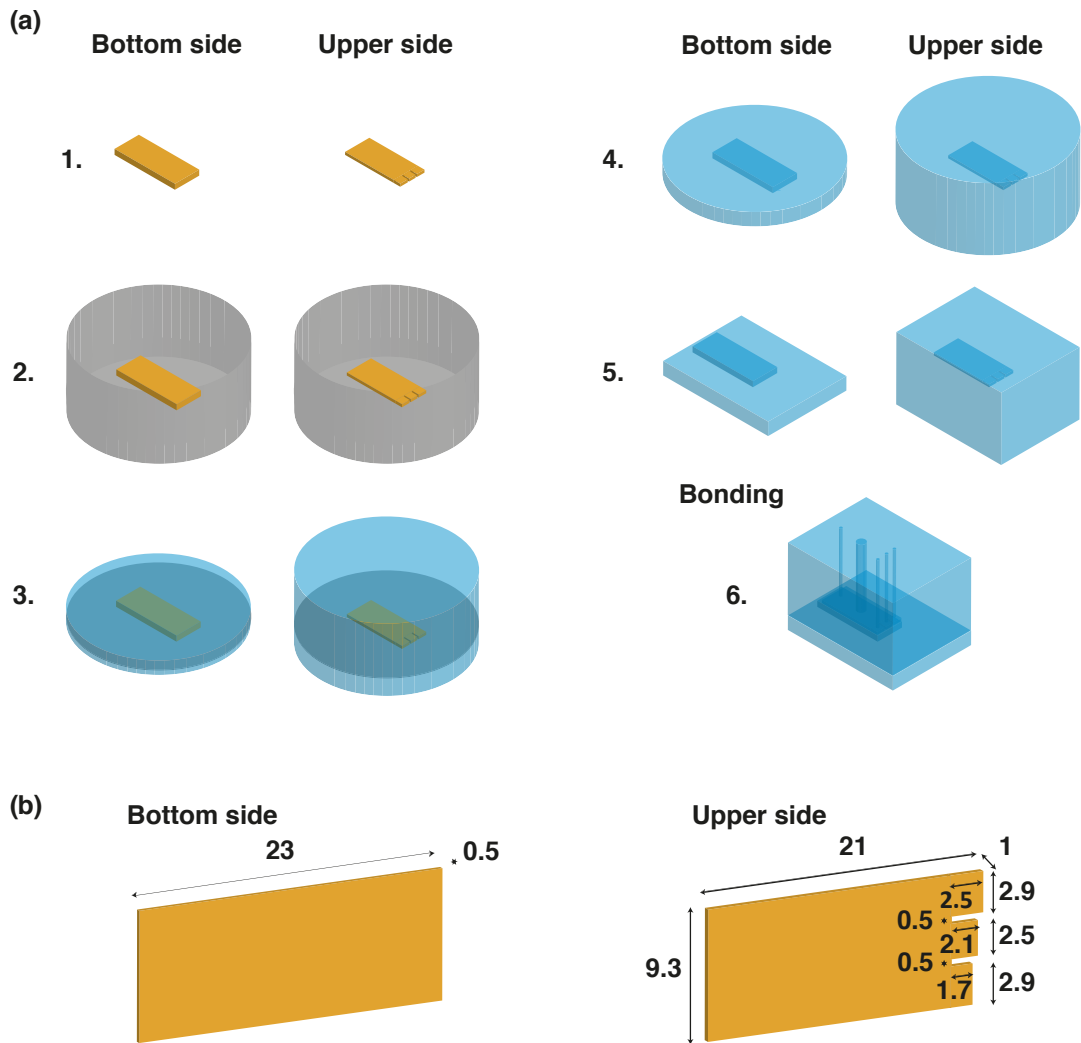


Figure 7.8 – Process flow of the fluidic system hosting the microfabricated sensor (a). Bottom and upper part of the fluidic system and their dimensions in mm (b).

from Rat Tail (Gibco, Life Technologies) and incubated for 2 hours at 37 °C. HepG2/C3A cells were then seeded in the bioreactor at 20×10^6 and left to attach for 24 hours.

7.4.2 Characterisation in HEPES buffer, DI water and cell media

The nanopetal-based K^+ SE showed a sensitivity near to Nernstian with a flow rate of 16.7 $\mu\text{l}/\text{min}$ as seen in Fig. 7.9 (a) where the potential change is shown by increasing first and then decreasing the ion concentration. The respective calibration curves are illustrated in Fig. 7.9 (b).

Chapter 7. A biological application of solid-contact potassium-selective electrode based on Pt nanopetals

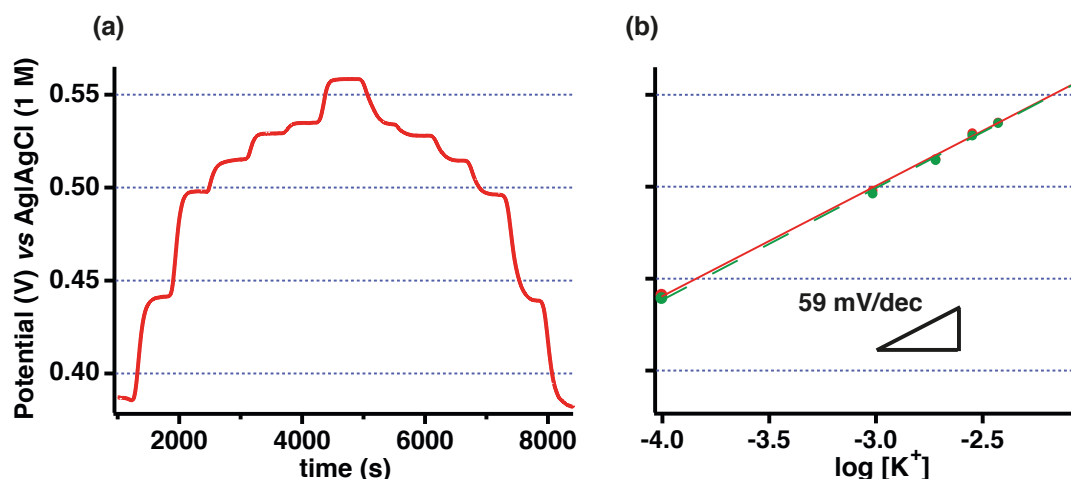


Figure 7.9 – Potentiometric measurement in a fluidic system (flow rate: 16.7 $\mu\text{l}/\text{min}$, K^+ concentrations: 0.1, 1, 2, 3, 4, 10 mM in HEPES, pH 5) (a) and calibration curves by increasing (red solid line) and by decreasing (green broken line) the ion concentration (b).

The nanopetal-based K^+ SE behaviour was still near to Nernstian when DI water and cell media were used as calibration solutions. Fig. 7.10 (a) shows the calibration curve for increased concentrations of K^+ from 0.05 mM to 10 mM in DI water and Fig. 7.10 (b) shows the calibration curve for increased concentrations of K^+ in cell media. The biosample had a starting K^+ concentration already in the millimolar range (6 mM) and, to calibrate the electrodes, K^+ level was increased up to 16 mM covering most of the pathological conditions of hyperkalemia. For this reason, K^+ concentrations investigated in cell media do not cover decades of variation as in DI water (see x axes of Fig. 7.10 (a) and (b)). Considering the presence of multiple and high concentrated ions in cell media, that makes difficult the computation of K^+ activities, the logarithm of K^+ concentrations (instead of K^+ activities) was taken for calibrating the nanopetal-based K^+ SE from the present section. Despite the electrochemical cell responds to changes of ion activities, the cell can be calibrated in terms of concentration since the activity is equal to the concentration multiplied by the activity coefficient. To do this, calibration solutions and test solutions were chosen so that the activity coefficient of K^+ was identical (cells were cultured in the same media used for calibrating the nanopetal-based K^+ SEs). Calibrations in DI water were carried out with respect to K^+ concentrations to extract easily the concentration of the ion from real samples.

The sensitivity decreased of about 20% by reducing the flow rate down to 9.3 $\mu\text{l}/\text{min}$ because of the detrimental effect of a decreased ion flux, as explained in Section 7.3. The ageing of the membrane on the Pt nanopetals was also evaluated. The nanopetal-based K^+ SE was kept for one week in the conditioning solution (0.01 M KCl) and a sensitivity drop of 30% was observed with respect to a Nernstian slope. The ageing is absent when the membrane is stored in a dry condition.

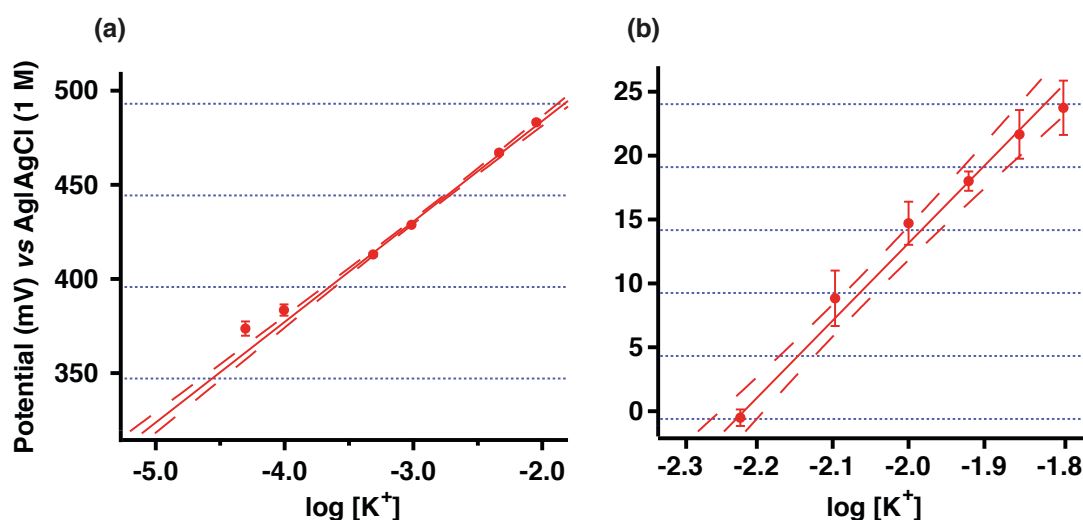


Figure 7.10 – Calibration curves in DI water (flow rate: 16.7 $\mu\text{l}/\text{min}$, K^+ concentrations: 0.05, 0.1, 0.5, 1, 5, 10 mM) (a) and in cell media (flow rate: 16.7 $\mu\text{l}/\text{min}$, K^+ concentrations: 6, 8, 10, 12, 14, 16 mM) (b). Error bars refer to intrasample triplicate measurements [183].

7.5 Acute cell death monitoring

Cell death by osmotic shock Shock by DI water produces cell expansion till the membrane is disrupted and the intracellular content, including K^+ , is emptied into the water. HepG2/C3A cells were exposed to DI water in a 96 well plate for several time points. Cell viability was evaluated and the K^+ released was measured after each interval time of exposure to DI water that caused cell death. With the electrodes previously calibrated, K^+ concentrations were evaluated after 1, 5, 15 and 30 minutes of cell exposure to DI water. A significant decrease of viability, corresponding to the highest increase of K^+ , started at minute 1. Fig. 7.11 shows the concentration of K^+ released by the cells and fluorescence images after 1, 5, 15 and 30 minutes of DI water exposure in the case of single cells (a) and spheroids (b). The percentage of live and dead cells (single cells only - Fig. 7.11 (a)) correlates well with the measured ion concentration demonstrating the reliability of our electrodes as a standard for cell death.

Chapter 7. A biological application of solid-contact potassium-selective electrode based on Pt nanopetals

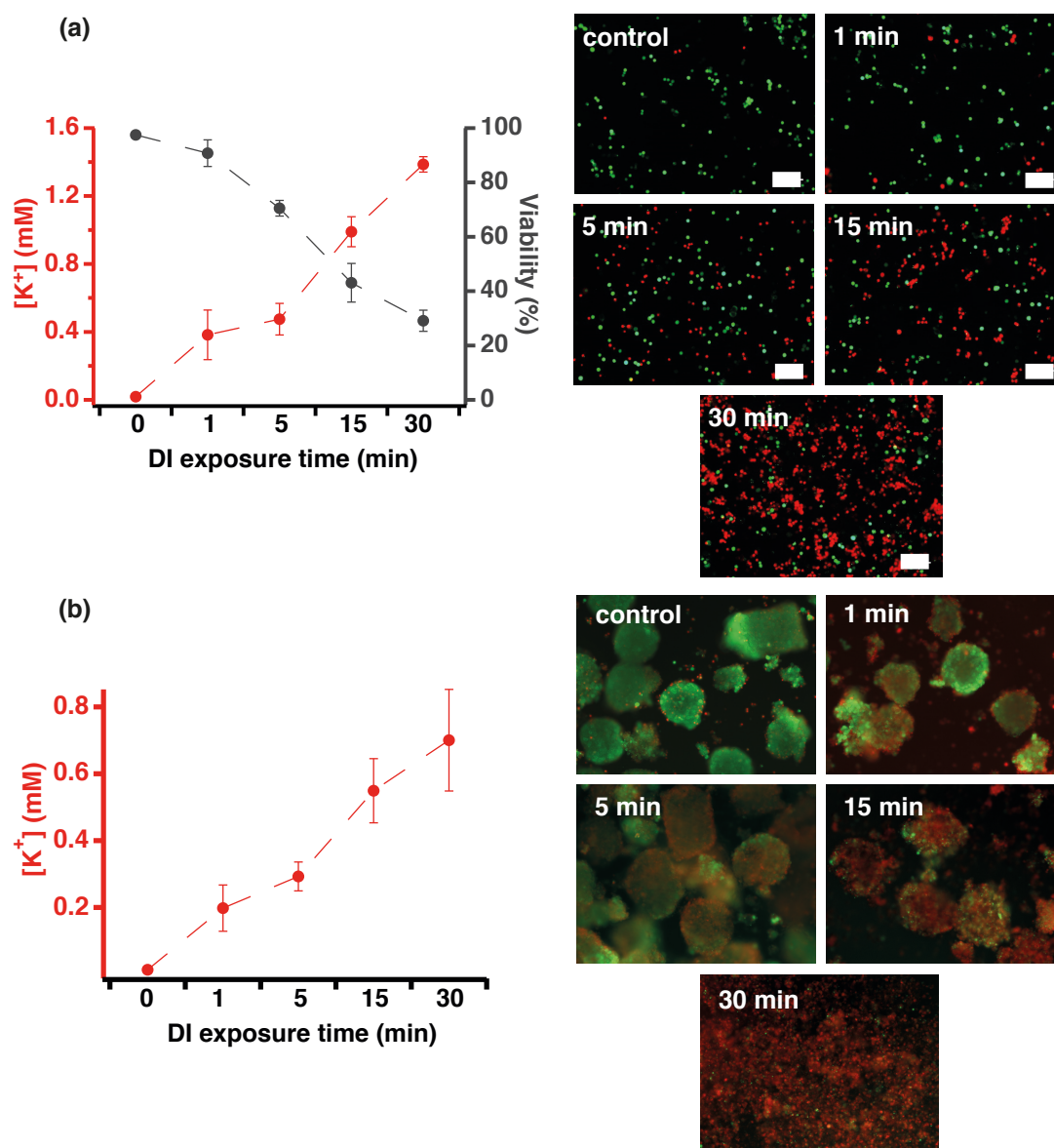


Figure 7.11 – Plot of the K⁺ concentration by exposing single cells to DI water for 1, 5, 15 and 30 min and live/dead cells in percentage. Microscope images of live (green) and dead (red) cells after 1, 5, 15 and 30 min of exposure to DI water. Bars: 100 μm (a). Plot of the K⁺ concentration by exposing spheroids to DI water for 1, 5, 15 and 30 min. Microscope images of live (green) and dead (red) cells after 1, 5, 15 and 30 min of exposure to DI water (b). Error bars refer to measurements done with three samples per each exposure time to DI water.

Cell death by drug treatment Acetaminophen is one of the most popular drugs [192] and extensively used for *in vitro* testing [193]. Doses over the limits reported in the literature [194] were selected to evaluate the drug cytotoxic effect. By inducing acute necro-apoptosis in HepG2/C3A cells, the resulting K⁺ efflux can be also measured and then compared with live and dead results. The concentrations of acetaminophen used were 5, 25 and 50mM in media

over a period of 36 hours in a 96 well plate. After calibrating the sensor in cell media, samples from the wells showed an elevation in the potentiometric signal in accordance to the live and dead assays (Fig. 7.12). While treatment in 5 mM acetaminophen does not show a significant decrease in viability or ion increase, treatment in media containing 25 and 50 mM of drug caused cell damage even after only 36 hours and an increase of K^+ concentration was detected with the nanopetal-based K^+ SE. The novel electrode was able to detect K^+ in undiluted media that already contained homeostatic amounts of K^+ and under pharmacological treatment both conditions first attempted with a K^+ selective electrode for cell culture monitoring. This finding demonstrates the definitely good performance of the realised electrode in monitoring cells apoptosis/necrosis. K^+ potentiometric measurements have been reported in previous works [176] but they required K^+ free sample (DI water). To the best of our knowledge, this is the first experimental proof in which potentiometric quantification of K^+ effluxes from cells is achieved in undiluted cell media.

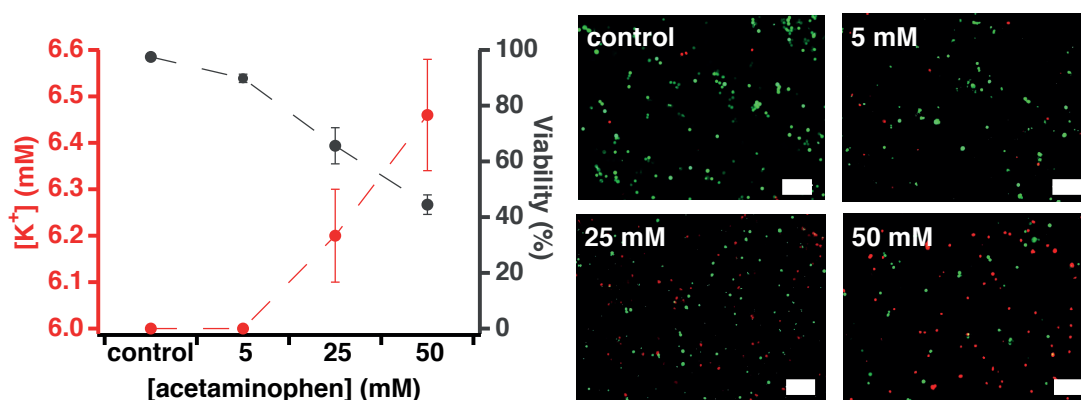


Figure 7.12 – Plot of the K^+ concentration by exposing single cells to media containing 5, 25 and 50 mM acetaminophen for 36 hours and live/dead cells in percentage. Microscope images of live (green) and dead (red) cells after culturing them in media containing 0, 5, 25 and 50 mM acetaminophen for 36 hours. Bars: 100 μ m. Error bars refer to measurements done with three samples per each drug concentration.

Continuous cell death monitoring The cell death was monitored continuously in incubator. The sensing parameters were not compromised by working at a temperature of 37 $^{\circ}$ C. Fig. 7.13 shows a picture (a) and a schematic (b) of the experimental setup used for continuous K^+ monitoring. A peristaltic pump is connected to a reservoir that perfuses the bioreactor, the sensor chamber and the rest of the system. Media or DI water flow into a waste container from the three outlets of the sensor chamber.

Chapter 7. A biological application of solid-contact potassium-selective electrode based on Pt nanopetals

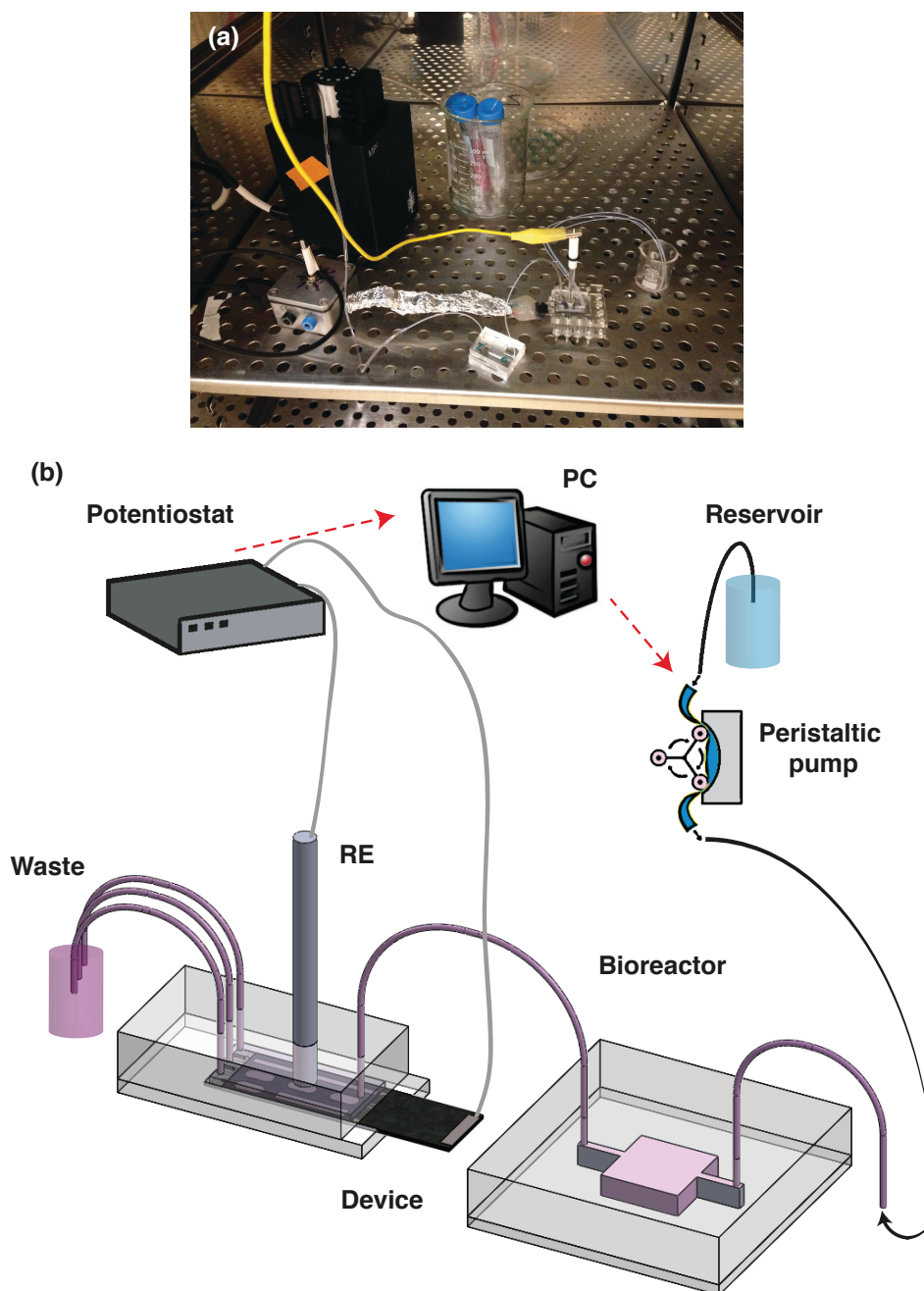


Figure 7.13 – Picture (a) and schematic (b) of the experimental setup used to monitor K^+ efflux after cell exposure to DI water.

Before each experiment, the fluidic chamber hosting the sensor was filled with DI water and the stabilisation of the signal was achieved (Fig. 7.14 (a) in green). Then, the bioreactor was filled with DI water and immediately connected with the inlet of the fluid system hosting the microfabricated sensor including the nanopetal-based K^+ SE. DI water in the bioreactor causes cell swelling and K^+ leaking to be monitored by the nanopetal-based K^+ SE (Fig. 7.14

(a). The maximum K^+ release was acquired after ≈ 30 min corresponding to $\approx 90\%$ of dead cells (Fig. 7.14 (b)). The entire system was then rinsed with DI water and calibration was carried out. Successful non-stop readings at 37°C carried out by keeping cells in a separate chamber from that of the sensor makes our nanopetal-based K^+ SE suitable and reliable for K^+ measurements in biomimetic platforms to monitor cells death. The decrease of the potential during the washing step showed a trend similar to that reported in [176]. Continuous cell death monitoring *via* potentiometric quantification of K^+ has been previously realised by Generelli and coworkers [176]. Nevertheless, their experiments were not performed in incubator and, more importantly, the cells were floating around the sensing site so that K^+ dilution issues were limited with respect to our setup.

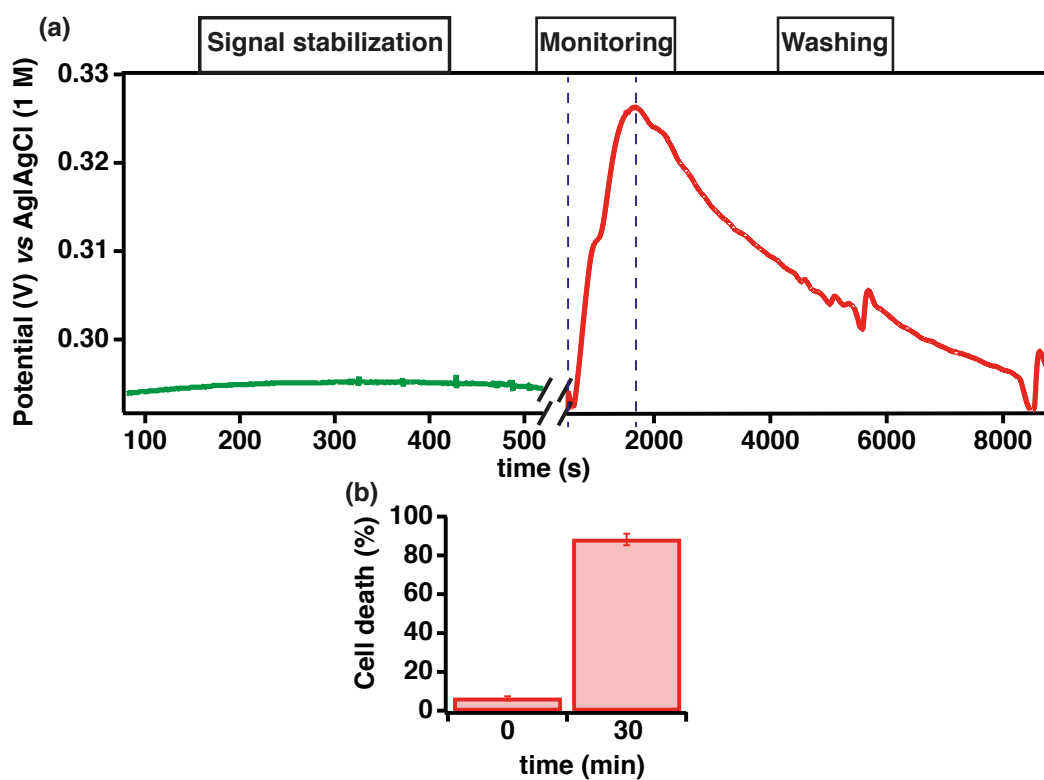


Figure 7.14 – Signal stabilisation (green), monitoring in incubator of K^+ efflux from cells in a bioreactor after exposure to DI water (red). Rinsing with DI water (red) (a). Cell death percentage after exposure to DI water ($n=4$) for 30 minutes (b).

7.6 Building an integrated all-solid-state RE

RE plays a crucial role in potentiometric devices and more generally in all electrochemical measurements. Basic requirements for a RE are the high exchange current densities, the non polarisability and a minimum drift over time [195]. A stable RE is important especially for potentiometric measurements in which the RE is responsible of half of the signal. Its stability ensures the sensor to work effectively.

Commonly used REs contain an inner-filling solution that causes numerous disadvantages such as the need of good maintenance, the high cost of manufacture, the contamination of the sample due to problems of leakage, their use only in a vertical position to keep the contact sample/liquid junction and the difficulty of miniaturisation.

Potentiometric sensors for point of care and/or continuous health monitoring need a durable miniature RE fully integrated with the platform. The most promising approach reported up to now has been the microfabrication of a *solid-state* (SS) Ag|AgCl RE covered with a membrane to ensure a constant and high chloride concentration (Polyurethane, Nafion, silicon rubber) as well as to minimise AgCl dissolution (PVC, epoxy) [195]. Silver is deposited by a thin film deposition technique (metal evaporation, sputtering or CVD), electrodeposition or screen printing and then oxidised either electrochemically or chemically [195].

7.6.1 Preparation procedures

Ag was deposited on Pt electrodes (area = 12.56 cm²) by electrodeposition from a solution containing 10 mM Ag₂SO₄ (extra pure, SLR, FisherSci), 1.5 M KSCN (Fluka), 2.5 M NH₄Cl (BioChemica, Applichem) at -1 V for 10 s. Glassy carbon and silver electrodes were used as CE and RE, respectively. Electrodeposition allows us to obtain a thicker and rougher layer of Ag (Fig. 7.15 (a) on the left) compared to other deposition techniques providing a much larger active surface area that is important for improving the stability of the RE. Both an electrochemical anodisation (-0.5 V for 20 s and +20 μA for 1800 s in 0.1 M KCl buffer - pH adjusted to 2.2 with HCl) and chemical anodisation (1 min in 50 mM FeCl₃ [196]) were investigated. Chemical treatment was selected because faster than the electrochemical one and equally well-performing. Fig. 7.15 (a) on the right shows the AgCl particles formed after the chemical treatment. The increase of Cl on the Ag surface is clear from the EDX spectra before and after the chemical anodisation and shown in Fig. 7.15 (b). A solution of polyvinylbutyral (79.1 mg) and NaCl (50 mg) was prepared in 1 ml methanol. Finally, a drop of 10 μl of the solution was cast on the Ag|AgCl electrode and let dry for 24 h.

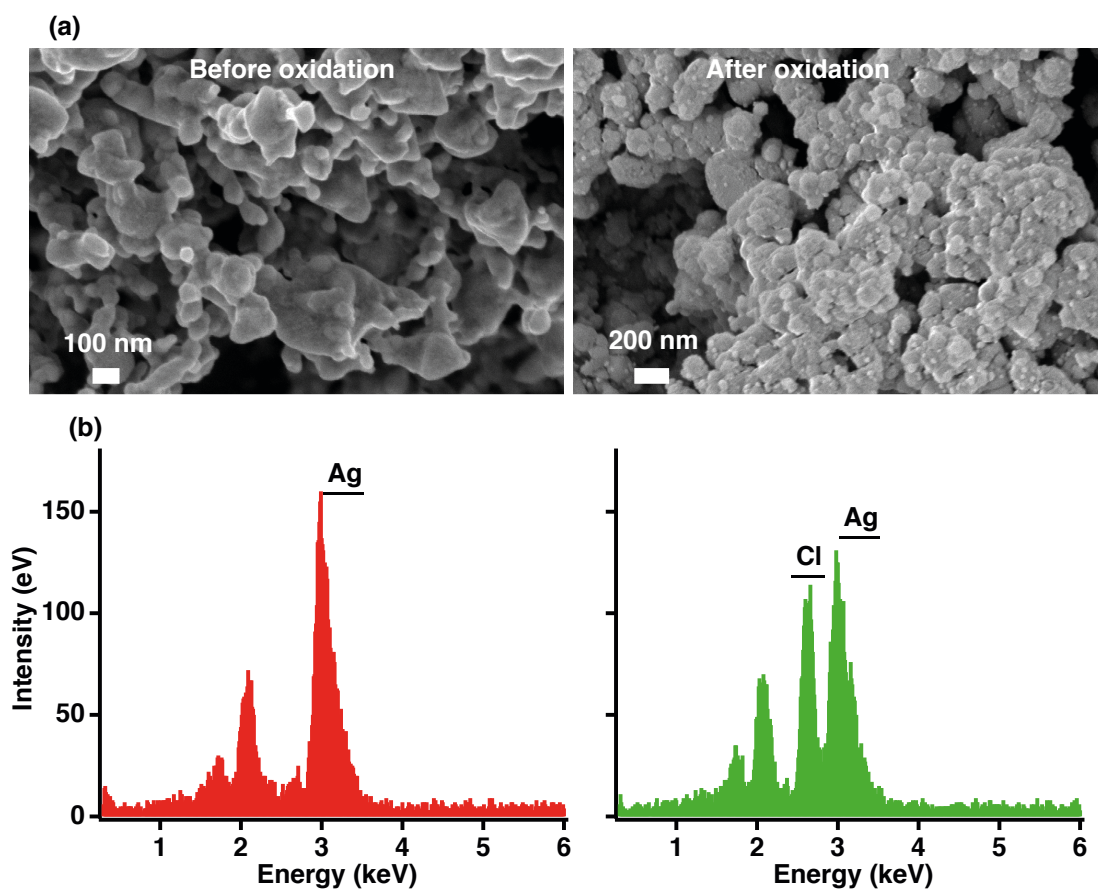


Figure 7.15 – High magnification SEM images (a) and EDX spectra (b) of electrodeposited Ag before (left) and after (right) the chemical oxidation.

7.6.2 Results

Fig. 7.16 (a) shows the CVs of a glassy carbon WE *vs* two SS REs and *vs* double junction RE Ag|AgCl (3M) in 0.5 M potassium hexacyanoferrate (III) (reagentplus, TM, 99%) solution. The potential shift towards more negative potentials by using the microfabricated RE of about 110 mV. The voltammograms were coincident when the two SS REs were used. Values of peak currents and of peak-to-peak separations were equal by using SS REs and the commercial RE.

As shown in Fig. 7.16 (b), the sensitivities in cell media towards the K^+ detection were similar when a SS RE and a commercial Ag|AgCl RE (3 M) were used.

The SS RE was proven to be insensitive to the addition of the most common ions of biological significance (K^+ , Na^+ , Ca^{2+}) and a slight sensitivity to the pH change as shown in the Fig. 7.16 (c).

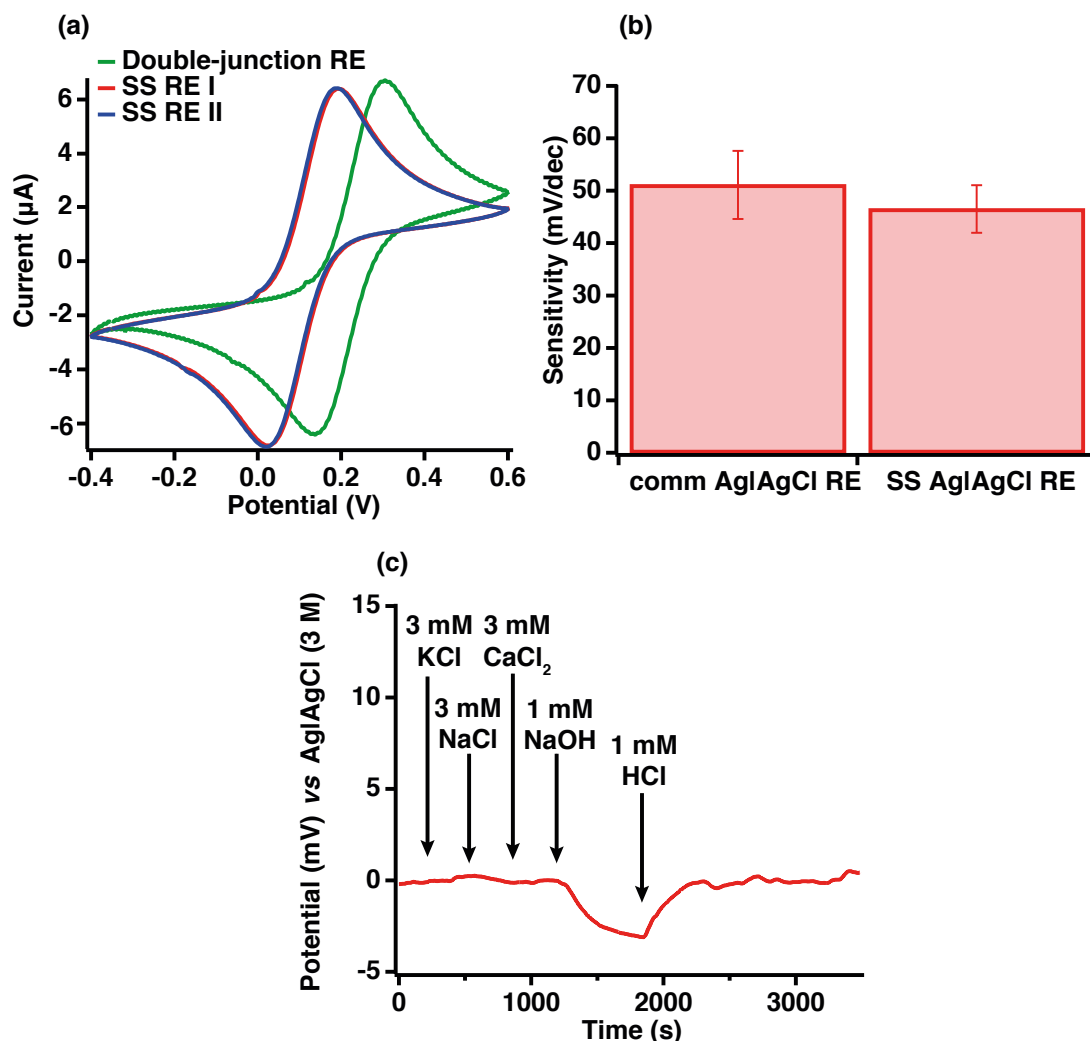


Figure 7.16 – CVs of glassy carbon WE *vs* two SS REs (in red and in blue) and glassy carbon WE *vs* double junction RE Ag|AgCl (3M) (in green) (a). Sensitivities of K⁺ sensors by using SS REs (n=4) and a commercial RE Ag|AgCl (3M) (n=3) (b). Responses of a SS RE *vs* commercial RE Ag|AgCl (3M) by adding 3 mM KCl, 3 mM NaCl, 3 mM CaCl₂, 1 mM NaOH, 1 mM HCl in cell media (c).

7.7 Summary and contributions

The most commonly used techniques for sensing ions in biosamples have numerous selectivity problems and limited *off-line* detection with repetitive sampling. Potentiometric devices enable continuous and highly selective detection of an ion even in complex samples as human fluids. *Solid-contact ion-selective electrodes* (SC-ISEs) based on nanomaterials have been recently employed to obtain small sensing sites with exceptional potential stability and reproducible measurements.

The main achievements and contributions of the present chapter are described below.

- Pt nanostructured electrodes, produced by template electrodeposition, have been previously employed as solid contacts to build pH [197] and reference [38] electrodes. Our nanostructured coatings were obtained by a simpler and faster one-step procedure than the method employed by Park [197] and Han [38] and are the first examples of Pt nanostructured films used as solid contacts of electrodes selective to ions (here K^+).
- In this chapter, a solid-contact K^+ -selective electrode is used for the first time for a real biological application. Unlike previous works [176], this chapter shows the first experimental proof of acute cell death monitoring as effect of a drug treatment by potentiometric measurements. Therefore, our electrodes are suitable for K^+ detection in biosamples that already contains K^+ .
- Cell lysis was continuously monitored for the first time at 37 °C in a sterile environment enabling the nanopetal-based K^+ -selective electrode to run long-term monitoring of biological samples.
- In previous works, potentiometric measurements of K^+ for cell culture were realised with cells in the sensor chamber. This chapter describes cell death in a separate chamber from that containing the sensor. The proposed nanopetal-based K^+ -selective electrode can sense K^+ despite the high dilution that our setup entails.
- Considering the high demand of miniaturised sensing sites in medicine, a stable solid-state Ag|AgCl reference electrode has been fabricated to substitute the big external reference electrode with another fully integrated on the platform for potentiometric ion readings.

8 Conclusions and Future Research Directions

Nanomaterial- and nanoporous-based electrodes are novel emerging electrodes that can be used to increase the performance of electrochemical sensors. In particular, easy and rapid nanostructuring steps at low cost and without using any binders as additional materials are highly desirable. In diagnosis, nanostructuring protocols should be compatible with micro-sized electrodes of invasive, wearable or portable devices that are going to substitute conventional laboratory tests. It is worth to mention that nanostructured materials, if appropriately integrated, may confer higher sensitivity, better measurement stability, excellent selectivity towards a biomolecule than flat electrodes.

My research focused on the development of novel electrodic nanostructurations and on their optimisation by looking at the ease and the reproducibility of the procedure, at the film stability and at the final electrochemical performance. Two classes of nanostructures were considered: carbon nanomaterials and nanostructured films of noble metals (monometallic Pt and bimetallic Au-Pt systems).

Achievements are summarised below.

- **Integration of carbon nanomaterials and electrochemical measurements.** A new protocol to directly grow a wide range of carbon nanomaterials by *chemical vapour deposition* (CVD) onto specific micro-sized sites of an implantable CMOS device was proposed in this thesis. This method ensured a close nanostructure-metal electric contact avoiding the use of additional binders, ever-present by using other nanointegration techniques. Binders hinder the nanomaterial properties and make the nanostructuring unstable in water-based environment. By a fine tuning of the deposition parameters, growths were obtained down to CMOS compatible temperatures opening the possibility to a direct integration nanostructures/front-end CMOS data acquisition circuits. Such nanostructured devices were proven to be powerful for sensing biomarkers within physio-pathological ranges independently from interfering species. In addition, CVD grown nanomaterials exhibited competitive biosensing performance and an excellent resistance to biofouling.

- **Integration of noble metal nanostructured films and electrochemical measurements.** This work also presents an innovative and optimised integration of different Pt and Pt-Au nanostructured films (nanospheres, nanopetals and nanoferns) onto electrodes by rapid electrodeposition processes. Novel template-free methods were described for the first time. Template-free electrodeposition was selected to reduce the effect of other material residues which may unfavourably change the electrocatalytic features of metal nanostructures. Two major advantages were achieved by employing our metal nanostructures: unprecedented reduction of the oxidation potential towards hydrogen peroxide (reaction product of oxydase-based sensors) with simultaneous increase of the signal response (a) and highly-sensitive non-enzymatic glucose detection even in undiluted biosample (b). Note that this last finding makes considerable promise for using the present technology as better alternative to commercially established devices for diabetes monitoring (85% of the whole biosensor market) which lifetime is limited by the stability of the enzyme.
- **Nanotechnology to boost continuous metabolic assessment of Cell-On-Chip.** A novel solid-contact potassium selective electrode based on Pt nanopetals was successfully designed, fabricated and tested as standard for acute cell death evaluation and continuous monitoring. Such finding opens the possibility to use the proposed nanostructured electrodes fabricated on miniaturised electrochemical sensing platforms to monitor organ and tissue necrosis.

Possible future works of this PhD thesis are described below.

- **Integration of nanostructured sensors with miniaturised custom-made potentiostat for multisensing.** Miniaturised medical devices require the combination of microfabricated electrochemical platforms with *ad hoc* low-noise electronics on a *printed circuit board* (PBC). A PBC-based chip was recently realised in our lab to carry out continuous electrochemical measurements and signal readings of different metabolites and ions. Simultaneous measurements of more than one analyte (glucose and lactate) were also carried out by using our multipanel electrochemical sensor in a fluidic system and an integrated electronics. Specific nanostructures were integrated onto the working electrodes of the platform to improve sensing performance and time stability. Electrode nanostructurations helped to reproducibly immobilise enzymes on different micro-sized electrodes while preventing protein leakage and denaturation.

Considering our recent accomplishments, a possible direction of the present work could be the simultaneous sensing of metabolites and ions directly from human fluids with an *on-board* electronics. By carefully selecting the type of nanostructuration, multiple detection can be achieved within adequate concentration ranges. The chemical crosstalk, resulting from multiple measurements with one platform, and the influence of interfering species improve by selecting appropriate nanostructures for each electrode.

-
- **Nanoporous electrodes.** Further optimisation of template-free electrodeposition processes to obtain other differently sized and shaped (dendrites, spheres, cubes, spikes, petals) nanostructured metals, binary-metals or alloys for enhanced electrochemical properties could be of enormous scientific interest. Voltammetry and potentiometry but also other electroanalytical techniques and other biomarkers could be considered. Post-treatments should be taken into account to further boost the sensing capabilities and to minimise fouling and biofouling.
 - **Exploiting advanced micro-nanofabrication technologies for continuous health monitoring.** The investigation of nanostructured miniaturised electrochemical devices for continuous monitoring of Organ-on-Chips or animals could be an interesting point to develop. In both cases, low-volume microdevices are required for fast and non-stop metabolic analysis. In the field of Organ-On-Chip systems, an appropriate design and long-term testing of single or multipanel nanostructured devices fully-integrated with microfluidic components is expected. The main challenges in the case of *in vivo* experiments are the efficient integration of nanostructures on devices that are always more frequently fabricated on flexible or stretchable materials.

A Electrochemical sensing parameters

A.1 Performance evaluation from voltammetric measurements

Calibration curve In CA, the average currents corresponding to a certain analyte concentration were computed by averaging points related to an interval time (20 s or 60 s) per each steady-state signal. From voltammetric measurements, the heights of the peak currents were evaluated by fitting peaks with Gaussian (principally peaks in DPV and SWV) or Exponentially Modified Gaussian (peaks in CV) models [198]. Before starting each fitting, a linear or cubic baseline (Fig. A.1; case of BR) was subtracted. The Igor Pro (Wavemetrics, Lake Oswego, OR, USA) software was employed for data analysis. Calibration curves were obtained by plotting the steady-state currents (CA) or the peak height currents (CV, DPV, SWV) *vs* the analyte concentration.

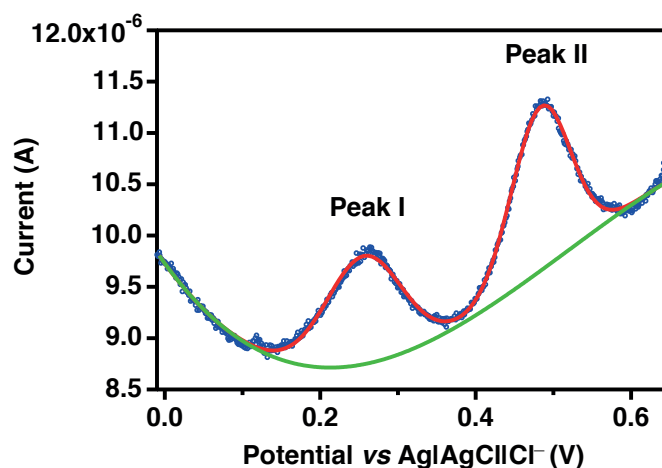


Figure A.1 – Fitting (red) of the two voltammetric peaks related to the oxidation of BR (Peak I; blue) and BV (Peak II; blue) by using Gaussian curves. Cubic baseline in green. BR concentration: 150 μ M in PBS 10 mM, pH 7.4.

Appendix A. Electrochemical sensing parameters

Linear range An ordinary least squares model has been used to fit the data. The linear range has been identified on the basis on the determination coefficient ($R^2 > 0.99$) and by verifying the residual values were randomly distributed about the regression line [199].

Sensitivity Slope of the calibration curve in the linear range.

LOD Defined as the concentration of an analyte which gives a signal significantly different from the blank response. Many approaches have been used so far taking into account: the signal-to-noise ratio [200], statistical parameters resulting from the linear fitting [199], the standard deviation of the measurements in blank [199, 201]. In this work, the IUPAC definition of LOD was considered that is defined as [199, 201]

$$LOD = 3\delta_{\text{blank}}/S \quad (\text{A.1})$$

where δ_{blank} is the standard deviation referred to the blank signal and S is the sensor sensitivity. In CA, three steady-state currents of the blank were acquired (intervals of 20 s) and the standard deviation of the average per each stream was computed. In CVs, SWVs and DPVs three voltammograms of the blank were acquired and then the standard deviation of voltammogram portions corresponding to the position of the peak potentials of interest was computed.

A.2 Performance evaluation from potentiometric measurements

Calibration curve Plot of the emf (electromotive force $-E$) measured between a K^+ SE and a reference electrode *vs* the logarithm of K^+ activities (DI water or HEPES buffer) or K^+ concentrations (cell media) (red dots in Fig. A.2) [183].

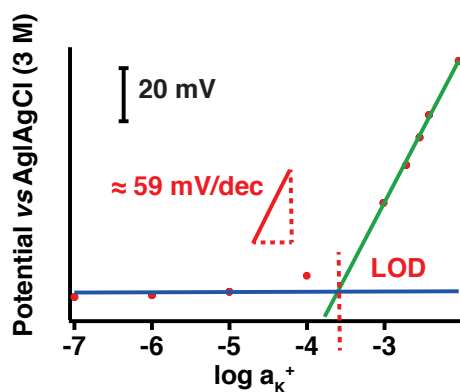


Figure A.2 – Typical K^+ calibration graph.

A.2. Performance evaluation from potentiometric measurements

Sensitivity Slope of the linear curve (95% confidence interval according to the IUPAC definition [183]) fitting the data points in the linear range. The linear range was taken for K⁺ concentrations higher than 1 mM for measurements in beaker at stirring < 140 rpm or higher than 0.05 mM for measurements in beaker at stirring > 140 rpm and measurements under flow conditions (green line in Fig. A.2). A minimum of five data points was taken to evaluate the sensor sensitivity and measurements were taken minimum three times (inter- or intra-sample). The measurements in the fluidic system were taken by increasing, decreasing and then increasing again the level of K⁺.

LOD K⁺ activity at the point of intersection of the curve fitting the data points in the linear range and the average E corresponding to low concentrations of K⁺ at which the electrode is insensitive to the K⁺ increase (blue line Fig. A.2) [183].

Drift Slope E *vs* time in a certain interval time [183].

Selectivity coefficient It was evaluated according to the *separate solution method* (SSM) in which the E of the cell is measured in two separate solutions, one containing the ion of interest (K⁺) and the other containing the interfering ion (Na⁺ or Ca²⁺) both at a concentration of 0.1 M. Then the selectivity coefficient $K_{(\text{ion}, \text{int})}$ can be calculated from the equation below [183]

$$\log K_{(\text{ion}, \text{int})} = ((E_{\text{ion}} - E_{\text{int}})z_{\text{ion}}F)/(2.303 R T) + (1 + z_{\text{ion}}/z_{\text{int}}) \log a_{\text{ion}} \quad (\text{A.2})$$

R, T and F have the usual significance, z_{ion} and z_{int} are the charges of the ion of interest (K⁺) and of the interfering ion (Na⁺ or Ca²⁺) and a_{ion} and a_{int} are the activities of the ion of interest (K⁺) and of the interfering ion (Na⁺ or Ca²⁺).

B Taguchi method

Genichi Taguchi developed a method to design experiments in order to investigate how different parameters (control factors) affect mean and variance of a particular process outcome (objective function) [202]. This experimental design involves the use of orthogonal arrays¹ to organise the parameters affecting the process and the levels at which they should be varied. These methods utilise two-, three-, and mixed-level fractional factorial designs². Instead of testing all possible combinations, the Taguchi method tests subsets of possible combinations. This allows us to determine which factors mainly affect a certain output with a minimum amount of experimentation, saving time and resources.

The most innovative part of Taguchi method is the parameter design that can be summarised by the following steps.

- Identification of the control factors and the levels.
- Construction of the Orthogonal Array.
- Realisation of experiments.
- Evaluation of the Signal-to-Noise Ratio (S/N), called performance statistic. It depends on the experimental situation analysed.
- Use of S/N values to determine the optimal combination of levels for each factor.
- Control the effective improvement obtained by the result of the previous phase.

¹represent a versatile class of combinational arrangements useful for conducting experiments. They determine the levels of each factor for an optimal process output

²A *full factorial experiment* is an experiment whose design consists of two or more factors, each with discrete levels, and whose experiments test all possible combinations of these levels across all such factors. Such an experiment allows studying the effect of each factor on the response variable, as well as the effects of interactions between factors on the response variable. If the number of combinations in a full factorial design is too high to be logistically feasible, a *fractional factorial design* may be done, in which some of the possible combinations (usually at least half) are omitted.

Appendix B. Taguchi method

The choice of the S/N type can vary. To minimise a process feature (*smaller-is-better analysis*), the S/N ratio is calculated according to the following Equation B.1

$$S/N_i = -10 \frac{1}{N_i} \sum_{u=1}^{N_i} y_u^2 \quad (\text{B.1})$$

To maximise a process feature (*larger-is-better analysis*), the S/N ratio should be calculated according to the following Equation B.2

$$S/N_i = -10 \log \frac{1}{N_i} \sum_{u=1}^{N_i} \frac{1}{y_u^2} \quad (\text{B.2})$$

where:

- N_i is the number of levels in which each parameter is investigated and
- y_u is the u^{th} value of the objective functions.

To study the effect of the electrodeposition parameters on some characteristics of the resulting Pt nanostructured films the following procedure was used.

1. Identification of *parameters* affecting the process (control factors) and their *levels* (possible values for each parameter);
2. Selection of the *orthogonal array matrix of experiments* (number of experiments and the level of the parameters for each experiments);
3. Identification of the *objective function* to be optimised;
4. Realisation of the experiments;
5. Application of Equations B.1 and B.2 for minimising or maximising the objective functions;
6. Plot the results;
7. Identification of the level for each parameter that optimised the selected objective function.

The optimisation of the electrodeposition from tetravalent Pt-based solutions required to examine the following three parameters with two levels of variation each.

- Applied voltage (-1 or -0.2 V)
- Solution composition (3 mM H₂PtCl₆ and 500 mM H₂SO₄ or 25 mM H₂PtCl₆ and 50mM H₂SO₄).
- Time (90 or 200 s)

Four experiments organised in a L₄ Taguchi's Orthogonal Array were carried out. The parameter design is shown in Table 5.1. The objective functions of the growth process selected were: R_f, nanostructure coverage area in percentage, petal dimensions in nm. Graphs showing the S/N ratio for the *smaller-is-better* analysis of petal dimensions and for the *larger-is-better* analysis of R_f and of nanostructure coverage area are in Fig 5.4. Considerations about the obtained results are in the Section 5.4.

Bibliography

- [1] J. Ochei and A. Kolhatkar. Medical laboratory science: Theory and practice. *Copyright*, pages 801–804, 2000.
- [2] Carl D Deaton, Kameron W Maxwell, Richard S Smith, and Robert L Creveling. Use of laser nephelometry in the measurement of serum proteins. *Clinical chemistry*, 22(9):1465–1471, 1976.
- [3] Søren Blirup-Jensen. Protein standardization III: method optimization. Basic principles for quantitative determination of human serum proteins on automated instruments based on turbidimetry or nephelometry. *Clinical chemistry and laboratory medicine*, 39(11):1098–1109, 2001.
- [4] Ivan Lefkovits and Benvenuto Pernis. *Immunological methods*, volume 3. Elsevier, 2014.
- [5] Kirill V Larin, Taner Akkin, Rinat O Esenaliev, Massoud Motamedi, and Thomas E Milner. Phase-sensitive optical low-coherence reflectometry for the detection of analyte concentrations. *Applied optics*, 43(17):3408–3414, 2004.
- [6] Florinel-Gabriel Banica. *Chemical sensors and biosensors: fundamentals and applications*. John Wiley & Sons, 2012.
- [7] Jonathan M. Yuen, Nilam C. Shah, Joseph T. Walsh Jr, Matthew R. Glucksberg, and Richard P. Van Duyne. Transcutaneous glucose sensing by surface-enhanced spatially offset raman spectroscopy in a rat model. *Analytical chemistry*, 82(20):8382–8385, 2010.
- [8] Miguel A. Pleitez, Tobias Lieblein, Alexander Bauer, Otto Hertzberg, Hermann von Lilienfeld-Toal, and Werner Mäntele. In vivo noninvasive monitoring of glucose concentration in human epidermis by mid-infrared pulsed photoacoustic spectroscopy. *Analytical chemistry*, 85(2):1013–1020, 2012.
- [9] Xia Cai, Jilin Yan, Haihong Chu, Meisheng Wu, and Yifeng Tu. An exercise degree monitoring biosensor based on electrochemiluminescent detection of lactate in sweat. *Sensors and Actuators B: Chemical*, 143(2):655–659, 2010.
- [10] Vincenzo F. Curto, Shirley Coyle, Robert Byrne, Nikolay Angelov, Dermot Diamond, and Fernando Benito-Lopez. Concept and development of an autonomous wearable micro-

Bibliography

- fluidic platform for real time pH sweat analysis. *Sensors and Actuators B: Chemical*, 175:263–270, 2012.
- [11] Yumei Hu, Xiaomei Jiang, Laiying Zhang, Jiao Fan, and Weitai Wu. Construction of near-infrared photonic crystal glucose-sensing materials for ratiometric sensing of glucose in tears. *Biosensors and Bioelectronics*, 48:94–99, 2013.
- [12] Ramachandram Badugu, Joseph R. Lakowicz, and Chris D. Geddes. A glucose-sensing contact lens: from bench top to patient. *Current opinion in biotechnology*, 16(1):100–107, 2005.
- [13] Bin Xie, Kumaran Ramanathan, and Bengt Danielsson. Mini/micro thermal biosensors and other related devices for biochemical/clinical analysis and monitoring. *TrAC Trends in Analytical Chemistry*, 19(5):340–349, 2000.
- [14] Siqi Li, Xian Huang, Erin N. Davis, Qiao Lin, and Qian Wang. Development of novel glucose sensing fluids with potential application to microelectromechanical systems-based continuous glucose monitoring. *Journal of diabetes science and technology*, 2(6):1066–1074, 2008.
- [15] Xian Huang, Charles Leduc, Yann Ravussin, Siqi Li, Erin Davis, Bing Song, Qian Wang, Domenico Accili, Rudolph Leibel, and Qiao Lin. Continuous monitoring of glucose in subcutaneous tissue using microfabricated differential affinity sensors. *Journal of diabetes science and technology*, 6(6):1436–1444, 2012.
- [16] Eric Bakker. Electrochemical sensors. *Analytical chemistry*, 76(12):3285–3298, 2004.
- [17] Anthony P.F. Turner. Biosensors-sense and sensitivity. *Science*, 290(5495):1315–1317, 2000.
- [18] G. Piechotta, J. Albers, and R. Hintsche. Novel micromachined silicon sensor for continuous glucose monitoring. *Biosensors and Bioelectronics*, 21(5):802–808, 2005.
- [19] Tomàs Guinovart, Marc Parrilla, Gastón A. Crespo, E. Xavier Rius, and Francisco J. Andrade. Potentiometric sensors using cotton yarns, carbon nanotubes and polymeric membranes. *Analyst*, 138(18):5208–5215, 2013.
- [20] Jayoung Kim, Gabriela Valdés-Ramírez, Amay J. Bandodkar, Wenzhao Jia, Alexandra G. Martinez, Julian Ramírez, Patrick Mercier, and Joseph Wang. Non-invasive mouthguard biosensor for continuous salivary monitoring of metabolites. *Analyst*, 139(7):1632–1636, 2014.
- [21] Andrea Kagie, Daniel K. Bishop, Jared Burdick, Jeffrey T. La Belle, Robert Dymond, Robin Felder, and Joseph Wang. Flexible rolled thick-film miniaturized flow-cell for minimally invasive amperometric sensing. *Electroanalysis*, 20(14):1610–1614, 2008.

- [22] Qinyi Yan, Bo Peng, Gang Su, Bruce E. Cohan, Terry C. Major, and Mark E. Meyerhoff. Measurement of tear glucose levels with amperometric glucose biosensor/capillary tube configuration. *Analytical chemistry*, 83(21):8341–8346, 2011.
- [23] Huanfen Yao, Angela J. Shum, Melissa Cowan, Ilkka Lähdesmäki, and Babak A. Parviz. A contact lens with embedded sensor for monitoring tear glucose level. *Biosensors and Bioelectronics*, 26(7):3290–3296, 2011.
- [24] Nicole Thomas, Ilkka Lähdesmäki, and Babak A. Parviz. A contact lens with an integrated lactate sensor. *Sensors and Actuators B: Chemical*, 162(1):128–134, 2012.
- [25] S. Zhang, G. Wright, and Y. Yang. Materials and techniques for electrochemical biosensor design and construction. *Biosensors and Bioelectronics*, 15(5):273–282, 2000.
- [26] Joshua Ray Windmiller and Joseph Wang. Wearable electrochemical sensors and biosensors: a review. *Electroanalysis*, 25(1):29–46, 2013.
- [27] Chengzhou Zhu, Guohai Yang, He Li, Dan Du, and Yuehe Lin. Electrochemical sensors and biosensors based on nanomaterials and nanostructures. *Analytical chemistry*, 2015.
- [28] Dale A.C. Brownson, Maria Gómez-Mingot, and Craig E. Banks. CVD graphene electrochemistry: biologically relevant molecules. *Physical Chemistry Chemical Physics*, 13(45):20284–20288, 2011.
- [29] Soma Das and Mitali Saha. Synthesis of carbon nanosheet from barley and its use as non-enzymatic glucose biosensor. *Journal of Pharmaceutical Analysis*, 4(6):351–359, 2014.
- [30] Wang Liang and Yuan Zhuobin. Direct electrochemistry of glucose oxidase at a gold electrode modified with single-wall carbon nanotubes. *Sensors*, 3(12):544–554, 2003.
- [31] Jian-Shan Ye, Ying Wen, Wei De Zhang, Leong Ming Gan, Guo Qin Xu, and Fwu-Shan Sheu. Nonenzymatic glucose detection using multi-walled carbon nanotube electrodes. *Electrochemistry Communications*, 6(1):66–70, 2004.
- [32] A. Michalska, A. Hulanicki, and A. Lewenstam. All-solid-state potentiometric sensors for potassium and sodium based on poly (pyrrole) solid contact. *Microchemical journal*, 57(1):59–64, 1997.
- [33] Wei Feng and Peijun Ji. Enzymes immobilized on carbon nanotubes. *Biotechnology advances*, 29(6):889–895, 2011.
- [34] Masato Tominaga, Shinya Nomura, and Isao Taniguchi. D-fructose detection based on the direct heterogeneous electron transfer reaction of fructose dehydrogenase adsorbed onto multi-walled carbon nanotubes synthesized on platinum electrode. *Biosensors and Bioelectronics*, 24(5):1184–1188, 2009.

Bibliography

- [35] Dan Zheng, Jianshan Ye, and Weide Zhang. Some properties of sodium dodecyl sulfate functionalized multiwalled carbon nanotubes electrode and its application on detection of dopamine in the presence of ascorbic acid. *Electroanalysis*, 20(16):1811–1818, 2008.
- [36] Yi-Jae Lee and Jae-Yeong Park. A coral-like macroporous gold–platinum hybrid 3D electrode for enzyme-free glucose detection. *Sensors and Actuators B: Chemical*, 155(1):134–139, 2011.
- [37] Stuart A.G. Evans, Joanne M. Elliott, Lynn M. Andrews, Philip N. Bartlett, Peter J. Doyle, and Guy Denuault. Detection of hydrogen peroxide at mesoporous platinum microelectrodes. *Analytical Chemistry*, 74(6):1322–1326, 2002.
- [38] Ji-Hyung Han, Sejin Park, Hankil Boo, Hee Chan Kim, Jongmin Nho, and Taek Dong Chung. Solid-state reference electrode based on electrodeposited nanoporous platinum for microchip. *Electroanalysis*, 19(7-8):786–792, 2007.
- [39] Ewa Jaworska, Michał Wójcik, Anna Kisiel, Józef Mieczkowski, and Agata Michalska. Gold nanoparticles solid contact for ion-selective electrodes of highly stable potential readings. *Talanta*, 85(4):1986–1989, 2011.
- [40] Xinyu Pang, Dongmei He, Shenglian Luo, and Qingyun Cai. An amperometric glucose biosensor fabricated with Pt nanoparticle-decorated carbon nanotubes/TiO₂ nanotube arrays composite. *Sensors and Actuators B: Chemical*, 137(1):134–138, 2009.
- [41] Tarushee Ahuja, Devendra Kumar, et al. Recent progress in the development of nanostructured conducting polymers/nanocomposites for sensor applications. *Sensors and Actuators B: Chemical*, 136(1):275–286, 2009.
- [42] Jen-Lin Chang, Kuo-Hsin Chang, Chi-Chang Hu, Wan-Ling Cheng, and Jyh-Myng Zen. Improved voltammetric peak separation and sensitivity of uric acid and ascorbic acid at nanoplatelets of graphitic oxide. *Electrochemistry Communications*, 12(4):596–599, 2010.
- [43] Karin Pihel, Q. David Walker, and R. Mark Wightman. Overoxidized polypyrrole-coated carbon fiber microelectrodes for dopamine measurements with fast-scan cyclic voltammetry. *Analytical chemistry*, 68(13):2084–2089, 1996.
- [44] Jing-Fang Huang. 3-D nanoporous Pt electrode prepared by a 2-D UPD monolayer process. *Electroanalysis*, 20(20):2229–2234, 2008.
- [45] Irene Taurino, Sandro Carrara, Mauro Giorelli, Alberto Tagliaferro, and Giovanni De Micheli. Comparing the enhanced sensing interfaces of differently oriented carbon nanotubes onto silicon for bio-chip applications. In *Advances in Sensors and Interfaces IWASI, 2011 4th IEEE International Workshop on*, pages 90–93. IEEE, 2011.
- [46] Richard L. McCreery. Advanced carbon electrode materials for molecular electrochemistry. *Chem. Rev.*, 108(7):2646–2687, 2008.

- [47] Jue Lu, Lawrence T. Drzal, Robert M. Worden, and Ilsoon Lee. Simple fabrication of a highly sensitive glucose biosensor using enzymes immobilized in exfoliated graphite nanoplatelets nafion membrane. *Chemistry of Materials*, 19(25):6240–6246, 2007.
- [48] Haojie Zhou, Zipin Zhang, Ping Yu, Lei Su, Takeo Ohsaka, and Lanqun Mao. Noncovalent attachment of NAD^+ cofactor onto carbon nanotubes for preparation of integrated dehydrogenase-based electrochemical biosensors. *Langmuir*, 26(8):6028–6032, 2010.
- [49] Anthony Guiseppi-Elie, Chenghong Lei, and Ray H. Baughman. Direct electron transfer of glucose oxidase on carbon nanotubes. *Nanotechnology*, 13(5):559, 2002.
- [50] Yu-Chen Tsai, Shih-Ci Li, and Jie-Ming Chen. Cast thin film biosensor design based on a nafion backbone, a multiwalled carbon nanotube conduit, and a glucose oxidase function. *Langmuir*, 21(8):3653–3658, 2005.
- [51] Maogen Zhang, Audrey Smith, and Waldemar Gorski. Carbon nanotube-chitosan system for electrochemical sensing based on dehydrogenase enzymes. *Analytical Chemistry*, 76(17):5045–5050, 2004.
- [52] Chenxin Cai and Jing Chen. Direct electron transfer of glucose oxidase promoted by carbon nanotubes. *Analytical biochemistry*, 332(1):75–83, 2004.
- [53] Quanping Yan, Faqiong Zhao, Guangzu Li, and Baizhao Zeng. Voltammetric determination of uric acid with a glassy carbon electrode coated by paste of multi-walled carbon nanotubes and ionic liquid. *Electroanalysis*, 18(11):1075–1080, 2006.
- [54] Sandro Carrara, Léandre Bolomey, Cristina Boero, Andrea Cavallini, Eric Meurville, Giovanni De Micheli, Tanja Rezzonico Jost, Michele Proietti, and Fabio Grassi. Remote system for monitoring animal models with single-metabolite bio-nano-sensors. *Sensors Journal, IEEE*, 13(3):1018–1024, 2013.
- [55] Xi-Liang Luo, Jing-Juan Xu, Jin-Li Wang, and Hong-Yuan Chen. Electrochemically deposited nanocomposite of chitosan and carbon nanotubes for biosensor application. *Chem. Commun.*, (16):2169–2171, 2005.
- [56] Liuyun Chen, Yanhong Tang, Ke Wang, Chengbin Liu, and Shenglian Luo. Direct electrodeposition of reduced graphene oxide on glassy carbon electrode and its electrochemical application. *Electrochemistry Communications*, 13(2):133–137, 2011.
- [57] C.T.J. Low, F.C. Walsh, M.H. Chakrabarti, M.A. Hashim, and M.A. Hussain. Electrochemical approaches to the production of graphene flakes and their potential applications. *Carbon*, 54:1–21, 2013.
- [58] Mei Gao, Liming Dai, and Gordon G. Wallace. Biosensors based on aligned carbon nanotubes coated with inherently conducting polymers. *Electroanalysis*, 15(13):1089–1094, 2003.

Bibliography

- [59] Zhipeng Wang, Mao Shoji, and Hironori Ogata. Electrochemical determination of NADH based on MPECVD carbon nanosheets. *Talanta*, 99:487–491, 2012.
- [60] Yan-Shi Chen, Jin-Hua Huang, and Chia-Chih Chuang. Glucose biosensor based on multiwalled carbon nanotubes grown directly on Si. *Carbon*, 47(13):3106–3112, 2009.
- [61] Irene Taurino, Sandro Carrara, Mauro Giorcelli, Alberto Tagliaferro, and Giovanni De Micheli. Comparing sensitivities of differently oriented multi-walled carbon nanotubes integrated on silicon wafer for electrochemical biosensors. *Sensors and Actuators B: Chemical*, 160(1):327–333, 2011.
- [62] Irene Taurino, Sandro Carrara, Mauro Giorcelli, Alberto Tagliaferro, and Giovanni De Micheli. Carbon nanotubes with different orientations for electrochemical biodevices. *Sensors Journal, IEEE*, 12(12):3356–3362, 2012.
- [63] Serin Park, Park Dong-Won, Cheol-Soo Yang, Kwang-Rok Kim, Jun-Hyuk Kwak, Hye-Mi So, Chi Won Ahn, Beom Soo Kim, Hyunju Chang, and Jeong-O Lee. Vertically aligned carbon nanotube electrodes directly grown on a glassy carbon electrode. *ACS nano*, 5(9):7061–7068, 2011.
- [64] Iñigo Martin-Fernandez, Gemma Gabriel, Gemma Rius, Rosa Villa, Francesc Perez-Murano, Emilio Lora-Tamayo, and Philippe Godignon. Vertically aligned multi-walled carbon nanotube growth on platinum electrodes for bio-impedance applications. *Microelectronic engineering*, 86(4):806–808, 2009.
- [65] Yuehe Lin, Fang Lu, Yi Tu, and Zhifeng Ren. Glucose biosensors based on carbon nanotube nanoelectrode ensembles. *Nano letters*, 4(2):191–195, 2004.
- [66] Rachel M. Snider, Madalina Ciobanu, Amy E. Rue, and David E. Cliffel. A multiwalled carbon nanotube/dihydropyran composite film electrode for insulin detection in a microphysiometer chamber. *Analytica chimica acta*, 609(1):44–52, 2008.
- [67] S. Sara Ghoreishizadeh, Camilla Baj-Rossi, Sandro Carrara, and Giovanni De Micheli. Nano-sensor and circuit design for anti-cancer drug detection. In *Life Science Systems and Applications Workshop (LiSSA), 2011 IEEE/NIH*, pages 28–33. IEEE, 2011.
- [68] Koichi Aoki, Minoru Ishida, Koichi Tokuda, and Kiyoshi Hasebe. Electrode kinetics of the oxidation of hydrogen peroxide at pretreated glassy carbon and carbon fiber electrodes. *Journal of electroanalytical chemistry and interfacial electrochemistry*, 251(1):63–71, 1988.
- [69] Arkady A. Karyakin. Prussian blue and its analogues: electrochemistry and analytical applications. *Electroanalysis*, 13(10):813–819, 2001.
- [70] Prashanth Asuri, Sandeep S. Karajanagi, Hoichang Yang, Tae-Jin Yim, Ravi S. Kane, and Jonathan S. Dordick. Increasing protein stability through control of the nanoscale environment. *Langmuir*, 22(13):5833–5836, 2006.

- [71] Joseph Wang, Mustafa Musameh, and Yuehe Lin. Solubilization of carbon nanotubes by Nafion toward the preparation of amperometric biosensors. *Journal of the American Chemical Society*, 125(9):2408–2409, 2003.
- [72] James G. Roberts, Keri L. Hamilton, and Leslie A. Sombers. Comparison of electrode materials for the detection of rapid hydrogen peroxide fluctuations using background-subtracted fast scan cyclic voltammetry. *Analyst*, 136(17):3550–3556, 2011.
- [73] Hao Tang, Jinhua Chen, Shouzhuo Yao, Lihua Nie, Guohong Deng, and Yafei Kuang. Amperometric glucose biosensor based on adsorption of glucose oxidase at platinum nanoparticle-modified carbon nanotube electrode. *Analytical Biochemistry*, 331(1):89–97, 2004.
- [74] Xiehong Cao, Zhiyuan Zeng, Wenhui Shi, Peiru Yep, Qingyu Yan, and Hua Zhang. Three-dimensional graphene network composites for detection of hydrogen peroxide. *Small*, 9(9-10):1703–1707, 2013.
- [75] Yongjin Zou, Cuili Xiang, Li-Xian Sun, and Fen Xu. Glucose biosensor based on electrodeposition of platinum nanoparticles onto carbon nanotubes and immobilizing enzyme with chitosan-SiO₂ sol-gel. *Biosensors and Bioelectronics*, 23(7):1010–1016, 2008.
- [76] Sabahudin Hrapovic, Yali Liu, Keith B. Male, and John H.T. Luong. Electrochemical biosensing platforms using platinum nanoparticles and carbon nanotubes. *Analytical chemistry*, 76(4):1083–1088, 2004.
- [77] Rajanish Ná Tiwari, S Ká Nandi, et al. Facile synthesis of continuous Pt island networks and their electrochemical properties for methanol electrooxidation. *Chemical Communications*, (48):6516–6518, 2008.
- [78] Hankil Boo, Sejin Park, Bonkyung Ku, Yunmee Kim, Jin Hyung Park, Hee Chan Kim, and Taek Dong Chung. Ionic strength-controlled virtual area of mesoporous platinum electrode. *Journal of the American Chemical Society*, 126(14):4524–4525, 2004.
- [79] Na Tian, Zhi-You Zhou, Shi-Gang Sun, Yong Ding, and Zhong Lin Wang. Synthesis of tetrahedral platinum nanocrystals with high-index facets and high electrooxidation activity. *Science*, 316(5825):732–735, 2007.
- [80] Na Tian, Zhi-You Zhou, Neng-Fei Yu, Li-Yang Wang, and Shi-Gang Sun. Direct electrodeposition of tetrahedral Pd nanocrystals with high-index facets and high catalytic activity for ethanol electrooxidation. *Journal of the American Chemical Society*, 132(22):7580–7581, 2010.
- [81] Zhi-You Zhou, Zhi-Zhong Huang, De-Jun Chen, Qiang Wang, Na Tian, and Shi-Gang Sun. High-index faceted platinum nanocrystals supported on carbon black as highly efficient catalysts for ethanol electrooxidation. *Angewandte Chemie International Edition*, 49(2):411–414, 2010.

Bibliography

- [82] Yi Jae Lee and Jae Yeong Park. A highly miniaturized dissolved oxygen sensor using a nanoporous platinum electrode electroplated on silicon. *Journal of the Korean Physical Society*, 58(5):1505–1510, 2011.
- [83] Je Hyun Bae, Ji-Hyung Han, Donghyeop Han, and Taek Dong Chung. Effects of adsorption and confinement on nanoporous electrochemistry. *Faraday discussions*, 164:361–376, 2013.
- [84] Haihui Zhou, Hong Chen, Shenglian Luo, Jinhua Chen, Wanzhi Wei, and Yafei Kuang. Glucose biosensor based on platinum microparticles dispersed in nano-fibrous polyaniline. *Biosensors and Bioelectronics*, 20(7):1305–1311, 2005.
- [85] Juan Ren, Wentao Shi, Kai Li, and Zhanfang Ma. Ultrasensitive platinum nanocubes enhanced amperometric glucose biosensor based on chitosan and nafion film. *Sensors and Actuators B: Chemical*, 163(1):115–120, 2012.
- [86] J.H. Yuan, Kang Wang, and X.H. Xia. Highly ordered platinum-nanotubule arrays for amperometric glucose sensing. *Advanced Functional Materials*, 15(5):803–809, 2005.
- [87] Yan-Yan Song, Dai Zhang, Wei Gao, and Xing-Hua Xia. Nonenzymatic glucose detection by using a three-dimensionally ordered, macroporous platinum template. *Chemistry-A European Journal*, 11(7):2177–2182, 2005.
- [88] Brandy Kinkead, Julia van Drunen, Michael T.Y. Paul, Katie Dowling, Gregory Jerkiewicz, and Byron D. Gates. Platinum ordered porous electrodes: Developing a platform for fundamental electrochemical characterization. *Electrocatalysis*, 4(3):179–186, 2013.
- [89] Jongmin Noh, Sejin Park, Hankil Boo, Hee Chan Kim, and Taek Dong Chung. Nanoporous platinum solid-state reference electrode with layer-by-layer polyelectrolyte junction for pH sensing chip. *Lab on a Chip*, 11(4):664–671, 2011.
- [90] Feng Ye, Ling Chen, Jingjing Li, Jianling Li, and Xindong Wang. Shape-controlled fabrication of platinum electrocatalyst by pulse electrodeposition. *Electrochemistry Communications*, 10(3):476–479, 2008.
- [91] Ming-Chi Tsai, Tsung-Kuang Yeh, and Chuen-Horng Tsai. Electrodeposition of platinum-ruthenium nanoparticles on carbon nanotubes directly grown on carbon cloths for methanol oxidation. *Materials Chemistry and Physics*, 109(2):422–428, 2008.
- [92] You-Jung Song, Jae-Kyung Oh, and Kyung-Won Park. Pt nanostructure electrodes pulse electrodeposited in PVP for electrochemical power sources. *Nanotechnology*, 19(35):355602, 2008.
- [93] Hongmei Zhang, Weiqiang Zhou, Yukou Du, Ping Yang, and Chuanyi Wang. One-step electrodeposition of platinum nanoflowers and their high efficient catalytic activity for methanol electro-oxidation. *Electrochemistry Communications*, 12(7):882–885, 2010.

- [94] You Xu, Huan Wang, Yifu Yu, Lei Tian, Weiwei Zhao, and Bin Zhang. *Cu₂O* nanocrystals: Surfactant-free room-temperature morphology-modulated synthesis and shape-dependent heterogeneous organic catalytic activities. *The Journal of Physical Chemistry C*, 115(31):15288–15296, 2011.
- [95] Raffaella Lo Nigro, Graziella Malandrino, Patrick Fiorenza, and Ignazio L. Fragalà. Template-free and seedless growth of Pt nanocolumns: imaging and probing their nanoelectrical properties. *ACS nano*, 1(3):183–190, 2007.
- [96] Chih-Hung Chou, Jyh-Cheng Chen, Chia-Cheng Tai, I-Wen Sun, and Jyh-Myng Zen. A nonenzymatic glucose sensor using nanoporous platinum electrodes prepared by electrochemical alloying/dealloying in a water-insensitive zinc chloride-1-ethyl-3-methylimidazolium chloride ionic liquid. *Electroanalysis*, 20(7):771–775, 2008.
- [97] Qin Xu, Lina Yin, Chuantao Hou, Xiaoxian Liu, and Xiaoya Hu. Facile fabrication of nanoporous platinum by alloying–dealloying process and its application in glucose sensing. *Sensors and Actuators B: Chemical*, 173:716–723, 2012.
- [98] Kang Wang, Jing-Juan Xu, Da-Cheng Sun, Hui Wei, and Xing-Hua Xia. Selective glucose detection based on the concept of electrochemical depletion of electroactive species in diffusion layer. *Biosensors and Bioelectronics*, 20(7):1366–1372, 2005.
- [99] S. Ernst, J. Heitbaum, and C.H. Hamann. The electrooxidation of glucose in phosphate buffer solutions: Part I. reactivity and kinetics below 350 mV/RHE. *Journal of Electroanalytical Chemistry and Interfacial Electrochemistry*, 100(1):173–183, 1979.
- [100] E. Skou. The electrochemical oxidation of glucose on platinum-I. the oxidation in 1 M H_2SO_4 . *Electrochimica Acta*, 22(4):313–318, 1977.
- [101] Jun Ho Shim, Kyung Jang, et al. Applications of porous Pt-filled micropore electrode: Direct amperometric glucose detection and potentiometric pH sensing. *Electroanalysis*, 23(9):2063–2069, 2011.
- [102] Yi-Jae Lee, Dae-Joon Park, Jae-Yeong Park, and Younghun Kim. Fabrication and optimization of a nanoporous platinum electrode and a non-enzymatic glucose micro-sensor on silicon. *Sensors*, 8(10):6154–6164, 2008.
- [103] Sejin Park, Taek Dong Chung, and Hee Chan Kim. Nonenzymatic glucose detection using mesoporous platinum. *Analytical Chemistry*, 75(13):3046–3049, 2003.
- [104] Sejin Park, Youn Joo Song, Ji-Hyung Han, Hankil Boo, and Taek Dong Chung. Structural and electrochemical features of 3D nanoporous platinum electrodes. *Electrochimica Acta*, 55(6):2029–2035, 2010.
- [105] Timoer Frelink, W. Visscher, and J.A.R. Van Veen. Particle size effect of carbon-supported platinum catalysts for the electrooxidation of methanol. *Journal of Electroanalytical Chemistry*, 382(1):65–72, 1995.

Bibliography

- [106] Sangyun Park, Sejin Park, Ran-A Jeong, Hankil Boo, Jeyoung Park, Hee Chan Kim, and Taek Dong Chung. Nonenzymatic continuous glucose monitoring in human whole blood using electrified nanoporous Pt. *Biosensors and Bioelectronics*, 31(1):284–291, 2012.
- [107] Segyeong Joo, Sejin Park, Taek Dong Chung, and Hee Chan Kim. Integration of a nanoporous platinum thin film into a microfluidic system for non-enzymatic electrochemical glucose sensing. *Anal. Sci.*, 23(3):277–281, 2007.
- [108] Qingming Shen, Liping Jiang, Hui Zhang, Qianhao Min, Wenhua Hou, and Jun-Jie Zhu. Three-dimensional dendritic Pt nanostructures: sonoelectrochemical synthesis and electrochemical applications. *The Journal of Physical Chemistry C*, 112(42):16385–16392, 2008.
- [109] M.Q. Guo, H.S. Hong, X.N. Tang, H.D. Fang, and X.H. Xu. Ultrasonic electrodeposition of platinum nanoflowers and their application in nonenzymatic glucose sensors. *Electrochimica Acta*, 63:1–8, 2012.
- [110] Simon B. Hall, Emad A. Khudaish, and Alan L. Hart. Electrochemical oxidation of hydrogen peroxide at platinum electrodes. Part 1. An adsorption-controlled mechanism. *Electrochimica Acta*, 43(5):579–588, 1998.
- [111] Yunli Wang, Yingchun Zhu, Jingjing Chen, and Yi Zeng. Amperometric biosensor based on 3D ordered freestanding porous Pt nanowire array electrode. *Nanoscale*, 4(19):6025–6031, 2012.
- [112] Yibo Zhou, Gang Yu, Fangfang Chang, Bonian Hu, and Chuan-Jian Zhong. Gold-platinum alloy nanowires as highly sensitive materials for electrochemical detection of hydrogen peroxide. *Analytica chimica acta*, 757:56–62, 2012.
- [113] Cuiling Li, Hongjing Wang, and Yusuke Yamauchi. Electrochemical deposition of mesoporous Pt–Au alloy films in aqueous surfactant solutions: towards a highly sensitive amperometric glucose sensor. *Chemistry-A European Journal*, 19(7):2242–2246, 2013.
- [114] Tanji Yin and Wei Qin. Applications of nanomaterials in potentiometric sensors. *TrAC Trends in Analytical Chemistry*, 51:79–86, 2013.
- [115] A. Magrez, J.W. Seo, R. Smajda, B. Korbely, J.C. Andresen, M. Mionć, S. Casimirius, and L. Forró. Low-temperature, highly efficient growth of carbon nanotubes on functional materials by an oxidative dehydrogenation reaction. *ACS Nano*, 4(7):3702–3708, 2010.
- [116] Arnaud Magrez, Jin W. Seo, Vladimir L. Kuznetsov, and László Forró. Evidence of an equimolar C₂H₂-CO₂ reaction in the synthesis of carbon nanotubes. *Angewandte Chemie*, 119(3):445–448, 2007.
- [117] Petr Klapetek, David Nečas, and Christopher Anderson. Gwyddion user guide. <http://gwyddion.net/>, 2004–2009.

- [118] Wayne S. Rasband. Imagej. <http://rsbweb.nih.gov/ij/>, 2008.
- [119] Bernt Ketterer, Martin Heiss, Emanuele Uccelli, Jordi Arbiol, and Anna Fontcuberta i Morral. Untangling the electronic band structure of wurtzite GaAs nanowires by Resonant Raman spectroscopy. *ACS Nano*, 5(9):7585–7592, 2011.
- [120] D. Olevik, A.V. Soldatov, M. Dossot, B. Vigolo, B. Humbert, and E. McRae. Stability of carbon nanotubes to laser irradiation probed by Raman spectroscopy. *Physica Status Solidi (b)*, 245(10):2212–2215, 2008.
- [121] A. Sadezky, H. Muckenhuber, H. Grothe, R. Niessner, and U. Pöschl. Raman microspectroscopy of soot and related carbonaceous materials: Spectral analysis and structural information. *Carbon*, 43(8):1731–1742, 2005.
- [122] Gilbert D. Nessim, Matteo Seita, Kevin P. O’Brien, A. John Hart, Ryan K. Bonaparte, Robert R. Mitchell, and Carl V. Thompson. Low temperature synthesis of vertically aligned carbon nanotubes with electrical contact to metallic substrates enabled by thermal decomposition of the carbon feedstock. *Nano Letters*, 9(10):3398–3405, 2009.
- [123] S. Osswald, M. Havel, and Y. Gogotsi. Monitoring oxidation of multiwalled carbon nanotubes by Raman spectroscopy. *Journal of Raman Spectroscopy*, 38(6):728–736, 2007.
- [124] R.A. DiLeo, B.J. Landi, and R.P. Raffaele. Purity assessment of multiwalled carbon nanotubes by Raman spectroscopy. *Journal of Applied Physics*, 101(6):064307–064307, 2007.
- [125] A.C. Ferrari and J. Robertson. Interpretation of raman spectra of disordered and amorphous carbon. *Physical Review B*, 61(20):14095, 2000.
- [126] A.C. Ferrari. Raman spectroscopy of graphene and graphite: Disorder, electron–phonon coupling, doping and nonadiabatic effects. *Solid State Communications*, 143(1):47–57, 2007.
- [127] C. Soldano, A. Mahmood, and E. Dujardin. Production, properties and potential of graphene. *Carbon*, 48(8):2127–2150, 2010.
- [128] Daiyu Kondo, Shintaro Sato, Katsunori Yagi, Naoki Harada, Motonobu Sato, Mizuhisa Nihei, and Naoki Yokoyama. Low-temperature synthesis of graphene and fabrication of top-gated field effect transistors without using transfer processes. *Applied Physics Express*, 3(2):025102, 2010.
- [129] Nikolay A. Vinogradov, A.A. Zakharov, Vancho Kocovski, Jan Rusz, K.A. Simonov, Olle Eriksson, A. Mikkelsen, E. Lundgren, A.S. Vinogradov, Nils Mårtensson, et al. Formation and structure of graphene waves on Fe (110). *Physical Review Letters*, 109(2):26101, 2012.

Bibliography

- [130] Chun Tak Chow, Mandy L.Y. Sin, Philip H.W. Leong, Wen J. Li, and K.P. Pun. Design and modeling of a CNT-CMOS low-power sensor chip. In *Nano/Micro Engineered and Molecular Systems, 2007. NEMS'07. 2nd IEEE International Conference on*, pages 1209–1214. IEEE, 2007.
- [131] Rajat Subhra Chakraborty, Seetharam Narasimhan, and Swarup Bhunia. Hybridization of CMOS with CNT-based nano-electromechanical switch for low leakage and robust circuit design. *Circuits and Systems I: Regular Papers, IEEE Transactions on*, 54(11):2480–2488, 2007.
- [132] Ying Zhou, Jason L. Johnson, Ant Ural, and Huikai Xie. Localized growth of carbon nanotubes on CMOS substrate at room temperature using maskless post-CMOS processing. *Nanotechnology, IEEE Transactions on*, 11(1):16–20, 2012.
- [133] Vincent T. Renard, Michael Jublot, Patrice Gergaud, Peter Cherns, Denis Rouchon, Amal Chabli, and Vincent Jousseume. Catalyst preparation for CMOS-compatible silicon nanowire synthesis. *Nature nanotechnology*, 4(10):654–657, 2009.
- [134] Jie Shen and Chung-Chiun Liu. Development of a screen-printed cholesterol biosensor: Comparing the performance of gold and platinum as the working electrode material and fabrication using a self-assembly approach. *Sensors and Actuators B: Chemical*, 120(2):417–425, 2007.
- [135] Yihong Wu, Bingjun Yang, Baoyu Zong, Han Sun, Zexiang Shen, and Yuanping Feng. Carbon nanowalls and related materials. *Journal of Materials Chemistry*, 14(4):469–477, 2004.
- [136] Thiruvolu Bhuvana, Anurag Kumar, Aditya Sood, Roger H. Gerzeski, Jianjun Hu, Venkata Srinu Bhadrani, Chandrabhas Narayana, and Timothy S. Fisher. Contiguous petal-like carbon nanosheet outgrowths from graphite fibers by plasma CVD. *ACS applied materials & interfaces*, 2(3):644–648, 2010.
- [137] Shihui Si, Li Si, Fenglian Ren, Derong Zhu, and Yingsing Fung. Study of adsorption behavior of bilirubin on human-albumin monolayer using a quartz crystal microbalance. *Journal of colloid and interface science*, 253(1):47–52, 2002.
- [138] Walter F. Boron and Emile L. Boulpaep. *Medical Physiology, 2e Updated Edition: with STUDENT CONSULT Online Access*. Elsevier Health Sciences, 2012.
- [139] Cong Wang, Guangfeng Wang, and Bin Fang. Electrocatalytic oxidation of bilirubin at ferrocenecarboxamide modified MWCNT-gold nanocomposite electrodes. *Microchimica Acta*, 164(1-2):113–118, 2009.
- [140] K. Ando, K. Shinke, S. Yamada, T. Koyama, T. Takai, S. Nakaji, and T. Ogino. Fabrication of carbon nanotube sheets and their bilirubin adsorption capacity. *Colloids and Surfaces B: Biointerfaces*, 71(2):255–259, 2009.

- [141] Salah Sommakia, Jenna L Rickus, and Kevin J Otto. Effects of adsorbed proteins, an antifouling agent and long-duration DC voltage pulses on the impedance of silicon-based neural microelectrodes. In *Engineering in Medicine and Biology Society, 2009. EMBC 2009. Annual International Conference of the IEEE*, pages 7139–7142. IEEE, 2009.
- [142] Bei Guo, Jun-ichi Anzai, and Tetsuo Osa. Adsorption behavior of serum albumin on electrode surfaces and the effects of electrode potential. *CHEMICAL AND PHARMACEUTICAL BULLETIN-TOKYO-*, 44:800–803, 1996.
- [143] D.W. Miwa, M.C. Santos, and S.A.S. Machado. A microgravimetric study of simultaneous adsorption of anions and copper on polycrystalline Pt surfaces. *Journal of the Brazilian Chemical Society*, 17(7):1339–1346, 2006.
- [144] R.J. Vink, K.L. and Van Dreumel, W. Schuurman, H. Wikkeling, R. Van Gansewinkel, C.J. Phielix, and H.C. Koedam. A candidate standard for use in calibration of total bilirubin in serum. *Clinical chemistry*, 33(10):1817–1821, 1987.
- [145] Meredith L. Porter and Beth L. Dennis. Hyperbilirubinemia in the term newborn. *American family physician*, 65(4):599–606, 2002.
- [146] J. Ye, H. Xiong, Q. Wang, X. Zhang, and S. Wang. Voltammetric behavior of bilirubin based on [bmim][PF6] as the supporting electrolyte in organic solvent and its analytical application. *Am. J. Biomed. Sci*, 3(3):191–198, 2011.
- [147] T.R. Koch and O.O. Akingbe. Feasibility of measuring free and total bilirubin electrochemically in serum. *Clinical Chemistry*, 27(7):1295–1299, 1981.
- [148] Nadia Nikolaus and Beate Strehlitz. Amperometric lactate biosensors and their application in (sports) medicine, for life quality and wellbeing. *Microchimica Acta*, 160(1-2):15–55, 2008.
- [149] Cristina Boero, Sandro Carrara, and Giovanni De Micheli. Sensitivity enhancement by carbon nanotubes: applications to stem cell cultures monitoring. In *Research in Microelectronics and Electronics, 2009. PRIME 2009. Ph. D.*, pages 72–75. IEEE, 2009.
- [150] Cristina Boero, Sandro Carrara, and Giovanni De Micheli. Design and optimization of a lactate amperometric biosensor based on lactate oxidase and multi walled-carbon nanotubes. *Nanotech, Montreux, November*, 2008.
- [151] T.S. Tracy. Atypical enzyme kinetics: their effect on in vitro-in vivo pharmacokinetic predictions and drug interactions. *Current drug metabolism*, 4(5):341–346, 2003.
- [152] Elisa Woolridge, Sandra L Turchi, and John R Edwards. The peroxidase-glucose oxidase enzyme system in the undergraduate laboratory. *Biochemical Education*, 14(2):82–83, 1986.

Bibliography

- [153] A.G. Rinzler, Jie Liu, H. Dai, P. Nikolaev, C.B. Huffman, F.J. Rodriguez-Macias, P.J. Boul, An Huai Lu, Dominique Heymann, D.T. Colbert, et al. Large-scale purification of single-wall carbon nanotubes: process, product, and characterization. *Applied Physics A: Materials Science & Processing*, 67(1):29–37, 1998.
- [154] R. Andrews, D. Jacques, D. Qian, and E.C. Dickey. Purification and structural annealing of multiwalled carbon nanotubes at graphitization temperatures. *Carbon*, 39(11):1681–1687, 2001.
- [155] Chao Chen, Qingji Xie, Dawei Yang, Hualing Xiao, Yingchun Fu, Yueming Tan, and Shouzhuo Yao. Recent advances in electrochemical glucose biosensors: a review. *RSC Advances*, 3:4473–4491, 2013.
- [156] Cristina Boero, Sandro Carrara, Giovanna Del Vecchio, Laura Calzà, and Giovanni De Micheli. Targeting of multiple metabolites in neural cells monitored by using protein-based carbon nanotubes. *Sensors and Actuators B: Chemical*, 157(1):216–224, 2011.
- [157] Jinwoo Park, Yoshiyuki Show, Veronika Quaiserova, James J Galligan, Gregory D Fink, and Greg M Swain. Diamond microelectrodes for use in biological environments. *Journal of Electroanalytical Chemistry*, 583(1):56–68, 2005.
- [158] Serhiy Cherevko and Chan-Hwa Chung. Direct electrodeposition of nanoporous gold with controlled multimodal pore size distribution. *Electrochemistry Communications*, 13(1):16–19, 2011.
- [159] Doyeon Kim, Inhwa Jung, Jaeyoung Lee, Inhwan Oh, Heungyong Ha, and Yongsug Tak. Investigation of hydrogen adsorption behaviours in the presence of methanol and dissolved oxygen using electrochemical quartz crystal microbalance. *Electrochimica acta*, 50(2):693–697, 2004.
- [160] Boris I. Kharisov. A review for synthesis of nanoflowers. *Recent patents on nanotechnology*, 2(3):190–200, 2008.
- [161] W.H. Yang and Y.S. Tarng. Design optimization of cutting parameters for turning operations based on the Taguchi method. *Journal of Materials Processing Technology*, 84(1):122–129, 1998.
- [162] L.M. Plyasova, I. Yu Molina, A.N. Gavrilov, S.V. Cherepanova, O.V. Cherstiouk, N.A. Rudina, E.R. Savinova, and G.A. Tsirlina. Electrodeposited platinum revisited: tuning nanostructure via the deposition potential. *Electrochimica Acta*, 51(21):4477–4488, 2006.
- [163] Kyung Tae Kim, Sung-Ho Jin, Seung-Cheol Chang, and Deog-Su Park. Green synthesis of platinum nanoparticles by electroreduction of a K_2PtCl_4 solid-state precursor and its electrocatalytic effects on H_2O_2 reduction. *Bulletin of the Korean Chemical Society*, 12(12), 2013.

- [164] A.M. Feltham and Michael Spiro. Platinized platinum electrodes. *Chemical Reviews*, 71(2):177–193, 1971.
- [165] Kun Zhao, Shuqi Zhuang, Zhu Chang, Haiyan Songm, Liming Dai, Pingang He, and Yuzhi Fang. Amperometric glucose biosensor based on platinum nanoparticles combined aligned carbon nanotubes electrode. *Electroanalysis*, 19(10):1069–1074, 2007.
- [166] Jianmin Wu and Longwei Yin. Platinum nanoparticle modified polyaniline-functionalized boron nitride nanotubes for amperometric glucose enzyme biosensor. *ACS applied materials & interfaces*, 3(11):4354–4362, 2011.
- [167] Xia Chu, Daxue Duan, Guoli Shen, and Ruqin Yu. Amperometric glucose biosensor based on electrodeposition of platinum nanoparticles onto covalently immobilized carbon nanotube electrode. *Talanta*, 71(5):2040–2047, 2007.
- [168] Adam T. Woolley, Kaiqin Lao, Alexander N. Glazer, and Richard A. Mathies. Capillary electrophoresis chips with integrated electrochemical detection. *Analytical Chemistry*, 70(4):684–688, 1998.
- [169] Kathryn E. Toghill and Richard G. Compton. Electrochemical non-enzymatic glucose sensors: a perspective and an evaluation. *Int J Electrochem Sci*, 5(9):1246–1301, 2010.
- [170] Young Wook Lee, Minjung Kim, Yena Kim, Shin Wook Kang, Joon-Hwa Lee, and Sang Woo Han. Synthesis and electrocatalytic activity of Au- Pd alloy nanodendrites for ethanol oxidation. *The Journal of Physical Chemistry C*, 114(17):7689–7693, 2010.
- [171] Jing-Jing Yu, Shuang Lu, Jiang-Wen Li, Fa-Qiong Zhao, and Bai-Zhao Zeng. Characterization of gold nanoparticles electrochemically deposited on amine-functioned mesoporous silica films and electrocatalytic oxidation of glucose. *Journal of Solid State Electrochemistry*, 11(9):1211–1219, 2007.
- [172] Ying Li, Yan-Yan Song, Chen Yang, and Xing-Hua Xia. Hydrogen bubble dynamic template synthesis of porous gold for nonenzymatic electrochemical detection of glucose. *Electrochemistry Communications*, 9(5):981–988, 2007.
- [173] Qingfeng Yi and Wenqiang Yu. Electrocatalytic activity of a novel titanium-supported nanoporous gold catalyst for glucose oxidation. *Microchimica Acta*, 165(3-4):381–386, 2009.
- [174] Francis D. Moore and Kandula S. Sastry. Intracellular potassium: 40K as a primordial gene irradiator. *Proceedings of the National Academy of Sciences*, 79(11):3556–3559, 1982.
- [175] Stephane Genet, Robert Costalat, and Jacques Burger. The influence of plasma membrane electrostatic properties on the stability of cell ionic composition. *Biophysical journal*, 81(5):2442–2457, 2001.

Bibliography

- [176] Silvia Generelli, Renaud Jacquemart, Nico F de Rooij, Mario Jolicoeur, Milena Koudelka-Hep, and Olivier T Guenat. Potentiometric platform for the quantification of cellular potassium efflux. *Lab on a Chip*, 8(7):1210–1215, 2008.
- [177] Chiun-Chien Huang, Andrew C Hall, and Poh-Hong Lim. Characterisation of three pathways for osmolyte efflux in human erythroleukemia cells. *Life sciences*, 81(9):732–739, 2007.
- [178] Jean-Jacques Lahet, François Lenfant, Carol Courderot-Masuyer, Frederic Bouyer, Julien Lecordier, Alain Bureau, Marc Freysz, and Bernard Chaillot. Comparison of three methods for oxidative stress-induced potassium efflux measurement. *Biomedicine & pharmacotherapy*, 61(7):423–426, 2007.
- [179] Niels Fertig, Robert H Blick, and Jan C Behrends. Whole cell patch clamp recording performed on a planar glass chip. *Biophysical journal*, 82(6):3056–3062, 2002.
- [180] Monia Fibbioli, Krisanu Bandyopadhyay, Sheng-Gao Liu, Luis Echegoyen, Olivier Enger, François Diederich, Philippe Bühlmann, and Ernö Pretsch. Redox-active self-assembled monolayers as novel solid contacts for ion-selective electrodes. *Chemical Communications*, (5):339–340, 2000.
- [181] Johan Bobacka. Conducting polymer-based solid-state ion-selective electrodes. *Electroanalysis*, 18(1):7–18, 2006.
- [182] Jianfeng Ping, Yixian Wang, Yibin Ying, and Jian Wu. Application of electrochemically reduced graphene oxide on screen-printed ion-selective electrode. *Analytical chemistry*, 84(7):3473–3479, 2012.
- [183] Richard P. Buck and Erno Lindner. Recommendations for nomenclature of ion selective electrodes (IUPAC Recommendations 1994). *Pure and Applied Chemistry*, 66(12):2527–2536, 1994.
- [184] A. Craggs, G.J. Moody, and J.D.R. Thomas. PVC matrix membrane ion-selective electrodes. construction and laboratory experiments. *Journal of Chemical Education*, 51(8):541, 1974.
- [185] Chun Ze Lai, Marti M. Joyer, Melissa A. Fierke, Nicholas D. Petkovich, Andreas Stein, and Philippe Buehlmann. Subnanomolar detection limit application of ion-selective electrodes with three-dimensionally ordered macroporous (3DOM) carbon solid contacts. *Journal of Solid State Electrochemistry*, 13(1):123–128, 2009.
- [186] Melissa A. Fierke, Chun-Ze Lai, Philippe Buehlmann, and Andreas Stein. Effects of architecture and surface chemistry of three-dimensionally ordered macroporous carbon solid contacts on performance of ion-selective electrodes. *Analytical Chemistry*, 82(2):680–688, 2009.

- [187] Jianfeng Ping, Yixian Wang, Jian Wu, and Yibin Ying. Development of an all-solid-state potassium ion-selective electrode using graphene as the solid-contact transducer. *Electrochemistry Communications*, 13(12):1529–1532, 2011.
- [188] Johan Bobacka. Potential stability of all-solid-state ion-selective electrodes using conducting polymers as ion-to-electron transducers. *Analytical chemistry*, 71(21):4932–4937, 1999.
- [189] Zsófia Szigeti, Tamás Vigassy, Eric Bakker, and Ernő Pretsch. Approaches to improving the lower detection limit of polymeric membrane ion-selective electrodes. *Electroanalysis*, 18(13-14):1254–1265, 2006.
- [190] Nupura S. Bhise, João Ribas, Vijayan Manoharan, Yu Shrike Zhang, Alessandro Polini, Solange Massa, Mehmet R. Dokmeci, and Ali Khademhosseini. Organ-on-a-chip platforms for studying drug delivery systems. *Journal of Controlled Release*, 190:82–93, 2014.
- [191] Yanina Shevchenko, Gulden Camci-Unal, Davide F. Cuttica, Mehmet R. Dokmeci, Jacques Albert, and Ali Khademhosseini. Surface plasmon resonance fiber sensor for real-time and label-free monitoring of cellular behavior. *Biosensors and Bioelectronics*, 56:359–367, 2014.
- [192] M. Józwiak-Bebenista and Jerzy Z. Nowak. Paracetamol: mechanism of action, applications and safety concern. *Acta poloniae pharmaceutica*, 71(1):11–23, 2013.
- [193] CP Babalola, FA Oladimeji, and MN Femi-Oyewo. Correlation between in vitro and in vivo parameters of commercial paracetamol tablets. *African journal of medicine and medical sciences*, 30(4):275–280, 2001.
- [194] Stephen J. Fey and Krzysztof Wrzesinski. Determination of drug toxicity using 3D spheroids constructed from an immortal human hepatocyte cell line. *Toxicological sciences*, page kfs122, 2012.
- [195] M. Waleed Shinwari, David Zhitomirsky, Imran A. Deen, P.R. Selvaganapathy, M. Jamal Deen, and D. Landheer. Microfabricated reference electrodes and their biosensing applications. *Sensors*, 10(3):1679–1715, 2010.
- [196] Brian J Polk, Anna Stelzenmuller, Geraldine Mijares, William MacCrehan, and Michael Gaitan. Ag/AgCl microelectrodes with improved stability for microfluidics. *Sensors and Actuators B: Chemical*, 114(1):239–247, 2006.
- [197] Sejin Park, Hankil Boo, Yunmee Kim, Ji-Hyung Han, Hee Chan Kim, and Taek Dong Chung. pH-sensitive solid-state electrode based on electrodeposited nanoporous platinum. *Analytical chemistry*, 77(23):7695–7701, 2005.
- [198] A. Economou, P.R. Fielden, and A.J. Packham. Data smoothing in stripping voltammetry by simplex function fitting. *Analytical letters*, 30(14):2595–2610, 1997.

Bibliography

- [199] James N. Miller and Jane Charlotte Miller. *Statistics and chemometrics for analytical chemistry*. Pearson Education, 2005.
- [200] R.R. Williams. Fundamental limitations on the use and comparison of signal-to-noise ratios. *Analytical Chemistry*, 63(15):1638–1643, 1991.
- [201] Gary L. Long and James D. Winefordner. Limit of detection. a closer look at the IUPAC definition. *Analytical Chemistry*, 55(7):712A–724A, 1983.
- [202] Raghu N. Kacker. Off-line quality control, parameter design, and the Taguchi method. *Journal of Quality Technology*, 17:176–188, 1985.

24, Chemin Vermont
1006 Lausanne, Switzerland
☎ +41 76 265 71 95
✉ irene.taurino@epfl.ch

IRENE TAURINO

Research experience

March 2011 – **Integrated Systems Laboratory, EPFL**, Lausanne, Switzerland, PhD student.
June 2015 PhD project: Carbon and Platinum Nanostructured Electrodes on Miniaturized Devices for Biomedical Diagnosis.

- Developed a new protocol to integrate by CVD down to CMOS compatible temperatures a wide range of carbon nanomaterials on working electrodes of a multipanel Si-based device
- Developed new methods to fabricate differently shaped and sized Pt and Au-Pt nanostructures by electrodeposition
- Electrochemical study of carbon nanomaterials and of Pt and Au-Pt nanostructured films for direct detection of metabolites, for enzyme-mediated detection of metabolites and as solid contacts for ion selective electrodes.

August-December 2014 **Khademhosseini Lab, Harvard-MIT Division of Health Sciences and Technology, Massachusetts Institute of Technology**, Cambridge, MA 02139, USA, Short term scholar.

- Developed an *in-line* solid-contact potassium-selective electrode for monitoring functional parameters of a bioreactor

2010 **Physics Department, PoliTo and Integrated Systems Laboratory, EPFL**, Torino, Italy and Lausanne, Switzerland, Master project: Fabrication and Electrochemical Characterisation of Differently Treated and Oriented Multi-Walled Carbon Nanotubes (MWCNTs) Directly Grown on Si.

2008 – 2010 **PoliTo and PoliMi**, Torino and Milano, Italy, Double degree Master project: Management, localisation and communication of wheelchair users living in a building by using an economically and technically feasible technology.

May 2005 **DI.PRO. S.A.S.**, San Mauro Torinese (To), Italy, Bachelor project: Surface Functionalization for Incisional Hernias Prostheses.

Teaching experience

Teaching assistant EPFL, Lausanne, Switzerland, EE-518: Analog Circuits for Biochip, Master in Electrical and Electronics Engineering (some lectures and exercise sessions)

Mentoring Integrated Systems Laboratory, EPFL, Lausanne, Switzerland: Mentoring PhD and Master students working on electrochemical devices, nanomaterials for electrochemical sensing, biocompatible membranes, microfluidic systems

Expertise

- Clean room facilities Photolithography, Thin Film Metal Evaporation, Ion Beam and Plasma Etching, Atomic Layer Deposition (ALD), Catalytic Chemical Vapour Deposition (CCVD), Sputtering.
- Sample characterisation Electroanalytical techniques, Optical and mechanical profilometers, Scanning Electron Microscopy with Energy Dispersive X-ray Spectroscopy (SEM/ EDX), Atomic Force Microscopy (AFM), Raman Spectroscopy.

Education

- March 2011 – June 2015 **EPFL**, Lausanne, Switzerland, PhD, Microsystems and Microelectronics.
- August 2014 – Dec 2014 **Harvard-MIT Division of Health Sciences and Technology, Massachusetts Institute of Technology**, Cambridge, MA 02139, USA, Short term scholar, Khademhosseini Lab.
- March 2010 – Sept 2010 **EPFL**, Lausanne, Switzerland, Exchange student (Erasmus scholarship, funded by European Union), Integrated Systems Laboratory.
- 2008–2010 **PoliTo**, Torino, Italy, Master of Science, Biomedical Engineering, 110 out of 110, summa cum laude.
- 2008–2010 **Alta Scuola Politecnica (ASP), PoliTo and PoliMi**, Torino and Milano, Italy, ASP diploma and double Master of Science degree, Biomedical Engineering.
- 2005–2008 **PoliTo**, Torino, Italy, Bachelor of Science, Biomedical Engineering, 110 out of 110, summa cum laude.

Languages

- Italian **Mother tongue**
- English **Advanced** *Pet Certificate in English, Cambridge University, 2008. IELTS Certificate in English, Cambridge University, 2008. Working experience in English*
- French **Intermediate** *Classes at EPFL Language Centre*

Computer skills

- Operating System Windows, Mac OSX
- Programming Applications Matlab, Simulink, C language, Mathematica, Igor Pro
- Microsoft Office (Word, PowerPoint, Excel), Latex, Bibtex
- Art and Graphics Adobe Illustrator, Image J, SolidWorks, Altair HyperWorks, Rhinoceros, Ansys
- Data treatment Igor Pro, Matlab, Simulink, Mathematica, Excel

Extracurricular activities

- Dance Teacher of dances from Southern Italy.

Publications

Peer-reviewed papers in international journals

- [1] **Irene Taurino**, Arnaud Magrez, Federico Matteini, Andrea Cavallini, László Forró, Giovanni De Micheli, and Sandro Carrara. High-performance multipanel biosensors based on a selective integration of nanographite petals. *Nano letters*, 14(6):3180–3184, 2014.
- [2] **Irene Taurino**, Viviane Van Hoof, Arnaud Magrez, László Forró, Giovanni De Micheli, and Sandro Carrara. Efficient voltammetric discrimination of free bilirubin from uric acid and ascorbic acid by a CVD nanographite-based microelectrode. *Talanta*, 130:423–426, 2014.
- [3] **Irene Taurino**, Arnaud Magrez, Federico Matteini, László Forró, Giovanni De Micheli, and Sandro Carrara. Direct growth of nanotubes and graphene nanoflowers on electrochemical platinum electrodes. *Nanoscale*, 5(24):12448–12455, 2013.
- [4] **Irene Taurino**, Renate Reiss, Michael Richter, Michael Fairhead, Linda Thöny-Meyer, Giovanni De Micheli, and Sandro Carrara. Comparative study of three lactate oxidases from *Aerococcus viridans* for biosensing applications. *Electrochimica Acta*, 93:72–79, 2013.
- [5] **Irene Taurino**, Viviane Van Hoof, Giovanni De Micheli, and Sandro Carrara. Superior sensing performance of multi-walled carbon nanotube-based electrodes to detect unconjugated bilirubin. *Thin Solid Films*, 548:546–550, 2013.
- [6] **Irene Taurino**, Sandro Carrara, Mauro Giorcelli, Alberto Tagliaferro, and Giovanni De Micheli. Comparison of two different carbon nanotube-based surfaces with respect to potassium ferricyanide electrochemistry. *Surface Science*, 606(3):156–160, 2012.
- [7] **Irene Taurino**, Sandro Carrara, Mauro Giorcelli, Alberto Tagliaferro, and Giovanni De Micheli. Carbon nanotubes with different orientations for electrochemical biodevices. *Sensors Journal, IEEE*, 12(12):3356–3362, 2012.
- [8] **Irene Taurino**, Giovanni De Micheli, and Sandro Carrara. Multiwalled carbon nanotubes for amperometric array-based biosensors. *BioNanoScience*, 2(4):185–195, 2012.
- [9] **Irene Taurino**, Sandro Carrara, Mauro Giorcelli, Alberto Tagliaferro, and Giovanni De Micheli. Comparing sensitivities of differently oriented multi-walled carbon nanotubes integrated on silicon wafer for electrochemical biosensors. *Sensors and Actuators B: Chemical*, 160(1):327–333, 2011.
- [10] Sandro Carrara, Sara Ghoreishizadeh, Jacopo Olivo, **Irene Taurino**, Camilla Baj-Rossi, Andrea Cavallini, Maaïke Op de Beeck, Catherine Dehollain, Wayne Burleson, Francis Gabriel Moussy, et al. Fully integrated biochip platforms for advanced healthcare. *Sensors*, 12(8):11013–11060, 2012.

- [11] Nima Aliakbarinodehi, **Irene Taurino**, Jagdale Pravin, Alberto Tagliaferro, Gianluca Piccinini, Giovanni De Micheli, and Sandro Carrara. Electrochemical nanostructured biosensors: carbon nanotubes versus conductive and semi-conductive nanoparticles. *Chemical Papers*, 69(1):134–142, 2015.
- [12] **Irene Taurino***, Gabriella Sanzó*, Franco Mazzei, Gabriele Favero, Giovanni De Micheli, and Sandro Carrara. Fast synthesis of platinum nanopetals and nanospheres for highly-sensitive non-enzymatic detection of glucose and selective sensing of ions. *Submitted to Scientific Reports*.
- [13] **Irene Taurino***, Solange Massa*, Gabriella Sanzó, Julio Aleman, Basilotta Flavia, Su Ryon Shin, Yu Shrike Zhang, Mehmet Dokmeci, Giovanni De Micheli, Sandro Carrara, and Ali Khademhosseini. Platinum nanopetals-based potassium sensors for acute cell death monitoring. *Submitted to ACS Applied Materials and Interfaces*.
- Chapter in referred books
- [14] **Irene Taurino**, Alessandro Sanginario, Giovanni De Micheli, Danilo Demarchi, and Sandro Carrara. Carbon nanomaterials for electrochemical and electrochemiluminescent medical sensors. In *Carbon for Sensing Devices*, pages 133–152. Springer, 2015.
- Peer-reviewed conference papers
- [15] Gabriella Sanzó*, **Irene Taurino***, Franco Mazzei, Gabriele Favero, Giovanni De Micheli, and Sandro Carrara. Highly sensitive electrodic materials based on Pt nanoflowers grown on Pt nanospheres for biosensor development. In *Nanotechnology (IEEE-NANO), 2015 IEEE 15th International Conference on*. IEEE, 2015.
- [16] **Irene Taurino**, Arnaud Magrez, Laszlo Forro, Giovanni De Micheli, and Sandro Carrara. Direct and selective synthesis of a wide range of carbon nanomaterials by CVD at CMOS compatible temperatures. In *Nanotechnology (IEEE-NANO), 2014 IEEE 14th International Conference on*, pages 843–848. IEEE, 2014.
- [17] Ismael Rattalino, Paolo Motto, **Irene Taurino**, Fernando Cortes-Salazar, Gianluca Piccinini, Danilo Demarchi, Giovanni De Micheli, and Sandro Carrara. Nanogap-based enzymatic-free electrochemical detection of glucose. In *Biomedical Circuits and Systems Conference (BioCAS), 2013 IEEE*, pages 130–133. IEEE, 2013.
- [18] Giovanni De Micheli, Cristina Boero, Camilla Baj-Rossi, **Irene Taurino**, and Sandro Carrara. Integrated biosensors for personalized medicine. In *Proceedings of the 49th Annual Design Automation Conference*, pages 6–11. ACM, 2012.
- [19] S. Sara Ghoreishizadeh, **Irene Taurino**, Sandro Carrara, and Giovanni De Micheli. A current-mode potentiostat for multi-target detection tested with different lactate biosensors. In *Biomedical Circuits and Systems Conference (BioCAS), 2012 IEEE*, pages 128–131. IEEE, 2012.
- [20] **Irene Taurino**, Sandro Carrara, Mauro Giorcelli, Alberto Tagliaferro, and Giovanni De Micheli. Comparing the enhanced sensing interfaces of differently oriented carbon nanotubes onto silicon for bio-chip applications. In *Advances in Sensors and*

Interfaces (IWASI), 2011 4th IEEE International Workshop on, pages 90–93. IEEE, 2011.

Patents

- [21] **Irene Taurino**, Arnaud Magrez, László Forró, Giovanni De Micheli, and Sandro Carrara. Close and selective integration of carbon nanomaterials by CVD onto working microelectrodes of multi sensing electrochemical biosensors, European patent application number EP 13184291.6 filed September 13 2013.

*These authors equally contributed to the work.